



QA: QA

ANL-EBS-MD-000001 REV 01

November 2004

Environment on the Surfaces of the Drip Shield and Waste Package Outer Barrier

Prepared for:
U.S. Department of Energy
Office of Civilian Radioactive Waste Management
Office of Repository Development
1551 Hillshire Drive
Las Vegas, Nevada 89134-6321

Prepared by:
Bechtel SAIC Company, LLC
1180 Town Center Drive
Las Vegas, Nevada 89144

Under Contract Number
DE-AC28-01RW12101

DISCLAIMER

This report was prepared as an account of work sponsored by an agency of the United States Government. Neither the United States Government nor any agency thereof, nor any of their employees, nor any of their contractors, subcontractors or their employees, makes any warranty, express or implied, or assumes any legal liability or responsibility for the accuracy, completeness, or any third party's use or the results of such use of any information, apparatus, product, or process disclosed, or represents that its use would not infringe privately owned rights. Reference herein to any specific commercial product, process, or service by trade name, trademark, manufacturer, or otherwise, does not necessarily constitute or imply its endorsement, recommendation, or favoring by the United States Government or any agency thereof or its contractors or subcontractors. The views and opinions of authors expressed herein do not necessarily state or reflect those of the United States Government or any agency thereof.

QA: QA

**Environment on the Surfaces of the Drip Shield and Waste Package
Outer Barrier**

ANL-EBS-MD-000001 REV 01

November 2004

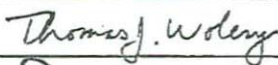
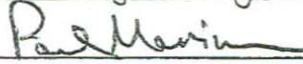

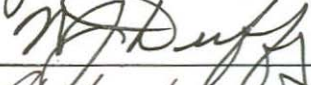

OCRWM	Scientific Analysis Signature Page/ Change History	Page iii
		1. Total Pages: 210

2. Scientific Analysis Title
Environment on the Surfaces of the Drip Shield and Waste Package Outer Barrier

3. DI (including Revision Number)
ANL-EBS-MD-000001 REV 01

4. Total Appendices
None

5. Number of Pages in Each Appendix

	Printed Name	Signature	Date
6. Originator	Tom Wolery		11/16/2004
7. Checker	Paul Mariner		11/16/2004
8. QER	James Graff		11/14/04
9. Responsible Manager/Lead	for Russell Jarek W.J. DUFFY		11/16/04
10. Responsible Manager	Ernest Hardin		11/16/04

11. Remarks

Change History

12. Revision No.	13. Description of Change
00/00	Initial Issue.
00/01	Changes to DTN numbers and references. Entries in Table 25 corrected.
00/02	Changes made to Sections 4.20, 4.21, 5 and 8.2.
01	Posted onto RIS Web. Changes to this version are too extensive to be indicated by change bars. This revision of the document is significantly reorganized and reformatted including renumbering of the figures and tables. This revision documents new work on the impacts that the mass transfer of trace-level acid-gas species has on the formulation of certain brine types.

INTENTIONALLY LEFT BLANK

CONTENTS

	Page
ACRONYMS.....	xvii
1. PURPOSE.....	1-1
1.1 PURPOSE AND SCOPE.....	1-1
1.2 ANALYSIS DESCRIPTION AND LIMITATIONS	1-3
1.3 RELATION TO ASSESSING SYSTEM PERFORMANCE	1-5
1.4 SUMMARY OF INFORMATION SOURCES AND USES OF OUTPUT INFORMATION.....	1-5
1.4.1 Information Sources	1-5
1.4.2 Users of Output Information	1-6
2. QUALITY ASSURANCE.....	2-1
3. USE OF SOFTWARE	3-1
4. INPUTS.....	4-1
4.1 DIRECT INPUTS	4-1
4.1.1 Miscellaneous Constants and Conversion Factors.....	4-2
4.1.2 Elevation of the Repository Above Sea Level	4-3
4.1.3 Vapor Pressure of Pure Water as a Function of Temperature.....	4-4
4.1.4 Vapor Pressure of Water over Saturated Solutions of Calcium Nitrate and Calcium Chloride.....	4-5
4.1.5 Boiling Points of Saturated Solutions of Some Pure Salts.....	4-8
4.1.6 Equilibrium RH of Selected Saturated Salt Solutions from 0°C to 100°C.....	4-8
4.1.7 Solubilities of Ca, Mg, Na, and K Salts in Water	4-11
4.1.8 Decomposition Temperatures of Some Salt Minerals.....	4-11
4.1.9 In-Drift Precipitates/Salts Model Including High Temperature Pitzer Thermodynamic Database.....	4-11
4.1.10 Standard Gibbs Energies of Formation and Standard Entropies at 298.15K for Selected Acid Gas Species.....	4-12
4.1.11 Thermodynamic Data Supporting Spreadsheet Files – <i>data0.ymp.R2</i> (Maier-Kelley Heat Capacity Coefficients of Selected Acid Gas Species)	4-13
4.1.12 Components of Atmospheric Air Exclusive of Water	4-14
4.1.13 Major Components of the Gas Phase in the Emplacement Drifts.....	4-14
4.1.14 Geochemical Composition of Dust Samples.....	4-17
4.1.15 Mean Atmospheric Pressure as a Function of Elevation (Equation)	4-22
4.1.16 Composition of J-13 Well Water	4-22
4.1.17 Composition of Porewaters from the TSw Unit.....	4-23
4.1.18 Calcium Chloride Acid Gas Volatility Experimental Data.....	4-24

CONTENTS (Continued)

	Page
4.1.19 Seepage Water Chemistry (Fugacities of Acid Gas Species in the Drift Wall).....	4-24
4.1.20 Solubility of Potassium Nitrate as a Function of Temperature	4-29
4.1.21 Barometric Pressure in the Repository.....	4-30
4.1.22 Solute Content of Precipitation (Rainfall) at Three Meteorological Stations in the Vicinity of Yucca Mountain.....	4-30
4.1.23 Leachable Compositions of Asian Dusts	4-31
4.1.24 Key Thermodynamic Relations for Gibbs Energies of Gas Species (Equations).....	4-32
4.1.25 Chemical Potential and Fugacity or Partial Pressure of a Gas Species (Equations).....	4-34
4.2 CRITERIA	4-35
4.3 CODES, STANDARDS, AND REGULATIONS.....	4-37
5. ASSUMPTIONS.....	5-1
5.1 VENTILATION WILL RESULT IN THE DEPOSITION OF DUST AND AEROSOLS ON THE SURFACES OF THE METAL BARRIERS.....	5-1
5.2 WATERS THAT HAVE BEEN SAMPLED AT YUCCA MOUNTAIN REPRESENT THE COMPOSITIONS OF SEEPAGE-DERIVED WATERS THAT CAN EVOLVE ON THE METAL BARRIER SURFACES.....	5-1
5.3 TOTAL PRESSURE IN THE DRIFTS WILL REMAIN CLOSE TO AMBIENT ATMOSPHERIC PRESSURE	5-2
5.4 THE GAS PHASE IN THE DRIFT, EXCLUSIVE OF WATER, HAS THE GROSS COMPOSITION OF ATMOSPHERIC AIR.....	5-3
5.5 THE TEMPERATURE, RH, AND CO ₂ PRESSURE AT A METAL BARRIER SURFACE ARE NOT PERTURBED BY EVAPORATION OR DELIQUESCENTE.....	5-3
5.6 THE COMPOSITION OF WATER CONTACTING METAL BARRIERS WILL NOT CHANGE SIGNIFICANTLY BECAUSE OF CHEMICAL INTERACTION WITH THE BARRIERS THEMSELVES.....	5-4
5.7 ACID GAS VOLATILES PRODUCED ON THE METAL BARRIERS ARE DISPERSED BY CONVECTION AND DIFFUSION TO THE DRIFT WALL.....	5-4
6. SCIENTIFIC ANALYSIS DISCUSSION.....	6-1
6.1 ANALYSIS OBJECTIVES	6-1
6.2 FEATURES, EVENTS, AND PROCESSES INCLUDED IN ANALYSIS.....	6-1
6.3 IN-DRIFT PRECIPITATES/SALTS CONCEPTUAL MODEL	6-2
6.4 CONSIDERATION OF ALTERNATIVE CONCEPTUAL MODELS	6-5
6.5 ANALYSIS FORMULATION.....	6-6
6.5.1 Mathematical Description of the In-Drift Precipitates/Salts Conceptual Model	6-10
6.5.2 Analysis Inputs.....	6-11
6.5.3 Summary of Computational Framework.....	6-11

CONTENTS (Continued)

	Page
6.6 NOT USED.....	6-11
6.7 ANALYSIS RESULTS	6-11
6.7.1 Overview	6-11
6.7.2 Discussion of Results	6-12
6.7.2.1 Atmospheric Pressure at the Repository Elevation	6-12
6.7.2.2 Vapor Pressure of Pure Water as a Function of Temperature	6-13
6.7.2.3 Vapor Pressure of Water as a Function of Temperature and Water Activity	6-15
6.7.2.4 Deliquescence Relative Humidity as a Function of Temperature for Several Salt Minerals.....	6-16
6.7.2.5 Boiling Point Elevation	6-18
6.7.2.6 Accessible Relative Humidity Conditions.....	6-19
6.7.2.7 Other Factors Governing Deliquescence RH-Temperature Relations	6-20
6.7.2.8 Other Information on Deliquescence, Dust, and Salt Minerals.....	6-22
6.7.2.9 EQ3/6 Calculations of Deliquescence Relative Humidities for Various Salt Minerals and Salt Mineral Assemblages	6-25
6.7.2.10 Analysis of Dust Compositions Taken from the Repository Drifts.....	6-50
6.7.2.11 Deliquescence of Salt Minerals Created by Evaporation of Seepage Waters	6-72
6.7.2.12 Additional Deliquescence RH Data for Saturated Calcium Nitrate and Saturated Calcium Chloride Solutions	6-75
6.7.2.13 Analysis of Deliquescence of Salt Minerals on the Metal Barriers	6-78
6.7.2.14 The Role of Acid Gas Volatility in Determining the Chemical Environment on the Metal Barriers	6-83
6.7.2.14.1 Background	6-83
6.7.2.14.2 Thermogravimetric Thin Aqueous Film Studies of Calcium Chloride Solutions at Elevated Temperature	6-96
6.7.2.14.3 EQ3/6 Calculations of the Evaporation to Near Dryness of a Dilute Calcium Chloride Solution, Subject to Fixed Fugacities of CO ₂ and HCl	6-101
6.7.2.15 Comments on In-Drift Precipitates/Salts Model Accuracy for the Present Analysis	6-103
6.7.2.16 Uncertainties.....	6-106
7. CONCLUSIONS.....	7-1
7.1 SUMMARY OF SCIENTIFIC ANALYSES	7-1
7.2 DEVELOPED OUTPUT	7-5
7.3 ACCEPTANCE CRITERIA SUMMARY	7-6

CONTENTS (Continued)

	Page
8. INPUTS AND REFERENCES.....	8-1
8.1 DOCUMENTS CITED.....	8-1
8.2 CODES, STANDARDS, REGULATIONS, AND PROCEDURES.....	8-12
8.3 SOURCE DATA, LISTED BY DATA TRACKING NUMBER.....	8-12
8.4 OUPUT DATA, LISTED BY DATA TRACKING NUMBER.....	8-14
8.5 SOFTWARE CODES.....	8-14

FIGURES

	Page
6.7-1. Vapor Pressure of Water as a Function of Temperature and Water Activity (Water Activity Values are Shown in the Legend).....	6-16
6.7-2. Vapor Pressure of Water as a Function of Temperature and Water Activity (Water Activity Values are Shown in the Legend; Pressure Range Reduced to 0 to 110 kPa).....	6-18
6.7-3. Maximum RH for “Wet” Conditions as a Function of Temperature, for Repository Ambient Pressure (left, the red curve) and Standard Atmospheric Pressure (right, the black curve)	6-20
6.7-4. Deliquescence RH as a Function of Temperature for Some Deliquescent Salts	6-26
6.7-5. Deliquescence RH Versus Temperature for Some Less-Deliquescent Salts	6-28
6.7-6. Deliquescence RH as a Function of Temperature for Some Moderately Deliquescent Salts.....	6-29
6.7-7. Deliquescence RH as a Function of Temperature for Antarcticite (CaCl ₂ :6H ₂ O), a Highly Deliquescent Salt, and (above 30°C to 31°C) its “Melt”	6-33
6.7-8. Deliquescence RH as a Function of Temperature for Successively Less Hydrous CaCl ₂ Minerals (Antarcticite, CaCl ₂ :6H ₂ O; CaCl ₂ :4H ₂ O; and CaCl ₂ :2H ₂ O).....	6-33
6.7-9. Deliquescence RH as a Function of Temperature for Ca(NO ₃) ₂ :4H ₂ O, a Highly Deliquescent Salt, and (above 45°C) its “Melt”	6-35
6.7-10. Deliquescence RH as a Function of Temperature for the Single Minerals Halite (NaCl) and Soda Niter (NaNO ₃) and the Two-Mineral Assemblage Halite and Soda Niter (NaCl-NaNO ₃).....	6-36
6.7-11. Deliquescence RH as a Function of Temperature for Several Two-Mineral Assemblages	6-36
6.7-12. Deliquescence RH as a Function of Temperature for Halite (NaCl) and Some Two-Mineral Assemblages Containing Halite.....	6-37
6.7-13. Deliquescence RH as a Function of Temperature for Some Three-Mineral Assemblages	6-39
6.7-14. Deliquescence RH as a Function of Temperature for the Three-Mineral Assemblage Halite–Niter–Soda Niter (NaCl-KNO ₃ -NaNO ₃) and the Three Contained Two-Mineral Assemblages.....	6-39
6.7-15. Deliquescence RH as a Function of Temperature for the Single Minerals Halite (NaCl), Niter (KNO ₃), and Soda Niter (NaNO ₃).....	6-40
6.7-16. RH versus Nitrate Mole Fraction [NO ₃ /(Cl + NO ₃)] in Aqueous Solution in the Halite-Soda Niter (NaCl-NaNO ₃) System at 25°C	6-41
6.7-17. Nitrate and Chloride Molalities versus Nitrate Mole Fraction [NO ₃ /(Cl + NO ₃)] in Aqueous Solution in the Halite-Soda Niter (NaCl-NaNO ₃) System at 25°C	6-42
6.7-18. RH versus Nitrate Mole Fraction [NO ₃ /(Cl + NO ₃)] in Aqueous Solution in the Halite–Soda Niter (NaCl-NaNO ₃) System at Temperatures of 25°C, 40°C, 60°C, 80°C, and 100°C	6-44
6.7-19. Nitrate and Chloride Molalities versus Nitrate Mole Fraction [NO ₃ /(Cl + NO ₃)] in Aqueous Solution in the Halite–Soda Niter (NaCl-NaNO ₃) System at Temperatures of 25°C, 40°C, 60°C, 80°C, and 100°C	6-44

FIGURES

	Page
6.7-20. RH versus Composite Normalized Reaction Progress (ξ) in Aqueous Solution in the Halite–Soda Niter (NaCl-NaNO ₃) System at Temperatures of 25°C, 40°C, 60°C, 80°C, and 100°C	6-45
6.7-21. Nitrate and Chloride Molalities versus Composite Normalized Reaction Progress (ξ) in Aqueous Solution in the Halite–Soda Niter (NaCl-NaNO ₃) System at Temperatures of 25°C, 40°C, 60°C, 80°C, and 100°C	6-45
6.7-22. RH versus Nitrate Mole Fraction [NO ₃ /(Cl + NO ₃)] in Aqueous Solution in the Halite–Niter (NaCl-KNO ₃) System at Temperatures of 25°C, 40°C, 60°C, 80°C, 100°C, and 120°C	6-47
6.7-23. Nitrate and Chloride Molalities versus Nitrate Mole Fraction [NO ₃ /(Cl + NO ₃)] in Aqueous Solution in the Halite–Niter (NaCl-KNO ₃) System at Temperatures of 25°C, 40°C, 60°C, 80°C, 100°C, and 120°C	6-47
6.7-24. RH versus Composite Normalized Reaction Progress (ξ) in Aqueous Solution in the Halite–Niter (NaCl-KNO ₃) System at Temperatures of 25°C, 40°C, 60°C, 80°C, 100°C, and 120°C	6-48
6.7-25. Nitrate and Chloride Molalities versus Composite Normalized Reaction Progress (ξ) in Aqueous Solution in the Halite–Niter (NaCl-KNO ₃) System at Temperatures of 25°C, 40°C, 60°C, 80°C, 100°C, and 120°C	6-48
6.7-26. RH Versus Composite Normalized Reaction Progress (ξ) in Aqueous Solution on the NaCl+KNO ₃ -NaNO ₃ +KNO ₃ join in the Halite–Niter–Soda Niter (NaCl-KNO ₃ -NaNO ₃) System at Temperatures of 25°C, 40°C, 60°C, 80°C, 100°C, and 120°C	6-49
6.7-27. Eutectic RH percent Values from EQ3/6 Calculations of Reconstituted Salt Minerals in Yucca Mountain Tunnel Dust	6-61
6.7-28. Deliquescence RH as a Function of Temperature for the Three-Mineral Assemblage Halite–Niter–KBr (NaCl-KNO ₃ -KBr)	6-62
6.7-29. Deliquescence RH as a Function of Temperature for the Assemblages Halite–Niter (NaCl-KNO ₃) and Halite–Niter–KBr (NaCl-KNO ₃ -KBr)	6-64
6.7-30. Deliquescence RH as a Function of Temperature for the Assemblages Halite–Niter–Soda Niter (NaCl-KNO ₃ -NaNO ₃) and Halite–Niter–Soda Niter–KBr (NaCl-KNO ₃ -NaNO ₃ -KBr)	6-64
6.7-31. Deliquescence RH and Minimum RH Values to Achieve NO ₃ /Cl Ratios of 1.0 and 0.2 as a Function of Temperature for the Assemblage Halite–Niter (NaCl-KNO ₃)	6-71
6.7-32. Deliquescence RH and Minimum RH Values to Achieve NO ₃ /Cl Ratios of 1.0 and 0.2 as a Function of Temperature for the Assemblage Halite–Niter–Soda Niter (NaCl- KNO ₃ -NaNO ₃)	6-71
6.7-33. Deliquescence RH as a Function of Temperature for the Three No-Dripping Cases	6-82
6.7-34. Deliquescence RH as a Function of Temperature for the Single Dripping Case	6-84
6.7-35. Weight Change Curve for a Typical Test at 150°C and 22.5 Percent RH for Alloy 22	6-98

FIGURES

	Page
6.7-36. Images of Alloy 22 Specimen (ID#TGA016) Before (left) and After (right) Reaction With a Thin Aqueous Layer of Calcium Chloride at 150°C and 19 Percent RH for Approximately 40 Hours	6-99
6.7-37. Comparison of Weight Changes of Alloy 22 Specimens Coated With a Thin Film of Calcium Chloride and Subjected to a 22.5 Percent RH Environment at the Various Temperatures Shown.....	6-99
6.7-38. Scanning Electron Microscopy (top left) and Energy Dispersive X-ray Spectroscopy Elemental Mapping (Cl, top right; Ca, bottom left; and O, bottom right) of Precipitate Constituents	6-100
6.7-39. In-Drift Precipitates/Salts Model Calculations versus Reported Measurements of the Solubility (Molality) of Niter (KNO ₃) from 25°C to 200°C.....	6-105
6.7-40. In-Drift Precipitates/Salts Model Calculations Versus Reported Measurements of the Solubility (Molality) of Niter (KNO ₃) from 25°C to 75°C (Showing More Detail in this Region than Figure 6.7-39)	6-105

INTENTIONALLY LEFT BLANK

TABLES

	Page
3-1. Summary List of Software Used.....	3-2
4.1-1. Direct Inputs.....	4-1
4.1-2. Miscellaneous Constants and Conversion Factors.....	4-2
4.1-3. Elevation of the Repository	4-3
4.1-4. Water Vapor Pressure as a Function of Temperature	4-4
4.1-5. Water Vapor Pressure of Saturated Calcium Nitrate Solutions as a Function of Temperature	4-6
4.1-6. Water Vapor Pressure of Saturated Calcium Chloride Solutions as a Function of Temperature	4-7
4.1-7. Boiling Points of Aqueous Solutions of Some Pure Salts	4-8
4.1-8. Equilibrium RH(%) of Saturated Aqueous Solutions of Various Pure Salts.....	4-9
4.1-9. Solubilities of Ca, Mg, Na, and K Salts in Water	4-10
4.1-10. Decomposition Temperatures of Some Salt Minerals	4-11
4.1-11. Standard Gibbs Energies of Formation and Standard Entropies at 298.15K for Selected Acid–Gas Species.....	4-13
4.1-12. Maier-Kelley Heat Capacity (Cp) Coefficients of Selected Acid–Gas Species (Joule Units).....	4-13
4.1-13. Components of Atmospheric Air Exclusive of Water Vapor	4-14
4.1-14. Some Measurements of Ambient CO ₂ Abundance in the Yucca Mountain Gas Phase (Borehole USW UZ-14)	4-15
4.1-15. Thermal-Hydrologic-Chemical Calculation Results for High Temperature and Low Carbon Dioxide Partial Pressure in the Tptpl Lithology for Seepage at the Crown of the Drift.....	4-16
4.1-16. Thermal-Hydrologic-Chemical Calculation Results for High Temperature and High Carbon Dioxide Partial Pressure in the Tptpl Lithology for Seepage at the Crown of the Drift.....	4-17
4.1-17. Thermal-Hydrologic-Chemical Calculation Results for Low Temperature and Low Carbon Dioxide Partial Pressure in the Tptpl Lithology for Seepage at the Crown of the Drift.....	4-17
4.1-18. Thermal-Hydrologic-Chemical Calculation Results for Low Temperature and High Carbon Dioxide Partial Pressure in the Tptpl Lithology for Seepage at the Crown of the Drift.....	4-17
4.1-19. Dust Leachate Compositions, Phase I.....	4-19
4.1-20. Dust Leachate Compositions, Phase II	4-20
4.1-21. Composition of J-13 Well Water	4-23
4.1-22. Major Ion Concentrations Reported for TSw Porewater at Ambient Temperature....	4-23
4.1-23. Log Fugacities of Five Acid–Gas Species in the Drift Wall as Functions of Time in Repository History	4-25
4.1-24. Solubility of Potassium Nitrate as a Function of Temperature.....	4-29
4.1-25. Measurements of the 2002 Mean Annual Solute Content of Precipitation at Three National Atmospheric Deposition Program Sites in the Vicinity of Yucca Mountain	4-30
4.1-26. Leachable Compositions of Asian Dust Samples (Statistical Composites).....	4-31

TABLES

	Page
4.2-1. Project Requirements and Yucca Mountain Review Plan Acceptance Criteria Applicable to This Report.....	4-36
6.2-1. Included FEPs in TSPA-LA Addressed in This Document.....	6-2
6.5-1. Considered Salt Minerals for Which Thermodynamic Data Extend to High Temperature.....	6-8
6.7-1. Calculated Atmospheric Pressure at the Repository Elevation.....	6-13
6.7-2. Measured Atmospheric Pressure in the Repository.....	6-13
6.7-3. Vapor Pressure of Pure Water as a Function of Temperature.....	6-14
6.7-4. Equilibrium RH of Saturated Aqueous Solutions of Various Pure Salts.....	6-17
6.7-5. Boiling Points of Aqueous Solutions of Pure Salts.....	6-19
6.7-6. Decomposition Temperatures of Some Salt Minerals.....	6-21
6.7-7. EQ3/6 Calculations of Reconstituted Salt Minerals in Dust Samples – Eutectic Mineral Assemblages at 25°C.....	6-53
6.7-8. EQ3/6 Calculations of Reconstituted Salt Minerals in Dust Samples – Eutectic Water Activities and Relative Humidities.....	6-55
6.7-9. (Table 6.7-7 with Additional Weighted Occurrences) EQ3/6 Calculations of Reconstituted Salt Minerals in Dust Samples at 25°C.....	6-57
6.7-10. Summary of Mineral Occurrences in the 16 Assemblages in Table 6.7-9.....	6-59
6.7-11. Key Sub-Assemblages of Reconstituted Salt Minerals in Dust Samples.....	6-60
6.7-12. Calculated Deliquescence RH Values for Key Assemblages at 25°C.....	6-61
6.7-13. Calculated Deliquescence RH values for Key Assemblages at 25°C, with and without KBr.....	6-63
6.7-14. Ionic Ratios (mol/mol) for the Soluble Fraction of Three Representative Tunnel Dusts, Three Regional Precipitation (Rainfall) Stations Surrounding Yucca Mountain, and Three Composite Results for Asian Dust.....	6-67
6.7-15. NO ₃ /Cl Ratios for Phase I Dust Samples.....	6-69
6.7-16. NO ₃ /Cl Ratios for Phase II Dust Samples.....	6-70
6.7-17. Water Vapor Pressure and RH of Saturated Calcium Nitrate Solutions as a Function of Temperature.....	6-75
6.7-17. Water Vapor Pressure and RH of Saturated Calcium Nitrate Solutions as a Function of Temperature (Continued).....	6-76
6.7-18. Water Vapor Pressure and RH of Saturated Calcium Chloride Solutions as a Function of Temperature.....	6-76
6.7-18. Water Vapor Pressure and RH of Saturated Calcium Chloride Solutions as a Function of Temperature (Continued).....	6-77
6.7-19. Cases, Associated Key Salts, and Percentage of Affected Waste Packages for the No-Dripping Condition (Dust Deliquescence).....	6-78
6.7-20. Case, Associated Key Salt, and Percentage of Affected Waste Packages for the Dripping Condition (Deliquescence of Salts Formed from Seepage Waters).....	6-78
6.7-21. Deliquescence RH as a Function of Temperature: No-Dripping Key Dust Assembly Case A (“NaCl-KNO ₃ ”).....	6-79
6.7-22. Deliquescence RH as a Function of Temperature: No-Dripping Key Dust Assembly Case B (“NaCl-KNO ₃ -NaNO ₃ ”).....	6-80

TABLES

	Page
6.7-23. Deliquescence RH as a Function of Temperature: No-Dripping Key Dust Assembly Case C (“NaCl-KNO ₃ -NaNO ₃ -Ca(NO ₃) ₂ ”)	6-81
6.7-24. Deliquescence RH as a Function of Temperature: Dripping Case (“CaCl ₂ ”)	6-83
6.7-25. Components of Atmospheric Air Exclusive of Water Vapor	6-84
6.7-26. Calculation Results for High Temperature and Low Carbon Dioxide Partial Pressure in the Tptpll Lithology for Seepage at the Crown of the Drift.....	6-86
6.7-27. Calculation Results for High Temperature and High Carbon Dioxide Partial Pressure in the Tptpll Lithology for Seepage at the Crown of the Drift.....	6-86
6.7-28. Calculation Results for Low Temperature and Low Carbon Dioxide Partial Pressure in the Tptpll Lithology for Seepage at the Crown of the Drift.....	6-86
6.7-29. Calculation Results for Low Temperature and High Carbon Dioxide Partial Pressure in the Tptpll Lithology for Seepage at the Crown of the Drift.....	6-87
6.7-30. Log Fugacities of Five Acid–Gas Species in the Drift Wall as Functions of Time in Repository History	6-89
6.7-31. The Apparent Standard Gibbs Energy of Formation (J/mol) of the gases HF, HCl, HBr, HNO ₃ , and N ₂ O ₅ as a Function of Temperature.....	6-95
6.7-32. Calculated Log Fugacities for HCl, RH Percent Values, and Ca and Cl Molalities Obtained in EQ3/6 Calculations of the Evaporation to Near-Dryness of Dilute CaCl ₂ Solution	6-102
6.7-33. Calculated RH Percent Values and Ca and Cl ⁻ Molalities Obtained in EQ3/6 Calculations of the Evaporation to Near-Dryness of Dilute CaCl ₂ Solution at Fixed Log Fugacities of CO ₂ and HCl.....	6-102
6.7-34. Estimated In-Drift Precipitates/Salts Model Uncertainties for Temperatures Between 25°C and 140°C	6-111
7.2-1. Output DTN Packages	7-5

INTENTIONALLY LEFT BLANK

ACRONYMS AND ABBREVIATIONS

ASTM	American Society for Testing and Materials
DIRS	Document Input Reference System
DS	drip shield
EBS	engineered barrier system
ESP	Environmental Simulation Program
FEPs	features, events, and processes
ICN	interim change notice
LA	license application
RH	relative humidity
TGA	thermogravimetric analyzer
TSw	Topopah Spring welded unit
TH	thermal-hydrologic
THC	thermal-hydrologic-chemical
TSPA	total system performance assessment
UZ	unsaturated zone
WPOB	waste package outer barrier
YMP	Yucca Mountain Project

INTENTIONALLY LEFT BLANK

1. PURPOSE

1.1 PURPOSE AND SCOPE

This report provides supporting analysis of the conditions at which an aqueous solution can exist on the drip shield or waste package surfaces, including theoretical underpinning for the evolution of concentrated brines that could form by deliquescence or evaporation, and evaluation of the effects of acid-gas generation on brine composition. This analysis does not directly feed the total system performance assessment for the license application (TSPA-LA), but supports modeling and abstraction of the in-drift chemical environment (BSC 2004 [DIRS 169863]; BSC 2004 [DIRS 169860]). It also provides analyses that may support screening of features, events, and processes, and input for response to regulatory inquiries.

This report emphasizes conditions of low relative humidity (RH) that, depending on temperature and chemical conditions, may be dry or may be associated with an aqueous phase containing concentrated electrolytes. Concentrated solutions at low RH may evolve by evaporative concentration of water that seeps into emplacement drifts, or by deliquescence of dust on the waste package or drip shield surfaces. The minimum RH for occurrence of aqueous conditions is calculated for various chemical systems based on current understanding of site geochemistry and equilibrium thermodynamics. The analysis makes use of known characteristics of Yucca Mountain waters and dust from existing tunnels, laboratory data, and relevant information from the technical literature and handbooks.

This report is written in accordance with *Technical Work Plan For: Near-Field Environment and Transport In-Drift Geochemistry Model Report Integration* (BSC 2004 [DIRS 171156]). The analyses presented in this report are for the current repository design (BSC 2004 [DIRS 168489]). In this design, drip shields are placed over the waste packages and no backfill is used. The LA waste package design consists of two layers: an Alloy 22 outer barrier (waste package output barrier) and a 316 stainless steel inner shell (BSC 2004 [DIRS 169480]) providing structural support. The drip shields placed over the waste packages are fabricated from Titanium Grade 7 (BSC 2004 [DIRS 169220]). The space between the drip shield and the emplacement drift wall is open for gas-phase circulation. The repository is ventilated for at least 50 years before permanent closure (e.g., BSC 2001 [DIRS 154276]).

This report contributes to definition of the environment as required by the “Problem Definition” section of the American Society for Testing and Materials standard (ASTM C 1174-97 1998 [DIRS 105725]), that is concerned with predicting the long-term behavior of materials used in the engineered barrier system (EBS) for the geological disposal of high-level radioactive waste. In its objectives and methodologies, this report links and overlaps with *Engineered Barrier System: Physical and Chemical Environment* (BSC 2004 [DIRS 169860]) and *In-Drift Precipitates/Salts Model* (BSC 2004 [DIRS 169863]). One link concerns the EQ3/6 Version 8.0 software (BSC 2003 [DIRS 162228]; SNL 2003 [DIRS 162494]) and its supporting Pitzer-based thermodynamic database: *data0.ypf.R1* (DTN: SN0302T0510102.002 [DIRS 162572]). This database is based on the phenomenology of Pitzer (1991 [DIRS 152709]), which addresses the thermodynamic behavior of aqueous salt solutions to high concentration. The database and the phenomenology are not exclusive to highly concentrated solutions, however. There is also a non-Pitzer thermodynamic database: *data0.ymp.R2* (DTN: MO0302SPATHDYN.000

[DIRS 161756]), which is applicable to a wider range of chemical components but restricted to the treatment of more dilute aqueous solutions. The database file *data0.ymp.R2* is not used in this report, although one spreadsheet from the set of supporting materials used to construct it (and taken from DTN: MO0302SPATHDYN.001 [DIRS 161886]) is used in the discussion of the role of acid–gas volatiles in Section 6.7.2.14. *In-Drift Precipitates/Salts Model* (BSC 2004 [DIRS 169863]) is the source of the high-temperature Pitzer-based thermodynamic model, hereafter referred to as the IDPS model. This report and *Engineered Barrier System: Physical and Chemical Environment* (BSC 2004 [DIRS 169860]) use the IDPS model in various analyses.

This report uses the IDPS model to analyze salt mineral deliquescence on the metal barrier surfaces, for application to the prediction of deliquescence associated with dust. The analysis identifies key assemblages of salt minerals and calculates the corresponding RH and temperature ranges for existence of an aqueous phase. The analysis applies the general limitation on the existence of liquid water imposed by the maximum total gas-phase pressure (and thus the maximum partial pressure of water vapor) in the repository environment.

The output of this report includes tables that describe “no-dripping” and “dripping” cases. The no-dripping case corresponds to deliquescence of the salt component of dust. The dripping case corresponds to the deliquescence of salts that may have formed due to the evaporation of seepage water. This output indicates, as a function of temperature and RH, whether or not an aqueous phase is present, and the major-component composition of the aqueous phase. Environmental conditions of temperature, RH, and partial pressure of CO₂ (pCO₂) are extracted from other reports and used as boundary conditions for estimating the evolution of the no-dripping and dripping cases with time in the repository. Many of the inputs listed in Section 4.1 are used for these calculations. However, this output is generated for expository purposes only and is not a feed to the TSPA-LA. *Engineered Barrier System: Physical and Chemical Environment* (BSC 2004 [DIRS 169860]) provides that feed to the TSPA-LA, and is constructed using the same principles described here and the same IDPS model. There are differences between the output of this analysis and the abstraction used in TSPA-LA, but these differences are caused by the use of different assumptions and inputs that describe the repository environment, and are not important differences in technical approach.

Care is taken in this report revision cycle to minimize inconsistencies among this report, *Engineered Barrier System: Physical and Chemical Environment* (BSC 2004 [DIRS 169860]), and *In-Drift Precipitates/Salts Model* (BSC 2004 [DIRS 169863]). The differences that remain are associated with: (1) different approximations, for example, different approaches to grouping of dust types based on experimental data; and (2) the use of certain published data for physical or chemical properties that may differ slightly from related information in the EQ3/6 thermodynamic database files. For example, one might use handbook data for the deliquescence RH of a salt mineral as a function of temperature, whereas a different value would be calculated using the IDPS model. The impact of this is insignificant because the magnitude of such differences is within the stated ranges of uncertainty on model output.

This report is a collection of analyses and supporting information. As noted previously, the principal output is an analysis of deliquescence. The role of acid–gas volatiles (which may affect seepage water evaporation and deliquescence processes) is addressed, but not included in the calculations used to construct the “no-dripping” and “dripping” case deliquescence tables that are

the principal output of this analysis report. If acid-gas volatilization were included, the ranges of temperature and RH for existence of an aqueous phase would likely be reduced. Also, the chemistry of the remaining fluids could be rendered less corrosive. Discussion of new experimental data pertinent to this topic is included.

Deviations from the Technical Work Plan—Section 1.2.3 of the technical work plan includes the requirement to “Incorporate the results of ongoing experiments on the boiling points of salt solutions at Lawrence Livermore National Laboratory” (BSC 2004 [DIRS 171156]). These results are not included because they were not available in time.

Section 2.2.3 of the technical work plan states, “The *Environment on the Surfaces of DS and WPOB* report, a scientific analysis, will use the IDPS model within its validation range for the stated purpose of the report” (BSC 2004 [DIRS 171156]). This report includes some results obtained from using the IDPS model outside its validation range in order to discuss trends, model adequacy, and uncertainties in parts of the analysis. None of these out-of-range results are used for the TSPA-LA. In Section 6.7.2.15, calculations of the solubility and relative humidity for saturated KNO_3 solutions are extended beyond the validation limit of 140°C to as much as 200°C in order to illustrate the limitations of the IDPS model in dealing with this important salt. In Sections 6.7.2.9 and 6.7.2.13, some calculations for solutions with very high (near saturation) concentrations of $\text{Ca}(\text{NO}_3)_2$ lie partially out of the validation range of the IDPS model. Here the solubility results are within the validation range but some deliquescence RH results are out-of-range. The validation range criteria for the IDPS model are listed in *In-Drift Precipitates/Salts Model* (BSC 2004 [DIRS 169863], Table 7-1). The out-of-validation-range results are clearly identified in this report where they are presented.

Section 3.2 of the technical work plan states that five acceptance criteria from *Yucca Mountain Review Plan, Final Report* (NRC 2003 [DIRS 163274]) will be addressed in this report. Sections 4.2 and 7.3 address four of these criteria but the fifth was not addressed because it pertains to output from model abstractions used in TSPA-LA, and this report does not feed TSPA-LA, nor does it discuss abstraction of a model.

1.2 ANALYSIS DESCRIPTION AND LIMITATIONS

The characteristics of the environment on the drip shield and waste package outer barrier are discussed in terms of the compositions of Yucca Mountain waters, the temperature of the EBS components, the effective RH at the EBS components, the gas-phase composition, and dust and aerosol deposition of hygroscopic (deliquescent) salts. This report includes thermodynamic calculations using the EQ3/6 Version 8.0 software (BSC 2003 [DIRS 162228]; SNL 2003 [DIRS 162494]) with the *data0.yppf.R1* database (DTN: SN0302T0510102.002 [DIRS 162572]) noted in Section 1.1.

For purposes of this analysis, most interactions among aqueous solutions and minerals on the metal surfaces and the components of the adjoining gas phase are effectively governed by thermodynamic equilibrium (local equilibrium). Thus, mineral and gas solubilities are key elements to understanding whether an aqueous solution is present under given conditions (e.g., temperature, RH, and pCO_2), and the composition of the solution. The expectation of local thermodynamic control is supported by several factors: (1) the long time periods available for

equilibrium to be reached (e.g., temperature and RH are relatively constant for long periods), and (2) the small thickness of any aqueous film or layer, and the ready availability of nucleation sites (“rough” surfaces and small particles). Still, some minerals such as dolomite and quartz will likely be prevented from forming due to extremely slow kinetics. This is factored into the analysis.

In the absence of salts, water is present on the metal surfaces only under conditions approaching 100 percent RH. At lower RH, pure water would quickly dry out, and without salt minerals present, condensation could not occur. Dissolved salts lower the RH at which dryout of an aqueous solution occurs, and salt minerals in a dry system lower the RH required for an aqueous solution to form. If equilibrium thermodynamics is controlling, and other conditions such as temperature are constant, deliquescence (condensation assisted by the presence of salt minerals) is simply the reverse of dryout. Under these conditions, if dryout occurs at a certain RH, then the salts deposited will deliquesce when the RH increases to the RH at dryout.

The equivalence of temperatures for dryout and deliquescence occurs only in laboratory-controlled systems. In practice, dryout and deliquescence may occur at different moisture conditions, and even at different locations. Importantly, much of the salt mineral mass present in dust on the metal barrier surfaces is likely to be brought into the repository from the outside by ventilation. Such salts will have a different origin (e.g., precipitation in what are now dry lakebeds, formation or modification by atmospheric chemistry processes), and may be distinct from salts formed by evaporation of seepage in the repository.

The deliquescence RH of a salt mineral (or assemblage of salt minerals) is the minimum RH at which aqueous solution can be formed from an initially dry system. Deliquescent salts are also termed “hygroscopic.” The best-known deliquescent salts include halides and nitrates of the alkali and alkaline earth metals, and the sulfates of some such metals. In principle any mineral, even a non-salt mineral such as quartz, has some deliquescence RH less than 100 percent. However, in the case of quartz and other relatively insoluble minerals, that deliquescence RH is not readily distinguishable from 100 percent. Deliquescent minerals tend to be highly soluble, with deliquescence RH generally correlating inversely with solubility. Examples of moderately to highly deliquescent minerals (which are moderately to highly soluble) include halite (NaCl), sylvite (KCl), antarcticite ($\text{CaCl}_2 \cdot 6\text{H}_2\text{O}$), niter (KNO_3), soda niter (NaNO_3 ; also known as nitratine), nitrocalcite [$\text{Ca}(\text{NO}_3)_2 \cdot 4\text{H}_2\text{O}$], and epsomite ($\text{MgSO}_4 \cdot 7\text{H}_2\text{O}$). The deliquescence RH, like solubility, is a function of temperature.

The deliquescence RH of a mineral assemblage is lower than the deliquescence RH of any individual mineral in the assemblage, and lower than the deliquescence RH of any contained subassemblage. In some cases (e.g., NaCl and NaNO_3 at 25°C; Section 6.7.2.9), the deliquescence RH of the assemblage is markedly lower than the deliquescence RH of any of the components. However, the deliquescence RH of a mineral assemblage need not be much lower than that of a highly deliquescent member or subassemblage. Consequently, for assemblages of as many as ten or more salt minerals, the deliquescence RH is often effectively determined by only one to three of the members. This factor supports categorization and analysis, and is a key result of this report (Sections 6.7.2.10 and 6.7.2.11).

Aqueous solutions on the metal surfaces can result from water absorption by deliquescent salts present on these surfaces (as well as from deposition of seepage waters). Deliquescent salts are deposited on the surfaces from dust and aerosols entrained in ventilation air, by any waters that completely evaporate on contact with the surfaces, and by deposition of aerosols formed in the repository by the dripping (splashing) of seepage water.

This report presents analyses of deliquescence of dust that may be deposited on the metal barrier surfaces, particularly during the ventilation period. A limitation of these analyses is that the quantity and composition of such dust are uncertain. Dust samples from the existing tunnels have been collected and analyzed, but they are influenced by recent construction activities and have been exposed to ventilation air for much less time than the duration of the repository ventilation period. Therefore, regional atmospheric dust compositions are also relevant.

An important concept developed in this report is that mass transfer of trace-level acid-gas species, including HCl, HBr, HF, and N₂O₅ (the anhydride of nitric acid), may significantly limit the existence or possible formation of certain brine types from either seepage-water evaporation or dust deliquescence. For example, a CaCl₂ solution would gain CO₂ and lose HCl, forming calcite (CaCO₃) and potentially drying out in the process. This report introduces the concept that the partial pressure of a gas like HCl on a metal barrier surface is limited by the partial pressure in the external environment (e.g., in the surrounding rock). This report presents thermodynamic calculations and experimental evidence that support this concept.

1.3 RELATION TO ASSESSING SYSTEM PERFORMANCE

This report contributes to definition of the environment for potential degradation of the drip shield and waste package outer barrier, although (as discussed above) the information developed here does not feed the TSPA-LA. This report demonstrates the methodology for estimating the critical RH for aqueous corrosion as the result of salt mineral deliquescence, which describes the process of dust deliquescence, and redissolution of certain salts (e.g., NaCl) that may be precipitated by the evaporative concentration of seepage waters. At RH values below the critical RH, aqueous solutions are not expected to form, and hence, aqueous electrochemical corrosion processes are not expected to occur. For RH greater than the critical value, this report demonstrates the methodology for estimating solution composition, which describes the further deliquescence of dust, and the evaporative concentration of seepage waters.

1.4 SUMMARY OF INFORMATION SOURCES AND USES OF OUTPUT INFORMATION

1.4.1 Information Sources

The principal information source for this report is *In-Drift Precipitates/Salts Model* (BSC 2004 [DIRS 169863]). This report uses the IDPS model (Section 4.1.9), an EQ3/6-based thermodynamic model for aqueous geochemical systems including salt minerals and concentrated brines. It is validated for use up to 140°C. The IDPS model is extensively applied in the present analysis in various parts of Section 6.7.2.

A second information source is *Engineered Barrier System: Physical and Chemical Environment* (BSC 2004 [DIRS 169860]). That report is the source of a set of EQ3/6 calculations of the chemistries of anticipated seepage waters, including computed values of equilibrium fugacities or partial pressures of acid–gas species of potential relevance (Section 6.7.2.14.1). This input is further discussed in Section 4.1.19.

1.4.2 Users of Output Information

Engineered Barrier System Features, Events, and Processes (BSC 2004 [DIRS 169898]) uses information from this report regarding dust sources and expected water compositions. *Engineered Barrier System: Physical and Chemical Environment* (BSC 2004 [DIRS 169860]) cites this report regarding several topics of common interest. The TSPA-LA does not directly use information from this report.

2. QUALITY ASSURANCE

Development of this report and supporting activities have been determined to be subject to the OCRWM quality assurance program (BSC 2004 [DIRS 171156], Section 8.1, Work Package ARTM02). Approved quality assurance procedures identified in the technical work plan (BSC 2004 [DIRS 171156], Section 4) have been used to conduct and document activities described in this report. The technical work plan also identifies the methods used to control the electronic management of data (BSC 2004 [DIRS 171156], Section 8.4) during the analysis and documentation activities.

This report analyzes the aqueous environment on the surfaces of the drip shield or waste package, which can influence the long-term performance of these components of the engineered barrier system. These components are classified in *Q-List* (BSC 2004 [DIRS 168361] as Safety Category because they are important to safety and waste isolation, as defined in AP-2.22Q, *Classification Analyses and Maintenance of the Q-List*. The results of this report are, therefore, important to the demonstration of compliance with the performance objectives prescribed in 10 CFR 63.113 [DIRS 156605]. The report contributes to the analysis of data used to support postclosure performance assessment; the conclusions do not directly impact preclosure engineered features important to safety, as defined in AP-2.22Q.

INTENTIONALLY LEFT BLANK

3. USE OF SOFTWARE

Microsoft Excel 97 (on a Windows 98 PC) and Microsoft Excel 2000 (on a Windows 2000 PC) were used to perform support calculations and graphics. Microsoft Excel is a standardized commercial spreadsheet program designed to assist in routine calculations and graphics. The program provides built-in mathematical functions that can be used to automate the calculation process. It also includes a graphics package to assist in data presentation. Microsoft Excel is exempt from software qualification because, in accordance with LP-SI.11Q-BSC, *Software Management*, Section 2.1.1, office automation systems such as word processors and spreadsheets are not required to be qualified. Furthermore, the graphical representation use of Microsoft Excel can be exempted under LP-SI.11Q-BSC, Section 2.1.2; and the calculations using built-in mathematical functions can be exempted under LP-SI.11Q-BSC, Section 2.1.6. When Microsoft Excel is used for calculations in this report (Sections 6.7.2.1, 6.7.2.2, 6.7.2.3, 6.7.2.5, 6.7.2.6, 6.7.2.9, 6.7.2.10, 6.7.2.12, 6.7.2.13, 6.7.2.14, and 6.7.2.15), information required for an independent person to reproduce the work (including formula or algorithm used, and listing of inputs and outputs) is provided.

Geochemical calculations are made using EQ3/6 version 8.0 (BSC 2003 [DIRS 162228]; SNL 2003 [DIRS 162494]) on a Windows 98 PC and a Windows 2000 PC. EQ3/6 is a software package for running the IDPS model on aqueous geochemical systems. This package contains two principal codes, EQ3NR and EQ6.

The EQ3NR code computes analyses of the thermodynamic state of aqueous solutions from analytical data or equivalent assumptions (e.g., the concentration of dissolved calcium is controlled by equilibrium with the mineral calcite). This code computes a simultaneous solution to a mélange of mass balance, electrical balance, mass action (equilibrium), and nonideality (e.g., activity coefficient) equations, using a hybrid Newton-Raphson method.

The EQ6 code computes reaction-path models of an aqueous solution reaction with minerals or other “reactant” substances, treating extents of reaction of the “reactants,” the identities of any secondary products and their extent of formation, and the evolution of the composition of the aqueous solution. Rate equations may include the use of arbitrary “relative rates” (as in a titration process), various theoretical rate law forms, or a combination of such equations. The temperature may be constant or vary as specified by the user.

In simple form, a reaction path calculation involves transferring mass from the “reactants” into a system including the aqueous solution and any secondary products. After any increment of mass transfer, the code performs essentially a heterogeneous equilibrium calculation, using essentially the same hybrid Newton-Raphson method to solve nearly the same set of equations used in an EQ3NR calculation. The main difference is that in EQ6, the mass of solvent water is not fixed, but calculated, and that mass action (equilibrium) equations for secondary products are also employed. If the rates of reaction of the “reactants” are all arbitrarily specified, then the calculation of mass transfer increments is straightforward. However, if the rate of reaction of a “reactant” is specified by a theoretical rate law (e.g., one formulated after transition state theory), then that rate law poses an ordinary differential equation. The mass transfer increments must then be determined by numerical integration. This applies whether all the rate laws in a given problem are of theoretical form, or whether they consist of a mix of theoretical rate laws with

arbitrary specified rates. For this purpose, EQ6 (beginning with version 8.0) employs a full ordinary differential equation predictor-corrector algorithm, including a so-called “stiff system” corrector.

In the present report, EQ3/6 is only used to make thermodynamic calculations. These calculations address two primary topics: the deliquescence of salt minerals on the surfaces of the drip shield and waste package outer barrier (due to deposition of dust or evaporation of seepage water) and the role of volatile acid–gas species in controlling the development of potential brine chemistries.

Limitations on outputs—No specific limitations on the outputs of this report are defined. None of the outputs are intended to be used as inputs to the total systems performance assessment for the license application (TSPA-LA).

Software is used in accordance with its intended use. This report uses the EQ3/6 code as part of implementing the IDPS model (BSC 2004 [DIRS 169863]), and the IDPS is used within its range of validation except as specified in Section 1.2. For the out-of-range conditions described in Section 1.2 the EQ3/6 code is valid; the validation range of the IDPS is associated with use of the *data0.yppf.R1* database (DTN: SN0302T0510102.002 [DIRS 162572]).

A summary list of the software used in this report is shown in Table 3-1.

Table 3-1. Summary List of Software Used

Software Name	Version Number	Software Tracking Number
Microsoft Excel 97	97	Exempt
Microsoft Excel 2000	2000	Exempt
EQ3/6	8.0	10813-8.0-00

4. INPUTS

4.1 DIRECT INPUTS

The individual input data sets are described below. Those data sets consisting of Yucca Mountain site-specific data are used to establish initial or boundary conditions for the analysis. The majority of the remaining inputs consist of thermodynamic data. Data sets not falling in one of these categories are generally experimental data used for comparison to calculated results, or are used in the analysis discussion to directly answer a question of interest (e.g., how does the composition of a given aqueous solution evolve in response to boiling?).

Some input data have specific associated uncertainties given by the data sources. When such data are presented in the tables that follow, these uncertainties are included. Otherwise, the input data are assumed to be accurate (certain) to the number of significant figures presented. Table 4.1-1 summarizes the direct inputs for this report.

Table 4.1-1. Direct Inputs

Section in This Report	Data Name or Descriptor	Data Source
4.1.1	Miscellaneous constants and conversion factors	Weast and Astle 1981 [DIRS 100833], Sections B and F (see Table 4.1-2 for the various page numbers)
4.1.2	Elevation of the repository above sea level	BSC 2003 [DIRS 161727]
4.1.3	Vapor pressure of pure water as a function of temperature	Weast and Astle 1981 [DIRS 100833], pp. D-168 and D-169
4.1.4	Vapor pressure of water over saturated solutions of calcium nitrate and calcium chloride	Kracek 1928 [DIRS 122125], p. 368
4.1.5	Boiling points of saturated solutions of some pure salts	Kracek 1928 [DIRS 122125], pp. 368 to 369, 371 to 373
4.1.6	Equilibrium RH of selected saturated salt solutions from 0 to 100°C	DTN: LL991212305924.108 [DIRS 144927]
4.1.7	Solubilities of Ca, Mg, Na, and K salts in water	Weast and Astle 1981 [DIRS 100833], pp. B-73 to B-166
4.1.8	Decomposition temperatures of some salt minerals	Weast and Astle 1981 [DIRS 100833], Section B (see Table 4.1-10 for the various page numbers)
4.1.9	In-Drift Precipitates/ Salts Model Including High-Temperature Pitzer Thermodynamic Database Pitzer thermodynamic database (data0.ypf, Rev. 1) and Baseline Set of Minerals Whose Precipitation is to be Suppressed	DTNs: SN0302T0510102.002 [DIRS 162572]; MO0312SPAESMUN.002 [DIRS 166329]; MO0303SPAMNSUP.000 [DIRS 171426]
4.1.10	Standard Gibbs Energies of Formation and Standard Entropies at 298.15K for Selected Acid-Gas Species	Barin and Platzki 1995 [DIRS 157865]
4.1.11	Thermodynamic Data Supporting Spreadsheet Files – <i>data0.ymp.R2</i> (Maier-Kelley Heat Capacity Coefficients of Selected Acid-Gas Species)	DTN: MO0302SPATHDYN.001 [DIRS 161886]
4.1.12	Components of atmospheric air exclusive of water	Weast and Astle 1981 [DIRS 100833], p. F-172

Table 4.1-1. Direct Inputs (Continued)

Section in This Report	Data Name or Descriptor	Data Source
4.1.13	Major Components of the Gas Phase in the Emplacement Drifts	DTN: GS970908312271.003 [DIRS 111467]
4.1.14	Geochemical composition of dust samples	DTNs: MO0207EBSDUSTS.020 [DIRS 162556]; MO0209EBSDUST2.030 [DIRS 162557]
4.1.15	Mean Atmospheric Pressure as a Function of Elevation (Equation)	Fleagle and Businger 1980 [DIRS 108591], pp. 10, 34, and 40
4.1.16	Composition of J-13 well water	DTN: MO0006J13WTRCM.000 [DIRS 151029]
4.1.17	Composition of porewaters from Topopah Spring welded unit (TSw)	DTN: MO0005PORWATER.000 [DIRS 150930]
4.1.18	Calcium chloride acid–gas volatility experimental data	DTNs: LL030308812251.017 [DIRS 163775]; LL030309012251.018 [DIRS 163774]
4.1.19	Seepage water chemistry (fugacities of selected acid–gas species in the drift wall)	DTN: MO0303MWDSCMAB.000 [DIRS 162551]
4.1.20	Solubility of potassium nitrate as a function of temperature	Linke 1965 [DIRS 166191], p. 250
4.1.21	Barometric pressure in the repository	DTN: GS030108312242.001 [DIRS 163118]
4.1.22	Solute content of precipitation (rainfall) at three meteorological stations bracketing Yucca Mountain	National Atmospheric Deposition Program: NADP/NTN 2003 [DIRS 171291]; NADP/NTN 2003 [DIRS 171292]; NADP/NTN 2003 [DIRS 171293]
4.1.23	Leachable compositions of Asian dusts	Topping et al. 2004 [DIRS 171290], Table 1 (p. 2113) and Table 2 (p. 2116)
4.1.24	Key Thermodynamic Relations for Gibbs Energies of Gas Species (Equations)	Helgeson et al. 1978 [DIRS 101596], pp. 28 to 29
4.1.25	Chemical Potential and Fugacity or Partial Pressure of a Gas Species (Equations)	Nordstrom and Munoz 1986 [DIRS 153965], p. 129

4.1.1 Miscellaneous Constants and Conversion Factors

Miscellaneous constants and conversion factors used in various calculations in this report are given in Table 4.1-2.

Table 4.1-2. Miscellaneous Constants and Conversion Factors

Datum	Value	Units	Source Page Number
Atmospheric Pressure at Sea Level	1,013.2500	mbar	F-168
Standard Atmosphere (atm)	1,013,250	dyn/cm ²	F-81
Standard Atmosphere (atm)	760	Torr	F-282
Standard bar	10 ⁶	dyn/cm ²	F-82
Standard bar	0.986923	atm	F-283
Standard Pascal (Pa)	1	Newton/m ²	F-108
mm Hg (0°C)	1	Torr	F-297
Standard dyne	1	g-cm/s ²	F-90

Table 4.1-2. Miscellaneous Constants and Conversion Factors (Continued)

Datum	Value	Units	Source Page Number
Standard Newton	10 ⁵	dynes	F-298
Mean acceleration due to gravity (<i>g</i>)	980.7±0.9	cm/s ²	F-144
Gas Constant (<i>R</i>)	8.3143	J/K-mol	F-96
Gas Constant (<i>R</i>)	8.20562 × 10 ⁻²	m ³ -atm/kmol-K	F-204
Effective Molecular Weight of Air [<i>MW</i> (<i>air</i>)]	28.966	g/mol*	F-168
Molecular Weight of H ₂ O	18.0153	g/mol	B-105
Molecular weight of KNO ₃	101.11	g/mol	B-135

Source: Weast and Astle 1981 [DIRS 100833].

*The source does not give units for this, apparently to avoid the issue of what is a mole of air. Nevertheless, "g/mol" is the appropriate set of units for any molecular weight following modern chemical practice. Also, these units are consistent with those of the gas constant, *R*, in subsequent calculations.

Some of these data are used to calculate the atmospheric pressure at the elevation of the repository in Section 6.7.2.1. These data are also used elsewhere in Section 6.7.2 for converting units when cited data are not in the units desired.

4.1.2 Elevation of the Repository Above Sea Level

The elevation range of the repository (BSC 2004 [DIRS 164519]) is given in Table 4.1-3. The specified range is 1,039 to 1,107 m. The elevation is of interest because the lower atmospheric pressure at higher elevation lowers the boiling point of water (and that of aqueous salt solutions). These data are used in Section 6.7.2.1 to calculate the atmospheric pressure at the elevation of the repository. The purpose of this calculation is to support the choice of a value for the expected maximum pressure in the repository (maximum exclusive of short-term spikes associated with weather phenomena). The elevation data are used in Section 6.7.2.1 as inputs to the pressure-elevation equation introduced later in Section 4.1.15. Other inputs include various constants introduced in Section 4.1.1 (Table 4.1-1).

Table 4.1-3. Elevation of the Repository

Datum	Value	Units	Source
Minimum Elevation	1,038	m	BSC 2003 [DIRS 161727]
Maximum Elevation	1,107	m	BSC 2003 [DIRS 161727]
Minimum Elevation	1,039	m	BSC 2004 [DIRS 164519]*
Maximum Elevation	1,107	m	BSC 2004 [DIRS 164519]*

NOTE: * Used as corroborative information.

The actual elevation data used in the calculations in Section 6.7.2.1 are from a superseded design document (BSC 2003 [DIRS 161727]), which gives the same maximum elevation as the current design document (BSC 2001 [DIRS 164519]), but a minimum elevation of 1,038 m, not 1,039 m, as shown above in Table 4.1-3. The data from *Repository Design, Repository/PA IED Subsurface Facilities* (BSC 2003 [DIRS 161727]) are judged to be suitable and qualified for their intended use in this report through corroboration with current design values in *D&E/PA/C IED*

Subsurface Facilities (BSC 2004 [DIRS 164519]). The older design document was superseded and changed to reflect changes in the repository layout, resulting in the elevation change.

As shown on Table 4.1-3, only the data for the minimum elevation are different between the current and superseded documents. The elevation data given in these documents are only specified to the nearest whole meter, which is also the difference between the two minimum elevation values. For the purposes of this report (to support the establishment of an expected maximum pressure in the repository), this difference is not significant, as is demonstrated in Section 6.7.2.1. Furthermore, the maximum pressure in the repository elevation range depends on the minimum elevation. Using a lower elevation value will result in a higher calculated pressure. Thus, for the purposes of this report, results using the older, lower elevation values would be more conservative than results based on the newer elevation values.

4.1.3 Vapor Pressure of Pure Water as a Function of Temperature

The vapor pressure of pure water as a function of temperature is given in Table 4.1-4. The vapor pressures are given in mm Hg. The vapor pressures are converted to kPa in Section 6.7.2.2.

Table 4.1-4. Water Vapor Pressure as a Function of Temperature

Temperature (°C)	mm Hg	Temperature (°C)	mm Hg
0	4.579	155	4,075.88
5	6.543	160	4,636.00
10	9.209	165	5,256.16
15	12.788	170	5,940.92
20	17.535	175	6,694.08
25	23.756	180	7,520.20
30	31.824	185	8,423.84
35	42.175	190	9,413.36
40	55.324	195	10,488.76
45	71.88	200	11,659.16
50	92.51	205	12,929.12
55	118.04	210	14,305.48
60	149.38	215	15,792.80
65	187.54	220	17,395.64
70	233.7	225	19,123.12
75	289.1	230	20,978.28
80	355.1	235	22,967.96
85	433.6	240	25,100.52
90	525.76	245	27,381.28
95	633.9	250	29,817.84
100	760.00	255	32,417.80
105	906.07	260	35,188.00
110	1,074.56	265	38,133.00
115	1,267.98	270	41,261.16
120	1,489.14	275	44,580.84
125	1,740.93	280	48,104.20

Table 4.1-4. Water Vapor Pressure as a Function of Temperature (Continued)

Temperature (°C)	mm Hg	Temperature (°C)	mm Hg
130	2,026.16	285	51,838.08
135	2,347.26	290	55,799.20
140	2,710.92	295	59,994.40
145	3,116.76	300	64,432.80
150	3,570.48	—	—

Source: Weast and Astle 1981 [DIRS 100833], pp. D-168 to D-169.

These data are used in parts of Section 6.7.2 to calculate constraints on the range of accessible RH values, and to calculate RH values from water vapor pressures over saturated salt solutions.

4.1.4 Vapor Pressure of Water over Saturated Solutions of Calcium Nitrate and Calcium Chloride

Table 4.1-5 contains data for the vapor pressure of water over saturated solutions of calcium nitrate. The saturating phases are specifically identified, as this “salt” is represented by a sequence with increasing temperature of progressively lower hydrates leading to the anhydrous salt. Table 4.1-6 contains the same kind of data for saturated solutions of calcium chloride. That “salt” also is represented by a sequence of progressively lower hydrates leading to the anhydrous form. The data in these tables are handbook data constituting established fact.

The data summarized in each table were collected by Kracek (1928 [DIRS 122125]) from multiple original sources and are not entirely mutually consistent. The degree of inconsistency should be interpreted as representing the likely uncertainty. The data in Table 4.1-5 indicate that α -Ca(NO₃)₂·4H₂O is the saturating solid up to about 42.7°C. Then Ca(NO₃)₂·3H₂O takes over and holds this role up to about 50°C (likely in the range 49.8°C to 51.9°C, though that probably underestimates the true uncertainty). It is not clear from the data whether or not Ca(NO₃)₂·2H₂O is really a stable saturating solid before Ca(NO₃)₂ takes over. If so, its range is likely to be only a degree or two. Ca(NO₃)₂ is clearly the stable saturating solid by 55°C, and continues as such up to 151°C (the apparent boiling point at atmospheric pressure).

The data in Table 4.1-6 indicate that CaCl₂·6H₂O is the saturating solid up to about 29.5°C to 30°C, after which α -CaCl₂·4H₂O takes over. That solid then holds up to 45.3°C, at which point CaCl₂·2H₂O becomes the saturating solid. That phase then holds this role up to at least 172°C. The corresponding reported vapor pressure at that temperature is 825 mm Hg (825 Torr), which is greater than atmospheric pressure (1 atm. = 760 Torr), implying that the boiling temperature for conditions of standard atmospheric pressure is less than 172°C. Indeed, the reported vapor pressures for 160°C and 170°C bracket standard atmospheric pressure, indicating that the boiling temperature lies in between. Subsequent data in the table (for 175.7°C and 175.5°C) suggest that the boiling temperature might be closer to 176°C. It is not clear if CaCl₂·2H₂O is the saturating solid all the way to the boiling temperature, or if CaCl₂ has a small range in which it is the saturating solid. The data suggest that the boiling temperature is likely between 164°C and 176°C.

Table 4.1-5. Water Vapor Pressure of Saturated Calcium Nitrate Solutions as a Function of Temperature

Temperature (°C)	(mm) Hg
α-Ca(NO₃)₂:4H₂O	
0	2.7
5	3.9
10	5.2
15	6.9
20	9.4
25	12.0
30	14.9
35	17.7
37	18.9
39	19.5
40	19.7 max
41	19.7
42	19.3
42.5	19.0
42.7	18.6
α-Ca(NO₃)₂:4H₂O + Ca(NO₃)₂:3H₂O	
42.7 ^(E)	18.0
Ca(NO₃)₂:3H₂O	
44	18.8
46	19.8
48	20.5
49	20.6 max
50	20.5
50.5	20.2
51.1	19.0
51	16.8
Ca(NO₃)₂:3H₂O + Ca(NO₃)₂:2H₂O	
50.6 ^(E)	15.4
Ca(NO₃)₂:3H₂O + Ca(NO₃)₂	
49.8 ^(m, E)	14.3
Ca(NO₃)₂:2H₂O + Ca(NO₃)₂	
51.9 ^(U)	16.0
Ca(NO₃)₂	
55	19
60	24.9
151	760.0

Source: Kracek 1928 [DIRS 122125], p. 368.

E = eutectic point; U = transition temperature or incongruent melting point; m = metastable; "max" = maximum.

Table 4.1-6. Water Vapor Pressure of Saturated Calcium Chloride Solutions as a Function of Temperature

Temperature (°C)	(mm) Hg
CaCl₂·6H₂O	
0	2.08
5	2.74
10	3.71
15	4.76
20	6.06
25	6.97
27	7.28
28.5	7.36 max
29	7.33
29.5	7.22
CaCl₂·6H₂O	
29.95 ^(m)	6.70
CaCl₂·6H₂O + α-CaCl₂·4H₂O	
29.93 ^(U)	6.85
α-CaCl₂·4H₂O	
35	8.63
40	10.53
α-CaCl₂·4H₂O + CaCl₂·2H₂O	
45.3 ^(U)	12.06
CaCl₂·2H₂O	
50	15.5
60	25.7
70	41.2
80	63.9
90	95.2
100	138
120	268
140	467.5
160	719
170	815
172	825
CaCl₂·2H₂O	
175.7 ^(m)	771
CaCl₂·2H₂O + CaCl₂·H₂O	
175.5 ^(U)	796

Source: Kracek 1928 [DIRS 122125], p. 368.

E = eutectic point; U = transition temperature or incongruent melting point; m = metastable; "max" = maximum.

4.1.5 Boiling Points of Saturated Solutions of Some Pure Salts

Table 4.1-7 lists the boiling points at sea level of the saturated aqueous solutions of several pure salts. The boiling point is defined as the temperature at which the water-vapor pressure is equal to the ambient pressure. At sea level, the ambient pressure is 101.325 kPa (760 Torr).

Table 4.1-7. Boiling Points of Aqueous Solutions of Some Pure Salts

Salt	Boiling Point (°C)	Source Page Number
K ₂ SO ₄	101.4	373
Na ₂ SO ₄	102.84	371
KCl	108.6	373
NaCl	108.67	369
KNO ₃	115.5	373
NaNO ₃	120.59	372
Ca(NO ₃) ₂	151	368

Source: Kracek 1928 [DIRS 122125].

As noted in Section 4.1.4, the boiling point for CaCl₂ carries fairly wide uncertainty. However, it appears to be bounded by 180°C.

4.1.6 Equilibrium RH of Selected Saturated Salt Solutions from 0°C to 100°C

Table 4.1-8 lists the equilibrium RHs of selected saturated salt solutions. These equilibrium RHs are the deliquescence RHs for the salt minerals with which the solutions are saturated. The data in Table 4.1-8 are taken from DTN: LL991212305924.108 [DIRS 144927]. The listed sources of these data for that DTN are Greenspan (1977 [DIRS 104945]) and Kracek (1928 [DIRS 122125]).

A subset of these data is from ASTM E 104-85, *Standard Practice for Maintaining Constant Relative Humidity by Means of Aqueous Solutions* (1996 [DIRS 146039]). Included in the ASTM standard are the data for magnesium chloride, potassium carbonate, magnesium nitrate, sodium chloride, potassium chloride, potassium nitrate, and potassium sulfate.

Qualification Status: These are Project data – qualified per the status of the cited DTN. The subsets of the data attributable to Kracek (1928 [DIRS 122125]) and ASTM E 104-85 (1996 [DIRS 146039]) would otherwise be considered established fact.

Table 4.1-8. Equilibrium RH(%) of Saturated Aqueous Solutions of Various Pure Salts

Temperature (°C)	KF	MgCl ₂	K ₂ CO ₃	MgNO ₃	NaNO ₃	NaCl	KCl	KNO ₃	NaOH	KOH	K ₂ SO ₄
0	—	33.66	43.13	60.35	—	75.51	88.61	96.33	—	—	98.77
5	—	33.60	43.13	58.86	78.57	75.65	87.67	96.27	—	14.34	98.48
10	—	33.47	43.14	57.36	77.53	75.67	86.77	95.96	—	12.34	98.18
15	—	33.30	43.15	55.87	76.46	75.61	85.92	95.41	9.57	10.68	97.89
20	—	33.07	43.16	54.38	75.36	75.47	85.11	94.62	8.91	9.32	97.59
25	30.85	32.78	43.16	52.89	74.25	75.29	84.34	93.58	8.24	8.23	97.30
30	27.27	32.44	43.17	51.40	73.14	75.09	83.62	92.31	7.58	7.38	97.00
35	24.59	32.05	—	49.91	72.06	74.87	82.95	90.79	6.92	6.73	96.71
40	22.68	31.60	—	48.42	71.00	74.68	82.32	89.03	6.26	6.26	96.41
45	21.46	31.10	—	46.93	69.99	74.52	81.74	87.03	5.60	5.94	96.12
50	20.80	30.54	—	45.44	69.04	74.43	81.20	84.78	4.94	5.72	95.82
55	20.60	29.93	—	—	68.15	74.41	80.7	—	4.27	5.58	—
60	20.77	29.26	—	—	67.35	74.50	80.25	—	3.61	5.49	—
65	21.18	28.54	—	—	66.64	74.71	79.85	—	2.95	5.41	—
70	21.74	27.77	—	—	66.04	75.06	79.49	—	2.29	5.32	—
75	22.33	26.94	—	—	65.56	75.58	79.17	—	1.63	—	—
80	22.85	26.05	—	—	65.22	76.29	78.90	—	—	—	—
85	23.20	25.11	—	—	65.03	—	78.68	—	—	—	—
90	23.27	24.12	—	—	65.00	—	78.50	—	—	—	—
95	—	23.07	—	—	—	—	—	—	—	—	—
100	—	21.97	—	—	—	—	—	—	—	—	—

Source: DTN: LL991212305924.108 [DIRS 144927].

Table 4.1-9. Solubilities of Ca, Mg, Na, and K Salts in Water

Compound	Formula	Note	Temperature (°C)	Solubility (g/100 cm ³)	Temperature (°C)	Solubility (g/100 cm ³)
Calcium sulfate	CaSO ₄	Natural anhydrite	30	0.209	100	0.1619
Calcium sulfate dihydrate	CaSO ₄ ·2H ₂ O	Natural gypsum	"low"	0.241	100	0.222
Calcium nitrate	Ca(NO ₃) ₂	—	18	121.2	100	376
Calcium chloride	CaCl ₂	—	20	74.5	100	159
Calcium fluoride	CaF ₂	Natural fluorite	18	0.0016	26	0.0017
Calcium carbonate	CaCO ₃	Natural calcite	25	0.0014	75	0.0018
Calcium hydroxide	Ca(OH) ₂	—	0	0.185	100	0.077
Sodium sulfate	Na ₂ SO ₄	Natural thenardite	0	4.76	100	42.7
Sodium nitrate	NaNO ₃	Soda niter	25	92.1	100	180
Sodium chloride	NaCl	Natural halite, common salt	0	35.7	100	39.12
Sodium fluoride	NaF	Natural villiumite	18	4.22	"high"	—
Sodium carbonate	Na ₂ CO ₃	—	0	7.1	100	45.5
Sodium bicarbonate	NaHCO ₃	—	0	6.9	60	16.4
Sodium hydroxide	NaOH	—	0	42.0	100	34.7
Magnesium sulfate	MgSO ₄	—	0	26	100	73.8
Magnesium nitrate, hexahydrate	Mg(NO ₃) ₂ ·6H ₂ O	—	"low"	125	"high"	"Very soluble"
Magnesium chloride	MgCl ₂	—	20	54.25	100	72.7
Magnesium fluoride	MgF ₂	Natural sellaite	18	0.0076	"high"	"Insoluble"
Magnesium carbonate	MgCO ₃	Natural magnesite	"low"	0.0106	"high"	—
Magnesium carbonate trihydrate	MgCO ₃ ·3H ₂ O	Natural nesquehonite	16	0.179	"high"	"Decomposes"
Magnesium hydroxide	Mg(OH) ₂	Natural brucite	18	0.0009	100	0.004
Potassium sulfate	K ₂ SO ₄	Natural arcanite	25	12	100	24.1
Potassium sulfate, hydrogen	KHSO ₄	Natural mercallite, misenite	0	36.3	100	121.6
Potassium nitrate	KNO ₃	Saltpeter	0	13.3	100	247
Potassium chloride	KCl	Natural sylvite	20	23.8	100	56.7
Potassium fluoride	KF	—	18	92.3	"high"	"Very soluble"
Potassium carbonate	K ₂ CO ₃	—	20	112	100	156
Potassium carbonate, hydrogen	KHCO ₃	—	"low"	22.4	60	60
Potassium hydroxide	KOH	—	15	107	100	178

Source: Weast and Astle 1981 [DIRS 100833], pp. B-73 to B-166.

NOTE: See text for discussion of "low" and "high" temperatures.

4.1.7 Solubilities of Ca, Mg, Na, and K Salts in Water

Table 4.1-9 is a list of solubilities of various salts of calcium, magnesium, sodium, and potassium (Weast and Astle 1981 [DIRS 100833], pp. B-73 to B-166). These solubility data are given at two temperatures, one at or near 25°C, the other at some higher value, often 100°C. In some cases, a verbal designation (“low” or “high”) is given for the temperature. In a few instances, the table provides a verbal descriptor in the solubility, such as “very soluble.” The source handbook does not provide further information concerning such terms.

4.1.8 Decomposition Temperatures of Some Salt Minerals

Table 4.1-10 lists the decomposition temperatures of some salt minerals. In most instances, the mechanism of decomposition is melting. However, examples are also included of decarbonation and dehydration. Note that the melting of hydrate minerals produces a “melt” that is actually an aqueous solution. The complete melting of a pure hydrate mineral produces a solution whose composition is stoichiometrically identical to the original mineral.

Table 4.1-10. Decomposition Temperatures of Some Salt Minerals

Salt Mineral	Decomposition Temp (°C)	Mechanism	Source Page Number
CaCl ₂ ·6H ₂ O	29.92	Melting	B-87
CaCl ₂ ·H ₂ O	260	Melting	B-87
CaCl ₂	782	Melting	B-87
Ca(NO ₃) ₂ ·4H ₂ O	α: 42.7 β: 39.7	Melting	B-88
Ca(NO ₃) ₂ ·3H ₂ O	51.1	Melting	B-88
Ca(NO ₃) ₂	561	Melting	B-88
KHCO ₃	100-200	Unspecified decomposition	B-131
KCl	770	Melting	B-132
KNO ₃	334	Melting	B-135
NaCl	801	Melting	B-147
Na ₂ CO ₃ ·10H ₂ O	32.5-34.5	Melting	B-147
Na ₂ CO ₃ ·7H ₂ O	32	Dehydration	B-147
Na ₂ CO ₃ ·H ₂ O	100	Dehydration	B-147
Na ₂ CO ₃	851	Melting	B-147
NaHCO ₃	270	Decarbonation	B-147
Na ₂ SO ₄ ·10H ₂ O	32.38	Melting	B-150

Source: Weast and Astle 1981 [DIRS 100833].

4.1.9 In-Drift Precipitates/Salts Model Including High Temperature Pitzer Thermodynamic Database

EQ3/6 Version 8.0 calculations presented in various parts of Section 6.7.2 of this report were made using *In-Drift Precipitates/Salts Model* (BSC 2004 [DIRS 169863]) (IDPS model). This model includes a high-temperature thermodynamic database based in part on the use of Pitzer’s

equations. This database is contained in the data file: *data0.ypf.R1* (DTN: SN0302T0510102.002 [DIRS 162572]). The data file nominally covers the temperature range 25°C to 200°C. However, the IDPS model is only validated to 140°C. The IDPS model report presents the relevant validation for the model. The IDPS model incorporates many data that are accurate to temperatures well above 140°C. In particular, this model builds on the earlier high temperature Pitzer models of Pabalan and Pitzer (1987 [DIRS 162096]), and Greenberg and Møller (1989 [DIRS 152684]). The former give numerous examples showing the successful application of their model to 200°C and higher. The latter present fewer actual examples but describe their model as being generally valid to 250°C. Many of the other data incorporated in the IDPS model are known to extend to temperatures of 200°C or greater. The current validation limit of 140°C is primarily associated with a small, but critical, subset of the overall Pitzer model dealing with aqueous nitrate (especially KNO_3 , see discussion in Section 6.7.2.15). The size of this data file precludes its reproduction in this report.

Uncertainties to apply to output from applications of the IDPS model are provided in DTN: MO0312SPAESMUN.002 [DIRS 166329]. This information is also summarized in Table 7-8 of *In-Drift Precipitates/Salts Model* (BSC 2004 [DIRS 169863]). These data are used in Section 6.7.2.16.

The IDPS model also includes a baseline set of twelve minerals whose precipitation should be suppressed (BSC 2004 [DIRS 169863], Section 6.6.2.6.4, Table 6.3; also DTN: MO0303SPAMNSUP.000 [DIRS 171426]). These are phases whose precipitation is known to be strongly inhibited by kinetic factors, at least at relatively low temperatures. The phases are: cristobalite(alpha) (SiO_2), dolomite [$\text{CaMg}(\text{CO}_3)_2$], glaserite [$\text{NaK}_3(\text{SO}_4)_2$], magnesite (MgCO_3), maximum microcline (KAlSi_3O_8), quartz (SiO_2), talc [$\text{Mg}_3\text{Si}_4\text{O}_{10}(\text{OH})_2$], Ca saponite [$\text{Ca}_{0.165}\text{Mg}_3\text{Al}_{0.33}\text{Si}_{3.67}\text{O}_{10}(\text{OH})_2$], Mg saponite [$\text{Mg}_{3.165}\text{Al}_{0.33}\text{Si}_{3.67}\text{O}_{10}(\text{OH})_2$], Na saponite [$\text{Na}_{0.33}\text{Mg}_3\text{Al}_{0.33}\text{Si}_{3.67}\text{O}_{10}(\text{OH})_2$], H saponite [$\text{H}_{0.33}\text{Mg}_3\text{Al}_{0.33}\text{Si}_{3.67}\text{O}_{10}(\text{OH})_2$], and K saponite [$\text{K}_{0.33}\text{Mg}_3\text{Al}_{0.33}\text{Si}_{3.67}\text{O}_{10}(\text{OH})_2$]. These phases were suppressed in the validation and demonstration runs in *In-Drift Precipitates/Salts Model* (BSC 2004 [DIRS 169863]) and the suppressions are considered a part of the qualified model. These phases are not explicitly suppressed in all EQ3/6 input files used to run the IDPS model as that is not necessary in most instances. Explicit suppression is only necessary if the phase would otherwise precipitate in the corresponding run. Thus, it is not necessary, for example, to explicitly suppress dolomite in a model system containing no magnesium. None of these phases appeared in the actual phase assemblages included in the calculational outputs of the present report. Therefore, consistency with this list is maintained throughout.

4.1.10 Standard Gibbs Energies of Formation and Standard Entropies at 298.15K for Selected Acid-Gas Species

Data for the standard Gibbs energies of formation and standard entropies of selected acid-gas species (HF, HBr, HCl, HNO_3 , and N_2O_5) at 298.15K are taken from *Thermochemical Data of Pure Substances* (Barin and Platzki 1995 [DIRS 157865]). These data are summarized in Table 4.1-11 and are used in conjunction with the heat capacity coefficient data (Section 4.1.11) to generate standard apparent Gibbs energies of formation for these gases as functions of temperature (Section 6.7.2.14).

Table 4.1-11. Standard Gibbs Energies of Formation and Standard Entropies at 298.15K for Selected Acid–Gas Species

Gas Species	Standard Gibbs Energy of Formation (kJ/mol)	Standard Entropy (joule/mol-K)	Source Page Number
HF	-274.645	173.779	790
HCl	-95.293	186.896	788
HBr	-53.449	198.695	785
HNO ₃	-73.964	266.475	795
N ₂ O ₅	118.014	346.545	1,098

Source: Barin and Platzki 1995 [DIRS 157865].

4.1.11 Thermodynamic Data Supporting Spreadsheet Files – *data0.ymp.R2* (Maier-Kelley Heat Capacity Coefficients of Selected Acid–Gas Species)

Data for the Maier-Kelley heat capacity (C_p) coefficients of selected acid–gas species (HF, HBr, HCl, HNO₃, and N₂O₅) are taken from the spreadsheet: *Gases_j_TJW_2.xls*, which is part of a larger collection of supporting spreadsheet files (DTN: MO0302SPATHDYN.001 [DIRS 161886]) utilized in the construction of the non-Pitzer EQ3/6 thermodynamic data file *data0.ymp.R2* (DTN: MO0302SPATHDYN.000 [DIRS 161756]). These heat capacity coefficients are given in Table 4.1-12. The coefficients are used in equations presented in Section 4.1.24. The purpose of the original spreadsheet is to calculate temperature grids for equilibrium constants for gas dissolution reactions, also using data for the 298.15K values of the standard Gibbs energy of formation and the standard entropy listed in Table 4.1-11 (and, in fact, those data are utilized on the spreadsheet). Standard apparent Gibbs energies of the gas species are calculated on the spreadsheet as an intermediate result. These results corresponded to the “classic” EQ3/6 temperature grid of 0°C, 25°C, 60°C, 100°C, 150°C, 200°C, 250°C, and 300°C, which is too coarse for the purposes of this report. Hence, that spreadsheet is modified to calculate a finer grid. That calculation and the results (which use as inputs the data in Table 4.1-11 and Table 4.1-12) are described in Section 6.7.2.14.

The heat capacity coefficients in Table 4.1-12 here are taken from the “Cp Data” worksheet of the spreadsheet: *Gases_j_TJW_2.xls*, which is part of DTN: MO0302SPATHDYN.001 [DIRS 161756]. These data are ultimately traceable to *Thermochemical Data of Pure Substances* (Barin and Platzki 1995 [DIRS 157865]) pages listed in Table 4.1-11 for the given species. The coefficients are calculated from gridded heat capacity values and incorporated into the spreadsheet: *Gases_j_TJW_2.xls*.

Table 4.1-12. Maier-Kelley Heat Capacity (C_p) Coefficients of Selected Acid–Gas Species (Joule Units)

Gas Species	A	b	c
HF	2.9080E+01	1.8285E-04	2.2256E+02
HCl	2.7730E+01	2.7648E-03	5.2166E+04
HBr	2.6345E+01	5.4114E-03	1.0595E+05
HNO ₃	4.2278E+01	6.1932E-02	-6.5243E+05
N ₂ O ₅	9.8612E+01	5.8437E-02	-1.7578E+06

Source: *Gases_j_TJW_2.xls*; DTN: MO0302SPATHDYN.001 [DIRS 161886].

4.1.12 Components of Atmospheric Air Exclusive of Water

The components of atmospheric air exclusive of water vapor are given in Table 4.1-13. Only the O₂ and CO₂ data are used quantitatively in this report.

4.1.13 Major Components of the Gas Phase in the Emplacement Drifts

The composition of the gas phase has a controlling influence on the water chemistry of any coexisting aqueous solutions. It is, therefore, important to know the partial pressures or fugacities of the chemically active gas species that may be present. The three major gas species are water vapor, O₂, and CO₂. Water vapor is most often treated via the RH instead of partial pressure or fugacity ($RH\% = 100p_w / p_w^o$, where p_w = partial pressure of water vapor and p_w^o = partial pressure of water vapor in equilibrium with pure liquid water). The RH is treated in all TH and THC modeling on the YMP. In TH modeling, O₂ is typically implicit in the “air fraction” of the gas phase, whereas in THC modeling, it may be more directly treated via the partial pressure or fugacity of this gas species.

Table 4.1-13. Components of Atmospheric Air Exclusive of Water Vapor

Constituent	Content (%) by Volume	Content (ppm) by Volume
N ₂	78.084 ± 0.004	—
O ₂	20.946 ± 0.002	—
CO ₂	0.033 ± 0.001	—
Ar	0.934 ± 0.001	—
Ne	—	18.18 ± 0.04
He	—	5.24 ± 0.004
Kr	—	1.14 ± 0.01
Xe	—	0.087 ± 0.001
H ₂	—	0.5
CH ₄	—	2
N ₂ O	—	0.5 ± 0.1

Source: Weast and Astle 1981 [DIRS 100833], p. F-172.

CO₂ in the drifts is expected to be present at much lower concentrations than water vapor or O₂, but is important nonetheless for its chemical reactivity. It is commonly included in the THC modeling. Other gas-phase components, such as HCl and HNO₃, likely present at still smaller concentrations, may also affect the water chemistry. However, these have not yet been included in YMP THC modeling.

For the purposes of this report, the maximum water-vapor pressure is assumed (Section 5.3) to be limited to that which corresponds to the ambient boiling point of pure water. No minimum value of the water-vapor pressure is explicitly assumed. The composition of the air in the mountain (excluding water vapor) is assumed (Section 5.4) to be that of normal atmospheric air based on O₂, N₂, and Ar abundances as reported by Yang et al. (1996 [DIRS 100194]) and Thorstenson et al. (1990 [DIRS 100831]). This report does not require specific data for O₂, N₂, or Ar, nor does it use such data to develop output; therefore, the data from these sources are not used as direct input. Rather, this analysis applies mildly oxidizing conditions. The EQ3/6

version 8.0 calculations reported in Section 6.7.2 employ a specific value of oxygen fugacity (normal atmospheric, log fugacity of -0.70) on the associated input files. However, the output from this report has no meaningful dependence on this value.

Of somewhat greater concern is CO_2 abundance. The data in Table 4.1-14 show a broad range of CO_2 abundance as a function of borehole depth. A partial pressure of $10^{-3.0}$ bar is equivalent to 1,000 ppm (by volume). For purposes of this analysis a value of $10^{-3.0}$ bar was used for the partial pressure of CO_2 .

Table 4.1-14. Some Measurements of Ambient CO_2 Abundance in the Yucca Mountain Gas Phase (Borehole USW UZ-14)

CO₂ (ppm)	Depth (ft)
375	1,445
399	1,445
390	1,445
375	1,445
414	1,445
879	1,445
683	1,490
697	1,490
600	1,490
546	1,490
568	1,490
661	1,490
826	1,540
494	1,540
1,644	1,540
1,394	1,540
1,300	1,540
450	1,540
396	1,590
477	1,590
380	1,590
373	1,590
394	1,590
385	1,590
1,074	1,640
482	1,640
408	1,640
536	1,640
717	1,640
381	1,640
2,325	1,690
433	1,690
972	1,690
1,417	1,690

Table 4.1-14. Some Measurements of Ambient CO₂ Abundance in the Yucca Mountain Gas Phase (Borehole USW UZ-14) (Continued)

CO ₂ (ppm)	Depth (ft)
1,205	1,690
1,112	1,690
1,180	1,738
384	1,738
1,175	1,738
1,200	1,738
1,313	1,738
1,540	1,738

Source: DTN: GS970908312271.003
[DIRS 111467].

Actual CO₂ abundance during the repository history is predicted to change considerably in response to thermohydrologic processes. The ambient CO₂ pressure is, therefore, of limited use. For the purposes of this report, only a general understanding of the range of anticipated CO₂ pressures is required. Some results from DTN: LB0108DSTTHC01.001 [DIRS 156285] are noted here to support this. These results are summarized in Tables 4.1-15 through 4.1-18, where “v. frac.” refers to volume fraction. Similar additional CO₂ data for a “cooler” repository are noted in Section 4.1.19, which mainly addresses data for trace acid-gas species. These results establish a range of pCO₂ conditions that may exist in the repository. All of the gas composition results presented in Tables 4.1-15 through 4.1-19 exhibit the strongest fluctuations from dilution of the air fraction of the gas phase by water vapor.

Note that Tables 4.1-15 through 4.1-18 also include values for the ambient concentration of CO₂. The low value is 4.39×10^{-4} (v. frac.), and the high is 7.67×10^{-4} .

Table 4.1-15. Thermal-Hydrologic-Chemical Calculation Results for High Temperature and Low Carbon Dioxide Partial Pressure in the Tptpl Lithology for Seepage at the Crown of the Drift

Parameter	Preclosure	Boiling	Cool Down	Extended Cool Down	Transition to Ambient	Ambient
	(0 to 50 yr)	(51 to 1,500 yr)	(1,501 to 4,000 yr)	(4,001 to 25,000 yr)	(25,001 to 100,000 yr)	(100,001 to 1,000,000 yr)
Actual THC Model Run Time (yr)	49.97	300.00	1,800.01	10,000.00	50,001.50	Averaged
Temperature (°C)	79.30	122.87	95.80	54.02	27.37	23.60
pCO ₂ (v.frac)	9.20E-04	8.91E-06	1.66E-05	1.62E-03	5.71E-04	4.39E-04

Source: DTN: LB0108DSTTHC01.001 [DIRS 156285].

yr = year.

Table 4.1-16. Thermal-Hydrologic-Chemical Calculation Results for High Temperature and High Carbon Dioxide Partial Pressure in the Tptpl Lithology for Seepage at the Crown of the Drift

Parameter	Preclosure	Boiling	Cool Down	Extended Cool Down	Transition to Ambient	Ambient
	(0 to 50 yr)	(51 to 1,500 yr)	(1,501 to 4,000 yr)	(4,001 to 25,000 yr)	(25,001 to 100,000 yr)	(100,001 to 1,000,000 yr)
Actual THC Model Run Time (yr)	49.97	300.00	1,800.01	10,000.00	50,001.50	Averaged
Temperature (°C)	79.30	122.86	95.80	54.02	27.37	23.20
pCO ₂ (v.frac)	9.20E-04	8.92E-06	2.26E-05	3.45E-03	1.06E-03	7.67E-04

Source: DTN: LB0108DSTTHC01.001 [DIRS 156285].

yr = year.

Table 4.1-17. Thermal-Hydrologic-Chemical Calculation Results for Low Temperature and Low Carbon Dioxide Partial Pressure in the Tptpl Lithology for Seepage at the Crown of the Drift

Parameter	Preclosure	Postclosure Hot	Cool Down	Transition to Ambient	Ambient
	(0 to 300 yr)	(301 to 10,000 yr)	(10,001 to 30,000 yr)	(30,001 to 100,000 yr)	(100,001 to 1,000,000 yr)
Actual THC Model Run Time (yr)	53.00	700.00	20,000.00	51,411.30	Averaged
Temperature (°C)	52.92	73.40	35.59	25.89	23.60
pCO ₂ (v.frac)	1.19E-03	1.48E-03	8.75E-04	5.11E-04	4.39E-04

Source: DTN: LB0108DSTTHC01.001 [DIRS 156285].

yr = year.

Table 4.1-18. Thermal-Hydrologic-Chemical Calculation Results for Low Temperature and High Carbon Dioxide Partial Pressure in the Tptpl Lithology for Seepage at the Crown of the Drift

Parameter	Preclosure	Postclosure Hot	Cool Down	Transition to Ambient	Ambient
	(0 to 300 yr)	(301 to 10,000 yr)	(10,001 to 30,000 yr)	(30,001 to 100,000 yr)	(100,001 to 1,000,000 yr)
Actual THC Model Run Time (yr)	53.00	700.00	20,000.00	51,411.30	Averaged
Temperature (°C)	52.92	73.40	35.59	25.89	23.20
pCO ₂ (v.frac)	1.19E-03	1.48E-03	1.71E-03	9.38E-04	7.67E-04

Source: DTN: LB0108DSTTHC01.001 [DIRS 156285].

yr = year.

4.1.14 Geochemical Composition of Dust Samples

Dust samples were collected from the Exploratory Studies Facility in two separate phases. The samples were analyzed by leaching with water, and chemical analysis of the leachate. The results are reported by chemical element and some common chemical compounds. Only leachable components are used in this report, to represent soluble salts present in the dust. The

leachate data for Phase I samples (DTN: MO0207EBSDUSTS.020 [DIRS 162556]) are given in Table 4.1-19; those for Phase II samples (DTN: MO0209EBSDUST2.030 [DIRS 162557]) are given in Table 4.1-20. Of particular interest here are the data for soluble nitrate and chloride. The leachate data are thought to reflect the actual salt mineral content of the dust. Mineralogical data on the dust, or its salt components, are not available. Section 6.7.2.10 describes EQ3/6 calculations that estimate the original salt component mineralogy by simulating evaporation to dryness (or near dryness) of the leachate solutions.

Table 4.1-19. Dust Leachate Compositions, Phase I

Lab No.	Field Number	Meters	Ca	Mg	Na	K	Si	Cl	F	NO ₃	SO ₄	Br	P	As	Pb
			ppm	ppm	Ppm	ppm	ppm	ppm	ppm	ppm	ppm	ppm	ppm	ppb	ppb
C-186098	SPC00573629	202	268	26.7	346	126	34.5	184	10	240	360	38	9.6	92	1.20
C-186091	SPC00573622	558	980	83.6	358	183	43.5	182	6	800	1,120	10	1.8	43	0.88
C-186099	SPC00573630	669	392	42.0	344	149	27.9	196	8	280	480	28	4.6	74	2.50
C-186092	SPC00573623	901	638	79.7	431	193	46.6	180	6	580	980	22	3.5	69	1.30
C-186093	SPC00573624	901	332	35.7	386	128	14.9	240	10	280	340	54	0.8	116	3.10
C-186100	SPC00573631	1,100	630	31.4	389	150	82.5	220	40	260	640	64	4.6	158	1.80
C-186094	SPC00573625	1,272	974	79.1	617	260	58.7	300	8	680	1,340	26	3.2	100	1.10
C-186101	SPC00573632	1,510	229	18.9	262	101	42.3	220	8	114	300	28	5	74	3.00
C-186102	SPC00573633	1,720	543	9.76	158	80	97.5	114	18	62	320	22	2.2	63	1.40
C-186095	SPC00573626	1,808	575	34.3	415	206	94.9	200	14	400	660	26	5.7	99	1.50
C-186096	SPC00573627	2,273	394	53.4	511	237	65.0	260	32	420	1,020	34	196.0	152	0.91
C-186097	SPC00573628	2,708	480	34.8	287	142	61.2	160	8	380	620	18	40.2	86	1.10
C-186090	SPC00573620	3,109	226	10.6	157	101	79.1	56	4	82	162	6	3.6	34	0.80
C-186089	SPC00573619	3,514	635	43.6	397	214	100.0	200	24	420	720	22	10.9	108	1.40
C-186088	SPC00573618	3,900	439	13.7	345	479	120.0	114	12	300	400	16	5.5	67	0.81
C-186087	SPC00573617	4,300	919	32.8	332	221	96.4	140	18	440	1,180	20	6.1	81	0.94
C-186086	SPC00573616	4,721	893	35.7	374	248	107.0	130	12	400	1,480	26	5.6	97	0.80
C-186085	SPC00573615	5,040	863	25.9	369	220	134.0	162	12	380	740	22	6.5	97	0.54
C-186084	SPC00573614	5,300	939	27.1	343	219	121.0	130	12	380	1,160	24	5.6	103	0.85
C-186082	SPC00573612	6,297	630	28.3	388	231	95.1	154	10	340	1,060	50	5.5	132	0.75
C-186081	SPC00573611	6,700	941	6.32	378	242	213.0	200	30	340	840	56	3.1	186	0.30
C-186080	SPC00573610	6,895	430	19.4	304	221	89.2	162	24	220	640	34	4.4	102	0.40
C-186077	SPC00573607	7,798	2,490	12.8	455	350	173.0	260	8	1,820	2,200	14	4.2	81	1.10
Mean	—	—	607	34.2	363	204	81.7	181	14.5	418	816	28.7	6.5	96.2	1.24
Median	—	—	630	31.4	369	214	89.2	182	12.0	380	720	26.0	5.0	96.5	1.10
Std. Dev.	—	—	258	21.9	98	87	49.2	56	9.4	351	472	14.9	7.9	35.6	0.74
Min	—	—	226	6	157	80	14.9	56	4.0	62	162	6.0	0.8	33.5	0.30
Max	—	—	2,490	84	617	479	213.0	300	40.0	1,820	2,200	64.0	196.0	186.0	3.10
% Soluble	—	—	5.3	1.8	1.5	0.6	—	15.1	2.1	—	43.4	56.7	3.7	1.2	0.004
Micromoles/g	—	—	15.14	1.41	15.78	5.23	—	5.11	0.76	6.74	8.49	0.36	—	—	—

Source: DTN: MO0207EBSDUSTS.020 [DIRS 162556].

- NOTES: (1) SPC in the field number denotes specimen.
(2) "Meters" denotes distance inside the tunnel from the North Portal.

Table 4.1-20. Dust Leachate Compositions, Phase II

Lab No.	Sample No.	Ca	Mg	K	Na	Si	Cl	Br	F	NO ₃	SO ₄	PO ₄	Pb	As
		ppm	ppm	ppm	Ppm	ppm	ppm	ppm	ppm	ppm	ppm	ppm	ppb	ppb
C-203112	00574979A	147	16.3	159	55.4	161	<24	<1.6	8	<7	<32	7.67	3.7	41.6
C-203113	00574979B	91.7	9.47	127	46.4	96.5	<24	<1.6	4	10	<32	14.1	3.4	26.4
C-203114	00574979C	119	12.6	174	66.0	144	<24	<1.6	8	24	<32	19.0	3.9	43.2
C-203115	00574980A	270	34.3	193	115	169	76	<1.6	18	220	220	11.7	1.7	28.1
C-203116	00574980B	466	49.3	181	124	76.6	98	4	4	400	360	6.75	4.1	24.2
C-203117	00574980C	1,080	80.1	206	195	176	154	8	12	640	840	7.05	1.2	56.2
C-203118	00574981A	772	44.1	280	188	33.4	74	4	8	116	3,800	3160	2.0	94.6
C-203119	00574981B	1,060	39.5	389	471	287	280	44	22	360	1,000	15.0	2.7	126
C-203120	00574981C	2,340	130	389	392	42.8	320	6	8	1,760	4,600	4,380	1.6	166
C-203121	00574982A	246	39.6	196	262	164	86	4	20	240	320	17.2	4.0	36.0
C-203122	00574982B	458	64.1	244	339	51.6	118	6	4	520	520	14.4	3.6	30.6
C-203123	00574982C	1,010	99.6	345	556	99.2	170	12	6	1,000	1,060	14.1	2.7	42.4
C-203124	00574983A	262	23.7	281	296	94.9	114	8	12	198	380	17.8	3.6	46.6
C-203125	00574983B	770	50.8	303	425	57.3	260	10	4	540	720	11.0	5.3	39.6
C-203126	00574983C	1,240	85.9	369	666	62.7	360	10	10	980	1,200	10.7	3.0	45.3
C-203127	00574984A	335	49.4	339	265	87.3	128	10	10	220	440	166	4.8	57.4
C-203128	00574984B	—	—	—	—	—	—	—	—	—	—	—	—	—
C-203129	00574984C	—	—	—	—	—	220	18	10	500	1,040	—	—	—
C-203130	00574985A	994	65.4	303	349	248	170	20	18	340	880	15.9	1.6	97.8
C-203131	00574985B	1,260	52.4	333	461	181	168	14	22	480	1,180	24.8	1.5	83.1
C-203132	00574985C	1,030	54.7	275	480	130	166	16	22	500	1,220	22.1	1.8	90.3
C-203133	00574986A	248	23.4	234	222	75.4	96	6	6	146	320	5.21	3.5	39.0
C-203134	00574986B	806	38.0	220	292	131	170	10	12	300	740	9.51	1.8	52.6
C-203135	00574986C	1,190	51.4	260	408	159	220	14	18	440	1,140	12.9	1.9	70.4
C-203136	00574987A	1,290	84.6	257	201	21.8	188	2	8	600	5,800	12,700	2.5	266
C-203137	00574987B	1,180	64.1	313	564	135	360	42	22	540	1,400	19.3	2.9	117
C-203138	00574987C	1,280	70.5	288	570	143	320	32	24	520	1,480	19.0	1.6	110
C-203139	00574990A	274	19.8	186	149	44.7	88	10	8	170	500	3.99	1.4	31.1

Table 4.1-20. Dust Leachate Compositions, Phase II (Continued)

Lab No.	Sample No.	Ca	Mg	K	Na	Si	Cl	Br	F	NO ₃	SO ₄	PO ₄	Pb	As
		ppm	ppm	ppm	Ppm	ppm	ppm	ppm	ppm	ppm	ppm	ppm	ppb	ppb
C-203140	00574990B	434	25.9	151	186	38.9	102	16	6	220	760	7.05	2.0	39.1
C-203141	00574990C	689	34.7	251	370	82.2	136	22	14	300	940	12.9	1.9	69.8
C-203142	00574991A	281	55.4	139	128	161	88	12	22	122	440	4.91	1.6	39.6
C-203143	00574991B	319	56.8	114	121	79.4	76	10	4	156	520	7.05	4.7	29.7
C-203144	00574991C	622	53.6	177	196	215	82	12	10	164	700	7.97	1.2	51.0
C-203145	00574992A	122	10.3	155	171	57.4	98	6	8	70	116	5.52	3.2	44.2
C-203146	00574992B	110	9.48	121	126	12.3	82	<1.6	2	68	124	6.44	2.1	13.1
C-203147	00574992C	305	19.8	173	187	60.2	166	2	6	150	280	10.1	2.3	33.1

Source: DTN: MO0209EBSDUST2.030 [DIRS 162557], Table 4.

NOTE: The terminal letters of the sample numbers designate sample particle size range: A = 60 to 200 mesh (74 to 200 microns), B = 200 to 325 mesh (44 to 74 microns), and C = <325 mesh (<44 microns).

4.1.15 Mean Atmospheric Pressure as a Function of Elevation (Equation)

The mean atmospheric pressure as a function of elevation is described by Fleagle and Businger (1980 [DIRS 108591]):

$$P = P(0) \exp(-gz/R_m T), \quad (\text{Eq. 4.1.15-1})$$

where $P(0)$ is the atmospheric pressure at sea level, g is acceleration due to gravity, z is elevation, T is the absolute temperature, and R_m is the gas constant, R , divided by the effective molecular weight of air. Here “mean” atmospheric pressure refers to time-averaged pressure (exclusive of weather related variations). This equation is used in Section 6.7.2.1 to calculate the atmospheric pressure at the repository elevation, using data from Sections 4.1.1 and 4.1.2. Those results are then compared with some actual pressure measurements (DTN: GS030108312242.001 [DIRS 163118]) referenced in Section 4.1.21.

The equation is appropriate to use, as it represents the property of interest (mean atmospheric pressure) as a function of elevation. The equation is used in this report because the elevation range covered in the handbooks is much greater than required for the purposes of this report (extending to very high altitude) and the handbook tables are consequently too coarse to be directly used here.

Equation 4.1.15-1 is given in somewhat different forms in many textbooks and monographs, and is fairly easily derived from first principles as applied to an isothermal column of air of homogenous composition. The source (Fleagle and Businger 1980 [DIRS 108591]) is a textbook on atmospheric physics published in at least three editions, starting in 1963. The authors are currently emeriti faculty in the Department of Atmospheric Sciences, University of Washington. The purpose of using this equation in this report is only to establish an expected maximum pressure (time average for some reasonable period, excluding any spikes due to weather phenomena) in the Yucca Mountain repository. The data calculated from this equation are compared in Section 6.7.2.1 against a set of pressure measurements at one location in the existing Yucca Mountain tunnels (Section 4.1.21).

4.1.16 Composition of J-13 Well Water

Two types of waters are characteristic of those in volcanic units at the Yucca Mountain region. One type is saturated zone water and perched water in the UZ, and the other type is porewater in the UZ. The first type of water is dominated by rock/mineral interaction and is sodium-bicarbonate base water. J-13 well water is typical of this type of water (Harrar et al. 1990 [DIRS 100814]). Its composition from a qualified source (DTN: MO0006J13WTRCM.000 [DIRS 151029]) is listed in Table 4.1-21 (see Section 4.1.17 for discussion of the porewater).

Table 4.1-21. Composition of J-13 Well Water

Species	Concentration (mg/L)
Ca ²⁺	13.0 ± 0.99
Cl ⁻	7.14 ± 0.61
F ⁻	2.18 ± 0.29
HCO ₃ ^{- (a)}	128.9 ± 8.6
K ⁺	5.04 ± 0.61
Mg ²⁺	2.01 ± 0.21
NO ₃ ⁻	8.78 ± 1.03
Na ⁺	45.8 ± 2.29
SO ₄ ²⁻	18.4 ± 1.03
Si _(aq) ^(b)	28.5 ± 1.85
pH	7.41 ± 0.44

Source: DTN: MO0006J13WTRCM.000 [DIRS 151029].

^aAlkalinity is expressed as mg/L HCO₃⁻.

^bThe conversion from Si to SiO₂ is 1 mg/L Si = 2.14 mg/L SiO₂.

NOTE: These values represent the mean concentration values of water collected from this well over the course of about 20 years of sampling. These values represent the mean value of 15 to 20 analyses, each of which is the mean of replicate sampling in many cases.

4.1.17 Composition of Porewaters from the TSw Unit

Table 4.1-22 lists the concentrations of the major ions in two porewaters that were collected from the TSw unit at Yucca Mountain. The data for the porewaters do not list the concentrations for the bicarbonate component. The source (DTN: MO0005PORWATER.000 [DIRS 150930]) also gives data for trace elements including B, Al, and Fe that are not used in this report. See Section 4.1.16 for a discussion of the perched and saturated zone waters.

Table 4.1-22. Major Ion Concentrations Reported for TSw Porewater at Ambient Temperature

Ions	ESF-HD PERM-2 Concentration (mg/L)	ESF-HD PERM-3 Concentration (mg/L)
Na ⁺	61	62
K ⁺	7	9
Mg ²⁺	16.6	17.4
Ca ²⁺	106	97
SiO _{2(aq)}	66	75
HCO ₃ ⁻	Not reported	Not reported
SO ₄ ²⁻	111	120
Cl ⁻	110	123
F ⁻	0.96	0.76
NO ₃ ⁻	3	10
pH	8.32	8.31

Source: DTN: MO0005PORWATER.000 [DIRS 150930].

ESF = Exploratory Studies Facility.

4.1.18 Calcium Chloride Acid–Gas Volatility Experimental Data

These data (DTNs: LL030308812251.017 [DIRS 163775] and LL030309012252.018 [DIRS 163774]) present the results of an experiment to characterize the interaction between an aqueous calcium chloride thin film and Alloy 22 at elevated temperature and low RH. A concentrated aqueous solution of calcium chloride was sprayed on a coupon of Alloy 22 and dried, producing a thin coating of salt. The coupon was then placed in a thermogravimetric analyzer test apparatus, which allowed measurement of minute changes in the weight of the coupon during the progress of the experiment. The first experiment (at 150°C and 22.5 percent RH) showed an expected weight gain due to the deliquescence of the deposited salt. This was then followed by a slower weight loss. The weight loss appears to be the result of volatilization of HCl, which was apparently stripped from the system by the gas stream. Additional experiments of this type were run at 100°C and 125°C, with the 125°C experiment giving results qualitatively similar to those obtained at 150°C. The phenomenon of slow weight loss after an initial gain was not observed at 100°C. Other tests were performed at 150°C with glass and platinum substrates. These experiments gave similar results to those obtained with Alloy 22 at the same temperature. These experimental data are discussed in more detail in Section 6.7.2.14.2. The data taken from the source DTN are graphical (plots and pictures). They are not reproduced here in Section 4, rather only in Section 6 where they are used and discussed.

4.1.19 Seepage Water Chemistry (Fugacities of Acid–Gas Species in the Drift Wall)

Table 4.1-23 contains data for the fugacities of five acid–gas species (CO₂, HF, HCl, HNO₃, and N₂O₅) in the drift wall at various times in the repository history. These data are taken from the in-drift chemical environment calculations (DTN: MO0303MWDSCMAB.000 [DIRS 162551]), documented in *Engineered Barrier System: Physical and Chemical Environment* (BSC 2004 [DIRS 169860]). The data represent a sampling of calculated water compositions near the top (TF4) and bottom (BF4) of the drift. The data represent five different THC simulations (BSC 2004 [DIRS 170531] and BSC 2004 [DIRS 169858]), each starting with a different parent (ambient) porewater composition (designated W0, W4, W5, W6, and W7).

It is important to note that the THC simulations account for the transport of CO₂ through the gas phase. However, transport of the other four acid–gas species in the gas phase is not included in the THC model. The reported fugacities for these gas species are equilibrium values corresponding to the computed water chemistries. Nevertheless, these data are reasonable estimates for the magnitudes of the fugacities of these gases. Consequently, they provide a means of estimating the chemical potentials of these gases at these locations, and thus a point of comparison with the chemical potentials of these same gases on the metal barrier surfaces. This difference in chemical potential defines the thermodynamic driving force for the transport of acid–gases from the metal barrier surfaces to the drift wall. The data contained in Table 4.1-23 are used in Section 6.7.2.14 to illustrate the likely magnitude of such driving forces and the corresponding limits they may imply for aqueous solution compositions.

Table 4.1-23. Log Fugacities of Five Acid-Gas Species in the Drift Wall as Functions of Time in Repository History

W0 THC Abstraction													
TF4							BF4						
Time (yrs)	Temp (°C)	CO ₂	HF	HCl	HNO ₃	N ₂ O ₅	Time (yrs)	Temp (°C)	CO ₂	HF	HCl	HNO ₃	N ₂ O ₅
10	52.50	-2.978	-11.703	-15.703	-17.407	-39.928	10	51.30	-2.897	-11.724	-15.713	-17.412	-39.935
51	91.80	-3.215	-10.336	-14.222	-15.991	-37.148	51	86.10	-2.776	-10.334	-14.266	-16.026	-37.212
100	96.10	-3.485	-10.249	-14.609	-16.388	-37.944	100	111.00	-3.607	-9.973	-12.438	-14.233	-33.641
150	95.90	-3.453	-10.120	-14.309	-16.085	-37.339	150	110.00	-3.322	-9.864	-12.937	-13.934	-33.042
250	95.50	-3.400	-10.030	-13.790	-15.534	-36.237	250	109.00	-3.361	-9.913	-13.171	-14.432	-34.037
350	95.70	-3.461	-9.978	-13.352	-15.115	-35.398	350	108.00	-3.611	-10.067	-13.324	-14.774	-34.721
500	95.90	-3.164	-9.850	-12.793	-14.546	-34.259	500	106.00	-3.431	-10.035	-13.456	-14.976	-35.125
750	95.70	-2.707	-9.900	-13.864	-15.637	-36.443	750	103.00	-2.805	-9.814	-13.523	-15.094	-35.360
1,000	94.60	-2.405	-9.812	-13.918	-15.694	-36.554	1,000	100.00	-2.457	-9.658	-13.456	-15.087	-35.345
2,401	88.30	-2.126	-9.899	-14.024	-15.787	-36.738	2,401	88.30	-1.995	-9.765	-13.744	-15.507	-36.176
5,003	73.20	-2.218	-10.407	-14.613	-16.354	-37.857	5,003	73.30	-2.083	-10.281	-14.467	-16.205	-37.558
10,006	56.20	-2.202	-11.165	-15.334	-17.047	-39.216	10,006	56.30	-2.179	-11.142	-15.305	-17.015	-39.153
20,013	40.20	-2.393	-11.962	-16.129	-17.815	-40.716	20,013	40.30	-2.418	-11.986	-16.151	-17.837	-40.760
50,034	27.00	-2.712	-12.703	-16.880	-18.548	-42.142	50,034	27.00	-2.922	-12.900	-17.079	-18.748	-42.542
W4 THC Abstraction													
TF4							BF4						
Time (yrs)	Temp (°C)	CO ₂	HF	HCl	HNO ₃	N ₂ O ₅	Time (yrs)	Temp (°C)	CO ₂	HF	HCl	HNO ₃	N ₂ O ₅
10	52.50	-2.401	-11.496	-16.382	-17.620	-40.354	10	51.30	-2.351	-11.500	-16.381	-17.618	-40.348
51	91.90	-2.534	-10.287	-15.200	-16.505	-38.175	51	86.20	-2.061	-9.999	-14.962	-16.257	-37.674
100	96.10	-2.718	-9.977	-15.172	-16.484	-38.136	100	111.00	-2.825	-9.602	-12.926	-14.262	-33.699
150	96.00	-2.516	-9.833	-14.898	-16.209	-37.586	150	110.00	-2.493	-9.468	-13.469	-13.935	-33.043
250	95.50	-2.405	-9.703	-14.566	-15.855	-36.878	250	109.00	-2.393	-9.445	-13.453	-14.440	-34.053
350	95.70	-2.580	-9.651	-14.141	-15.434	-36.035	350	108.00	-2.583	-9.567	-13.589	-14.747	-34.668
500	95.90	-3.051	-9.715	-13.725	-15.024	-35.217	500	106.00	-3.102	-9.887	-14.033	-15.206	-35.585

Table 4.1-23. Log Fugacities of Five Acid-Gas Species in the Drift Wall as Functions of Time in Repository History (Continued)

W4 THC Abstraction													
TF4							BF4						
Time (yrs)	Temp (°C)	CO ₂	HF	HCl	HNO ₃	N ₂ O ₅	Time (yrs)	Temp (°C)	CO ₂	HF	HCl	HNO ₃	N ₂ O ₅
750	95.70	-2.861	-9.982	-14.696	-16.006	-37.179	750	103.00	-3.056	-9.953	-14.354	-15.546	-36.263
1,000	94.60	-2.481	-9.890	-14.753	-16.062	-37.291	1,000	100.00	-2.542	-9.765	-14.304	-15.524	-36.219
2,401	88.30	-2.107	-9.888	-14.786	-16.084	-37.330	2,401	88.30	-1.985	-9.762	-14.486	-15.780	-36.723
5,003	73.20	-2.117	-10.344	-15.339	-16.610	-38.369	5,003	73.30	-1.992	-10.239	-15.188	-16.460	-38.069
10,006	56.20	-2.002	-11.105	-16.003	-17.247	-39.616	10,006	56.30	-1.983	-11.092	-15.971	-17.215	-39.552
20,013	40.20	-2.080	-11.876	-16.735	-17.954	-40.993	20,013	40.30	-2.085	-11.891	-16.736	-17.956	-40.997
50,034	27.00	-2.391	-12.679	-17.519	-18.720	-42.485	50,034	27.00	-2.521	-12.802	-17.645	-18.846	-42.738
W5 THC Abstraction													
TF4							BF4						
Time (yrs)	Temp (°C)	CO ₂	HF	HCl	HNO ₃	N ₂ O ₅	Time (yrs)	Temp (°C)	CO ₂	HF	HCl	HNO ₃	N ₂ O ₅
10	52.50	-2.565	-11.526	-16.460	-17.814	-40.743	10	51.30	-2.522	-11.546	-16.470	-17.822	-40.756
51	91.80	-2.811	-10.367	-15.299	-16.719	-38.603	51	86.10	-2.288	-10.098	-15.073	-16.483	-38.126
100	96.10	-3.024	-10.068	-15.321	-16.748	-38.664	100	111.00	-3.133	-9.750	-13.166	-14.619	-34.411
150	96.00	-2.833	-9.949	-15.090	-16.517	-38.202	150	110.00	-2.818	-9.626	-13.803	-14.352	-33.878
250	95.50	-2.761	-9.819	-14.787	-16.184	-37.537	250	109.00	-2.772	-9.625	-13.928	-14.833	-34.839
350	95.70	-3.021	-9.811	-14.364	-15.770	-36.707	350	108.00	-3.046	-9.789	-13.951	-15.158	-35.490
500	95.90	-3.264	-9.813	-14.010	-15.421	-36.010	500	106.00	-3.526	-10.092	-14.365	-15.609	-36.390
750	95.70	-2.760	-9.965	-14.845	-16.268	-37.704	750	103.00	-2.915	-9.874	-14.487	-15.757	-36.685
1000	94.60	-2.428	-9.864	-14.858	-16.281	-37.729	1,000	100.00	-2.495	-9.678	-14.425	-15.736	-36.643
2,401	88.30	-2.112	-9.891	-14.877	-16.290	-37.744	2,401	88.30	-2.006	-9.772	-14.426	-15.828	-36.818
5,003	73.20	-2.171	-10.373	-15.471	-16.859	-38.867	5,003	73.30	-2.016	-10.248	-15.286	-16.674	-38.495
10,006	56.20	-2.125	-11.115	-16.155	-17.515	-40.151	10,006	56.30	-2.098	-11.097	-16.112	-17.471	-40.065
20,013	40.20	-2.249	-11.881	-16.898	-18.234	-41.553	20,013	40.30	-2.251	-11.896	-16.897	-18.232	-41.550
50,034	27.00	-2.596	-12.690	-17.698	-19.016	-43.076	50,034	27.00	-2.725	-12.813	-17.824	-19.142	-43.329

Table 4.1-23. Log Fugacities of Five Acid-Gas Species in the Drift Wall as Functions of Time in Repository History (Continued)

W6 THC Abstraction													
TF4							BF4						
Time (yrs)	Temp (°C)	CO ₂	HF	HCl	HNO ₃	N ₂ O ₅	Time (yrs)	Temp (°C)	CO ₂	HF	HCl	HNO ₃	N ₂ O ₅
10	52.50	-2.424	-11.384	-16.257	-16.835	-38.785	10	51.30	-2.389	-11.404	-16.277	-16.853	-38.818
51	91.80	-2.591	-10.293	-15.080	-15.725	-36.615	51	86.00	-1.942	-9.898	-14.745	-15.379	-35.919
100	96.10	-2.850	-9.982	-15.210	-15.862	-36.892	100	111.00	-2.962	-9.650	-13.051	-13.727	-32.628
150	95.80	-2.707	-9.864	-14.948	-15.599	-36.367	150	110.00	-2.733	-9.564	-13.750	-14.064	-33.302
250	95.30	-2.783	-9.929	-14.871	-15.516	-36.200	250	109.00	-2.768	-9.608	-14.279	-14.696	-34.565
350	95.60	-3.063	-9.933	-14.465	-15.111	-35.389	350	108.00	-3.098	-9.798	-14.425	-14.200	-33.574
500	95.90	-3.390	-9.993	-14.193	-14.840	-34.849	500	106.00	-3.650	-10.136	-14.606	-14.987	-35.148
750	95.60	-2.724	-9.936	-14.788	-15.436	-36.040	750	103.00	-2.948	-9.869	-14.467	-14.979	-35.129
1,000	94.50	-2.453	-9.872	-14.837	-15.484	-36.136	1,000	100.00	-2.525	-9.690	-14.430	-14.985	-35.140
2,401	88.30	-2.131	-9.903	-14.844	-15.482	-36.127	2,401	88.30	-2.041	-9.790	-14.211	-14.846	-34.856
5,003	73.20	-2.235	-10.411	-15.481	-16.093	-37.334	5,003	73.30	-2.051	-10.266	-15.272	-15.883	-36.914
10,006	56.20	-2.222	-11.075	-16.136	-16.720	-38.561	10,006	56.30	-2.191	-11.058	-16.090	-16.674	-38.470
20,013	40.20	-2.413	-11.867	-16.916	-17.477	-40.039	20,013	40.30	-2.414	-11.892	-16.842	-17.395	-39.876
50,034	27.00	-2.672	-12.615	-17.656	-18.197	-41.440	50,034	27.00	-2.790	-12.729	-17.771	-18.313	-41.671
W7 THC Abstraction													
TF4							BF4						
Time (yrs)	Temp (°C)	CO ₂	HF	HCl	HNO ₃	N ₂ O ₅	Time (yrs)	Temp (°C)	CO ₂	HF	HCl	HNO ₃	N ₂ O ₅
10	52.50	-2.428	-11.438	-15.885	-17.279	-39.673	10	51.30	-2.415	-11.487	-15.924	-17.314	-39.740
51	92.00	-2.670	-10.187	-14.649	-16.107	-37.380	51	86.20	-2.309	-10.104	-14.616	-16.064	-37.290
100	96.10	-2.921	-10.009	-14.830	-16.298	-37.764	100	111.00	-3.030	-9.692	-12.586	-14.075	-33.325
150	96.00	-2.740	-9.863	-14.547	-16.012	-37.193	150	110.00	-2.715	-9.564	-13.049	-13.738	-32.649
250	95.50	-2.668	-9.709	-14.097	-15.542	-36.252	250	109.00	-2.673	-9.572	-13.164	-14.235	-33.644
350	95.70	-2.912	-9.755	-13.622	-15.068	-35.303	350	108.00	-2.942	-9.736	-13.320	-14.590	-34.354
500	95.90	-3.326	-9.915	-13.271	-14.720	-34.607	500	106.00	-3.474	-10.056	-13.779	-15.082	-35.337
750	95.70	-2.790	-9.946	-14.290	-15.755	-36.677	750	103.00	-2.935	-9.878	-13.920	-15.245	-35.661
1,000	94.60	-2.443	-9.870	-14.359	-15.825	-36.817	1,000	100.00	-2.499	-9.699	-13.847	-15.212	-35.595
2,401	88.30	-2.121	-9.896	-14.437	-15.889	-36.942	2,401	88.30	-2.014	-9.777	-14.237	-15.692	-36.547

Table 4.1-23. Log Fugacities of Five Acid-Gas Species in the Drift Wall as Functions of Time in Repository History (Continued)

W7 THC Abstraction													
TF4							BF4						
Time (yrs)	Temp (°C)	CO ₂	HF	HCl	HNO ₃	N ₂ O ₅	Time (yrs)	Temp (°C)	CO ₂	HF	HCl	HNO ₃	N ₂ O ₅
5,003	73.20	-2.171	-10.379	-15.005	-16.433	-38.013	5,003	73.30	-2.047	-10.260	-14.865	-16.291	-37.730
10,006	56.20	-2.115	-11.127	-15.691	-17.089	-39.300	10,006	56.30	-2.090	-11.103	-15.656	-17.056	-39.235
20,013	40.20	-2.227	-11.891	-16.438	-17.812	-40.710	20,013	40.30	-2.238	-11.906	-16.445	-17.822	-40.729
50,034	27.00	-2.524	-12.672	-17.209	-18.564	-42.173	50,034	27.00	-2.689	-12.826	-17.366	-18.722	-42.490

Source: DTN: MO0303MWDSCMAB.000 [DIRS 162551].

4.1.20 Solubility of Potassium Nitrate as a Function of Temperature

Table 4.1-9 gave the solubility of potassium nitrate at two temperatures, 0°C and 100°C.

That is not entirely sufficient for the purposes of this report. A more detailed listing of the solubility of this salt, as presented in Table 4.1-24, is used in the analysis described in Section 6.7.2.15.

Table 4.1-24. Solubility of Potassium Nitrate as a Function of Temperature

Temp (°C)	Solubility g/100g of saturated solution
-2.84 ^(E)	10.9
0	11.7
10	24.0
20	24.0
25	27.5
30	31.3
40	39.0
50	46.0
60	52.2
70	57.8
80	62.8
90	67.0
100	71.0
110	74.8
120	77.5
140	81.5
160	85.0
180	87.0
200	89.0
225	91.7
250	93.5
275	96.0
300	98.0
336 ^(M)	100.0

Source: Linke 1965 [DIRS 166191], p. 250.

E = eutectic point; M =melting point.

4.1.21 Barometric Pressure in the Repository

Direct measurements of barometric pressure in the repository are reported in DTN: GS030108312242.001 [DIRS 163118]. The pressure was measured twice at each of 12,541 times from June 22, 2000 to August 26, 2002. Summary data are presented in Section 6.7.2.1.

4.1.22 Solute Content of Precipitation (Rainfall) at Three Meteorological Stations in the Vicinity of Yucca Mountain

Table 4.1-25 shows the 2002 annual mean solute compositions of precipitation (rainfall) at three National Atmospheric Deposition Program field stations that are located to the southeast, the northeast, and west of Yucca Mountain. The three stations are: NV00 (Red Rock Canyon, Clark County, NV); NV05 (Great Basin National Park, White Pine County, NV); and CA95 (Death Valley National Park, Inyo County, CA, respectively). The solute content of rainfall samples contributions from various sources in the atmosphere: dust, liquid aerosols, and reactive volatiles such as $\text{HCl}_{(g)}$ and $\text{HNO}_{3(g)}$. Its solute content is thought to be reflective of that in prevailing atmospheric dust, which itself reacts with liquid aerosols and reactive volatiles. Thus, this content is expected to be a compositional proxy of salts in atmospheric dusts. These data are compared with data for the leachable fraction of Yucca Mountain tunnel dusts in Section 6.7.2.10. Sea salts do not make a significant contribution at these three inland sites, as indicated by the relatively low concentrations of Na and Cl (principal components of sea salt) compared with those of NH_4 and NO_3 (principal products of atmospheric reactions; Arimoto 2001 [DIRS 163485]).

Table 4.1-25. Measurements of the 2002 Mean Annual Solute Content of Precipitation at Three National Atmospheric Deposition Program Sites in the Vicinity of Yucca Mountain

Station	Na (mg/L)	K (mg/L)	Mg (mg/L)	Ca (mg/L)	Cl (mg/L)	SO ₄ (mg/L)	NO ₃ (mg/L)	NH ₄ (mg/L)	pH (lab)	pH (field)
NV00	0.263	0.055	0.137	1.21	0.36	1.35	3.24	1.01	6.38	5.57
NV05	0.166	0.032	0.040	0.46	0.14	0.59	0.94	0.33	5.63	5.26
CA95	1.114	0.145	0.191	2.91	0.83	2.27	4.31	1.10	6.20	5.51

Source: Station NV00: NADP/NTN (National Atmospheric Deposition Program/National Trends Network) 2003 [DIRS 171291].
 Station NV05: NADP/NTN 2003 [DIRS 171292].
 Station CA95: NADP/NTN 2003 [DIRS 171293].

The data cited in Table 4.1-25 are meteorological data produced by the National Atmospheric Deposition Program, a cooperative research support program of the state agricultural experiment stations, federal and state agencies, and nongovernmental research organizations. The operating or sponsoring agency for station NV00 is the U.S. Bureau of Land Management and for stations CA95 and NV05 is the U.S. National Park Service.

4.1.23 Leachable Compositions of Asian Dusts

Table 4.1-26 shows leachable composition data for statistical composite samples of Asian dusts sampled during the ACE-ASIA (Asian-Pacific Regional Aerosol Characterization Experiment) project (Topping et al. 2004 [DIRS 171290]). These dusts originated in northern China and Mongolia and blow to the east; they were sampled in Korea. Asian dust is an analogue for southwest United States regional dusts. For example, both kinds of dusts tend to originate much of their material mass from playas (dry lake beds). However, Asian dust is also of much interest because of its extent of global transport; it actually reaches the western United States, including Nevada. These data are compared with data for Yucca Mountain tunnel dusts in Section 6.7.2.10 (and with the data for the solute composition of Nevada regional precipitation described in Section 4.1.22).

Table 4.1-26. Leachable Compositions of Asian Dust Samples (Statistical Composites)

	Na (nmol/m ³)	K (nmol/m ³)	Mg (nmol/m ³)	Ca (nmol/m ³)	Cl (nmol/m ³)	SO ₄ (nmol/m ³)	NO ₃ (nmol/m ³)	NH ₄ (nmol/m ³)
Whole Campaign	38.17	9.03	3.88	11.69	17.60	43.52	30.87	82.20
Chinese Course	72.55	21.44	11.66	48.44	55.44	93.08	79.84	124.44
Korean Course	47.84	11.09	4.71	13.98	21.53	43.18	37.01	87.00
	Na (µg/m ³)	K (µg/m ³)	Mg (µg/m ³)	Ca (µg/m ³)	Cl (µg/m ³)	SO ₄ (µg/m ³)	NO ₃ (µg/m ³)	NH ₄ (µg/m ³)
Total PM10	0.54	0.28	0.27	0.30	0.39	3.58	1.40	1.32

Source: Topping et al. 2004 [DIRS 171290], Tables 1 and 2.

NOTES: The "Whole Campaign," "Chinese Course," and "Korean Course" data are from Table 2 of the source document. These are given as "total" values, though they appear to be summations over size ranges encompassing 0.2 to 10 microns. The "Total PM10" data are the "average" data for the "whole campaign" from Table 1 of the source document. "PM10" refers to particulate matter up to 10 microns in size.

The gross salt composition was determined by leaching into aqueous solution, followed by chemical analysis. This is a common methodology for analyzing the salt content of dust. The same methodology has been applied in the analysis of the Yucca Mountain tunnel dusts (Section 4.1.14). These two sets of data are compared in Section 6.7.2.10.

The source document (Topping et al. 2004 [DIRS 171290]) was written by a ten-member team, and presents results from the ACE-ASIA Project, an international global atmospheric chemistry project with support and participation by various government agencies including the Instituto di Scienza dell'Atmosfera e del Clima [Bologna, Italy], the (U.S.) National Oceanic and Atmospheric Administration and the U.S. Department of Energy. The source journal, *Atmospheric Environment*, is one of the premier peer-reviewed journals of atmospheric chemistry. One of the authors, Professor Keith Bower (University of Manchester) is a Fellow of the Royal Meteorological Society, a member of several international committees involved in the study of atmospheric aerosols, and the author of numerous technical publications in this subject area.

4.1.24 Key Thermodynamic Relations for Gibbs Energies of Gas Species (Equations)

The apparent partial molar Gibbs energy of formation of the i -th chemical species is defined as (e.g., Helgeson et al. 1978 [DIRS 101596], p. 28, Equation 16, but with subscript T , P , T_r and P_r raised and put in parentheses):

$$\begin{aligned} \Delta G_{f,i}^{\circ}(T, P) = & \Delta G_{f,i}^{\circ}(T_r, P_r) - S_i^{\circ}(T_r, P_r)[T - T_r] \\ & + \int_{T_r}^T c_{p,i}^{\circ}(T, P_r) dT - T \int_{T_r}^T c_{p,i}^{\circ}(T, P_r) d \ln T + \int_{P_r}^P V_i^{\circ}(T, P) dP \end{aligned} \quad (\text{Eq. 4.1.24-1})$$

where $\Delta G_{f,i}^{\circ}(T_r, P_r)$ is the partial molar Gibbs energy of formation at reference absolute temperature T_r and pressure P_r (generally 298.15K and 1 bar, respectively), T is the absolute temperature, P is the total pressure, $S_i^{\circ}(T_r, P_r)$ is the partial molar entropy at the reference temperature and pressure, $c_{p,i}^{\circ}(T, P_r)$ is the partial molar heat capacity at the reference pressure (this heat capacity being generally a function of temperature), and $V_i^{\circ}(T, P)$ is the partial molar volume (generally a function of temperature and pressure). The apparent Gibbs energy of formation is equal to the Gibbs energy of formation at the reference temperature and pressure. At temperatures other than the reference temperature, however, the apparent Gibbs energy of formation is not equal to the true Gibbs energy of formation from the chemical elements in their stable reference states. To obtain the latter, one would need to replace $S_i^{\circ}(T_r, P_r)$ in Equation 4.1.24-1 with the partial molar entropy of formation, similarly replace $c_{p,i}^{\circ}(T, P_r)$ with the partial molar heat capacity of formation, and factor in corrections for any phase transitions or other changes in the reference elemental compounds. The apparent Gibbs energy of formation is thus tied to the elemental reference forms only at the reference temperature and pressure. It is more convenient to work with, and it is adequate for use in calculating Gibbs energy differences for balance reactions (or pseudo-reactions, as in estimating the Gibbs energy difference for a single chemical species at two different temperatures). The apparent Gibbs energy of formation is the working form of the Gibbs energy of a chemical species in the code SUPCRT92 (Johnson et al. 1992 [DIRS 101632]). That is a qualified software code on the Yucca Mountain Project (LBNL 1999 [DIRS 153218]).

The heat capacity of solids and gases is often represented by the Maier-Kelley equation (Maier and Kelley 1932 [DIRS 101691]). This is given by Helgeson et al. (1978 [DIRS 101596], p. 29, Equation 19) as:

$$c_{p,i}^{\circ}(T, P_r) = a_i + b_i T - c_i T^{-2} \quad (\text{Eq. 4.1.24-2})$$

where a_i , b_i , and c_i are the Maier-Kelley heat capacity coefficients. Most modern usage (e.g., Barin and Platzki (1995 [DIRS 157865], p. I-21; Weast and Astle 1981 [DIRS 100833], p. D-61) has the sign of the third term defined as positive:

$$c_{p,i}^{\circ}(T, P_r) = a_i + b_i T + c_i T^{-2} \quad (\text{Eq. 4.1.24-3})$$

This reverses the sign of the associated coefficient (c_i). Caution is required when taking data from a source so as not to introduce a sign error in subsequent results. Often at least one additional term (each such term introduces an additional coefficient) is used (e.g., Barin and Platzki (1995 [DIRS 157865], p. I-21; Weast and Astle 1981 [DIRS 100833], p. D-61) and implicit scaling factors are sometimes employed; for example, see Page D-61 of Weast and Astle. Caution is also required in dealing with implicit scaling factors. In the present report, only the basic Maier-Kelley equation, as shown in Equation 4.1.24-3 (with no implicit scaling), is considered.

Substitution of Equation 4.1.24-3 into Equation 4.1.24-1, followed by integration, then yields:

$$\begin{aligned} \Delta G_{f,i}^o(T, P) &= \Delta G_{f,i}^o(T_r, P_r) - S_i^o(T_r, P_r)[T - T_r] \\ &+ a_i[T - T_r] + \frac{b_i}{2}(T^2 - T_r^2) - c_i\left(\frac{1}{T} - \frac{1}{T_r}\right) \\ &- a_i T \ln\left(\frac{T}{T_r}\right) - b_i(T^2 - TT_r) + \frac{c_i}{2}\left(\frac{1}{T} - \frac{T}{T_r^2}\right) \\ &+ \int_{P_r}^P V_i^o(T, P) dP \end{aligned} \quad (\text{Eq. 4.1.24-4})$$

(Compare Helgeson et al. 1978 [DIRS 101596], pp. 28 to 29, Equations 16, 20, and 21, carrying through the $-T$ before the second integral in Equation 4.1.24-1 and accounting for the change in the sign of c_i). When P equals P_r , the above relation takes the form:

$$\begin{aligned} \Delta G_{f,i}^o(T, P_r) &= \Delta G_{f,i}^o(T_r, P_r) - S_i^o(T_r, P_r)[T - T_r] \\ &+ a_i[T - T_r] + \frac{b_i}{2}(T^2 - T_r^2) - c_i\left(\frac{1}{T} - \frac{1}{T_r}\right) \\ &- a_i T \ln\left(\frac{T}{T_r}\right) - b_i(T^2 - TT_r) + \frac{c_i}{2}\left(\frac{1}{T} - \frac{T}{T_r^2}\right) \end{aligned} \quad (\text{Eq. 4.1.24-5})$$

The partial molar apparent Gibbs energy of formation on the left-hand side is now $\Delta G_{f,i}^o(T, P_r)$. This equation is used in Section 6.7.2.14.1 to compute Gibbs energies for various acid-gas species as a function of temperature.

These equations represent the properties of interest (apparent Gibbs energy of formation of a gas species; heat capacity of a gas species) as a function of temperature, and are, thus, appropriate to calculate the apparent Gibbs energy of formation of some acid-gas species as a function of temperature in Section 6.7.2.14.1. The results are used in the discussion of thermodynamic driving forces on the migration of acid-gas species in the repository drifts.

The above equations for the apparent Gibbs energy of formation, as a function of temperature and various derivative equations (corrected where necessary to the positive convention of the c_i term in the Maier-Kelley heat capacity equation), are taken or assembled from a paper by

Helgeson et al. (1978 [DIRS 101596], pp. 28 to 29). This is a highly cited paper in the geochemical literature. The Maier-Kelley heat capacity equation also appears in two handbooks (Barin and Platzki 1995 [DIRS 157865], p. I-21; Weast and Astle 1981 [DIRS 100833], p. D-61). The equations presented here (apart from the issue of the sign of c_i) are a key part of the mathematical core of SUPCRT92 (Johnson et al. 1992 [DIRS 101632]), which is widely used in the geochemical community and is a qualified Yucca Mountain Project software code (LBNL 1999 [DIRS 153218]). These equations are also used in many of the spreadsheets in DTN: MO0302SPATHDYN.001 [DIRS 161886], a data package noted previously in Sections 4.1.11 and 4.1.12). These equations, through SUPCRT92, have long been a basis for the construction of thermodynamic databases that support other codes such as EQ3/6 Version 8.0 (e.g., BSC 2003 [DIRS 162228]). Those databases in turn have supported many publications in the geochemical literature over the years. “Summary and Critique of the Thermodynamic Properties of Rock Forming Minerals” (Helgeson et al. (1978 [DIRS 101596]) was written by a highly respected group of scientists at the University of California, Berkeley, that has produced many highly cited papers addressing thermodynamics and thermodynamic data in aqueous geochemistry. Prof. H.C. Helgeson, the founder of the group and lead author of this paper, is the recipient of the Goldschmidt Medal of the Geochemical Society and has a global reputation in the development and application of thermodynamics and thermodynamic data in aqueous geochemical systems.

4.1.25 Chemical Potential and Fugacity or Partial Pressure of a Gas Species (Equations)

The chemical potential of the i -th gas species is related to the fugacity f_i of the gas by (e.g., Nordstrom and Munoz 1986 [DIRS 153965], p. 129, Equation 5-52):

$$\mu_i = \mu_i^o + RT \ln \frac{f_i}{f_i^o} \quad (\text{Eq. 4.1.25-1})$$

where μ_i^o is the chemical potential at absolute temperature T and reference pressure P_r , R is the gas constant (which is introduced in Section 4.1.1), f_i is the fugacity (closely related to the partial pressure p_i), and f_i^o is the reference fugacity in the standard state (defined as 1 bar). Here μ_i^o equates to $\Delta G_{f,i}^o(T, P_r)$. For the purposes of the present report, fugacity can be equated to partial pressure and Equation 4.1.25-1 can be written as:

$$\mu_i = \mu_i^o + RT \ln \frac{p_i}{p_i^o} \quad (\text{Eq. 4.1.25-2})$$

where p_i^o is the reference partial pressure in the standard state (also defined as 1 bar). Because the reference fugacity and partial pressure have unit values, these quantities are sometimes omitted in writing the above equations. Equation 4.1.25-2, for example, then becomes:

$$\mu_i = \mu_i^o + RT \ln p_i \quad (\text{Eq. 4.1.25-3})$$

This equation is used in Section 6.7.2.14.1 to account for the thermodynamic driving force for the migration of acid-gas volatiles between two locations (e.g., one point on the surface of a

waste package and another on the drift wall) that do not have the same temperature. Given the partial pressure or fugacity of a gas species at one location, the “equilibrium” partial pressure at the other location can be calculated (in essence applying a temperature correction for comparing partial pressures).

The equating of fugacity with partial pressure is only approximate. Technically, the fugacity is related to the partial pressure by a fugacity coefficient χ_i :

$$f_i = \chi_i P_i \quad (\text{Eq. 4.1.25-4})$$

Fugacity coefficients may differ significantly from unity even at relatively low pressure. Garrels and Christ (1990 [DIRS 144877], pp. 22 to 26) discuss this and provide a table and chart for graphical estimation of fugacity coefficients from the reduced temperature and pressure ($T_r = T/T_c$ and $P_r = P/P_c$, where T_c and P_c are the critical temperature and pressure of a specific gas). In the temperature and pressure range of interest in the present report, for most gases T_r is generally greater than about 1 and P_r is generally less than about 0.2. Under these conditions, fugacity coefficients are expected to have values between about 0.9 and 1.0. In Section 6.7.2.14.1, the partial pressures or fugacities vary over orders of magnitude and fugacity coefficients can be ignored. In most instances in that section, comparisons are drawn between the partial pressure or fugacity at one location or temperature versus that at another. Under these circumstances, the fugacity coefficients largely cancel out.

These equations appropriately represent the properties of interest (relation of chemical potential of a gas species to its fugacity or partial pressure) to be used in Section 6.7.2.14 to calculate the thermodynamic driving forces on the migration of acid-gas species in the repository drifts.

Equations 4.1.25-1, 4.1.25-2, and 4.1.25-3 are well-known relations in thermodynamics, though they are not easily found in handbooks. They are instead common in monographs and textbooks addressing the subject of thermodynamics, and are commonly given in slightly different forms. These equations can be compared, for example, with Equation 14.15 by Lewis and Randall (1961 [DIRS 119458], p. 156) and Equations 51 and 56 by Stumm and Morgan (1996 [DIRS 125332], pp. 35 to 38).

4.2 CRITERIA

Technical requirements to be satisfied by performance assessment are based on 10 CFR 63.114 and 63.115 ([DIRS 156605]). These technical requirements are also identified in *Project Requirements Document* (Canori and Leitner 2003 [DIRS 166275], Section 3). The acceptance criteria that are expected to be used by the Nuclear Regulatory Commission to determine whether the technical requirements have been met are identified in *Yucca Mountain Review Plan, Final Report* (NRC 2003 [DIRS 163274]). The pertinent requirements and acceptance criteria for this report are summarized in Table 4.2-1.

Table 4.2-1. Project Requirements and Yucca Mountain Review Plan Acceptance Criteria Applicable to This Report

Requirement Number	Requirement Title	10 CFR 63 Link	YMRP Acceptance Criteria
PRD-002/T-015	Requirements for Performance Assessment (Canori and Leitner 2003 [DIRS 166275])	10 CFR 63.114 (a)-(c) and (e)-(g) [DIRS 156605]	Criteria 1 to 4 for “Quantity and Chemistry of Water Contacting Engineered Barriers and Waste Forms Model Abstraction” (NRC 2003 [DIRS 163274], Section 2.2.1.3.3.3)

YMRP = *Yucca Mountain Review Plan, Final Report*

Section 3.2 of *Technical Work Plan For: Near-Field Environment and Transport In-Drift Geochemistry Model Report Integration* (BSC 2004 [DIRS 171156]) identified the following acceptance criteria based on the requirements listed in *Yucca Mountain Review Plan, Final Report* (NRC 2003 [DIRS 163274]). The main purpose of this Section 4.2 is to identify the applicable subcriteria for each of the four criteria. Section 7.3 describes how and where each applicable subcriterion is addressed in this report. The subcriterion is omitted below if the subcriterion is not applicable to this report. The listing of applicable criteria and subcriteria is as follows.

Acceptance Criterion 1. System Description and Model Integration are Adequate

AC1(1) – Total system performance assessment adequately incorporates important design features, physical phenomena, and couplings, and uses consistent and appropriate assumptions throughout the quantity and chemistry of water contacting engineered barriers and waste forms abstraction process.

AC1(2) – The abstraction of the quantity and chemistry of water contacting engineered barriers and waste forms uses assumptions, technical bases, data, and models, that are appropriate and consistent with other related U.S. Department of Energy abstractions...[examples omitted here]. The descriptions and technical bases provide transparent and traceable support for the abstraction of quantity and chemistry of water contacting engineered barriers and waste forms.

AC1(4) – Spatial and temporal abstractions appropriately address physical couplings (thermal-hydrologic-mechanical-chemical).

AC1(10) – Likely modes for container corrosion (Section 2.2.1.3.1 of the Yucca Mountain Review Plan) are identified and considered in determining the quantity and chemistry of water entering the engineered barriers and contacting waste forms.

Acceptance Criterion 2. Data are Sufficient for Model Justification

AC2(1) – Geological, hydrological, and geochemical values used in the license application are adequately justified. Adequate description of how the data were used, interpreted, and appropriately synthesized into the parameters is provided.

AC2(2) – Sufficient data were collected on the characteristics of the natural system and engineered materials to establish initial and boundary conditions for conceptual models of thermal-hydrologic-mechanical-chemical coupled processes that affect seepage and flow and the engineered barrier chemical environment.

AC2(4) – Sufficient information to formulate the conceptual approach(es) for analyzing water contact with the drip shield, engineered barriers, and waste forms is provided.

Acceptance Criterion 3. Data Uncertainty Is Characterized and Propagated Through the Model Abstraction

AC3(1) – Models use parameter values, assumed ranges, probability distributions, and bounding assumptions that are technically defensible, reasonably account for uncertainties and variabilities, and do not result in an under-representation of the risk estimate.

AC3(4) – Adequate representation of uncertainties in the characteristics of the natural system and engineered materials is provided in parameter development for conceptual models, process-level models, and alternative conceptual models. The U.S. Department of Energy may constrain these uncertainties using sensitivity analyses or conservative limits.

Acceptance Criterion 4. Model Uncertainty Is Characterized and Propagated Through the Model Abstraction

AC4(3) – Consideration of conceptual model uncertainty is consistent with available site characterization data, laboratory experiments, field measurements, natural analog information and process level modeling studies; and the treatment of conceptual model uncertainty does not result in an under representation of the risk estimate.

4.3 CODES, STANDARDS, AND REGULATIONS

The acceptance criteria listed above are consistent with the methodology described in the ASTM Standard Practice C-1174 for prediction of the long-term behavior of EBS components in a geologic repository (ASTM C 1174-97 1998 [DIRS 105725]). This report also cites *Standard Practice for Maintaining Constant Relative Humidity by Means of Aqueous Solutions* (ASTM E 104-85 1996 [DIRS 146039]) as an indirect input.

INTENTIONALLY LEFT BLANK

5. ASSUMPTIONS

The following assumptions are used in the analysis contained in this report. The assumptions concern the anticipated temperature and RH histories at the drip shield and waste package outer barrier surfaces, the occurrence and nature of the waters contacting these surfaces, and the efficacy of certain processes expected to affect the occurrence and compositions of such waters.

5.1 VENTILATION WILL RESULT IN THE DEPOSITION OF DUST AND AEROSOLS ON THE SURFACES OF THE METAL BARRIERS

Assumption: The ventilation of the emplacement drifts will result in the deposition of dust and aerosols on the drip shield and the waste package outer barrier. It is assumed that the air used for ventilation is unfiltered and that dust from outside the tunnels is brought into the repository as a consequence.

Basis: This assumption is based on the current repository design (BSC 2004 [DIRS 168489]). The velocity of the ventilation-induced airflow may act to limit the settling of dust on the metal barrier surfaces. The actual efficacy of this is not known, particularly along the length of the tunnels. Although the quantity and distribution of atmospheric dust deposited during ventilation are uncertain, the presence of such dust on some or all of the waste packages is not in question.

Confirmation Status: This assumption represents the current repository design and does not require confirmation.

Use in the Analysis: This assumption is used to justify the analyses of the effects of dust deliquescence in the no-dripping case analysis (Section 6.7.2.13).

5.2 WATERS THAT HAVE BEEN SAMPLED AT YUCCA MOUNTAIN REPRESENT THE COMPOSITIONS OF SEEPAGE-DERIVED WATERS THAT CAN EVOLVE ON THE METAL BARRIER SURFACES

Assumption: The characteristics (e.g., compositions) of the waters that develop on the drip shield and waste package outer barrier surfaces because of groundwater seepage are represented by the types of concentrated solutions (brines) that evolve by evaporative concentration of the waters that have been sampled at Yucca Mountain. An acceptable alternative to the direct use of sampled waters for this purpose is the use of seepage water compositions obtained from numerical THC models, or the use of comparable water compositions obtained from bench scale or field tests. It is assumed that temperature and RH conditions for the formation of deliquescent aqueous conditions on the drip shield and waste package outer barrier are bounded by the most deliquescent salt occurring naturally in geologic systems that cannot be readily excluded. That is assumed to be one or more of the forms of calcium chloride (Sections 6.7.2.9, 6.7.2.11, and 6.7.2.12).

Basis: As discussed in Section 6.7.2.11, it is known that the types of brines in natural systems are limited, and their evolution from dilute waters can be explained by the relative ratios of certain ionic solution species according to the principles of chemical divide theory (though the analyses presented in this report are actually based on EQ3/6 calculations, not the ternary diagrams of classical chemical divide theory as illustrated in the classic works of Hardie and

Eugster (1970 [DIRS 162776]) and Eugster and Hardie (1978 [DIRS 100743]). The principles underlying this assumption can be demonstrated, for example, by the analysis presented by Drever (1997 [DIRS 147480], Chapter 15). The analysis includes extensive cataloging of natural brines. Three major types of brines are noted. Calcium chloride brine contains the most hygroscopic components. Classic chemical divide theory does not address the formation of brines from dilute solutions relatively rich in components such as fluoride, nitrate, and anionic silica species. Therefore, the classic theory, intended to describe the evaporation of surface waters in desert playas, is incomplete in regard to application to subsurface seepage waters of the sort expected at Yucca Mountain. Additional evidence, however, supports this assumption. The formation of magnesium chloride or magnesium sulfate brines is ruled out by arguments presented in Section 6.7.2.11. Only high-nitrate brines appear to be highly deliquescent alternatives to calcium chloride brines. Analysis of seepage water evolution is also contained in *Engineered Barrier System: Physical and Chemical Environment* (BSC 2004 [DIRS 169860]).

Confirmation Status: This assumption represents current understanding and appears reasonable and conservative. Confirmation for the purposes of this report is not required.

Use in the Analysis: This assumption is used to specify the deliquescence relative humidity (RH) of deposited salts from seepage (dripping) on the drip shield and waste package outer barrier. The deliquescence RH is used in other analyses for initiation of general corrosion of the drip shield and waste package outer barrier. This is discussed in Section 6.7.2.13.

5.3 TOTAL PRESSURE IN THE DRIFTS WILL REMAIN CLOSE TO AMBIENT ATMOSPHERIC PRESSURE

Assumption: The total pressure in the drifts in the postclosure period is limited to a value close to the ambient nominal atmospheric value at the repository horizon. Here “close to” can be taken to mean that the pressure will not exceed approximately 0.90 bar (900 mbar or 90 kPa). The ambient pressure at the repository is discussed in Section 6.7.2.1.

Basis: The repository rock is highly fractured and barometric fluctuations recorded at the site (e.g., in sealed boreholes, not the open tunnels) show that atmospheric pressure transients propagate to depth through the unsaturated zone. Therefore, the pressure excursions within the repository will be readily propagated into the surrounding host rock. Development of any significant “overpressure” seems unlikely and is not consistent with current thermohydrologic and THC models.

Confirmation Status: The gas transport features of the repository site (e.g., the highly fractured rock) are discussed in *Multiscale Thermohydrologic Model* (BSC 2004 [DIRS 169565]). Calculated postclosure pressures in the drift are within the expected range of ambient pressures. The assumption is reasonable based on present knowledge and does not require confirmation.

Use in the Analysis: This assumption is used in analyses leading to the no-dripping (dust deliquescence) and dripping (seepage) analyses (Section 6.7.2.13). This assumption is quantitatively significant because the total pressure is an important determinant of the range of as temperature for existence of aqueous conditions.

5.4 THE GAS PHASE IN THE DRIFT, EXCLUSIVE OF WATER, HAS THE GROSS COMPOSITION OF ATMOSPHERIC AIR

Assumption: The gross gas phase composition of the drift air, exclusive of water, is nominally that of atmospheric air. This assumption does not apply to components other than O₂, N₂, and Ar.

Basis: This assumption is largely based on information contained in Yang et al. (1996 [DIRS 100194]) and Thorstenson et al. (1990 [DIRS 100831]) for the major components of “air” in the mountain: O₂, N₂, or Ar. However, with regard to such components, this report only requires an assumption of mildly oxidizing conditions.

Confirmation Status This report does not use data for N₂ or Ar. It does require some value of O₂ fugacity (0.21 atm) in the EQ3/6 calculations described in Section 6 but none of the results are sensitive to the exact value. It is only necessary that the elements are present in their expected valence states under mildly oxidizing conditions (S is present as SO₄²⁻, Cl as Cl⁻, Na as Na⁺, and so forth). This assumption is reasonable and does not require confirmation for the purposes of this report.

Use in the Analysis: This assumption is used in analyses leading to the no-dripping (dust deliquescence) and dripping (seepage) analyses (Section 6.7.2.13).

5.5 THE TEMPERATURE, RH, AND CO₂ PRESSURE AT A METAL BARRIER SURFACE ARE NOT PERTURBED BY EVAPORATION OR DELIQUESCENT

Assumption: The temperature, RH, and CO₂ pressure at the surface of a metal barrier are not perturbed either by seepage-water evaporation or by the deliquescence of dust. In both cases, it is assumed that the amounts of liquid water vaporized or condensed are small in comparison with the amount of water vapor in and around the drifts. The evaporation of seepage water would tend to lower the local temperature and increase the local RH. Ignoring this effect may lead to an overestimation of the degree of evaporation and the concentration level of any residual brine. The deliquescence of salts would tend to increase the local temperature and reduce the local RH. Ignoring this effect may lead to an overestimation of the amount of aqueous solution formed and an underestimation of the concentration level of the brine that is formed. The CO₂ pressure is assumed to be unperturbed because the flux of consumption or production associated with these processes is expected to be small in comparison to the reservoir of CO₂ present in and near the drifts.

Basis: This assumption is consistent with current understanding of likely in-drift conditions (low water fluxes for seepage, limited amounts of dust on metal barrier surfaces). The low water fluxes for seepage are discussed in *Abstraction of Drift Seepage* (BSC 2004 [DIRS 169131]). It is recognized that there may be certain conditions, such as greater than expected flux of seepage water, or high focusing of seepage water in a few locales in the drifts, for which the assumption may not hold at all times and places. However, these conditions are infrequent on the time scale relevant for corrosion of the drip shield and waste package outer barrier. Note that a very high seepage flux would imply a transition to a regime in which the in-drift temperature would be lowered and the RH increased, such that evaporation would be suppressed. The effect of high-

temperature deliquescence would be minimized by a shorter period of conditions of high temperature and low RH, and seepage water after first penetrating the drifts would rapidly dilute any brines formed by deliquescence.

Confirmation Status: The analysis using this assumption bounds the concentrations for aqueous species, and confirmation is not required. For the case of deliquescence of deposited salts, the amount of aqueous solution formed is small due to the limited amounts of deposited salts, hence the effect on local temperature, RH, and CO₂ pressure is insignificant. This assumption is reasonable based on the bounding relationships and the likely amounts of dust deposition, and confirmation is not required.

Use in the Analysis: This assumption is used in analyses leading to the no-dripping (dust deliquescence) and dripping (seepage) analyses (Section 6.7.2.13).

5.6 THE COMPOSITION OF WATER CONTACTING METAL BARRIERS WILL NOT CHANGE SIGNIFICANTLY BECAUSE OF CHEMICAL INTERACTION WITH THE BARRIERS THEMSELVES

Assumption: The present revision of this report assumes that the composition of the water that contacts the drip shield and waste package outer barrier (via seepage or deliquescence) will not change significantly because of chemical interaction with the metal barriers themselves.

Basis: This is based on the slow general corrosion of the drip shield and waste package outer barrier materials and the modeling of generalized and localized corrosion based on the “initial” water chemistry in contact with the drip shield and waste package outer barrier materials. Expected low corrosion rates (BSC 2004 [DIRS 169845]; BSC 2004 [DIRS 169984]) imply a low extent of reaction for long periods of time. Thus, the evolution of water chemistry in this analysis is considered a function of temperature, RH, and gas phase composition, but not of the extent of corrosion. In the case of the drip shield, which is chemically simple and would corrode to form a simple oxide, a significant effect on water chemistry would not be expected even for a high extent of reaction. In the case of the WPOB, which is composed of the more chemically complex Alloy 22 and whose components exhibit more complexity of chemical behavior, significant effects on water chemistry would be expected for high extents of reaction. The argument for the WPOB thus depends solely on the expectation of very low rates of corrosion.

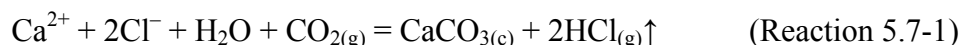
Confirmation Status: No confirmation of the assumption is required.

Use in the Analysis: This assumption is used in analyses leading to the no-dripping (dust deliquescence) and dripping (seepage) analyses (Section 6.7.2.13).

5.7 ACID-GAS VOLATILES PRODUCED ON THE METAL BARRIERS ARE DISPERSED BY CONVECTION AND DIFFUSION TO THE DRIFT WALL

Assumption: Acid-gas species (such as HCl_(g) and HNO_{3(g)}) volatilized by heating of concentrated salt solutions present on the drip shield and waste package outer barrier surfaces are dispersed by convection and diffusion to the drift wall, where they advect or diffuse into the rock and react with it. In particular, it is assumed that volatilized acid-gas species will not be

condensed into highly acidic solutions formed directly on the metal surfaces, or dripping onto them, except as a very transient event. Acid–gas volatility can occur through reactions such as:



The “↑” in this reaction denotes the volatilization of $\text{HCl}_{(\text{g})}$. For the waste package outer barrier, part of this assumption is that the drip shield will not be an effective vapor barrier between the waste package outer barrier and the drift wall.

Basis: This is based on several factors. One is the expectation of an actively convecting gas phase in the drifts. Another factor is that the chemical potentials of acid–gas species will necessarily be lower at the drift wall than on the metal surfaces (because of the lower temperature, the fact that conditions at the drift wall are expected to be neutral to alkaline, and the fact that acid–gas species are expected to be generated mainly on the hotter metal surfaces). This assures that the fundamental thermodynamic driving force will support transport to the drift wall. Even in the absence of convection, diffusion in the gas phase is quite rapid and would likely suffice. The potential amounts of acid–gas volatiles and rates of formation are limited by such factors as seepage rates, the amount of dust on the metal barrier surfaces, and the rate of rehumidification of the drifts. Those amounts and rates will likely be dwarfed by convective flux and if need be, by the gas phase diffusion flux.

Confirmation Status: The transport of acid–gas within the drifts is analogous to water vapor transport due to differences in chemical potentials. The driving force is from regions of high chemical potential to low chemical potential. Transport of water vapor due to natural convection is documented in *In-Drift Natural Convection and Condensation* (BSC 2004 [DIRS 164327]). The assumption is reasonable and confirmation is not necessary for the purposes of this report.

Use in the Analysis: This assumption is used to justify limits on the expected range of conditions pertaining to the chemical environment on the metal barrier surfaces (e.g., Section 6.7.2.14).

INTENTIONALLY LEFT BLANK

6. SCIENTIFIC ANALYSIS DISCUSSION

This section discusses the analysis objectives; features, events, and processes (FEPs); conceptual IDPS model; alternatives; and results.

6.1 ANALYSIS OBJECTIVES

The objective of this scientific analysis is to describe the anticipated chemical environment on the drip shield and waste package outer barrier surfaces and to provide useful bounds on that environment. As is noted in Section 1.1, this report is focused on the role of salt mineral deliquescence. This report uses the EQ3/6 version 8.0 software to implement the IDPS model for analyses of salt mineral deliquescence. The product of this report includes tables for the no-dripping and dripping cases. The no-dripping case corresponds to deliquescence of the salt component of dust. The dripping case corresponds to the deliquescence of salts that may have formed from seepage water, for example by dryout of small floating droplets created by splashing, followed by deposition on metal barrier surfaces. *Engineered Barrier System: Physical and Chemical Environment* (BSC 2004 [DIRS 169860]) uses the IDPS model for more extensive treatment of seepage-water evaporation.

This report presents background material on the process of deliquescence and determines bounds associated with the repository location and design. The relevance of equilibrium thermodynamics is discussed, along with the calculational tools and underlying data. Section 6.7.2.13 analyzes a no-dripping (deliquescence) and a dripping (seepage) case. For the no-dripping case, this report considers potential dust salts and their sources, and analyzes the key features of dust deliquescence using chemical data obtained from dusts taken from the repository drifts. For the dripping case, it provides an analysis based on a pure calcium chloride system, which is highly deliquescent and highly corrosive. Uncertainties in the analyses presented are discussed in Section 6.7.2.16.

Section 6.7.2.14 discusses potential bounds on aqueous solution compositions that may arise due to the formation of volatile acid-gas species, particularly HCl and HNO₃. Key concepts are described, and relevant thermodynamic and experimental data are discussed. Due to present limited understanding, no credit is taken for the potential beneficial effects of acid-gas volatilization in the analysis presented in Section 6.7.2.13. The discussion of such effects is limited to additional confidence building.

6.2 FEATURES, EVENTS, AND PROCESSES INCLUDED IN ANALYSIS

Table 6.2-1 provides a list of FEPs (that are included in TSPA-LA models) described in this analysis document, and provides specific references to sections within this document. *Technical Work Plan For: Near-Field Environment and Transport In-Drift Geochemistry Model Report Integration* (BSC 2004 [DIRS 171156], Table 3, p. 7) calls for these two TSPA-LA FEPs to be addressed by this report. The FEPs themselves are included on the LA FEP list (DTN: MO0407SEPFEP.LA.000 [DIRS 170760]).

Table 6.2-1. Included FEPs in TSPA-LA Addressed in This Document

FEP No.	FEP Name	Section Where Disposition is Described
2.1.09.28.0A	Deliquescence on Waste Package Outer surface	Section 6.7.2
2.1.09.28.0B	Deliquescence on Drip Shield Outer surface	Section 6.7.2

In essence, the treatment of each of these FEPs by this report is the same: a description of the expected chemical environment on the surface of the metal barriers. This description consists of an analysis of the presence or absence of liquid water as a function of T and RH along with an analysis of aqueous solution composition when such a solution is present. The analysis further consists of a dripping case (seepage evaporation) and a no-dripping case (deliquescence of dust), along with supporting data and other information.

6.3 IN-DRIFT PRECIPITATES/SALTS CONCEPTUAL MODEL

This scientific analysis uses the IDPS model (BSC 2004 [DIRS 169863]), which is a high-temperature Pitzer model utilizing the EQ3/6 Version 8.0 software (BSC 2003 [DIRS 162228]). This section describes that model as it is used in this analysis. The IDPS model consists of three elements. The first is the thermodynamic data file: *data0.yppf.R1* (DTN: SN0302T0510102.002 [DIRS 162572]). The second is a set of solids whose precipitation is to be suppressed (BSC 2004 [DIRS 169863], Section 6.6.2.6.4, Table 6.3; also DTN: MO0303SPAMNSUP.000 [DIRS 171426]). These solids are also identified in the text in Section 4.1.9 of the present report. The third element is a table (DTN: MO0312SPAESMUN.002 [DIRS 166329]) used to estimate uncertainties in IDPS model outputs. The IDPS model is the conceptual model used in this report, and is applied to deliquescence.

EQ3/6 Version 8.0 (BSC 2003 [DIRS 162228]; SNL 2003 [DIRS 162494]) is a package of geochemical codes. It incorporates provision for equilibrium thermodynamics and chemical kinetics. In this report, all calculations assume equilibrium thermodynamics as the controlling factor and no usage is made of the capability for treating chemical kinetics. The EQ3/6 software is not a model; rather, it is a tool to implement the IDPS model (BSC 2004 [DIRS 169863]). The IDPS model develops and utilizes the Pitzer-based supporting thermodynamic data file: *data0.yppf.R1* (DTN: SN0302T0510102.002 [DIRS 162572]), which covers a nominal temperature range of 25°C to 200°C. This data file is described in *In-Drift Precipitates/Salts Model* (BSC 2004 [DIRS 169863]). That report also presents the relevant validation for the IDPS model, which is validated to only 140°C owing primarily to limitations on the subset of the model dealing with aqueous nitrate (see discussion in Section 4.1.9).

The IDPS model (BSC 2004 [DIRS 169863]) utilizes the Pitzer (1991 [DIRS 152709]) approach to treating activity coefficients in aqueous solutions. This methodology is based on a combination of theoretical and empirical parts, the latter involving various coefficients for pairs and triplets of ions and electrically neutral solute species. This particular data file is based in part on the earlier high-temperature Pitzer models by Pabalan and Pitzer (1987 [DIRS 162096]) and Greenberg and Møller (1989 [DIRS 152684]). Those models in turn built on the 25°C Pitzer model by Harvie et al. (1984 [DIRS 118163]) for the “sea-salt” system, which was a classic in the early application of Pitzer’s equations to problems in the earth sciences. The

high-temperature IDPS (BSC 2004 [DIRS 169863]) Pitzer model in EQ3/6 can be utilized to deal with extremely concentrated solutions (e.g., ionic strength in excess of 20 molal).

The principal equations in EQ3/6 used in the present report include mass balance, electrical balance, mass action (thermodynamic equilibrium for individual chemical reactions), and activity coefficient equations. Subsidiary equations describe the temperature dependencies of parameters appearing in the mass action equations (equilibrium constants) and activity coefficient equations (e.g., and specifically in the present instance, the Pitzer interaction coefficients). These equations are solved using a hybrid Newton-Raphson method. The mathematical underpinnings of the model and the numerical methods employed are described in detail in *Software User's Manual, EQ3/6, Version 8.0* (SNL 2003 [DIRS 162494]). Furthermore, the model employed is not uniquely used by the present report, but also by *In-Drift Precipitates/Salts Model* (BSC 2004 [DIRS 169863]) and *Engineered Barrier System: Physical and Chemical Environment* (BSC 2004 [DIRS 169860]). The more general aspects of the model (e.g., application of equilibrium thermodynamics to aqueous geochemical systems) are also commonly discussed in textbooks and monographs in the geochemical literature (e.g., Garrels and Christ 1990 [DIRS 144877]; Stumm and Morgan 1996 [DIRS 125332]).

In the present scientific analysis, a submodel for thermodynamic activity coefficients valid in aqueous salt solutions extending to high concentration over the approximate temperature range 25°C to 140°C is essential. The “high temperature” Pitzer approach implemented in the IDPS model (BSC 2004 [DIRS 169863]) is used here to meet that need. EQ3/6 version 8.0 can use other activity coefficient submodels that are accurate only in fairly dilute solutions. However, those submodels are not used in the present report.

A key parameter in the EQ3/6 calculations is the activity of water (a_w), which is closely related to the RH. In the framework of thermodynamics, this is the product of the mole fraction of water and a mole fraction activity coefficient (calculated from the aqueous species activity coefficient model, here one based on Pitzer's equations). Conceptually, however, the activity of water is equivalent to:

$$a_w = f_w / f_w^o \quad (\text{Eq. 6.3-2})$$

where f_w is the fugacity of water vapor and f_w^o is the fugacity of water vapor in the standard state (in equilibrium with pure liquid water; this is different from the f_i^o noted in Section 4.1.25 that is fixed at 1 bar, despite the similarity in notation).

The relative humidity (RH), when defined on a fractional or decimal basis, has a closely analogous relationship with the partial pressure of water:

$$RH_{frac} = p_w / p_w^o \quad (\text{Eq. 6.3-3})$$

where p_w is the partial pressure of water vapor (e.g., above a sample of aqueous solution) and p_w^o is the partial pressure of water vapor in the standard state (e.g., pure water) at the same

temperature (this is different from the p_i^o noted in Section 4.1.25 that is fixed at 1 bar, despite the similarity in notation). For the purposes of this report, it may be taken that:

$$f_w / f_w^o = p_w / p_w^o \quad (\text{Eq. 6.3-4})$$

and hence that:

$$RH_{frac} = a_w \quad (\text{Eq. 6.3-5})$$

Equivalently, for the RH expressed as a percent, one has that:

$$RH(\%) = 100a_w \quad (\text{Eq. 6.3-6})$$

The IDPS conceptual model for deliquescence in this report is one in which salt minerals present on the drip shield and waste package outer barrier surfaces deliquesce during the cool down period due to decreasing temperature and rising relative humidity. These salt minerals are assumed to be present in dust deposited on the metal surfaces during the ventilation period (see Section 5.1). This dust will consist of local and regional dusts entrained in the ventilation flow as well as dusts originating in the repository as a result of tunneling and other operations. Negligible seepage occurs during the ventilation period owing to the dryness of the ventilation air (rock in the immediate vicinity of the drift wall is very dry). Negligible formation of salts on the metal barrier surfaces by evaporation of seepage water is expected in this period. Conditions in and adjacent to the drifts become even drier during the heating-up phase that follows closure of the repository.

In the cool-down phase, temperatures drop and local RH in and adjacent to the drifts increases. At some point in this phase, deliquescence may occur. The first instance of deliquescence is likely to be for the no-dripping (dust) case. Here no seepage has yet occurred in the cool-down phase. Upon the initiation of seepage, another case (the dripping case) becomes possible. Evaporation of seepage water dripping onto the metal surfaces deposits new salts, which may differ from those present in the dust. Some seepage may be aerosolized upon dripping, and transported by the convecting gas phase to a wider locus on the metal barrier surfaces, with the same effect. With continued cool down, these seepage-related salts may also deliquesce.

The IDPS conceptual model takes into account certain interactions between the gas phase, salt minerals, and deliquescing solutions. The transfer of water from vapor to aqueous solution is implicit. However, other volatiles also need to be considered. Conditions are assumed to be mildly oxidizing due to the presence of oxygen gas in the air fraction. The presence of CO₂ gas is also an important factor as this introduces an additional chemical component affecting the composition of any aqueous solution formed by deliquescence. In the interpretation of mineral assemblages, this gas functions much like an extra mineral. Lesser, but reactive, trace gases such as HCl and HNO₃ are other factors. Their potential behavior is discussed as part of the analysis presented in this report. Such acid-gases may be produced from the mixture of salts and water on the metal barrier surfaces. It is assumed that these are dispersed to the drift wall (with no inhibition by the drip shield, which is not designed to be a vapor barrier) and not generate

adverse conditions. Potential beneficial effects of such generation and dispersal are noted, but no credit for such effects is taken in the deliquescence analysis as discussed in Section 6.7.2.13.

6.4 CONSIDERATION OF ALTERNATIVE CONCEPTUAL MODELS

No alternative conceptual models were considered in this report. *In-Drift Precipitates/Salts Model* (BSC 2004 [DIRS 169863] Section 6.5) discusses six alternative conceptual models and should be consulted for further information.

The model used in this report for the analysis of deliquescence on metal barrier surfaces is the IDPS model. Conceptually, this is an equilibrium thermodynamics model incorporating provision for dealing with concentrated aqueous salt solutions. Deliquescence is generally understood to be a phenomenon controlled by equilibrium thermodynamics (e.g., Tang and Munkelwitz 1993 [DIRS 163124]; Tang and Munkelwitz 1994 [DIRS 163125]; Greenspan 1977 [DIRS 104945]; Ge et al. 1998 [DIRS 162165]; Ansari and Pandis 1999 [DIRS 162167]); and Pilinis 1999 [DIRS 163126]).

Other possible code–database combinations capable of calculations similar to those described in this report exist (though none are qualified for use on the YMP). One is a SOLGASMIX/Pitzer model used in thermodynamic modeling of Savannah River evaporators (Weber 2001 [DIRS 163110]). This model/database operates over a somewhat limited temperature range (25°C to 125°C), with a partial overlap with the EQ3/6 version 8.0 high-temperature Pitzer model in terms of the range of chemical components. The mathematical form of the temperature dependence of Pitzer interaction coefficients is almost identical: 25°C-centered with the same terms as in the formulation in the EQ3/6 model, but in a different order. The data given by Weber (2001 [DIRS 163110]) are in a form that could be used directly in EQ3/6.

Another possible code–database is the Environmental Simulation Program (ESP) of OLI Systems, Inc., Morris Plains, New Jersey. Pabalan et al. (2002 [DIRS 163067]) used ESP in a study conducted for the Nuclear Regulatory Commission of salt formation on the metals barriers in the Yucca Mountain repository. As described by Pabalan et al. (2002 [DIRS 163067], p. 10), the version 6 of ESP that was used has an ionic strength limit of 30 molal, which restricted the applicability of the calculations. ESP uses the Bromley (1973 [DIRS 163123]) and Pitzer (1991 [DIRS 152709]) approaches to deal with the activity coefficients. The thermodynamic database appears to be proprietary, as little detailed information on it seems to be available in the open literature.

No alternative code–database combination appear to be viable choices for YMP studies. In most cases, the scope of possible calculations is not a good match to YMP needs in terms of the permissible temperature range or the component sets covered in the supporting thermodynamic data, owing to a different set of target applications. Most of the potential alternatives are commercial products, with the supporting thermodynamic databases being proprietary with only limited or no open documentation. EQ3/6 is advantageous as it is a YMP standard with a history of qualified versions, and it is a familiar tool to people working on the YMP. The data files are nonproprietary, allowing them to be developed as needed.

Although other such “models” exist, it must be noted that these do not represent alternative *conceptual* models. All such code–data file combinations are tools for making thermodynamic calculations. Most of these that are capable of treating concentrated electrolyte solutions use some form of the Pitzer approach. While some do use or allow other approaches for this particular aspect, all these models are calibrated to explain what is largely the same set of physical chemistry measurements (including but not limited to osmotic coefficients, vapor pressures, and solubilities). Thus, to the extent that these models are equally accurate and overlapping in scope, they predict the same results.

Even for a given “model” (code–data file combination), strikingly different results can be obtained by using different assumptions regarding defining problem inputs. For example, if evaporation is simulated as merely the removal of solvent water, a given groundwater might appear to evolve into calcium chloride brine. However, if the calculation also factors in reasonable limits on the partial pressures of acid–gas volatiles such as CO₂ and HCl, the result could be very different (no calcium chloride brine).

6.5 ANALYSIS FORMULATION

The details of the IDPS model formulation is described in *Software User’s Manual, EQ3/6, Version 8.0* (SNL 2003 [DIRS 162494]) and *In-Drift Precipitates/Salts Model* (BSC 2004 [DIRS 169863]).

Certain details regarding the setup of the EQ3/6 runs for this report are noted here. Fundamentally, two different kinds of runs are made. One set is used to calculate the deliquescence RH of various salt minerals and salt mineral assemblages from 25°C to the IDPS model validation limit of 140°C, and to explore the IDPS model response for temperatures as high as 200°C. The other set is used to calculate aqueous solution composition and RH moving off the eutectic point of selected salt mineral assemblages. A run in this set would show how the solution composition and RH change when one or more of the minerals in an assemblage dissolves completely.

The salt deliquescence runs are made for sets of salt mineral assemblages that are selected as described in Section 6.7.2. In a typical instance, the deliquescence RH for a given salt mineral or assemblage of such minerals is determined over a temperature range starting at 25°C and potentially extending to 200°C (known to be above the IDPS model validation limit of 140°C). The initial part of the calculational approach is actually one in which salt minerals are added to originally dilute liquid water to the point of saturation (the eutectic point), rather than one in which water (in the form of vapor) is added to initially dry minerals (where the first formed liquid is also at the eutectic point). The temperature is then increased in the presence of excess amounts of the salt minerals, to assure that saturation is maintained. The actual starting point of a typical run is at 20°C. The salt mineral masses are added rapidly by specification of high rates of input (relative to the rate of increase of temperature), such that total saturation occurs prior to achieving a temperature of 25°C. Upon saturation, the sufficient reserve masses of the salt minerals are present to maintain saturation with further increase in temperature. The amounts of salt minerals to add are chosen to achieve saturation and provide such reserve masses. Sufficiency for this purpose is determined by examination of the code output, with adjustments made as necessary. Output data for temperatures below 25°C are discarded.

The other set of runs is used to calculate aqueous solution composition and RH moving off the eutectic point of selected salt mineral assemblages. The results of such a run show how aqueous solution and RH change when one or more of the minerals in a deliquescent salt mineral assemblage becomes completely dissolved. The system then moves off the corresponding eutectic point, and the deliquescence RH of that assemblage no longer governs the actual RH. In one sense, the system consisting of aqueous solution plus remaining minerals continues to deliquesce. In general, RH increases, and the continued dissolution of remaining salt minerals raises the concentrations of the corresponding aqueous solutes. The actual calculation can be thought of as running in reverse (toward instead of away from the eutectic point). A simple example of such a run would be an isothermal one for the NaCl-NaNO₃ system, in which NaNO₃ is added to a halite (NaCl) saturated solution (initially in the pure NaCl-H₂O system) until the solution becomes also saturated with soda niter (NaNO₃; also known as nitratine). This is the eutectic point for the NaCl-NaNO₃ assemblage. The calculation for this assemblage is completed by a complementary run in which NaCl is added to a soda niter saturated solution (initially in the pure NaNO₃-H₂O system) until the same eutectic point is reached. Isothermal calculations of this type are repeated at various temperatures to build a complete picture.

In the actual code calculations, the pressure is fixed at 1 atm (101.325 kPa) for temperatures up to 100°C. For temperatures above 100°C, the pressure is fixed at the value of the vapor pressure of pure water at the given temperature. This condition is built into the software as an integral part of the high-temperature IDPS Pitzer model. To determine the point at which the vapor pressure of water exceeds a reasonable limit on the total pressure in the repository, the following criterion is applied to the code output from both sets of runs.

First, the actual water vapor pressure (p_w) is as calculated from the following relation:

$$p_w = a_w p_{w,sat} \quad (\text{Eq. 6.5-1})$$

Here $p_{w,sat}$ is the vapor (saturation) pressure of pure water reported in the code output. This is functionally equivalent to p_w^o noted earlier. Results for actual water vapor pressures above 0.90 bar (90 kPa) are discarded. Actual water vapor pressures are limited to something very close to the atmospheric pressure at the repository elevation. Calculated values that exceed this pressure imply dryout (as is discussed in Sections 6.7.2.2 and 6.7.2.3). The value of 0.90 bar (90 kPa) is a reasonable limit (see the assumption in Section 5.3). The mean (over time) ambient pressure over the range of repository elevation is calculated in Section 6.7.2.1 (Table 6.7-1) to be 89.1±0.6 kPa. Actual measurements at a single location in the tunnel noted in Section 6.7.2.1 (Table 6.7-2) range from 87.1 to 90.9 kPa. This greater range reflects temporal variation associated with weather. The corresponding mean value is 88.87 kPa, with a standard deviation of 0.42 kPa. The mean plus two standard deviations is 89.71 kPa, which demonstrates the relative infrequency of the observed maximum 90.9 kPa.

In the majority of the EQ3/6 calculations, no actual values or limits on the partial pressure of CO₂ are included as inputs. CO₂ is not a factor in most of the systems for which calculations are made (e.g., NaCl-KNO₃-NaNO₃-H₂O). Runs involving bicarbonate or carbonate salts are examined to see if unrealistic pCO₂ values are generated (e.g., outside the expected range from THC calculations, and anything above the expected total pressure in the drifts). In some

instances, unrealistic values are obtained, and subsequent calculations are made in which the $p\text{CO}_2$ is set to a specified value. These calculations are called out in Section 6.7.2.

The IDPS model Pitzer data file: *data0.ypf.R1* (DTN: SN0302T0510102.002 [DIRS 162572]; BSC 2004 [DIRS 169860]) is like most EQ3/6 data files in that it contains some data that extend over the entire nominal temperature range of the data file (here 25°C to 200°C; known to be above the IDPS model validation limit of 140°C) and other data that are limited to some lesser range, commonly just at 25°C. For a number of the less common salt minerals reported by Harvie et al. (1984 [DIRS 118163]) included on this data file, there are only 25°C data. Valid high temperature calculations cannot be made for such minerals. Calculations in this report involving higher temperatures exclude such minerals by directives on the corresponding EQ3/6 input files. An option is selected to suppress all minerals on the data file except specified exceptions. Many of the excluded minerals are double salts or complex hydrates whose presence in addition to or in place of other, generally simpler salts (for which higher temperature data are available) would likely cause relatively minor changes. Furthermore, such phases tend to be less stable than simpler salts at elevated temperature. A fair number of the excluded salt minerals also appear to be rare or uncommon in the geologic environment. Therefore, the set of minerals for which high temperature data are available is sufficient for the purposes of this report.

The minerals considered in the calculations in this report (except the 25°C dust leachate evaporation calculations in Section 6.7.2.10) are listed in Table 6.5-1. The set of minerals in Table 6.5-1 consists of all the minerals in the data file that are considered potentially relevant and for which the thermodynamic data are not restricted to 25°C. This list includes those minerals allowed to precipitate, but such minerals actually appear in the calculations if thermodynamics favors their formation. Only a subset of these minerals typically appears in a given calculation. Some additional minerals do appear in the 25°C dust leachate evaporation calculations in Section 6.7.2.10. Note that none of the phases listed in the baseline suppression group in Section 4.1.9 are allowed to precipitate in any of the calculations in this report.

Table 6.5-1. Considered Salt Minerals for Which Thermodynamic Data Extend to High Temperature

Mineral	Formula
Anhydrite	CaSO_4
Antarcticite	$\text{CaCl}_2 \cdot 6\text{H}_2\text{O}$
Arcanite	K_2SO_4
Artinite	$\text{Mg}_2\text{CO}_3(\text{OH})_2 \cdot 3\text{H}_2\text{O}$
Bischofite	$\text{MgCl}_2 \cdot 6\text{H}_2\text{O}$
Brucite	$\text{Mg}(\text{OH})_2$
CaBr_2	CaBr_2
CaCl_2	CaCl_2
$\text{CaCl}_2 \cdot 2\text{H}_2\text{O}$	$\text{CaCl}_2 \cdot 2\text{H}_2\text{O}$
Calcite	CaCO_3
$\text{CaCl}_2 \cdot 4\text{H}_2\text{O}$	$\text{CaCl}_2 \cdot 4\text{H}_2\text{O}$

Table 6.5-1. Considered Salt Minerals for Which Thermodynamic Data Extend to High Temperature (Continued)

Mineral	Formula
Ca(NO ₃) ₂	Ca(NO ₃) ₂
Ca(NO ₃) ₂ ·2H ₂ O	Ca(NO ₃) ₂ ·2H ₂ O
Ca(NO ₃) ₂ ·3H ₂ O	Ca(NO ₃) ₂ ·3H ₂ O
Ca(NO ₃) ₂ ·4H ₂ O	Ca(NO ₃) ₂ ·4H ₂ O
Carnallite	KMgCl ₃ ·6H ₂ O
Carobbite	KF
Chloromagnesite	MgCl ₂
Darapskite	Na ₃ SO ₄ NO ₃ ·H ₂ O
Epsomite	MgSO ₄ ·7H ₂ O
Fluorite	CaF ₂
Glauberite	Na ₂ Ca(SO ₄) ₂
Gypsum	CaSO ₄ ·2H ₂ O
Halite	NaCl
Hemihydrate	CaSO ₄ ·0.5H ₂ O
Hexahydrate	MgSO ₄ ·6H ₂ O
Hydromagnesite	Mg ₅ (CO ₃) ₄ (OH) ₂ ·4H ₂ O
KBr	KBr
K ₂ CO ₃	K ₂ CO ₃
Kieserite	MgSO ₄ ·H ₂ O
Labile Salt	Na ₂ Ca ₅ (SO ₄) ₆ ·3H ₂ O
Leonhardtite	MgSO ₄ ·4H ₂ O
MgBr ₂	MgBr ₂
MgCl ₂ ·H ₂ O	MgCl ₂ ·H ₂ O
MgCl ₂ ·2H ₂ O	MgCl ₂ ·2H ₂ O
MgCl ₂ ·4H ₂ O	MgCl ₂ ·4H ₂ O
Mg(NO ₃) ₂	Mg(NO ₃) ₂
MgOHCl	MgOHCl
Mirabilite	Na ₂ SO ₄ ·10H ₂ O
NaBr	NaBr
Nahcolite	NaHCO ₃
Natrite	Na ₂ CO ₃
Nesquehonite	MgCO ₃ ·3H ₂ O
NH ₄ Cl	NH ₄ Cl
(NH ₄) ₂ SO ₄	(NH ₄) ₂ SO ₄
Niter	KNO ₃
Pentahydrate	MgSO ₄ ·5H ₂ O
Pentasalt	K ₂ Ca ₅ (SO ₄) ₆ ·H ₂ O
Portlandite	Ca(OH) ₂
Sellaite	MgF ₂
Sepiolite	Mg ₄ Si ₆ O ₁₅ (OH) ₂ ·6H ₂ O
SiO _{2(am)}	SiO _{2(am)}
Soda Niter	NaNO ₃
Sylvite	KCl

Table 6.5-1. Considered Salt Minerals for Which Thermodynamic Data Extend to High Temperature (Continued)

Mineral	Formula
Syngenite	$K_2Ca(SO_4)_2 \cdot H_2O$
Thenardite	Na_2SO_4
Thermonatrite	$Na_2CO_3 \cdot H_2O$
Villiaumite	NaF

Source: Output DTN: LL040903723121.042, EQ3/6 input files.

In general, when it is said that a mineral from the list in Table 6.5-1 is used, the intended sense is that it is specified as a “reactant” phase in one or more of the reported runs. A “reactant” (in the reaction-path sense) is a chemical species or phase that is “added” to an aqueous system, where it may react with the aqueous solution. When it is said that a mineral “appears” in the system, it means that the phase is either a “reactant” or that it appears as a secondary product of “reactants” with the aqueous solution. In the EQ3/6 calculations in this report, only some of the minerals in Table 6.5-1 are used as “reactants,” but any of these minerals has the potential to appear as a secondary or “product” mineral.

The actual number of known salt minerals far exceeds that presented in Table 6.5-1. Many of the known salt minerals are so-called “double” salts, implying the presence of at least two cations or two anions. Some double salts are included in the list, such as syngenite ($K_2Ca(SO_4)_2 \cdot H_2O$) and darapskite ($Na_3SO_4NO_3 \cdot H_2O$). However, thermodynamic data are lacking for many known salt minerals (generally double salts), even for 25°C. Nevertheless, the set of minerals represented in the table is sufficient for the purpose of this report.

EQ3/6 runs for specified salt mineral assemblages are actually defined in terms of the “reactant” mineral sets. Thus, the runs for the NaCl-KNO₃ assemblage use halite (NaCl) and niter (KNO₃) as “reactants.” However, other phases are permitted to form if the thermodynamics favors this. This is a choice made in setting up the runs. Other phases could have been disallowed, but this would not be realistic in that all of the phases included in Table 6.5-1 form readily. This is consistent with equilibrium thermodynamics. In the case of the NaCl-NaNO₃ (halite–oda niter) system at 25°C and higher, no other salt minerals appear. However, in the NaCl-KNO₃ (halite–niter) system, there is a region in which KCl (sylvite) is stable. These examples are included in calculations presented in Section 6.7.2.9.

An important aspect of the high-temperature IDPS Pitzer model used in this report is the ability to predict RH and brine compositions for the case of complex salt mixtures. If all one needed are the data for single salt systems (e.g., NaCl-H₂O or CaCl₂-H₂O), one could simply look the data up in a handbook (e.g., the data in Tables 4.1-5, 4.1-6, 4.1-7, 4.1-8, and 4.1-9) or perform a few measurements in the laboratory.

6.5.1 Mathematical Description of the In-Drift Precipitates/Salts Conceptual Model

Software User’s Manual, EQ3/6, Version 8.0 (SNL 2003 [DIRS 162494]) and *In-Drift Precipitates/Salts Model* (BSC 2004 [DIRS 169863]) provide descriptions of the relevant mathematics not covered in Section 6 of this report. Such mathematical relations describe mass balance, charge balance, mass action (equilibrium or partial equilibrium), thermodynamic

activity coefficients (including the Pitzer equations), and still more relations describing the temperature dependence of generally relevant thermodynamic parameters (e.g., equilibrium constants, Pitzer parameters). *Software User's Manual, EQ3/6, Version 8.0* also addresses kinetic rate laws and parameters such as surface areas that are required for kinetic modeling (SNL 2003 [DIRS 162494]). However, the IDPS model used in this report does not utilize those relations.

6.5.2 Analysis Inputs

The relevant IDPS model inputs for the EQ3/6 calculations in this report include the supporting high-temperature Pitzer data file: *data0.ypf.R1* (DTN: SN0302T0510102.002 [DIRS 162572]; BSC 2004 [DIRS 169860]), the list of baseline suppressed minerals noted in Section 4.1.9, the list of considered minerals in Table 6.5-1, and relevant salt mineral assemblages drawn from the latter list (these assemblages are determined in Section 6.7.2.10). The pressure limit of 0.90 bar (Section 6.5) is a criterion applied to filtering the EQ3/6 outputs.

6.5.3 Summary of Computational Framework

The computational framework used in this analysis is based on equilibrium thermodynamics and the IDPS model, a high-temperature (nominally from 25°C to the IDPS model limit of 140°C, but in some instances evaluated to 200°C) thermodynamic model that uses Pitzer's equations for the activity coefficients of aqueous species. The IDPS model is described in considerable detail in *Software User's Manual, EQ3/6, Version 8.0* (SNL 2003 [DIRS 162494]) and in *In-Drift Precipitates/Salts Model* (BSC 2004 [DIRS 169863]). A hybrid Newton-Raphson method is used to solve a system of mass balance, charge balance, mass action, and activity coefficient equations. The high-temperature IDPS model is capable of application to extremely concentrated salt solutions (e.g., ionic strength well in excess of 20 molal).

6.6 NOT USED

6.7 ANALYSIS RESULTS

6.7.1 Overview

Various analyses are presented in this subsection. The first deals with basic constraints on deliquescence phenomena with emphasis on conditions at the repository. For example, the first calculation describes the atmospheric pressure at the elevation of the repository. The dryout condition imposed by the limit of total pressure on actual water vapor pressure is dealt with in detail. Other background information on deliquescence is presented. EQ3/6 calculations are presented of deliquescence RH for a number of single salt minerals, of salt mineral pairs, and higher order salt mineral assemblages. Dust leachate analyses from the tunnels of the repository are examined. Salt mineral assemblages reconstructed by EQ3/6 calculations of these leachates are examined. Unique salt mineral assemblages are identified, and the key sub-assemblages that control the deliquescence RH in these reconstructed assemblages are determined. An analysis for the no-dripping (dust deliquescence) case and for the dripping (seepage-related) case is created. The potential roles of acid-gas generation from water and salts at elevated temperature are also discussed and analyzed from a thermodynamic point of view. This process may have beneficial effects, though some possible effects could be deleterious, such as concentration in

condensate on a metal barrier surface (Pulvirenti et al. 2003 [DIRS 163184]). It is assumed in the present analysis (Section 5.7) that acid-gas species will instead be effectively transported by convection and diffusion to the drift wall. It is noted, however, that such condensation would tend to be facilitated by the existence of any “cold traps” on the metal barrier surfaces.

6.7.2 Discussion of Results

6.7.2.1 Atmospheric Pressure at the Repository Elevation

The atmospheric pressure affects the boiling point of pure water and aqueous salt solutions. The ambient atmospheric pressure at the elevation of the repository is a function of elevation, temperature, and the effective molecular weight of the ambient “air.” The atmospheric pressure P can be calculated from Equation 6.7.2.1-1 (Fleagle and Businger 1980 [DIRS 108591]; introduced in Section 4.1.15):

$$P = P(0)\exp(-gz/R_m T). \quad (\text{Eq. 6.7.2.1-1})$$

Here $P(0)$ is the atmospheric pressure at sea level, g is acceleration due to gravity, z is elevation, T is the absolute temperature, and R_m is the gas constant, R , divided by the effective molecular weight of air.

Per the data in Table 4.1-2 (Section 4.1.1), $P(0)$ is 1,013.2500 mbar (Weast and Astle 1981 [DIRS 100833], p. F-168), or 1.01325 bar, or 101.325 kPa (from the data in the table for the definitions of the bar, the dyne, the Newton, and the Pascal, one may determine that 1 bar equals 100 kPa). The acceleration due to gravity g is 980.7 cm/s² (Weast and Astle 1981 [DIRS 100833], p. F-144). Here that is converted to 9.807 m/s² and rounded up to 9.81 m/s² for use in the calculations that follow. The gas constant, R , is given in Table 4.1-2 as 8.20562×10^{-2} m³-atm/kmol-K (Weast and Astle 1981 [DIRS 100833], p. F-204), equivalent to 8.20562×10^{-5} m³-atm/mol-K. Noting that 1 atm = 1.01325 bar and that 1 bar = 100 kPa, R can also be expressed as 8.20562×10^{-5} m³-atm/mol-K divided by 1.01325 atm/bar equals 8.09832×10^{-5} m³-bar/mol-K. The effective molecular weight of air is 28.966 g/mol (Weast and Astle 1981 [DIRS 100833], p. F-168). Hence, the constant R_m is 8.09832×10^{-5} m³-bar/mol-K divided by 28.966 g/mol, or 2.79580×10^{-6} m³-bar/g-K. However, R_m requires additional units conversion for consistency with g expressed in m/s². Since 1 bar = 10⁶ dyn/cm² (Weast and Astle 1981 [DIRS 100833], p. F-82) and 1 dyne = 1 g-cm/s² (Weast and Astle 1981 [DIRS 100833], p. F-90), one may calculate that 1 bar = 10⁶ dyn/cm² × 1 g-cm/s²-dyn = 10⁶ g/cm-s² or 10⁸ g/m-s². Then $R_m = 2.79580 \times 10^{-6}$ m³-bar/g-K times 10⁸ g/m-s²-bar = 279.580 m²/s²-K.

The elevation for the repository ranges from 1,038 to 1,107 m (BSC 2003 [DIRS 161727]; Section 4.1.2). Calculated pressures for the lowest elevation, the highest, and the midpoint elevation of 1,072.5 m are shown in Table 6.7-1 for temperatures of 288.15, 293.15, and 298.15K (15°C, 20°C, and 25°C, respectively). These temperatures span a reasonable range (note: the atmosphere is not an isothermal column and most of the mass is at higher altitude and generally cooler than at ground level). These pressures range from 88.5 to 89.7 kPa. More succinctly, the calculated ambient pressure can be described as 89.1±0.6 kPa (where the “±0.6 kPa” is a range limit, not a standard deviation).

Table 6.7-1. Calculated Atmospheric Pressure at the Repository Elevation

Pressure (P), kPa		Elevation (z), meters		
		1,038	1,072.5	1,107
Temperature (T), K	288.15	89.3	88.9	88.5
	293.15	89.5	89.1	88.8
	298.15	89.7	89.3	88.9

Source: Output DTN: LL030500612251.059, calculated in spreadsheet: *AmbRepPressure.xls*.

D&E/PA/C IED Subsurface Facilities (BSC 2004 [DIRS 164519]) now specifies the minimum elevation as 1,039 m. The effect of this is insignificant. Using, for example the data in Table 6.7-1 for the temperature 298.15K, the derivative of pressure with respect to elevation is $dP/dz = (88.9 - 89.7)/(1,107 - 1,038)$ kPa/m = -0.0116 kPa/m. The difference in pressure between 1,038 m and 1,039 m would, therefore, be about 0.012 kPa, whereas the data in Table 6.7-1 are only given to the nearest tenth of a kPa.

Direct measurements of barometric pressure at the repository level are reported in DTN: GS030108312242.001 [DIRS 163118]. The pressure was measured twice at each of 12,541 times over the period June 22, 2000 to August 26, 2002. Table 6.7-2 provides a summary of these measurements. The mean value of 88.87 kPa compares well with the calculated values of 89.1 ± 0.6 kPa. The minimum and maximum values (87.1 and 90.9 kPa) lie slightly outside the range of the calculated results (88.5 to 89.7 kPa) and reflect temporal variation associated with weather.

Table 6.7-2. Measured Atmospheric Pressure in the Repository

Datum	Pressure mbar	Pressure kPa
Mean	888.7	88.87
Standard Deviation	4.2	0.42
Minimum	871	87.1
Maximum	909	90.9

Source: Output DTN: LL030500612251.059, calculated in *YMBarometricPressure.xls*.

Further analysis (e.g., of deliquescence) requires establishing an expected maximum pressure in the repository, exclusive of very short time scales (e.g., hours, days). A reasonable value based on the preceding analysis is 90 kPa. Although actual pressure values measured at the repository have occasionally exceeded this limit, these values are clearly reflective of short-term meteorological effects. The 90 kPa value exceeds any of the expected mean (e.g., long-term) pressure values shown in Table 6.7-1. It is also greater than the mean plus two standard deviations shown in Table 6.7-2.

6.7.2.2 Vapor Pressure of Pure Water as a Function of Temperature

Water vapor pressure as a function of temperature is listed in Table 4.1-4 (Weast and Astle 1981 [DIRS 100833], pp. D-168 and D-169). The vapor pressure is given in mm Hg. The same data are presented in Table 6.7-3 after conversion to units of Torr and kPa). Note that 1 mm Hg = 1

Torr (Weast and Astle 1981 [DIRS 100833], p. F-297, cited in Table 4.1-2). The vapor pressure is obtained in kPa by applying the conversion factor 760 Torr = 101.325 kPa. Section 6.7.2.1 states that 1 atm = 1.01325 bar and that 1 bar = 100 kPa; therefore, 1 atm = 101.325 kPa. Noting that 1 atm also equals 760 Torr (Weast and Astle 1981 [DIRS 100833], p. F-282, cited in Table 4.1-2), 760 Torr = 101.325 kPa.

Table 6.7-3. Vapor Pressure of Pure Water as a Function of Temperature

Temp (°C)	kPa	Torr	Temp (°C)	kPa	Torr
0	0.6105	4.579	155	543.406	4075.88
5	0.8723	6.543	160	618.0825	4636.00
10	1.2278	9.209	165	700.7637	5256.16
15	1.7049	12.788	170	792.0575	5940.92
20	2.3378	17.535	175	892.4706	6694.08
25	3.1672	23.756	180	1,002.611	7520.20
30	4.2429	31.824	185	1,123.086	8423.84
35	5.6229	42.175	190	1,255.011	9413.36
40	7.3759	55.324	195	1,398.386	10,488.76
45	9.5832	71.88	200	1,554.427	11,659.16
50	12.3337	92.51	205	1,723.741	12,929.12
55	15.7374	118.04	210	1,907.24	14,305.48
60	19.9157	149.38	215	2,105.534	15,792.80
65	25.0033	187.54	220	2,319.228	1,7395.64
70	31.1574	233.7	225	2549.54	1,9123.12
75	38.5435	289.1	230	2,796.874	2,0978.28
80	47.3428	355.1	235	3,062.143	2,2967.96
85	57.8086	433.6	240	3,346.461	2,5100.52
90	70.0956	525.76	245	3,650.537	2,7381.28
95	84.5130	633.9	250	3,975.385	2,9817.84
100	101.3250	760.00	255	4,322.018	3,2417.80
105	120.7994	906.07	260	4,691.348	3,5188.00
110	143.2629	1,074.56	265	5,083.982	3,8133.00
115	169.0501	1,267.98	270	5,501.036	4,1261.16
120	198.5357	1,489.14	275	5,943.623	4,4580.84
125	232.1049	1,740.93	280	6,413.366	4,8104.20
130	270.1325	2,026.16	285	6,911.176	5,1838.08
135	312.9423	2,347.26	290	7,439.282	5,5799.20
140	361.4263	2,710.92	295	7,998.596	5,9994.40
145	415.5338	3,116.76	300	8,590.334	6,4432.80
150	476.0249	3,570.48	—	—	—

Source: Output DTN: LL030500712251.060, *WaterPressureTable.xls*.

The total pressure on an open system is often effectively fixed. This is the case at the earth's surface, where that pressure is a function of altitude as discussed in Section 6.7.2.1. When the vapor pressure of pure water becomes very close to the imposed total pressure, boiling occurs. Thus, at sea level, where the atmospheric pressure is 101.325 kPa, pure water boils at 100°C.

6.7.2.3 Vapor Pressure of Water as a Function of Temperature and Water Activity

The vapor pressure of water over aqueous salt solutions is reduced from that corresponding to pure water. Recall that the RH is defined by $RH\% = 100 p_w / p_w^o$, where p_w = the vapor pressure (partial pressure) of water, and p_w^o = vapor pressure over pure liquid water. Therefore, the vapor pressure of water is related to the vapor pressure of pure water by:

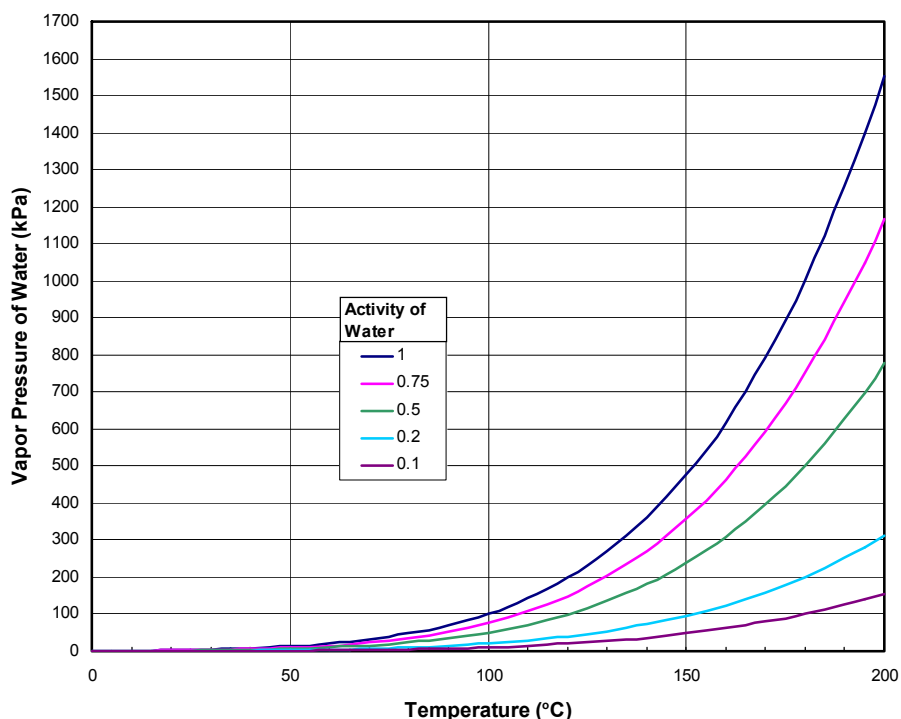
$$p_w = \left(\frac{RH\%}{100} \right) p_w^o \quad (\text{Eq. 6.7.2.3-1})$$

Because the RH expressed as a fraction is equivalent to the thermodynamic activity of water (a_w), this relation may also be expressed as (Equation 6.5-1, using slightly different notation):

$$p_w = a_w p_w^o \quad (\text{Eq. 6.7.2.3-2})$$

The more concentrated a solution containing a single dissolved salt is, the lower the activity of water. Quantitatively, the reduction of water activity depends on a number of factors, including the identity of the salt (or for a mixture, the identities of the salts and their relative proportions) and the temperature. At any given temperature, the activity of water achieves a minimum value when the solution becomes saturated with respect to some mineral corresponding to the single dissolved salt, or in the case of mixtures to saturation with a so-called eutectic mineral assemblage. Such a minimum water activity corresponds to the deliquescence RH of the single salt or salt mineral assemblage, when the deliquescence RH is expressed as a fraction.

The data for the vapor pressure of pure water in Table 6.7-3 are used in conjunction with Equation 6.7.2.3-2 to calculate the vapor pressure curves for constant water activities of 1.0, 0.75, 0.50, 0.20, and 0.10. The results are shown in Figure 6.7-1. The curve for unit water activity corresponds to the vapor pressure of pure water. The successively lower curves correspond to successively lower water activities. In general, the activity of water is not constant as a function of temperature for real saturated salts. The 0.75 curve is, as is shown in Section 6.7.2.4, a fairly accurate representation of the vapor pressure of water over a saturated sodium chloride (halite) solution. The 0.20 curve is a crude approximation of the vapor pressure over a saturated calcium chloride solution. The 0.10 curve is a fair approximation of the vapor pressure of a saturated solution of lithium bromide. This represents an extreme case of low water activity for a solution saturated with a single salt (or a eutectic assemblage).



Source: Output DTN: LL040601512251, *WaterPressureTableRev1.xls*.

NOTES: The condition of constant water activity with changing temperature is not in general a characteristic of real saturated salts. The activity of water for a solution saturated with a single salt or a eutectic salt mineral assemblage is not generally constant with respect to temperature. The curves shown here are only intended to illustrate the effect of the activity of water on water vapor pressure.

Figure 6.7-1. Vapor Pressure of Water as a Function of Temperature and Water Activity (Water Activity Values are Shown in the Legend)

6.7.2.4 Deliquescence Relative Humidity as a Function of Temperature for Several Salt Minerals

Table 4.1-8 is reproduced as Table 6.7-4. This table lists the deliquescence RH as a function of temperature for several salt minerals. Note that the deliquescence RH of NaCl (halite) is fairly constant in the 74 to 76 percent range. The deliquescence RH of K_2CO_3 is a nearly constant 43.1 to 43.2 percent, and the deliquescence RH of K_2SO_4 runs mainly in the 96 to 99 percent range. In the case of most of the other salts included in this table, the deliquescence RH generally decreases with increasing temperature. That is the case for example for KCl (88.61 percent at 0°C; 78.50 percent at 90°C) and $NaNO_3$ (78.57 percent at 5°C; 65.00 percent at 90°C). Increases with temperature are also seen, though less pronounced. The deliquescence RH of KF increases slightly starting at about 55°C, as does that of NaCl starting near 60°C.

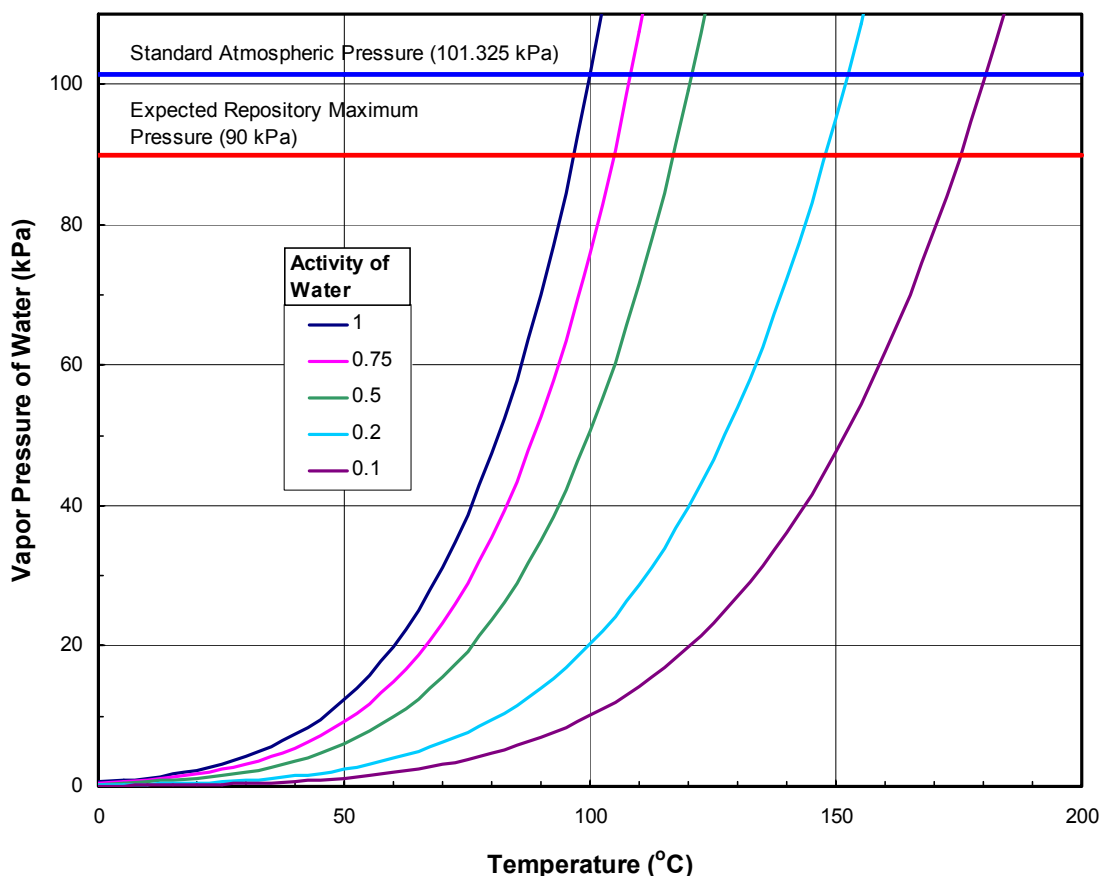
Table 6.7-4. Equilibrium RH of Saturated Aqueous Solutions of Various Pure Salts

Temperature (°C)	KF	MgCl ₂	K ₂ CO ₃	MgNO ₃	NaNO ₃	NaCl	KCl	KNO ₃	NaOH	KOH	K ₂ SO ₄
0	—	33.66	43.13	60.35	—	75.51	88.61	96.33	—	—	98.77
5	—	33.60	43.13	58.86	78.57	75.65	87.67	96.27	—	14.34	98.48
10	—	33.47	43.14	57.36	77.53	75.67	86.77	95.96	—	12.34	98.18
15	—	33.30	43.15	55.87	76.46	75.61	85.92	95.41	9.57	10.68	97.89
20	—	33.07	43.16	54.38	75.36	75.47	85.11	94.62	8.91	9.32	97.59
25	30.85	32.78	43.16	52.89	74.25	75.29	84.34	93.58	8.24	8.23	97.30
30	27.27	32.44	43.17	51.40	73.14	75.09	83.62	92.31	7.58	7.38	97.00
35	24.59	32.05	—	49.91	72.06	74.87	82.95	90.79	6.92	6.73	96.71
40	22.68	31.60	—	48.42	71.00	74.68	82.32	89.03	6.26	6.26	96.41
45	21.46	31.10	—	46.93	69.99	74.52	81.74	87.03	5.60	5.94	96.12
50	20.80	30.54	—	45.44	69.04	74.43	81.20	84.78	4.94	5.72	95.82
55	20.60	29.93	—	—	68.15	74.41	80.7	—	4.27	5.58	—
60	20.77	29.26	—	—	67.35	74.50	80.25	—	3.61	5.49	—
65	21.18	28.54	—	—	66.64	74.71	79.85	—	2.95	5.41	—
70	21.74	27.77	—	—	66.04	75.06	79.49	—	2.29	5.32	—
75	22.33	26.94	—	—	65.56	75.58	79.17	—	1.63	—	—
80	22.85	26.05	—	—	65.22	76.29	78.90	—	—	—	—
85	23.20	25.11	—	—	65.03	—	78.68	—	—	—	—
90	23.27	24.12	—	—	65.00	—	78.50	—	—	—	—
95	—	23.07	—	—	—	—	—	—	—	—	—
100	—	21.97	—	—	—	—	—	—	—	—	—

Source: DTN: LL991212305924.108 [DIRS 144927].

6.7.2.5 Boiling Point Elevation

The effect of decreased water activity on boiling temperature is better shown in Figure 6.7-2, which expands the relevant lower pressure region of Figure 6.7-1. This shows more detail in the range of standard atmospheric pressure (101.325 kPa), the repository ambient pressure of 89.1 ± 0.6 kPa (which is calculated in Section 6.7.2.1), and the expected repository maximum pressure of 90 kPa (also established in Section 6.7.2.1). The 0.75 water activity curve suggests a boiling temperature in the range 105°C to 108°C; the 0.50 curve, 116°C to 120°C, the 0.20 curve, 147°C to 152°C, and the 0.10 curve, 175°C to 180°C. The lower temperatures in these ranges correspond to the repository ambient pressure, the higher ones, standard atmospheric pressure.



Source: Output DTN: LL040601512251.103, *WaterPressureTableRev1.xls*.

Figure 6.7-2. Vapor Pressure of Water as a Function of Temperature and Water Activity (Water Activity Values are Shown in the Legend; Pressure Range Reduced to 0 to 110 kPa)

A particular point to be made here is that if concentrated salt solutions can form in the repository, the dissolved salt content is a much more important factor in determining boiling temperature than the reduction of atmospheric pressure at the elevation of the repository. High salt content can significantly elevate boiling temperature. The reduction in atmospheric pressure due to

increased elevation reduces the boiling temperature by 4°C to 5°C from what it would be at sea level.

Table 6.7-5 (reproducing here Table 4.1-7) lists the experimental boiling points of saturated aqueous solutions of several pure salts as tabulated in a handbook (Kracek 1928 [DIRS 122125]). These are defined for a standard atmospheric pressure of 101.325 kPa. At the reduced pressure associated with the elevation of the repository, these boiling points would be reduced by 4°C to 5°C. These data nevertheless confirm the picture of the significance of high salt content in raising boiling temperature. Experimental boiling point data for saturated salt solutions are available for only a relatively small number of single salts, and very few assemblages of more than one salt.

Table 6.7-5. Boiling Points of Aqueous Solutions of Pure Salts

Salt	Boiling Point (°C)	Source Page Number
K ₂ SO ₄	101.4	373
Na ₂ SO ₄	102.84	371
KCl	108.6	373
NaCl	108.67	369
KNO ₃	115.5	373
NaNO ₃	120.59	372
Ca(NO ₃) ₂	151	368

Source: Kracek 1928 [DIRS 122125].

As noted in Section 4.1.4, the boiling point for CaCl₂ carries fairly wide uncertainty, but appears bounded by 176°C.

To determine the maximum possible boiling temperatures that might apply to the repository, it is important to determine the relevant salt chemistry. In the case of dust deliquescence, this reduces to the question of which salt minerals are present on the metal barrier surfaces. In the case of seepage water evaporation, the question is what the chemistries of the anticipated seepage waters are.

6.7.2.6 Accessible Relative Humidity Conditions

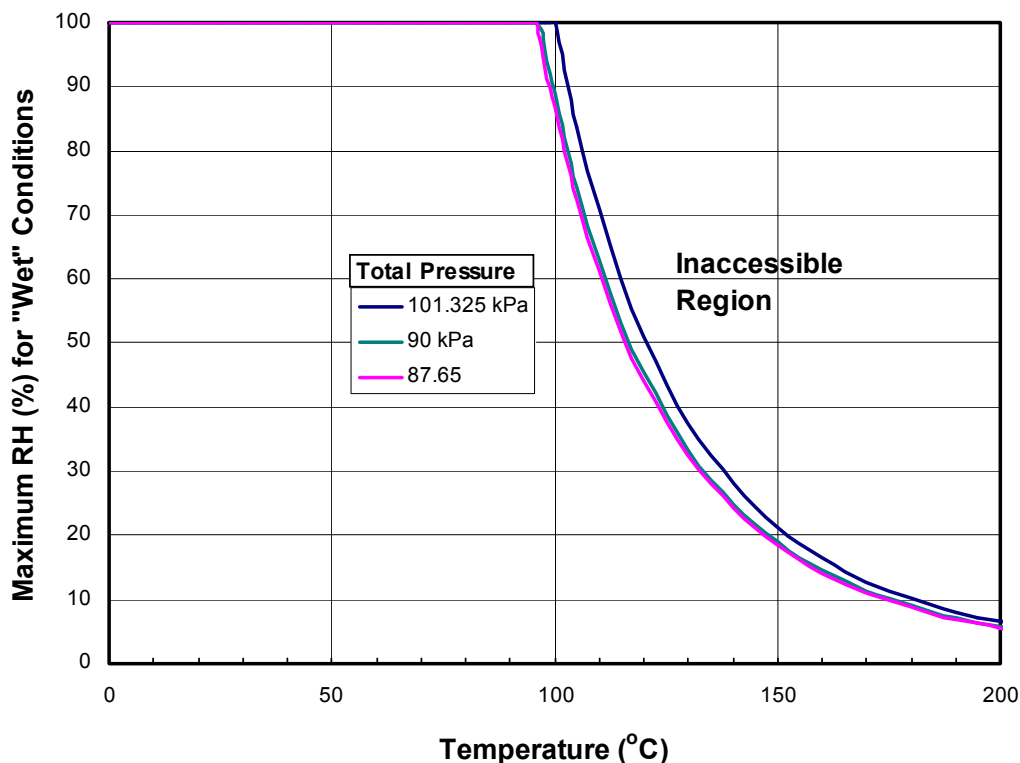
Another way of interpreting vapor pressure data in light of a limit on ambient total pressure (and hence on the water vapor pressure) is to place a limit on the maximum RH at which liquid water can be present. From the definition of RH,

$$RH\% = 100p_w / p_w^o \quad (\text{Eq. 6.7.2.6-1})$$

If the vapor pressure of water p_w is limited to some value defined by the ambient total pressure, then the maximum RH for “wet” conditions can be determined by substituting that value into the above equation. This result is interesting because it is independent of possible salt chemistry.

In Section 6.7.2.1, the nominal atmospheric pressure at the repository elevation is calculated to be 89.1±0.6 kPa; this corresponds to a boiling point somewhere between 96 and 97°C for pure

water. In the following discussion, the boiling point is rounded down to 96°C, for which the corresponding water vapor pressure is 87.65 kPa. Figure 6.7-3 shows the maximum RH for “wet” conditions as a function of temperature for the fixed total pressures of 87.65 kPa and, for reference, a pressure of 101.325 kPa. For a fixed total system pressure, the maximum RH for “wet” conditions decreases with increasing temperature, once the temperature is above the boiling point of pure water.



Source: Output DTN: LL040601512251.103, *WaterPressureTableRev1.xls*.

Figure 6.7-3. Maximum RH for “Wet” Conditions as a Function of Temperature, for Repository Ambient Pressure (left, the red curve) and Standard Atmospheric Pressure (right, the black curve)

If the RH for a saturated salt solution (the deliquescence RH of the corresponding salt or salt mineral assemblage) is plotted as a function of temperature, the intersection of that curve with the relevant curve for the maximum RH for existence of aqueous solution as shown in Figure 6.7-3 marks the point at which the solution dries out, leaving only solid salt and vapor. This point is similarly the point where deliquescence begins, starting from the “dry” side.

6.7.2.7 Other Factors Governing Deliquescence RH–Temperature Relations

A salt mineral (or a salt mineral assemblage) may have a simple deliquescence RH–temperature curve that continuously spans a wide temperature range. This is the case, for example, for NaCl (halite), which in the temperature range of interest here (roughly from 25°C to the IDPS model limit of 140°C, but in some instances evaluated to 200°C) is subject only to a limit associated with a fixed total ambient pressure. However, additional factors may come into play in other cases. One is that a mineral (or a mineral assemblage) may itself only be stable in a limited

range of temperature. A mineral may decompose at a certain temperature. The mechanism of decomposition may vary.

Table 6.7-6 (reproducing Table 4.1-10) lists a number of minerals that undergo decomposition. Also listed are the corresponding decomposition temperatures and mechanisms. These mechanisms include “melting,” dehydration, and decarbonation (loss of CO₂). The mechanisms and decomposition temperatures shown here are for single minerals, and do not require the presence of a preexisting aqueous solution. Note that “melting” of a hydrous salt mineral results in the creation of what may be called an aqueous solution, though such a solution might equally well be termed a hydrous molten salt. The melting of an anhydrous salt (such as Ca(NO₃)₂ in Table 6.7-6) simply produces a molten salt. In general, in the temperature range of primary interest to this report (roughly from 25°C to the IDPS model limit of 140°C, but in some instances evaluated to 200°C), all the “melts” are expected to be of the hydrous variety.

Table 6.7-6. Decomposition Temperatures of Some Salt Minerals

Salt Mineral	Decomposition Temperature (°C)	Mechanism	Source Page Numbers
CaCl ₂ :6H ₂ O	29.92	Melting	B-87
CaCl ₂ :H ₂ O	260	Melting	B-87
CaCl ₂	782	Melting	B-87
Ca(NO ₃) ₂ :4H ₂ O	α: 42.7 β: 39.7	Melting	B-88
Ca(NO ₃) ₂ :3H ₂ O	51.1	Melting	B-88
Ca(NO ₃) ₂	561	Melting	B-88
KHCO ₃	100 to 200	Unspecified decomposition	B-131
KCl	770	Melting	B-132
KNO ₃	334	Melting	B-135
NaCl	801	Melting	B-147
Na ₂ CO ₃ :10H ₂ O	32.5 to 34.5	Melting	B-147
Na ₂ CO ₃ :7H ₂ O	32	Dehydration	B-147
Na ₂ CO ₃ :H ₂ O	100	Dehydration	B-147
Na ₂ CO ₃	851	Melting	B-147
NaHCO ₃	270	Decarbonation	B-147
Na ₂ SO ₄ :10H ₂ O	32.38	Melting	B-150

Source: Weast and Astle 1981 [DIRS 100833].

If a salt mineral simply disappears, this can be referred to as decomposition of some sort. However, in addition to decomposition, a deliquescence RH temperature relation can be subject to replacement of a salt mineral by another or the appearance of another salt mineral. If no saturated salt mineral remains beyond a certain temperature, a deliquescence RH curve for the remaining solution can be defined. However, the nature of such deliquescence then refers to the RH above which the solution grows in mass due to the uptake of water. The temperature at which a mineral phase change (disappearance or appearance) occurs may vary in the case of salt mixtures. For example, the melting temperature of Na₂SO₄:10H₂O (mirabilite) may vary due to the presence of NaCl, present as either the solid (halite) or dissolved in coexisting aqueous solution. However, whether the temperature is constant or not for a phase assemblage change of

any type depends on whether or not the change involves a eutectic condition. The melting temperature of $\text{Na}_2\text{SO}_4 \cdot 10\text{H}_2\text{O}$ in the presence of solid NaCl (halite) would itself be a constant. However, that would be different from the melting temperature of $\text{Na}_2\text{SO}_4 \cdot 10\text{H}_2\text{O}$ by itself.

6.7.2.8 Other Information on Deliquescence, Dust, and Salt Minerals

The scientific and engineering literature on deliquescence is substantial but diverse. Most of the literature appears to be divided into two domains: engineering, including application of saturated salt solutions to the control of RH, and atmospheric chemistry.

The interest in deliquescence in the engineering domain is exemplified by compilation of data reported by Greenspan (1977 [DIRS 104945]). This domain is mainly interested in providing salt systems that can fix RH over a range of desired values. Because this goal is achievable with only single salt systems, data for assemblages of two or more minerals are uncommon in this literature. Interest tends to focus on temperatures close to 25°C , though not to the exclusion of higher temperatures. Because RH can now be well controlled in industrial and laboratory processes by other means, such as gas mixing, there is presently less interest in this topic in the engineering domain, apart from some specialty applications such as RH control in museum cases (e.g., Creahan 1991 [DIRS 163395]).

A wider interest in deliquescence, with more activity in recent times, exists in the domain of atmospheric chemistry (e.g., Tang and Munkelwitz 1993 [DIRS 163124]; Tang and Munkelwitz 1994 [DIRS 163125]; Ge et al. 1998 [DIRS 162165]; Ansari and Pandis 1999 [DIRS 162167]; Pilinis 1999 [DIRS 163126]). Here, the interest is focused on the generation of aqueous aerosols from salt aerosols, various reactions important to chemical budgets in the atmospheric, tie-ins to mechanisms governing climate and climatic change, and the fate and consequences of anthropogenic inputs. The atmospheric chemistry literature discriminates deliquescence RH from efflorescence RH. In this case, efflorescence is equivalent in meaning to dryout. Deliquescence is, as noted earlier in this report, closely governed by equilibrium thermodynamics. That is not always the case with efflorescence. Efflorescence relative humidity can be different from the deliquescence RH owing to the achievement of significant supersaturation with respect to some salt or salts before that salt or salts actually precipitates. The observation of a significant difference between efflorescence RH and deliquescence RH is mostly observed in the context of atmospheric science studies in which the systems of interest are colder and more “pristine” than those of common interest in geochemical studies. The time scales of interest are also typically much shorter, which also favors a lack of sensibly complete equilibrium. This is not to say that disequilibrium is not observed in evaporating systems of geologic interest, merely that such disequilibrium is rarer and of lesser magnitude.

In atmospheric science, the systems of interest are usually cooler than room temperature, and may be relatively “pristine” in the sense of lacking an abundance of suitable surfaces to assist mineral nucleation. Such a system might consist of an aerosol composed only of an aqueous solution, surrounded by “clean” atmosphere.

An experimental technique (single-particle levitation) meeting this description is described, for example, by Tang and Munkelwitz (1993 [DIRS 163124]). A well-defined efflorescence RH

different from a deliquescence RH is likely associated with a critical supersaturation for rapid precipitation of an associated salt mineral.

The concept of a distinct efflorescence RH is not relevant to conditions in the repository at Yucca Mountain for three reasons. First, the temperature range is higher than it would be up in the atmosphere (higher temperature promotes more rapid approach to thermodynamic equilibrium). Second, the time scale of interest is much longer (years at least versus hours). Finally, the conditions on the surfaces of the metal barriers are far less pristine than conditions in the upper atmosphere or a levitating droplet apparatus. The salt and nonsalt components of the dust itself will provide surfaces for nucleation, as will the metal barrier surfaces. Much, if not most, of the dust is expected to consist of relatively insoluble matter, mostly silicates (e.g., other data in DTNs: MO0207EBSDUSTS.020 [DIRS 162556] and MO0209EBSDUST2.030 [DIRS 162557]; see also Reheis et al. 2002 [DIRS 163132] and other papers cited on the characteristics of typical atmospheric dusts). Thus, it is expected that dryout (efflorescence) in the repository will for all practical purposes also be an equilibrium phenomenon.

Some discussion of the characteristics and origin of dust and its salt content is appropriate here. Dust was generated in the repository itself during tunneling operations (this is discussed in more detail in Section 6.7.2.10). To the extent that this includes rock dust, at least part of the salt content would originate from the rock itself. Other salt components may have been introduced during tunneling operations (e.g., use of lithium bromide in water used for dust control) and other operations following tunneling. The dust presently in the repository probably contains some component that was originally entrained in air outside the mountain and was subsequently brought into the tunnels by airflow including ventilation. Over the ventilation period, such outside dust is the major type of dust on the metal barrier surfaces.

Atmospheric dusts have local, regional, and global origins (e.g., Arimoto 2001 [DIRS 163485]; Blank et al. 1999 [DIRS 163486]; Reheis and Kihl 1995 [DIRS 106653]; Reheis et al. 2002 [DIRS 163132]; Orlovsky and Orlovsky 2001 [DIRS 163413]; Levy et al. 1999 [DIRS 163397]). Marine aerosols comprise one component of salt in atmospheric dust. In the western United States, these are more significant closer to the Pacific coast. Some salts are also created (or modified) by atmospheric processes (e.g., creation of nitrate by electrical discharges). Salts are also included in dusts stirred up from dry lake beds. Based on trace element geochemistry, Reheis et al. (2002 [DIRS 163132]) concluded that dust in the southwestern United States appears to come from four sources: (1) alluvial sediments, (2) playas, (3) the area of Owens Valley Dry Lake (a human-induced playa), and (4) anthropogenic or volcanic emissions, or both.

Levy et al. (1999 [DIRS 163397], pp. 53 to 55, 59 to 60) point out that Owens Valley Dry Lake is the source of the largest measured values of particulate air pollution in North America, and identified the minerals in the surface and shallow sediments of the dry lake. The most important quantitatively are quartz (SiO_2) and feldspar ($\text{Ca}_x\text{Na}_{1-x}\text{Al}_{1+x}\text{Si}_{3-x}\text{O}_8$), which are not salt minerals. The salt minerals included halite (NaCl), thenardite (Na_2SO_4), pirssonite ($\text{Na}_2\text{Ca}(\text{CO}_3)_2 \cdot 2\text{H}_2\text{O}$), nesquehonite ($\text{MgCO}_3 \cdot 3\text{H}_2\text{O}$) and trona [$\text{Na}_2\text{H}(\text{CO}_3)_2 \cdot 2\text{H}_2\text{O}$]. These salts tend to be concentrated at the surface.

Blank et al. (1999 [DIRS 163486]) report on dust collected from desert playa regions in Nevada. This study is somewhat notable in that it provides clear data (Blank et al. 1999 [DIRS 163486]),

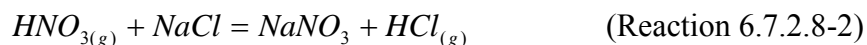
Table 2, p. 370) on the soluble salt fraction of aeolian dusts: 44.20±2.20 percent in playa samples, 0.46± 0.10 percent in beach samples, and 0.15± 0.02 percent in dune samples. These values are higher than, but reflective of, the soluble salt fraction in corresponding soil samples (9.36±1.05 percent in playa samples, 0.15± 0.08 percent in beach samples, and 0.01± 0.004 percent in dune samples). These differences are attributed (Blank et al. 1999 [DIRS 163486], p. 377) to recent changes in playa hydrology associated with climatic change and human activities. This report also notes the existence of pulses of nitrate-rich dust synchronous with the spring emergence (seasonal increase in biological activity).

Böhlke et al. (1997 [DIRS 163354]) studied stable isotope evidence for the origin of desert nitrate deposits and concluded that atmospheric deposition is the major mechanism. Oxidation of organic nitrogen in desert soils is another likely mechanism, but much less important quantitatively. The nitrate minerals in the samples studied by these authors are identified primarily as soda niter (NaNO_3 ; also known as nitratine) and darapskite ($\text{Na}_3\text{SO}_4\text{NO}_3\cdot\text{H}_2\text{O}$). These authors did not address in detail the origin of nitrate in the atmosphere.

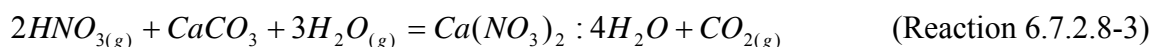
Various nitrate minerals may be created by atmospheric reactions involving $\text{HNO}_{3(g)}$ or $\text{N}_2\text{O}_{5(g)}$ created by electrochemical or photochemical reactions. The latter is considered as the acid anhydride of nitric acid. These two species are related by the reaction:



Soda niter may form from halite (NaCl), which itself is formed from sea salt aerosol or blown upward from salt playas:



Calcium nitrate [e.g., nitrocalcite $\text{Ca}(\text{NO}_3)_2\cdot 4\text{H}_2\text{O}$] may also be created from preexisting calcium carbonate by an atmospheric reaction such as noted by Arimoto (2001 [DIRS 163485], p. 37). Note that Arimoto omits the water of hydration shown here):



Niter (KNO_3), soda niter (NaNO_3 ; also known as nitratine), nitrocalcite [$\text{Ca}(\text{NO}_3)_2\cdot 4\text{H}_2\text{O}$], nitromagnesite [$\text{Mg}(\text{NO}_3)_2\cdot 4\text{H}_2\text{O}$], and darapskite ($\text{Na}_3\text{SO}_4\text{NO}_3\cdot\text{H}_2\text{O}$) are also known from cave deposits (Hill and Forti 1997 [DIRS 164320]; Duncan 1997 [DIRS 163338]; Hill 1999 [DIRS 163340]). These occurrences suggest that nitrate minerals relevant to Yucca Mountain might be derived from efflorescence deposits in fractures or voids in the tunneled rock.

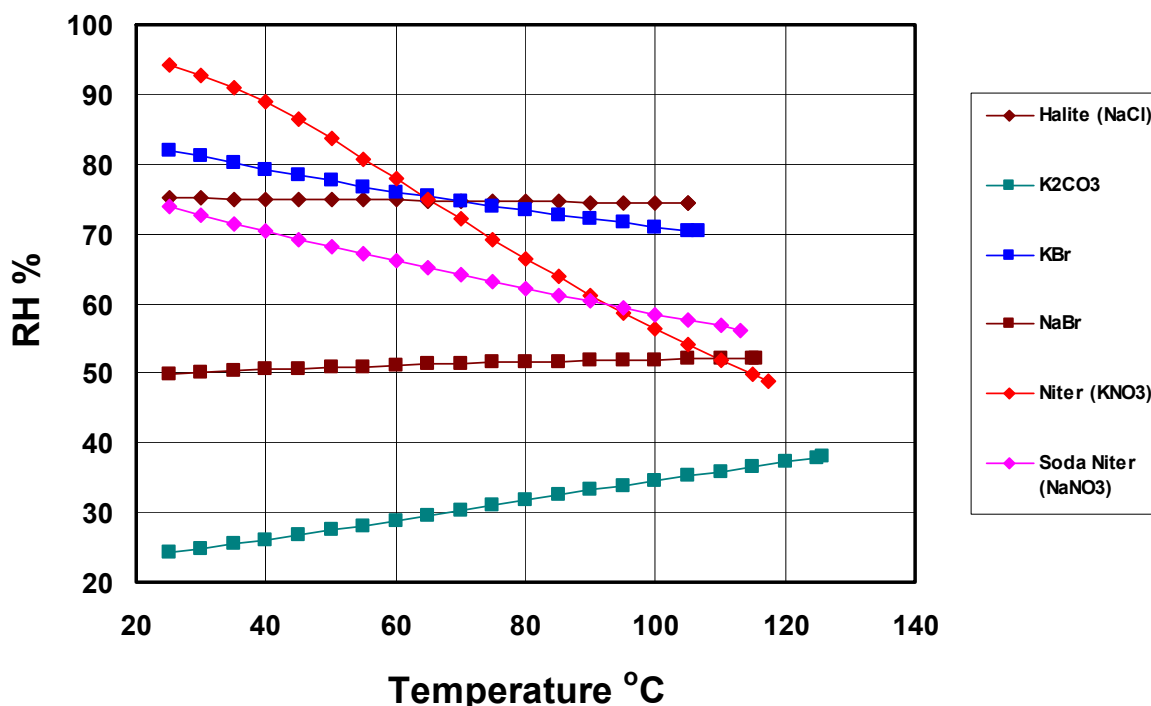
There is little evidence for the presence of calcium chloride minerals in dust or atmospheric aerosols. The stable form of calcium chloride at low temperature is antarcticite ($\text{CaCl}_2\cdot 6\text{H}_2\text{O}$). This is described from the type locality (a very shallow pond in Antarctica) by Torii and Osaka (1965 [DIRS 162577]). It is surmised that very low temperatures are in part responsible for the occurrence. A second occurrence is reported from Bristol Dry Lake, California, by Dunning and Cooper (1969 [DIRS 162578]). Here the antarcticite was found in the near-subsurface in the course of examining trenches and pits. Antarcticite is further discussed in Sections 6.7.2.9 and 6.7.2.12.

6.7.2.9 EQ3/6 Calculations of Deliquescence Relative Humidities for Various Salt Minerals and Salt Mineral Assemblages

EQ3/6 calculations of the deliquescence RH of single salts and salt mineral assemblages are made as described previously in Section 6. The deliquescence RH calculations are run from 25°C to the IDPS model limit of 140°C, and in most cases run on up to 200°C, with results obtained at 5°C increments. In general, the proper truncation of the results is the dryout temperature associated with the total pressure limit of 0.90 bar (90 kPa) as established in Section 6.7.2.1. Liquid water cannot exist under conditions in which the corresponding H₂O vapor pressure would exceed the total pressure. In nearly all cases, this requirement terminated the results at temperatures below 140°C, the limit of validation of the Pitzer IDPS model employed. Linear interpolation between the bounding temperatures (5°C apart) is used to calculate the dryout temperature. Any results otherwise extending beyond 140°C are discarded. For the few cases in which the analysis required data to higher temperatures (e.g., the CaCl₂-H₂O system), experimental data are used in place of calculated (IDPS model) data.

The relevant EQ3/6 files for the single-mineral assemblages are in the RHT×1 folder in *Pack048.zip* in output DTN: LL040903723121.042. A sampling of results for some single salts covering a wide range of RH is shown in Figure 6.7-4. The salts included here are halite (NaCl), K₂CO₃, KBr, NaBr, niter (KNO₃), and soda niter (NaNO₃; also known as nitratine). They are moderately to highly deliquescent (and moderately to highly soluble). The deliquescence RH of halite is nearly a constant 75 percent across the temperature range. In contrast, the deliquescence RH of K₂CO₃ increases significantly with increasing temperature, while that of soda niter and particularly niter decreases notably. The curves in Figure 6.7-4 terminate at temperatures below 140°C. These terminations are associated with the total pressure limit of 0.90 bar described previously (e.g., as represented in Figure 6.7-3).

Actual data for simple single salts such as those presented in Figure 6.7-4 can be found in handbooks (e.g., Weast and Astle 1981 [DIRS 100833]) and other published sources (e.g., Greenspan 1977 [DIRS 104945]). Few direct comparisons are made in this report, as it is not focused on the topic of model validation. For such comparisons, see *In-Drift Precipitates/Salts Model* (BSC 2004 [DIRS 169863]).



Source: Output DTN: LL040903723121.042, *RHTE_Minerals1_PlotsA_v2p1.xls*.

Figure 6.7-4. Deliquescence RH as a Function of Temperature for Some Deliquescent Salts

The curve for K_2CO_3 shown in Figure 6.7-4 requires some comment with regard to the implied partial pressure of CO_2 . These calculations are for a closed system and do not consider the effect of equilibrium with CO_2 in air. In general, the pCO_2 is very low, though it increases with increasing temperature. At 25°C it is 2.17×10^{-11} bar, at 135°C, 1.49×10^{-7} bar (file *k2co3.6o*, from output DTN: LL040903723121.042). These values lie below expected values in the repository. The low pCO_2 values are correlated with high pH values (12 and higher). The “v. frac.” value of 8.91×10^{-6} for the THC model “high-temperature, low carbon dioxide” case given in Table 4.1-15 (DTN: LB0108DSTTHC01.001 [DIRS 156285]) equates to a CO_2 pressure of 7.94×10^{-6} bar [$8.91 \times 10^{-6} \times 0.891$ bar (Section 6.7.2.1; 89.1 kPa = 0.891 bar) = 7.94×10^{-6} bar]. That is for the “boiling period,” for which the mean temperature (from the same table and source cited above) is 122.87°C. The CO_2 pressure is reduced because of expansion of the steam envelope. A nearly identical result would be obtained for the corresponding “high temperature, high carbon dioxide” case for which data are given in Table 4.1-16 (“v. frac.” of 8.92×10^{-6} and a temperature of 122.86°C). For a “cooler” (nonboiling or just-boiling) repository, as represented by the data in Table 4.1-17, Table 4.1-18, and Table 4.1-23, expected CO_2 pressures would be significantly higher. Thus, K_2CO_3 , if present in the repository, would not quite be stable under wet conditions, and would likely convert to some mixed carbonate-bicarbonate salt.

A similar but shorter EQ3/6 run (file *kalicini.6o*, output DTN: LL040903723121.042) for kalicinite ($KHCO_3$) yields a CO_2 pressure of 2.08 bar at 25°C, well above the expected limit on total pressure (the corresponding deliquescence RH was 89.5 percent). Thermodynamic data for this phase at other temperatures are not included in the current version of the EQ3/6 high-temperature Pitzer IDPS model, so only a special calculation (allowing this mineral to

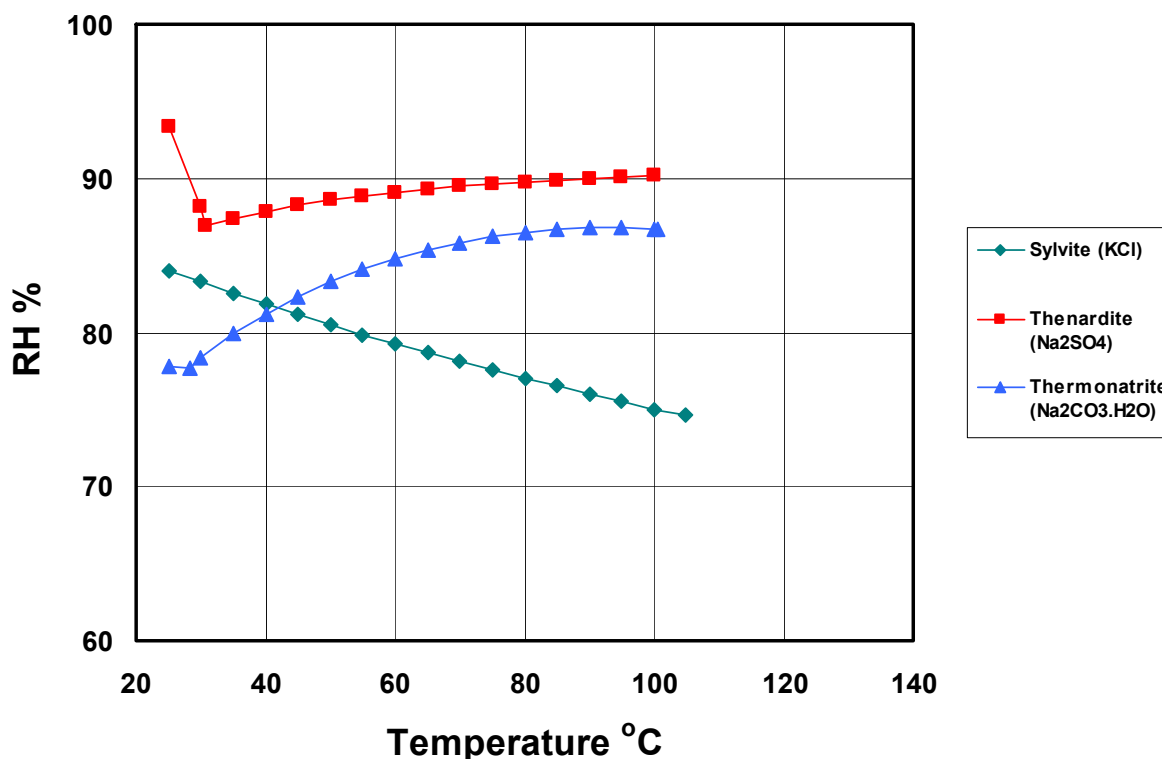
precipitate) for 25°C is made. One would expect still higher CO₂ pressures for higher temperatures. Nevertheless, it is clear that the presence of either K₂CO₃ or KHCO₃ is inconsistent with the expected range of CO₂ partial pressures in the repository. A similar calculation is also made for the mixed carbonate–bicarbonate phase K₈H₄(CO₃)₆·3H₂O, also for which only 25°C thermodynamic data are available. This yields (output DTN: LL040903723121.042, file *k8h4co36.6o*) an equilibrated system containing K₈H₄(CO₃)₆·3H₂O and KHCO₃ (which is also permitted to precipitate in this special run). It gives a CO₂ pressure of 8.09×10^{-6} bar and a deliquescence RH of 42.2 percent. This CO₂ pressure is closer to expected values in the repository, but still too low for the low temperature.

It is noted that the deliquescence RH data for niter (KNO₃) agree reasonably well with the handbook data in Table 4.1-8. However, the handbook data for this salt only extend to 50°C. The data for this salt at higher temperature represent an extrapolation of some uncertainty owing to the fact that the Pitzer binary interaction coefficient data for the KNO₃ electrolyte in the high-temperature Pitzer data file actually pertain only to 25°C. Nevertheless, the general correctness of the trend (RH decreasing strongly with increasing temperature) seems well established. The situation with the KNO₃ binary interaction coefficients is somewhat unique among the major electrolytes of significance to deliquescence on the metal barrier surfaces in the repository. It is further discussed in Section 6.7.2.15.

The curves shown in Figure 6.7-4 are generated using the IDPS model by adding a large amount (typically 10 to 30 moles) of the mineral associated with a given curve to a 1 kg mass of water, then heating from 25°C to as high as 200°C (known to be above the IDPS model validation limit of 140°C). For the cases shown in Figure 6.7-4, the mineral added is the only mineral present. However, the calculations are carried out such that any mineral listed in Table 6.5-1 is permitted to form if the composition of the system permits it and if the thermodynamic driving forces are favorable. The possible complications are illustrated in some of the results given in this section.

Figure 6.7-5 shows deliquescence RH–temperature curves for some moderately deliquescent salts. These include sylvite (KCl), thenardite (Na₂SO₄), and thermonatrite (Na₂CO₃·H₂O). The curve for thenardite (Na₂SO₄) takes a sharp turn near 30.7°C. This is because at lower temperature, the thenardite added to the system reacts with water to form mirabilite (Na₂SO₄·10H₂O). The curve from 25°C to 30.7°C is in actuality the deliquescence RH–T curve for that mineral. At 30.7°C, the mirabilite is no longer more stable than thenardite and water (specifically, water in mirabilite-saturated solution). In effect the mirabilite “melts,” forming thenardite and water. The part of the curve starting at 30.7°C is the true thenardite curve. A somewhat similar situation pertains to the curve for thermonatrite (Na₂CO₃·H₂O). The short segment up to 28.3°C is the actual curve for this salt. The following segment (most of the “thermonatrite” curve shown) is for natrite (Na₂CO₃), anhydrous sodium carbonate. At 25°C, the thermonatrite curve corresponds to a CO₂ pressure of 3.67×10^{-8} bar (output DTN: LL040903723121.042, file *thermona.6o*). Here the pH is about 12. At the 28.3°C phase boundary with natrite, that pressure is 5.44×10^{-8} bar. At 105°C, it is 2.13×10^{-5} bar, which is consistent with the notion of natrite being present under anticipated repository conditions. This is not the case at the lower temperatures, where a mixed carbonate-bicarbonate phase of sodium (e.g., trona, Na₃H(CO₃)₂·2H₂O) might be consistent, analogous to the case for potassium carbonate-bicarbonate. Trona is another salt mineral for which the data in the current version of the high-temperature IDPS Pitzer model are restricted to 25°C. A run restricted to that

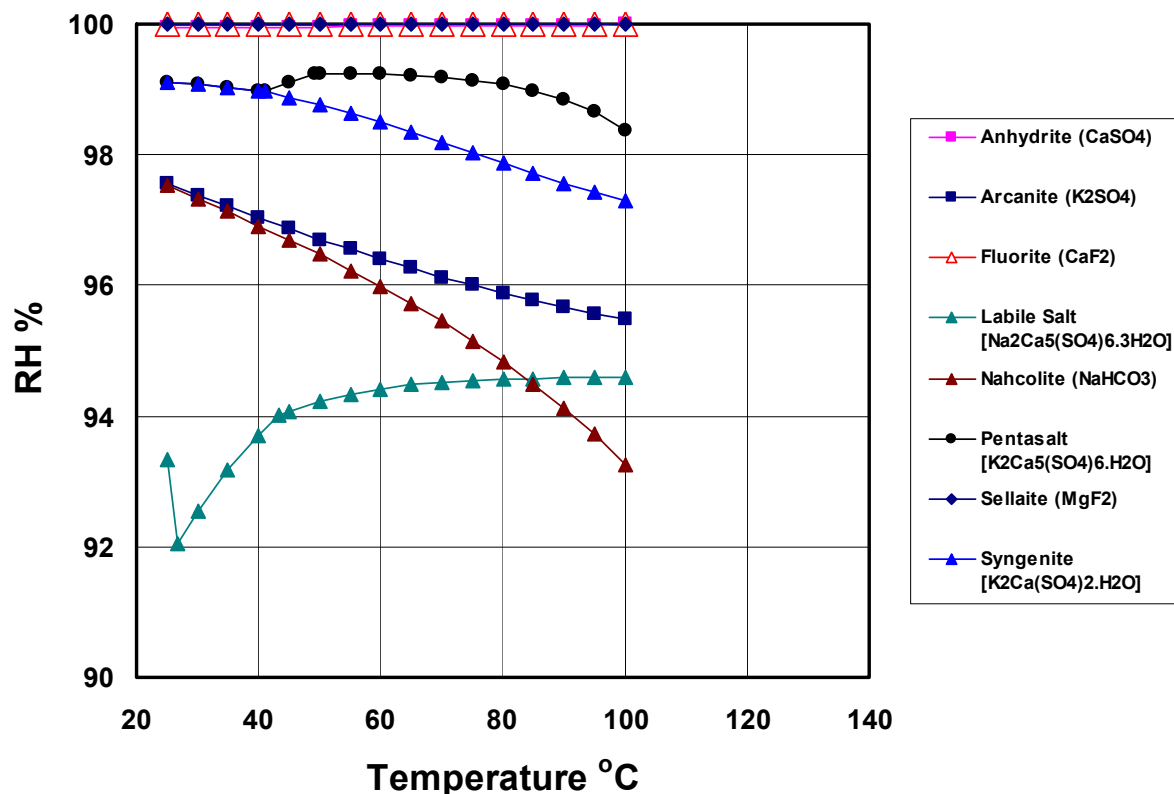
temperature (output DTN: LL040903723121.042, file: *trona.6o*) yields an equilibrated system containing trona and nahcolite (NaHCO_3), with a CO_2 pressure of 2.21×10^{-4} bar and a deliquescence RH of 88.2 percent. This CO_2 pressure is much closer to what would be expected in the repository at low temperature. The case for nahcolite itself is discussed in addressing the results shown in Figure 6.7-6.



Source: Output DTN: LL040903723121.042, *RHTE_Minerals1_PlotsA_v2p1.xls*.

Figure 6.7-5. Deliquescence RH Versus Temperature for Some Less-Deliquescent Salts

Figure 6.7-6 (which shows RH values in the 90-100 percent range) shows deliquescence RH-temperature curves for several slightly deliquescent salt minerals. Some of these are “simple” salts of the kind shown in the previous two figures. The ones of this type include anhydrite (CaSO_4), arcanite (K_2SO_4), fluorite (CaF_2), nahcolite (NaHCO_3), and sellaite (MgF_2). Fluorite (CaF_2) is a relatively insoluble salt, and it is not surprising that the calculated deliquescence RH over the temperature range is essentially fixed at a value indistinguishable from 100 percent. Anhydrite is considered to be only a slightly soluble salt, and a very similar result is obtained for it. Not apparent in the curve for anhydrite is a phase change. Up to 50.2°C , the salt actually present in the system is gypsum ($\text{CaSO}_4 \cdot 2\text{H}_2\text{O}$). The nahcolite (NaHCO_3) calculation (output DTN: LL040903723121.042, file: *nahcolite.6o*) gives a CO_2 pressure of 0.395 bar at 25°C , 1.02 bar at 45°C , and 11.0 bar at 105°C . These are high values compared to ones expected for the repository. However, the previously discussed 25°C -only calculation for trona (which yielded trona and nahcolite and a reasonable CO_2 pressure of 2.21×10^{-4} bar) shows that unreasonable CO_2 pressures associated with a mineral in a system comprised of only that mineral and water do not preclude that mineral being present in a more complex system that is characterized by more reasonable CO_2 pressures.



Source: Output DTN: LL040903723121.042, *RHTE_Minerals1_PlotsA_v2p1.xls*.

NOTE: The symbols and curve for anhydrite are obscured by those for fluorite and sellaite.

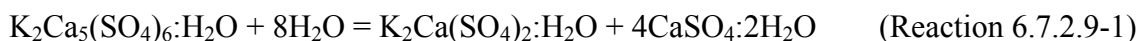
Figure 6.7-6. Deliquescence RH as a Function of Temperature for Some Moderately Deliquescent Salts

Also shown in Figure 6.7-6 are deliquescence RH–T curves for several “double” salts. In general, such a salt is characterized by the presence of at least two cations (usually excluding hydrogen ion) or at least two anions. Many double salts with two cations pair an alkali metal (Na, K) with an alkaline earth metal (Mg, Ca). The double salts whose curves are shown in the figure include labile salt [Na₂Ca₅(SO₄)₆:3H₂O], pentasalt [K₂Ca₅(SO₄)₆:H₂O], and syngenite [K₂Ca(SO₄)₂:H₂O]. The behavior of these double salt calculations is more complex than is the case for the “simple” salts. These calculations are discussed in reverse order starting with the simplest case.

In the run for syngenite [K₂Ca(SO₄)₂:H₂O] (reference the file *syngenit.6o*, folder RHTx1, in *Pack048.zip* in output DTN: LL040903723121.042), the system created by adding an excess of syngenite is saturated with gypsum (CaSO₄:2H₂O) as well as syngenite at 25°C. At 41.2°C the gypsum is replaced by pentasalt [K₂Ca₅(SO₄)₆:H₂O]. The curve for syngenite as shown in Figure 6.7-6 terminates near 100°C due to the restriction on total pressure. The actual dryout temperature for 0.90 bar total pressure actually lies between 96°C (the nominal boiling point for pure water at the repository elevation) and 100°C (the boiling point for pure water at sea level). Ignoring the limitation imposed by total pressure, at 111.4°C the pentasalt would be replaced by anhydrite (CaSO₄), which would hold up to at least the 140°C validation limit. The aqueous solution in this calculation does not become truly highly concentrated. At 25°C the ionic

strength is 0.686 molal; at 41.2°C, 0.812 molal; at 70°C, 1.47 molal; at 100°C, 2.31 molal. These values are well below those that would be obtained for other phases, for example halite (NaCl). Correspondingly, the water activities (RHs) remain relatively high.

In the run for pentasalt [$\text{K}_2\text{Ca}_5(\text{SO}_4)_6 \cdot \text{H}_2\text{O}$] (reference the file *pentasal.6o*, folder RHTx1, in *Pack048.zip* in output DTN: LL040903723121.042), similar results are obtained. In fact, the early part of the calculation produced identical results. At 25°C the system is saturated with gypsum and syngenite, with pentasalt replacing gypsum again at 41.2°C. Below this temperature, pentasalt plus water is unstable relative to gypsum plus syngenite. The reaction may be written as:



One could increase the mass of available pentasalt in the EQ3/6 calculation to the point where all the free water is consumed by the above reaction. However, saturation with pentasalt below 41.2°C would still not be achieved. At 49.4°C in this calculation, gypsum is replaced by anhydrite. The curve for pentasalt as shown in Figure 6.7-6 ends near 100°C owing to the restriction on the water vapor pressure. As is the case for syngenite, the actual dryout temperature lies between 96°C and 100°C. However, ignoring that restriction, at 111.3°C syngenite would reappear at the expense of pentasalt and this would hold at least up to the validation limit of 140°C. At 25°C the ionic strength is 0.686 molal; at 41.2°C, 0.812 molal; at 49.4°C, 0.588 molal; at 75°C, 0.667 molal; at 100°C, 1.34 molal. These are again not truly high values.

The curve for labile salt [$\text{Na}_2\text{Ca}_5(\text{SO}_4)_6 \cdot 3\text{H}_2\text{O}$] (reference the file *labilesa.6o*, folder RHTx1, in *Pack048.zip* in output DTN: LL040903723121.042) in Figure 6.7-6 clearly exhibits a phase change just above 25°C. At 25°C, the solids present are gypsum ($\text{CaSO}_4 \cdot 2\text{H}_2\text{O}$) and mirabilite ($\text{Na}_2\text{SO}_4 \cdot 10\text{H}_2\text{O}$). At 26.8°C glauberite [$\text{Na}_2\text{Ca}(\text{SO}_4)_2$] replaces the mirabilite. At 43.4°C, anhydrite (CaSO_4) replaces the gypsum. The assemblage anhydrite plus glauberite persists to the end of the curve at near 100°C. Ignoring the restriction on the water vapor pressure, this assemblage would persist to at least the validation limit of 140°C. Ionic strengths are significantly higher in this case, consistently with the lower water activities (RHs) shown by the curve in Figure 6.7-6. However, they decrease notably with increasing temperature. At 25°C, the ionic strength is 6.23 molal; at 50°C, 5.07 molal; at 100°C, 4.74 molal. These results are obtained by adding 3.0 moles of labile salt to 1 kg of water (input file *LabileSa.6i*). Adding 3.2 moles (input file *LabileS2.6i*) produced essentially identical results. Adding more than 3.2 moles results in total consumption of available water in the formation of gypsum and mirabilite. In yet another run (input file *LabileS3.6i*), gypsum and mirabilite are suppressed and the amount of added labile salt is increased to 500 moles. Here the assemblage anhydrite plus glauberite holds over the entire range. It is not possible to form labile salt itself by adding any mass of this salt to water. This does not mean that this salt can not be formed using the IDPS model employed, just that it can not be formed in this particular manner (adding some mass of it to water).

It is apparent that double salts are not necessarily associated with low water activities (RH) or highly concentrated solutions. This may seem somewhat surprising in view of geologic occurrence, as natural brines from which such salts typically precipitate are more highly concentrated. However, that association is somewhat fortuitous. Most natural brines that

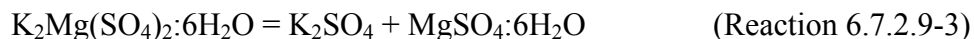
precipitate salt minerals have high sodium chloride content (Hardie and Eugster 1970 [DIRS 162776]; Eugster and Hardie 1978 [DIRS 100743]). That, by itself, has limited effect on double salt formation [the high sodium concentration favors precipitation of sodium-bearing double salts such as glauberite, $\text{Na}_2\text{Ca}(\text{SO}_4)_2$]. Potassium- and magnesium-bearing double salts tend to be associated with highly concentrated brines simply because dissolved potassium and magnesium are usually relatively unconcentrated in other aqueous solutions in the natural environment. Here the geologic association is meaningful, but it is driven by material distributions in nature, not by some fundamental aspect of double-salt chemistry or some principle of thermodynamics.

Each of the three double salts examined above can be thought of as a mixture of a relatively insoluble salt (the CaSO_4 component) and a more highly soluble salt (the Na_2SO_4 or K_2SO_4 component). The double salts tend to exhibit behavior that is somewhat intermediate between that of these component simple salts. Although a great many double salts appear to involve a component salt that is not highly soluble, that is not always the case, and some double salts (such as darapskite, $\text{Na}_3\text{SO}_4\text{NO}_3\cdot\text{H}_2\text{O}$) are composed of two more highly soluble components and solutions saturated with these are accordingly more concentrated. However, it appears to be generally true that one cannot always speak of the solubility of a double salt in the same way that one can of a simple salt. This is because the addition of a double salt to water may lead to the formation of saturated systems in which at least one simple salt is also present. In fact, as is shown, the double salt may be completely converted to other minerals, no matter how much is added.

The formation of double salts should act to reduce ionic concentration levels in aqueous solution and hence elevate the activity of water (and RH) relative to what would be obtained from the stoichiometric equivalent of single salts. Consider, for example, the decomposition of glauberite into thenardite and anhydrite:



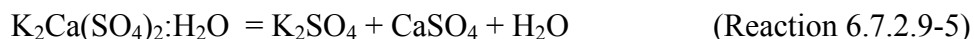
If the double salt is more stable than the two “component” single salts on the right hand side of this reaction, then its formation will necessarily reduce ionic concentrations in solution. In this particular case (two of these minerals not being all that soluble), that reduction might not be particularly notable. However, such a reduction might be more significant for a reaction involving more soluble minerals. An example would be the decomposition of picromerite [also known as schoenite; $\text{K}_2\text{Mg}(\text{SO}_4)_2\cdot 6\text{H}_2\text{O}$] to arcanite (K_2SO_4) and hexahydrate ($\text{MgSO}_4\cdot 6\text{H}_2\text{O}$):



Exact stoichiometric equivalence between a double salt and two simple salts may not obtain owing to a difference in bound water on the one side or the other. This is seen, for example, in the decomposition of syngenite to arcanite (K_2SO_4) and gypsum:



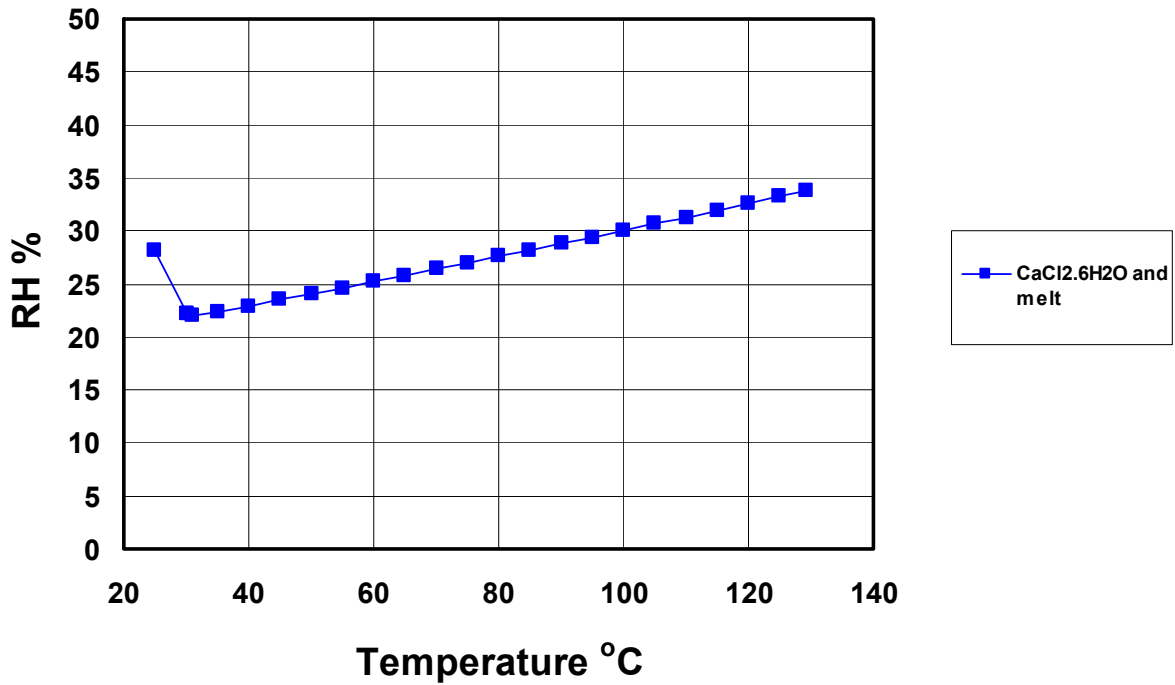
The imbalance persists if one substitutes anhydrite for gypsum:



It is possible to conduct IDPS modeling calculations for double salts in which the solubility or deliquescence RH of the hypothetical “pure” one-mineral systems, or both, are obtained. In this way, one could obtain data that cannot be obtained from corresponding experiments owing to the formation of additional minerals. However, the practical value, if any, of such calculations is at best uncertain. Consequently, they are not presented in this report.

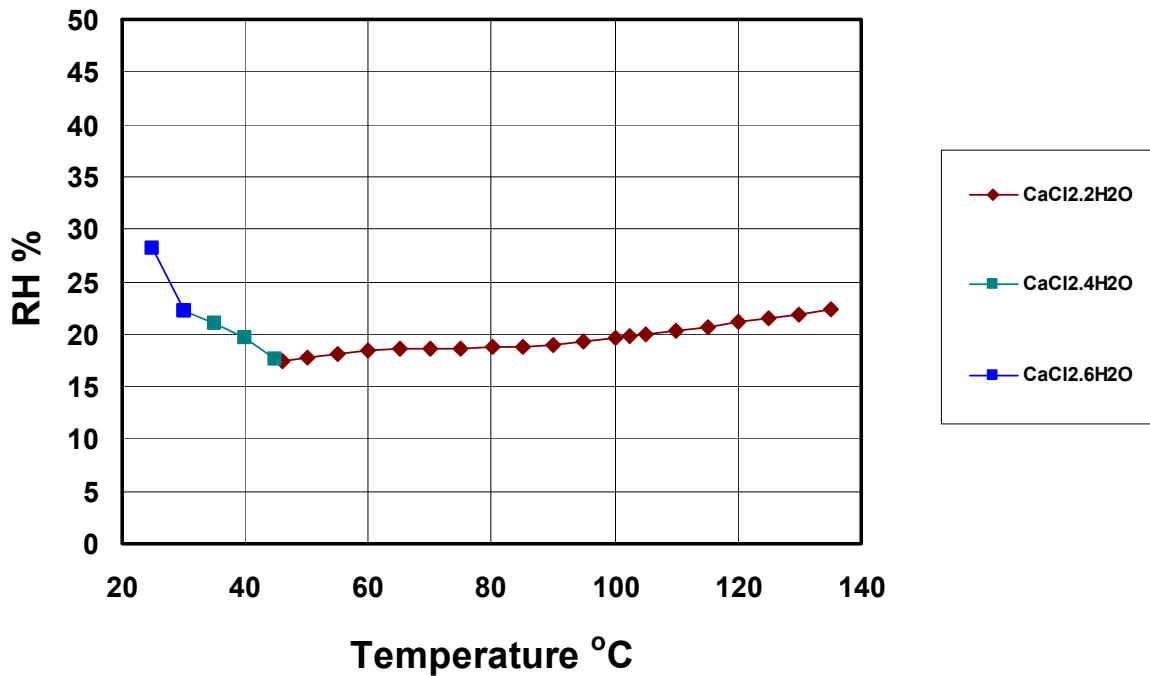
Figure 6.7-7 shows the deliquescence RH–T curve for antarcticite ($\text{CaCl}_2 \cdot 6\text{H}_2\text{O}$), a highly deliquescent salt mineral (reference the file *antarcti.6o*, folder RHTx1, in *Pack048.zip* in output DTN: LL040903723121.042). The deliquescence RH decreases rapidly with temperature from 25°C. At 30.0°C, the antarcticite is replaced by $\text{CaCl}_2 \cdot 4\text{H}_2\text{O}$, which itself dissolves completely at 31.0°C. At higher temperatures, no solid is present. In the run shown, 500 moles of antarcticite are added to 1 kg (55.51 moles) of water. The antarcticite contributes 3,000 moles of water, dwarfing the actual water the mineral was added to. A reasonable interpretation of these results is that near 30°C the antarcticite “melts” into an aqueous solution. At this melting point, it is very close to equilibrium with $\text{CaCl}_2 \cdot 4\text{H}_2\text{O}$. The portion of the deliquescence RH curve in Figure 6.7-7 for temperatures of 31°C and higher pertains to the deliquescence of an aqueous solution (“antarcticite melt”) whose composition is stoichiometrically the same as that of antarcticite. This part of the curve increases with temperature. The “melting” temperature of antarcticite in the IDPS model calculation agrees well with the decomposition (melting) temperature of 29.92°C cited in Table 6.7-6 and the 29.5°C, 29.95°C, and 29.93°C values cited in Table 4.1-6.

A more complete picture of phase equilibrium relations for CaCl_2 hydrates is given in Figure 6.7-8. This is a patchwork figure in which the parts of curves corresponding to “melt” only have been removed. Separate EQ3/6 runs are conducted for the two lesser hydrates $\text{CaCl}_2 \cdot 4\text{H}_2\text{O}$ and $\text{CaCl}_2 \cdot 2\text{H}_2\text{O}$. The run for the former began by adding 500 moles of $\text{CaCl}_2 \cdot 4\text{H}_2\text{O}$ to 1 kg of water, starting at close to 30°C. At about 45°C the solid then “melted,” being close to equilibrium with $\text{CaCl}_2 \cdot 2\text{H}_2\text{O}$. This melting temperature is quite close to the 45.3°C value cited for equilibrium between $\text{CaCl}_2 \cdot 4\text{H}_2\text{O}$ and $\text{CaCl}_2 \cdot 2\text{H}_2\text{O}$. The run for $\text{CaCl}_2 \cdot 2\text{H}_2\text{O}$ is similar, beginning near 46°C and continuing to the validation limit of 140°C, at which the results have the vapor pressure of water still below the total pressure limit of 0.90 bar.



Source: Output DTN: LL040903723121.042, *RHTE_Minerals1_PlotsA_v2p1.xls*.

Figure 6.7-7. Deliquescence RH as a Function of Temperature for Antarcticite ($\text{CaCl}_2 \cdot 6\text{H}_2\text{O}$), a Highly Deliquescent Salt, and (above 30°C to 31°C) its “Melt”



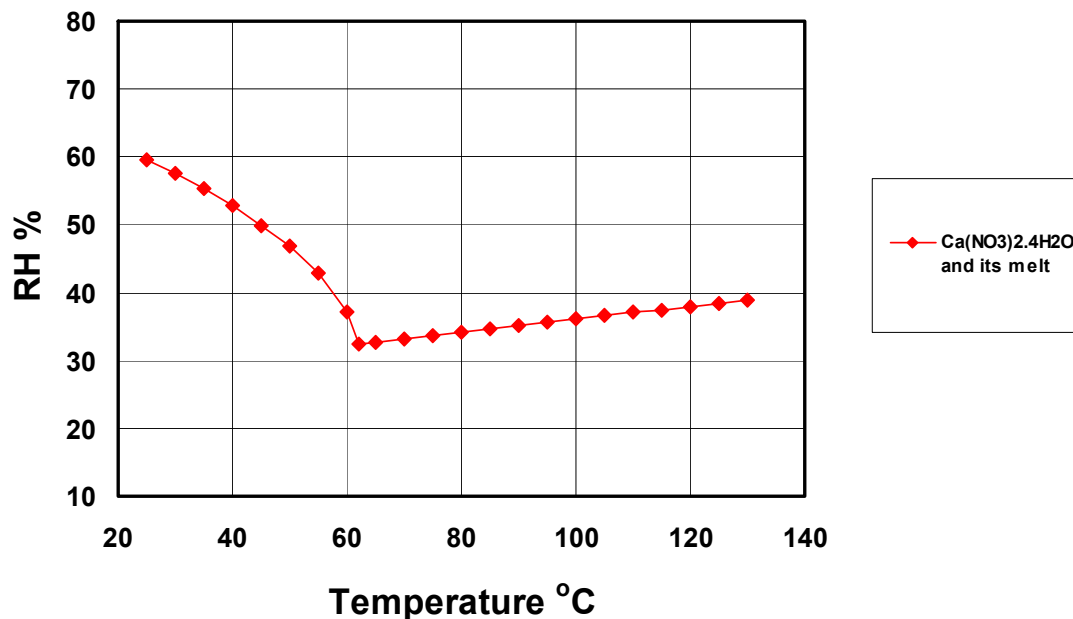
Source: Output DTN: LL040903723121.042, *RHTE_Minerals1_PlotsA_v2p1.xls*.

Figure 6.7-8. Deliquescence RH as a Function of Temperature for Successively Less Hydrated CaCl_2 Minerals (Antarcticite, $\text{CaCl}_2 \cdot 6\text{H}_2\text{O}$; $\text{CaCl}_2 \cdot 4\text{H}_2\text{O}$; and $\text{CaCl}_2 \cdot 2\text{H}_2\text{O}$)

Figure 6.7-9 shows the deliquescence RH–T curve for $\text{Ca}(\text{NO}_3)_2 \cdot 4\text{H}_2\text{O}$, another highly deliquescent salt mineral. It shows behavior that is similar to that of $\text{CaCl}_2 \cdot 6\text{H}_2\text{O}$, though it is not as highly deliquescent as that salt. The deliquescence RH decreases significantly with temperature from 25°C. At 62°C the $\text{Ca}(\text{NO}_3)_2 \cdot 4\text{H}_2\text{O}$ melts (being close to saturation with $\text{Ca}(\text{NO}_3)_2 \cdot 3\text{H}_2\text{O}$). The remainder of the curve describes the deliquescence of the melt (500 moles of the salt are added to 1 kg of water, so the composition of the melt is quite close to that of the solid). The IDPS model validation range is generally exceeded by the calculations shown in Figure 6.7-9, in that the deviation of calculated RH from experimental RH (e.g., Table 6.7-17) is greater than the 10 RH percent (0.1 unit in the activity of water) validation limit (BSC 2004 [DIRS 169863], Table 7-1) starting at a temperature between 25°C and 30°C. At 60°C, the difference is about 16 RH percent. Table 6.7-17 contains no data for the “melt” case, so further comparison is not possible.

The calculated 62°C melting point is notably higher than the 42.7°C decomposition (melting) temperature noted in Table 6.7-6. The 42.7°C temperature is also cited in Table 4.1-5 as the equilibrium temperature for the tetrahydrate and the trihydrate. In theory, in considering the progression of phase relations, $\text{Ca}(\text{NO}_3)_2 \cdot 4\text{H}_2\text{O}$ should be followed by $\text{Ca}(\text{NO}_3)_2 \cdot 3\text{H}_2\text{O}$, analogous to $\text{CaCl}_2 \cdot 6\text{H}_2\text{O}$ being followed by $\text{CaCl}_2 \cdot 4\text{H}_2\text{O}$. According to the data in Table 4.1-5, the trihydrate should be replaced by the dihydrate near 50.6°C. The anhydrous form [$\text{Ca}(\text{NO}_3)_2$] appears very soon thereafter (certainly by 55°C), and this should be the relevant form up to the boiling temperature of 151°C. An attempt to run a calculation for the trihydrate failed, however, as melting of this phase is predicted at essentially the same 62°C as for the tetrahydrate. All told, the calcium nitrate submodel of the current version of the high-temperature Pitzer IDPS model is more uncertain than many other parts, certainly compared to the calcium chloride submodel.

If the first rule of deliquescence is that it is an equilibrium phenomenon, the second rule must be that the deliquescence RH of any salt mineral assemblage is lower than that of any contained mineral or subassemblage. This point is illustrated in Figure 6.7-10, which compares the single-mineral deliquescence RH curves for halite (NaCl) and soda niter (NaNO_3 ; also known as nitratine) with the two mineral deliquescence RH curve for the same two minerals. Near 25°C the two salts are individually nearly as deliquescent (deliquescence RH close to 74 to 75 percent) and the deliquescence RH for the two-mineral assemblage is significantly lower (around 68 percent). At higher temperature, the deliquescence RH for soda niter is significantly reduced, near 55 percent at 120°C. At this temperature, the deliquescence RH for the two-mineral assemblage is lower than that, but almost insignificantly so. This example illustrates two cases. When two deliquescent minerals have roughly the same deliquescence RH, the deliquescence RH of the corresponding two-mineral assemblage is usually significantly lower than the deliquescence RH for either of the single minerals. When there is a significant difference between the deliquescence RH values of two single minerals, the deliquescence RH of the assemblage of these minerals is usually less than, but close to the deliquescence RH for the more deliquescent of the two single minerals.

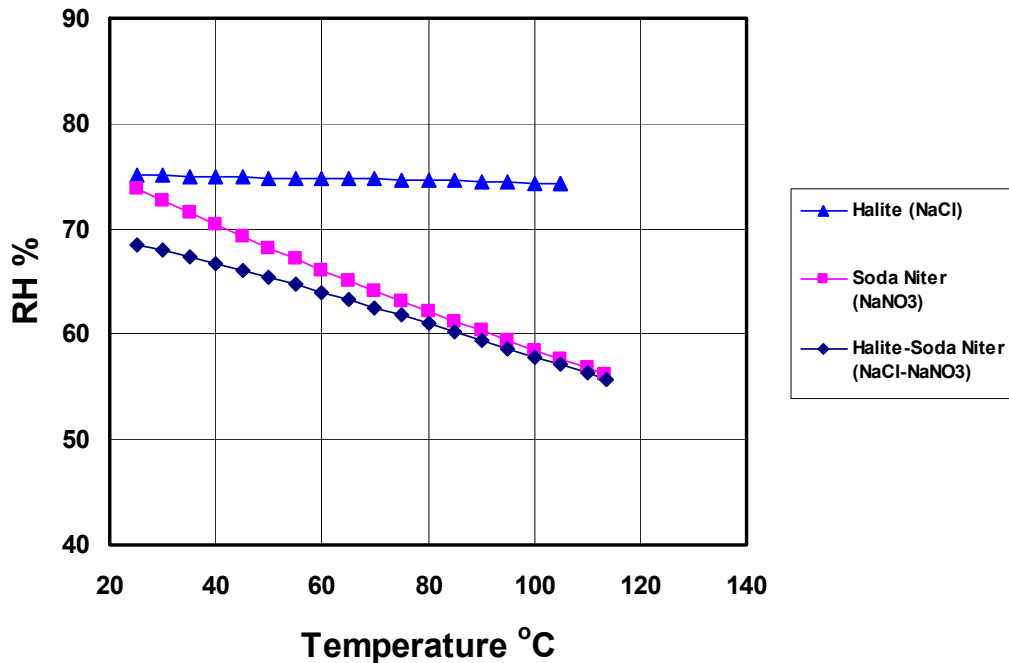


Source: DTN: LL040903723121.042, *RHTE_Minerals1_PlotsA_v2p1.xls*.

NOTE: Only the data at and very close to 25°C (somewhat less than 30°C) fall within the IDPS model validation criterion for error in calculating the RH. These results are presented only for purposes of describing limitations of the IDPS model. Actual experimental data are given in Table 6.7-17.

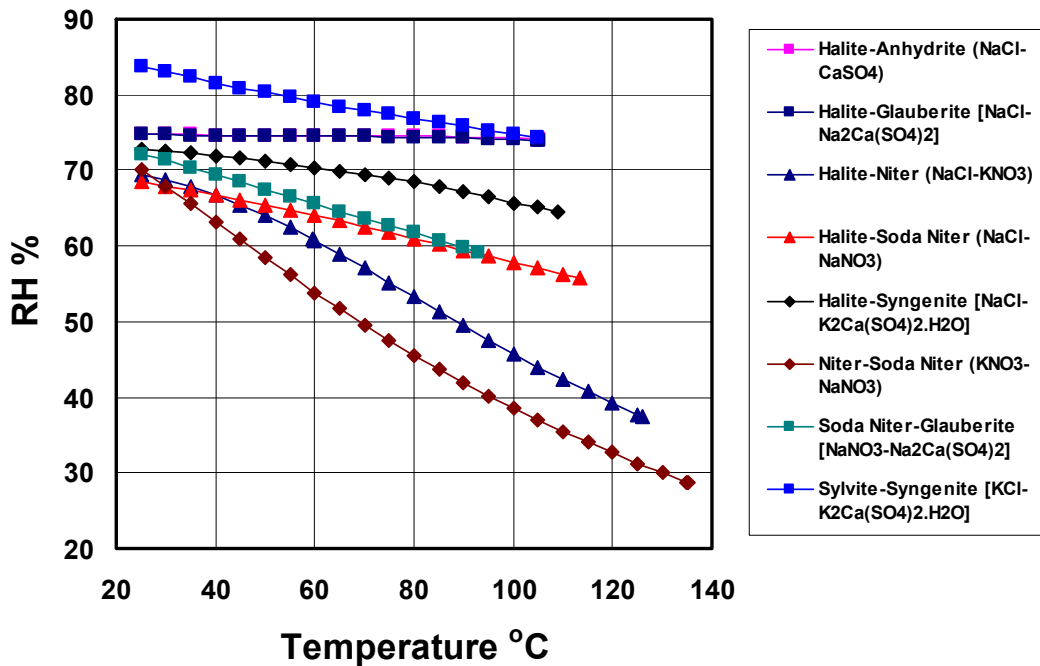
Figure 6.7-9. Deliquescence RH as a Function of Temperature for $\text{Ca}(\text{NO}_3)_2 \cdot 4\text{H}_2\text{O}$, a Highly Deliquescent Salt, and (above 45°C) its “Melt”

Figure 6.7-11 shows calculated deliquescence RH–T curves for several two-mineral assemblages. The relevant EQ3/6 files for two-mineral assemblages are in the folder: RHT×2 in *Pack048.zip* in output DTN: LL040903723121.042. This tends to mark the point at which IDPS modeling starts to provide information for more systems than existing experimental results. These calculations are subject to the same kinds of complications as have been described earlier for some of the nominally “single-mineral” systems. The halite-anhydrite and niter-soda niter calculations involve no complications. On the other hand, the curve for halite-syngenite [$\text{NaCl-K}_2\text{Ca}(\text{SO}_4)_2 \cdot \text{H}_2\text{O}$] (reference the file *halsyn.6o*, folder RHTx2, in *Pack048.zip* in output DTN: LL040903723121.042) presents quite a few. At 25°C the system contains glauberite ($\text{Na}_2\text{Ca}(\text{SO}_4)_2$) and pentasalt [$\text{K}_2\text{Ca}_5(\text{SO}_4)_6 \cdot \text{H}_2\text{O}$] in addition to halite and syngenite. At 111.4°C anhydrite (CaSO_4) replaces pentasalt. At 114.8°C, sylvite (KCl) replaces halite, and at 129.0°C, arcanite (K_2SO_4) replaces syngenite. The system then contains neither of the two salt minerals used to define the run. The assemblage anhydrite-arcanite-glauberite-sylvite holds up to at least the validation limit of 140°C. The curve shown in the figure is truncated at 109.07°C, consistent with the specified limit of 0.90 bar on the water vapor pressure. Thus, the final assemblage on the curve shown is anhydrite-glauberite-sylvite-syngenite. The calculated curve for soda niter-glauberite ($\text{NaNO}_3\text{-Na}_2\text{Ca}(\text{SO}_4)_2$) ends at 93°C. This is caused by an IDPS model convergence problem that appears to be associated with the Pitzer mixture parameters involving nitrate and sulfate.



Source: Output DTN: LL040903723121.042, *RHTE_Minerals1_PlotsA_v2p1.xls*.

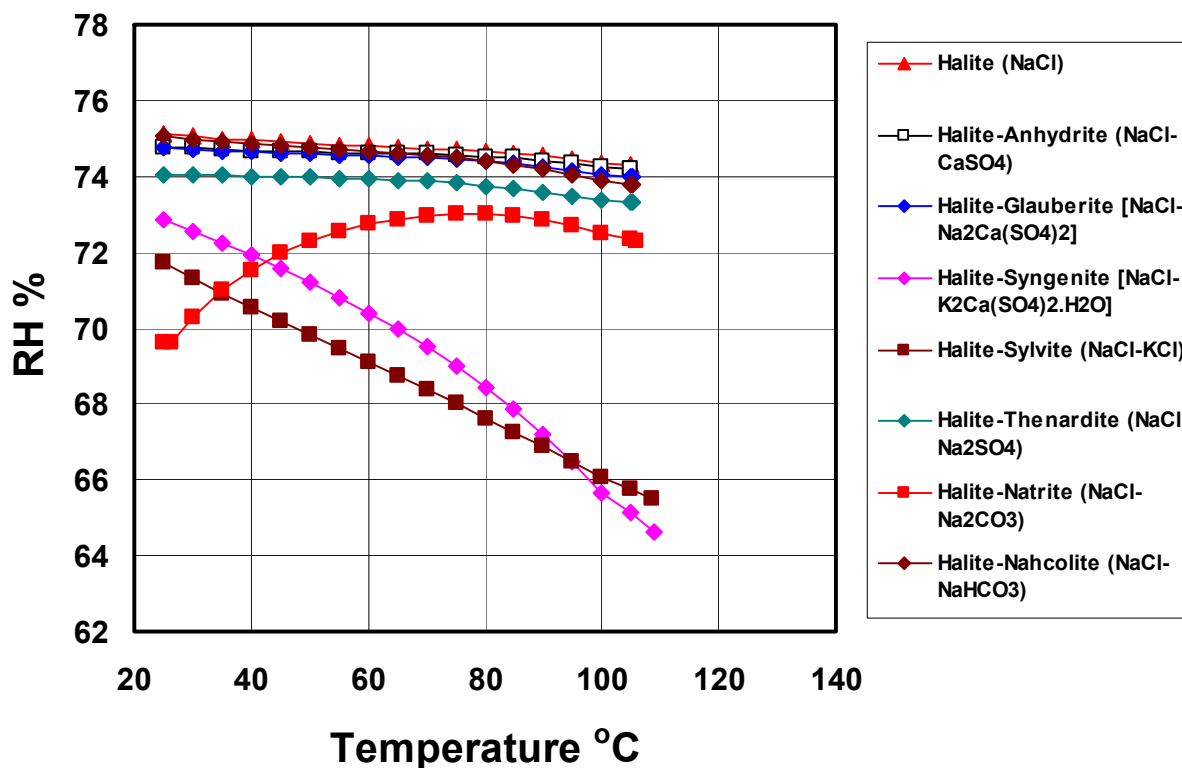
Figure 6.7-10. Deliquescence RH as a Function of Temperature for the Single Minerals Halite (NaCl) and Soda Niter (NaNO₃) and the Two-Mineral Assemblage Halite and Soda Niter (NaCl-NaNO₃)



Source: Output DTN: LL040903723121.042, *RHTE_Minerals1_PlotsA_v2p1.xls*.

Figure 6.7-11. Deliquescence RH as a Function of Temperature for Several Two-Mineral Assemblages

Figure 6.7-12 shows how the deliquescence RH-T curve for halite (NaCl) is altered by the addition to the assemblage of a second salt mineral. Slightly deliquescent salts like anhydrite (CaSO_4), glauberite ($\text{Na}_2\text{Ca}(\text{SO}_4)_2$), and nahcolite (NaHCO_3) make almost no difference (<1 percentage point in the RH), and even a somewhat more deliquescent salt like thenardite (Na_2SO_4) causes only a small perturbation of about one percentage point. Natrite (Na_2CO_3) causes a perturbation greater than five percentage points at 25°C; however, the perturbation declines to about 2 percentage points near 80°C. Sylvite (KCl) and syngenite [$\text{K}_2\text{Ca}(\text{SO}_4)_2 \cdot \text{H}_2\text{O}$] cause a generally stronger perturbation, especially at higher temperature, though the effect of either is somewhat less than that of natrite at 25°C.



Source: Output DTN: LL040903723121.042, *RHTE_Minerals1_PlotsA_v2p1.xls*.

Figure 6.7-12. Deliquescence RH as a Function of Temperature for Halite (NaCl) and Some Two-Mineral Assemblages Containing Halite

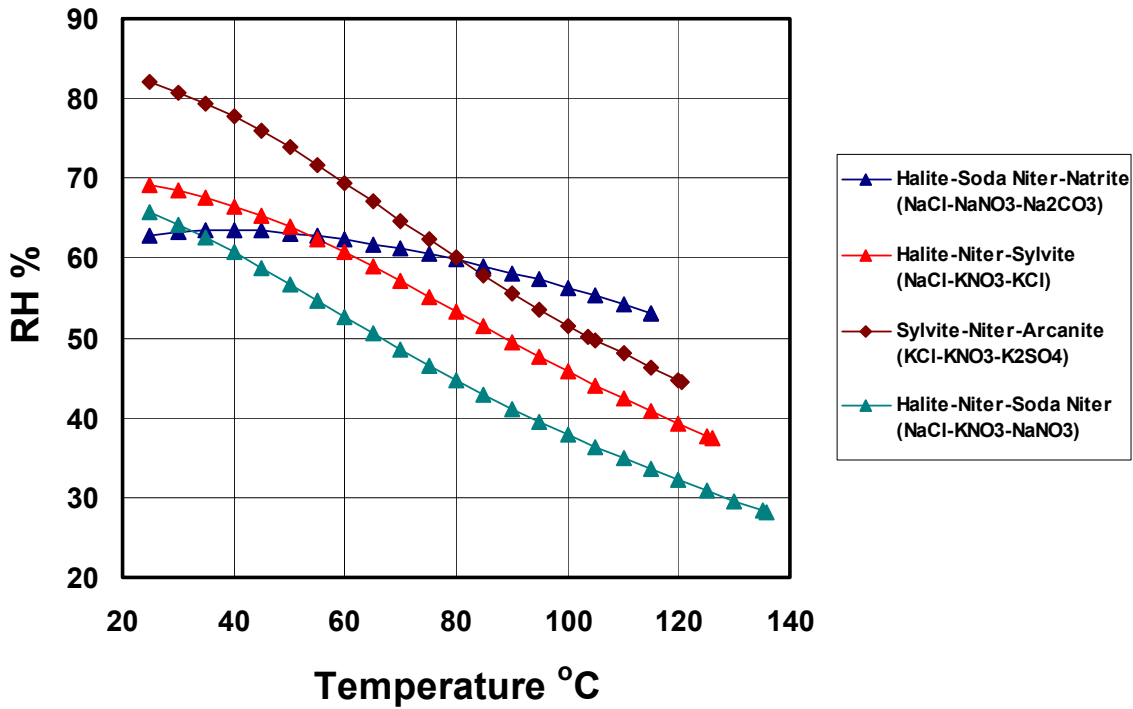
The main point introduced by Figure 6.7-12 is, as far as the deliquescence RH of an assemblage is concerned, minerals in the assemblage do not matter equally. The effect of adding anhydrite or glauberite to a significantly more deliquescent mineral such as halite makes little difference, and one could just use the deliquescence RH curve for halite alone for these assemblages with negligible error. This principle does not seem very useful in dealing with two-mineral assemblages which exhibit straightforward behavior. However, its extension to larger assemblages (more than 2 salts) provides a very useful tool. As the number of minerals in an assemblage becomes larger (ultimately limited only by the apparent or mineralogical phase rule for the number of components considered (Wolery 1979 [DIRS 156741], pp. 22 and 23), the number of possible permutations drawn on a set of minerals such as that in Table 6.5-1 may

become quite large. The utility of analyzing smaller and common sub-assemblages that control and adequately represent the details of interest (such as deliquescence RH versus temperature) then becomes apparent. As far as deliquescence RH is concerned, it is shown that even in ten-mineral assemblages, the deliquescence RH–T curve is generally adequately represented by one to three of the most deliquescent salt minerals. These are referred to as “key” or “driver” minerals.

Figure 6.7-13 shows deliquescence RH–T curves for some three-mineral assemblages. The relevant EQ3/6 files for three-mineral assemblages are in the folder: RHTx3 in *Pack048.zip* in output DTN: LL040903723121.042. The main point here is to show that calculations for such assemblages can be made. Experimental data on such systems tend to be scarce. As in the single- and two-mineral assemblage cases discussed previously, these calculations may or may not involve complications such as the presence of additional minerals. There are no complications in the case of the halite–niter–soda niter (NaCl-KNO₃-NaNO₃), the halite–niter–sylvite (NaCl-KNO₃-KCl), and the sylvite–niter–arcanite (KCl-KNO₃-K₂SO₄) assemblages. There are no mineralogical complications in the case of the halite–soda niter–natrite (NaCl-NaNO₃-Na₂CO₃) assemblage, but fairly low CO₂ pressures are implied: 4.86×10^{-8} bar at 25°C; 1.01×10^{-6} bar at 50°C; 5.29×10^{-6} at 75°C; 1.11×10^{-5} at 100°C; and 5.09×10^{-6} at 125°C. At the higher temperatures, these values are in the repository-relevant range (above boiling).

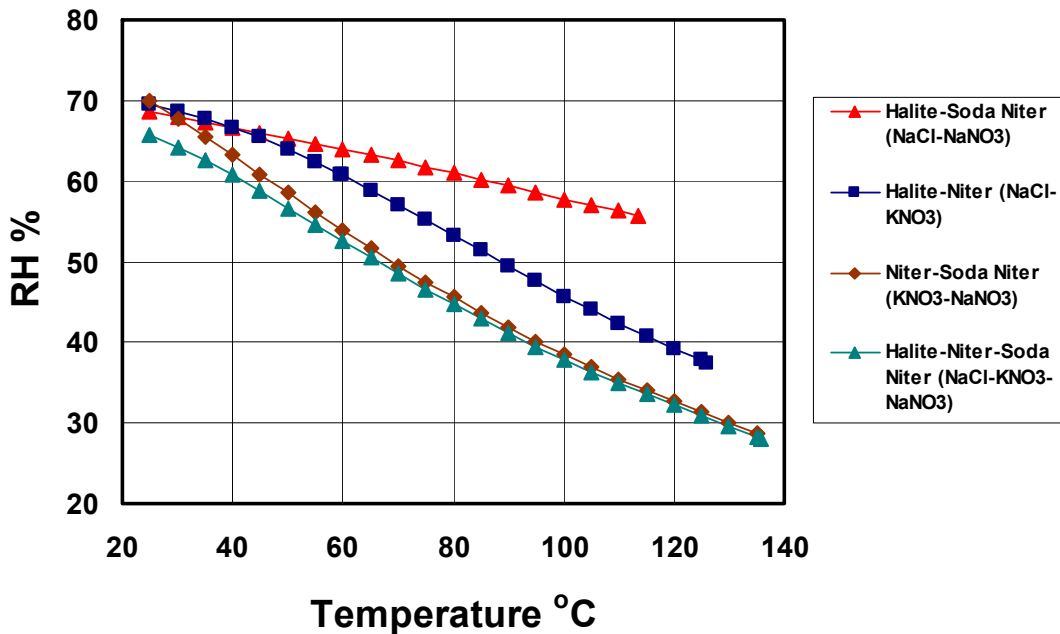
Figure 6.7-14 provides further illustration of the fact that the deliquescence RH of a mineral assemblage is lower than the deliquescence RH of any contained mineral or subassemblage. Deliquescence RH–T curves are shown for the three-mineral assemblage halite–niter–soda niter (NaCl-KNO₃-NaNO₃) and for the three contained two-mineral subassemblages. Note that the curve for the three-mineral assemblage and the two-mineral assemblage niter–soda niter (KNO₃-NaNO₃) are close, especially at the higher temperature. This indicates that the two nitrate minerals are the major drivers in regard to the deliquescence RH of the three-mineral assemblage. This is not surprising, as they are more deliquescent than halite. That point is shown in Figure 6.7-15, where the deliquescence RH curves for the three single minerals are presented.

In the case of a single-mineral system deliquescing, the composition of the aqueous solution is fixed (barring changes in temperature and pressure) as long as some of the solid phase remains. If that phase becomes completely dissolved, then the solution may become more dilute and the RH is no longer fixed at the deliquescence RH and may increase. Thus, if NaCl is placed in a dry atmosphere at 25°C and the RH is slowly increased (as by bringing in a gas mixture of desired RH), the salt phase would start to deliquesce at the deliquescence RH, here about 75 percent. By introducing a gas mixture of just slightly higher RH than the actual deliquescence RH, the solid salt mass would dissolve, the aqueous solution composition remaining constant as added water and added salt balance each other. Once the solid salt mass is gone, the aqueous salt solution will continue to deliquesce. As the RH is increased, the mass of aqueous solution will grow, but the dissolved salt concentration will decrease, becoming more and more undersaturated with respect to the no longer present solid.



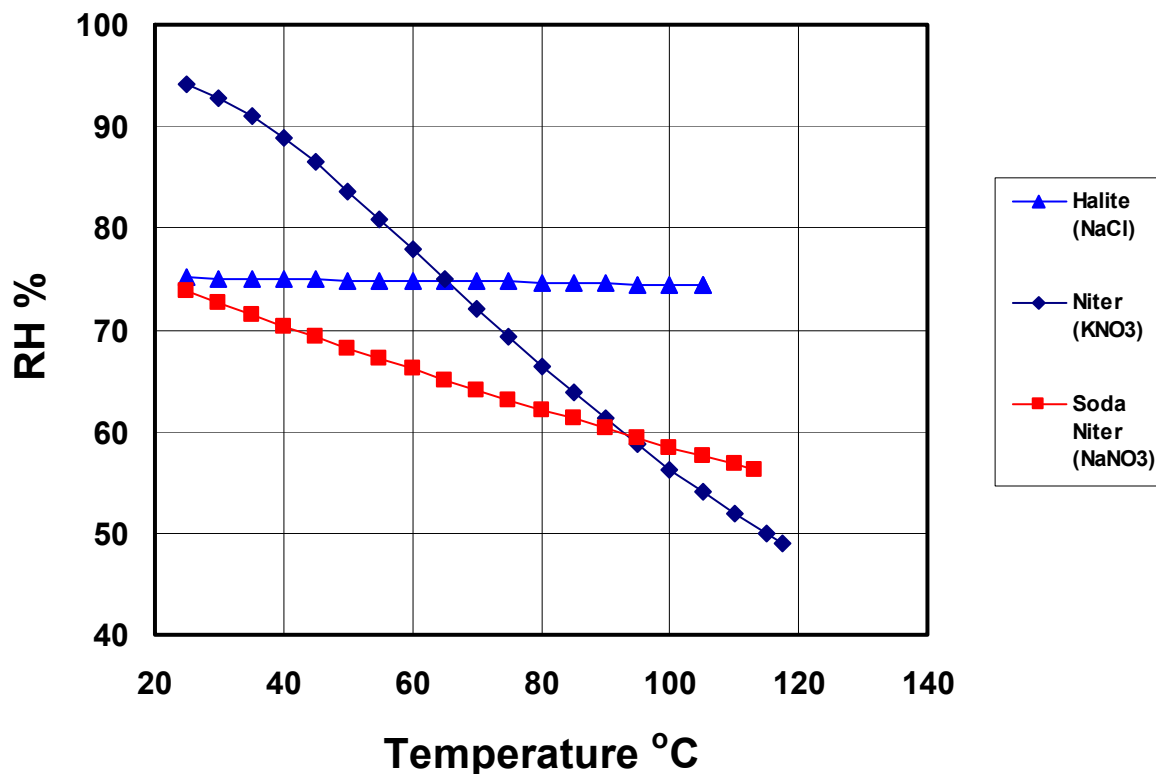
Source: Output DTN: LL040903723121.042, *RHTE_Minerals1_PlotsA_v2p1.xls*.

Figure 6.7-13. Deliquescence RH as a Function of Temperature for Some Three-Mineral Assemblages



Source: Output DTN: LL040903723121.042, *RHTE_Minerals1_PlotsA_v2p1.xls*.

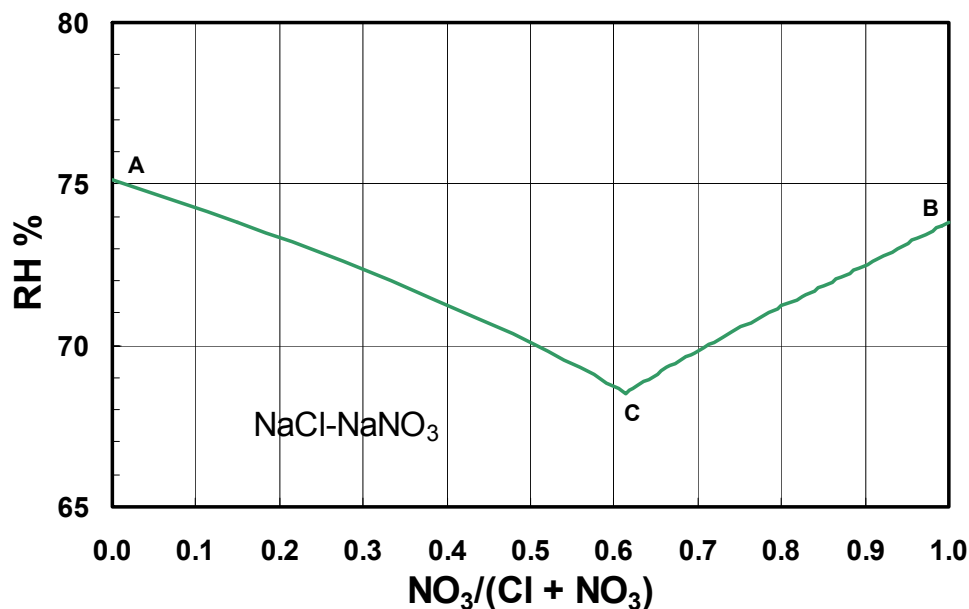
Figure 6.7-14. Deliquescence RH as a Function of Temperature for the Three-Mineral Assemblage Halite-Niter-Soda Niter (NaCl-KNO₃-NaNO₃) and the Three Contained Two-Mineral Assemblages



Source: Output DTN: LL040903723121.042, *RHTE_Minerals1_PlotsA_v2p1.xls*.

Figure 6.7-15. Deliquescence RH as a Function of Temperature for the Single Minerals Halite (NaCl), Niter (KNO₃), and Soda Niter (NaNO₃)

In the case of an assemblage of more than one mineral, the response to an externally driven increase in RH is complicated by the fact that not all of the minerals present will likely disappear at the same time. Rather, in general first one would disappear, then another, and so forth. A common method of showing the relationship of RH to aqueous solution composition for a two-salt system is exemplified by Figure 6.7-16, which shows RH as a function of the mole fraction of aqueous nitrate defined by the molality ratio $\text{NO}_3/(\text{Cl} + \text{NO}_3)$ for the system NaCl-NaNO₃-H₂O at 25°C. These data are taken from files *snha0a.csv* and *hasn0a.csv* in the folder Mixtures_HalSNi in *Pack048.zip* in output DTN: LL040903723121.042 (the “0a” is a code for 25°C, whereas for related files “04” denotes 40°C, “06” denotes 60°C, and so forth). Point A on the left side of the figure (the NaCl side) marks where the RH becomes equal to the deliquescence RH of halite (NaCl) in the system NaCl-H₂O. Point B on the right side (the NaNO₃ side) marks where the RH approaches the deliquescence RH of soda niter (NaNO₃) in the system NaNO₃-H₂O. Point C (just to the right of the middle of the plot) marks the deliquescence RH of the two-mineral assemblage halite plus soda niter. This diagram is consistent with the rule that the deliquescence RH of a mineral assemblage is lower than that of any contained mineral or mineral sub-assemblage. Note also that the two-salt deliquescence RH is also the lowest point on the composite curve, which is also necessary. The curve between point C and point A corresponds to saturation with halite (NaCl); the curve between point C and point D corresponds to saturation with soda niter (NaNO₃).



Source: Output DTN: LL040903723121.042, *RHTX_Minerals1_PlotsB_v2p1.xls*.

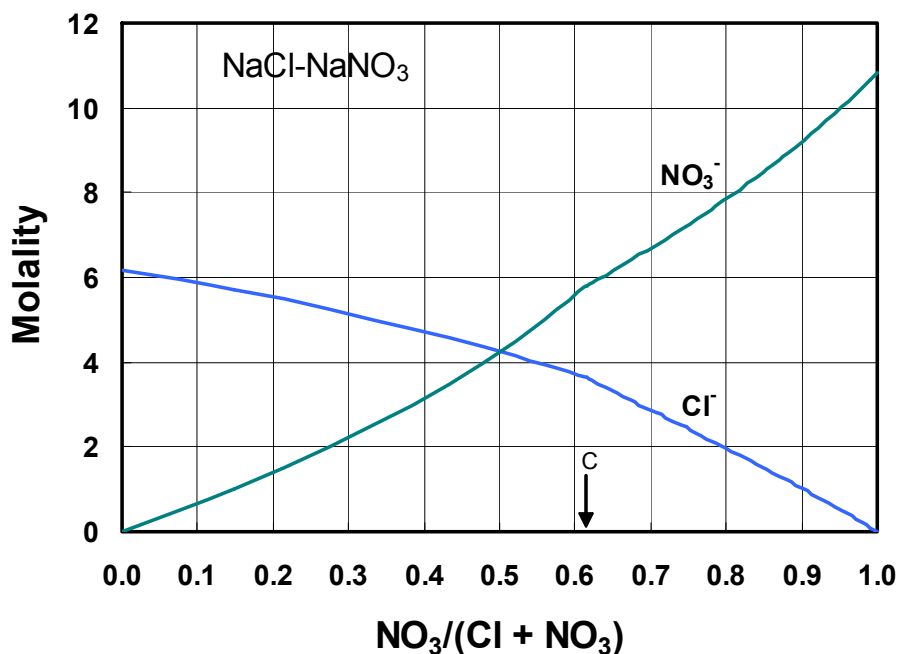
NOTE: Point A marks the deliquescence RH of halite in the system NaCl-H₂O, point B marks the deliquescence RH of soda niter in the system (NaNO₃-H₂O), and point C marks the deliquescence RH of halite and soda niter in the system NaCl-NaNO₃-H₂O.

Figure 6.7-16. RH versus Nitrate Mole Fraction [NO₃/(Cl + NO₃)] in Aqueous Solution in the Halite-Soda Niter (NaCl-NaNO₃) System at 25°C

If a physical mixture of halite and soda niter are used in an experiment at 25°C in which the RH is externally increased using controlled gas mixtures starting from some value below the deliquescence RH for the two-salt assemblage, the following events would occur. An aqueous solution would form at the two-salt deliquescence RH. The formation of this solution would maintain the local RH defined by point C (resisting the external driving force, a slightly higher RH in the introduced gas mixture) until one or both of the two solid salts is completely dissolved. If they disappear simultaneously, the RH would increase as the aqueous solution mass continued to grow. In this instance, the nitrate mole fraction would remain constant as the solution becomes more dilute. If the halite (NaCl) disappears first, the RH and composition will evolve along the curve leading from point C to point B. For a finite amount of halite initially present, the system cannot actually reach point B, which is a theoretical limit for the pure NaNO₃-H₂O system. If the soda niter (NaNO₃) disappears at some point along the curve from point C to point B, the relative humidity is no longer bound to the curve and will move vertically upward at a constant nitrate mole fraction that corresponds to the proportions of nitrate and chloride present in the initial salt masses. If the soda niter disappears before the halite, then the system will instead move along the curve from point C to point A, behaving in analogous manner (never reaching point A for a finite amount of soda niter initially present). If halite and soda niter disappear simultaneously, the RH will rise vertically above the nitrate mole fraction for the eutectic point.

The corresponding molalities of nitrate and chloride are shown in Figure 6.7-17 (the data are taken from files *snha0a.csv* and *hasn0a.csv*, folder: Mixtures_HalSNi in *Pack048.zip* in output

DTN: LL040903723121.042). The maximum for the nitrate curve is substantially greater than that for the chloride curve, reflecting the fact that soda niter is much more soluble than halite. There is a slight break in the slope of the two curves at the mole fraction of nitrate corresponding to the deliquescence RH for the two-salt assemblage (the ordinate for which is marked in the figure by "C").



Source: Output DTN: LL040903723121.042, *RHTX_Minerals1_PlotsB_v2p1.xls*.

NOTE: The x-axis coordinate for point C (the deliquescence RH for the two-salt assemblage) is marked by "C" and an arrow.

Figure 6.7-17. Nitrate and Chloride Molalities versus Nitrate Mole Fraction [$\text{NO}_3/(\text{Cl} + \text{NO}_3)$] in Aqueous Solution in the Halite-Soda Niter (NaCl-NaNO_3) System at 25°C

The NO_3/Cl ratio is a potential factor in localized corrosion modeling (NO_3 acting as an inhibitor, Cl as a promoter; e.g., Farmer et al. 2000 [DIRS 156521]). At the two-salt deliquescence RH in the $\text{NaCl-NaNO}_3\text{-H}_2\text{O}$ system, the aqueous solution contains more nitrate than chloride; hence the NO_3/Cl ratio is greater than unity at this point. A lower nitrate to chloride ratio can only be achieved if the soda niter can be completely dissolved away before the halite (so that the system then evolves to the left on Figures 6.7-16 and 6.7-17). To lower the NO_3/Cl to 0.25, the mole fraction of nitrate must be reduced to 0.2 (at which point the mole fraction of chloride is 0.8). Inspection of Figure 6.7-16 indicates that although the two-salt assemblages deliquesce at an RH of about 68 percent, the minimum RH required to achieve a NO_3/Cl ratio of 0.25 is about 74 percent. If halite disappears before soda niter, the system evolves to the right on Figures 6.7-16 and 6.7-17 and the NO_3/Cl ratio only increases with increasing RH.

RH and aqueous solution composition relationships of the type shown in Figures 6.7-16 and 6.7-17 depend on temperature. Figure 6.7-18 shows how the RH versus [$\text{NO}_3/(\text{Cl} + \text{NO}_3)$] curves for the system $\text{NaCl-NaNO}_3\text{-H}_2\text{O}$ vary over the range 25°C to 100°C. The curves for the

various temperatures considered do not change much on the NaCl side, but change quite markedly on the NaNO₃ side. This is a consequence of the near-constancy with increasing temperature of the deliquescence RH of halite in the system NaCl-H₂O and the notable decrease with increasing temperature of the deliquescence RH of soda niter in the system NaNO₃-H₂O. A related factor is that the solubility of halite increases slowly with temperature, while that of soda niter increases markedly. The solubility changes are evident in Figure 6.7-19, which shows the molality of nitrate and chloride as functions of NO₃/(Cl + NO₃) for the same temperatures considered in Figure 6.7-18.

Another way of expressing these RH-composition relationships is to replace the aqueous mole fraction variable with a composite normalized reaction progress variable (ξ). Consider that to get from a saturated halite (NaCl) solution in the NaCl-H₂O system to the deliquescence RH (mutual saturation) point in the system NaCl-NaNO₃-H₂O, one must dissolve x' moles of NaNO₃. Also, to get to the same point starting from a saturated soda niter (NaNO₃) solution in the NaNO₃-H₂O system, one must dissolve y' moles of NaCl. The normalized reaction progress variable is then defined in the following way. For the curve associated with the NaCl side, let x be the number of moles of NaNO₃ added. For $0 < x \leq x'$, the normalized progress variable is given by:

$$\xi = x/(x' + y') \quad (\text{Eq. 6.7.2.9-6})$$

For the curve associated with the NaNO₃ side, let y be the number of moles of NaCl added. For $0 < y \leq y'$, the normalized progress variable is given by:

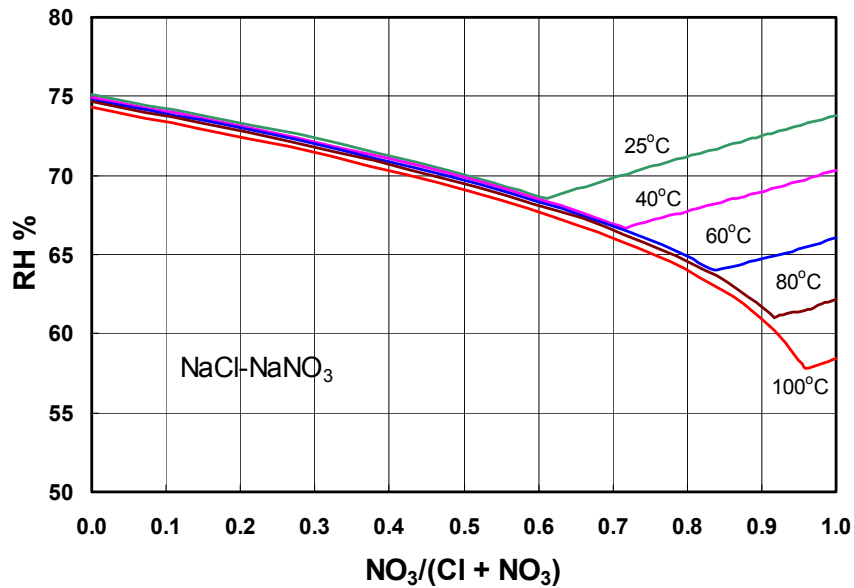
$$\xi = (x' + y' - y)/(x' + y') \quad (\text{Eq. 6.7.2.9-7})$$

By either formula, the normalized progress variable at the deliquescence RH (mutual saturation) point is given by:

$$\xi' = x'/(x' + y') \quad (\text{Eq. 6.7.2.9-8})$$

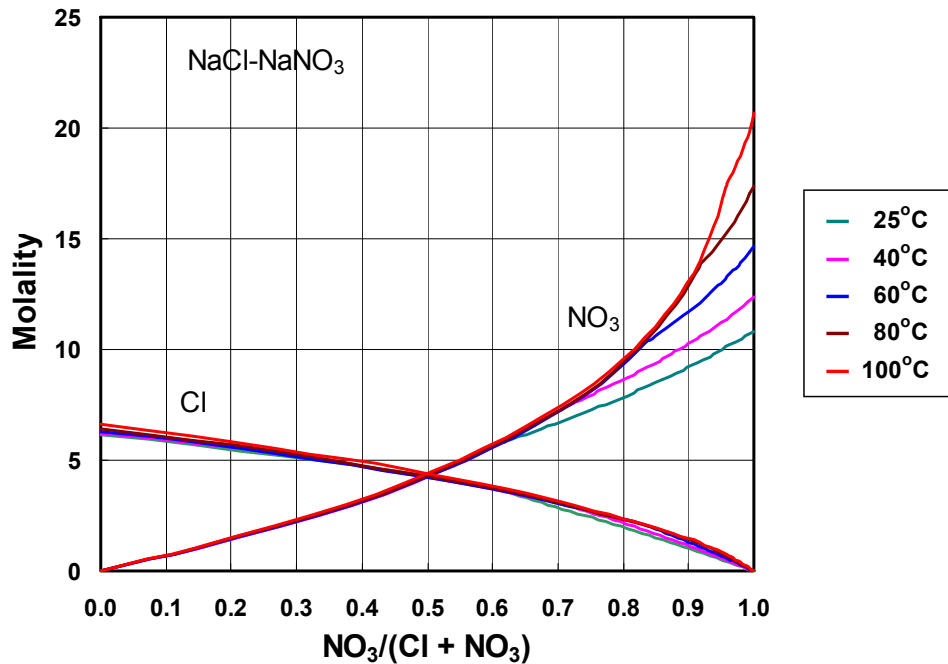
Figure 6.7-20 shows the RH versus the normalized progress variable. Note the similarity of these results versus those shown in Figure 6.7-18, in which RH is plotted versus [NO₃/(Cl + NO₃)] for the same temperatures considered here. The basic picture is similar, but the curves seem distorted when compared with their counterparts in Figure 6.7-18 owing to the change in the variable associated with the abscissa. The curves in the present figure appear more linear, at least in segments.

Figure 6.7-21 shows the nitrate and chloride molalities for the NaCl-NaNO₃-H₂O system versus the normalized progress variable, again for the same temperatures. Note the similarity of these results versus those shown in Figure 6.7-19, in which these same molalities are plotted versus [NO₃/(Cl + NO₃)] for the same temperatures considered here. The basic picture is similar, but these curves also seem distorted compared with their counterparts in Figure 6.7-19. The curves in the present figure appear much more linear, at least in segments. That is a direct and logical consequence of the usage of a reaction-progress based variable along the abscissa.



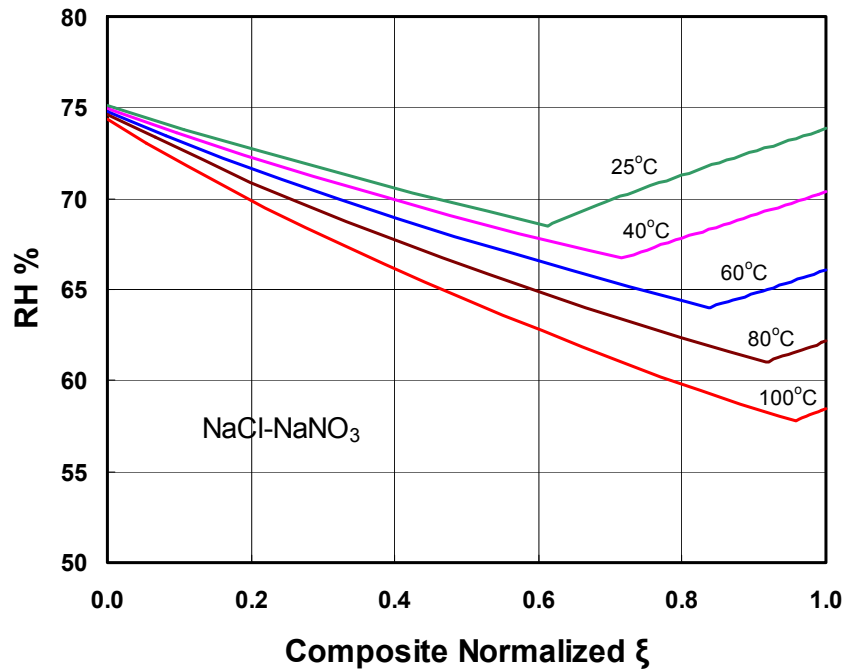
Source: Output DTN: LL040903723121.042, *RHTX_Minerals1_PlotsB_v2p1.xls*.

Figure 6.7-18. RH versus Nitrate Mole Fraction $[NO_3/(Cl + NO_3)]$ in Aqueous Solution in the Halite-Soda Niter (NaCl-NaNO₃) System at Temperatures of 25°C, 40°C, 60°C, 80°C, and 100°C



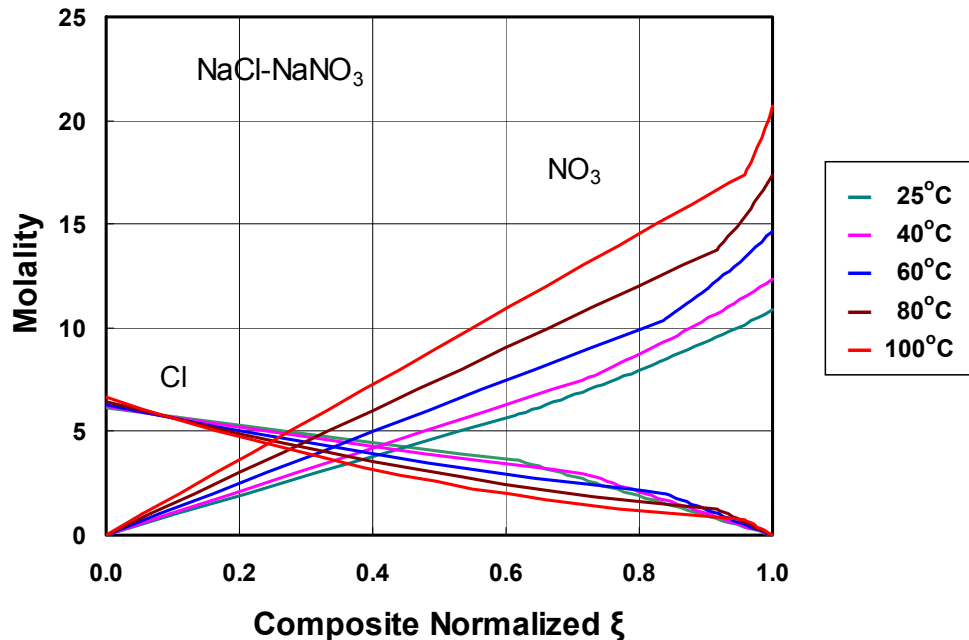
Source: Output DTN: LL040903723121.042, *RHTX_Minerals1_PlotsB_v2p1.xls*.

Figure 6.7-19. Nitrate and Chloride Molalities versus Nitrate Mole Fraction $[NO_3/(Cl + NO_3)]$ in Aqueous Solution in the Halite-Soda Niter (NaCl-NaNO₃) System at Temperatures of 25°C, 40°C, 60°C, 80°C, and 100°C



Source: Output DTN: LL040903723121.042, *RHTX_Minerals1_PlotsB_v2p1.xls*.

Figure 6.7-20. RH versus Composite Normalized Reaction Progress (ξ) in Aqueous Solution in the Halite–Soda Niter (NaCl–NaNO₃) System at Temperatures of 25°C, 40°C, 60°C, 80°C, and 100°C



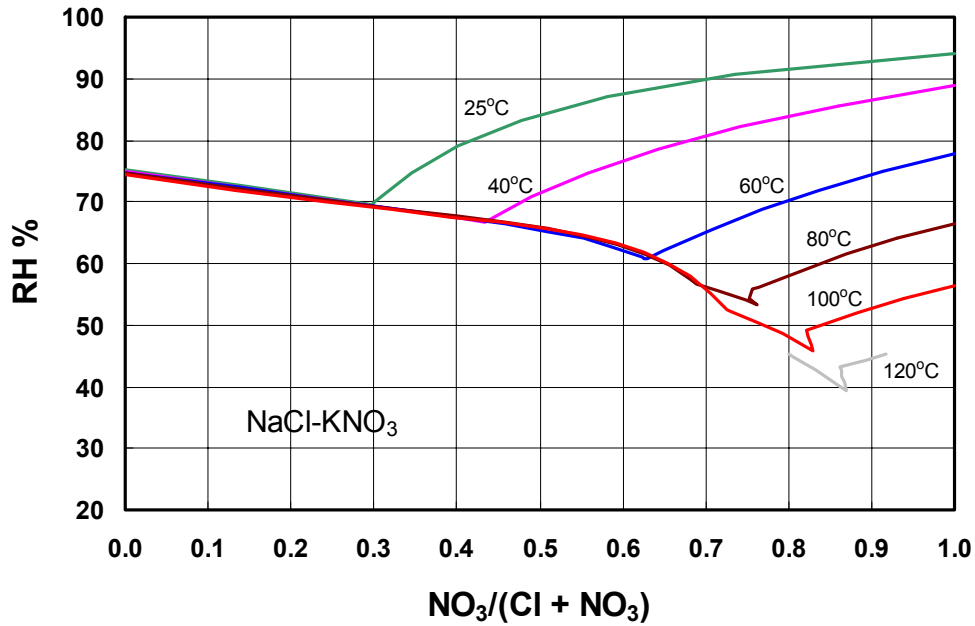
Source: Output DTN: LL040903723121.042, *RHTX_Minerals1_PlotsB_v2p1.xls*.

Figure 6.7-21. Nitrate and Chloride Molalities versus Composite Normalized Reaction Progress (ξ) in Aqueous Solution in the Halite–Soda Niter (NaCl–NaNO₃) System at Temperatures of 25°C, 40°C, 60°C, 80°C, and 100°C

The composite normalized reaction progress variable provides a more reliable metric of position between the two end-member systems in diagrams such as the figures presented above for the NaCl-NaNO₃-H₂O system. In essence, as one moves from one side of the end-member system to the other, this variable is guaranteed to be a monotonically increasing function. It might seem like a metric such as the aqueous nitrate mole fraction would also have that property. However, that is not always the case. Problems with the use of this variable may arise when additional solid phases appear between the end-member states. That does not occur in the NaCl-NaNO₃-H₂O system; hence, no problem is evident.

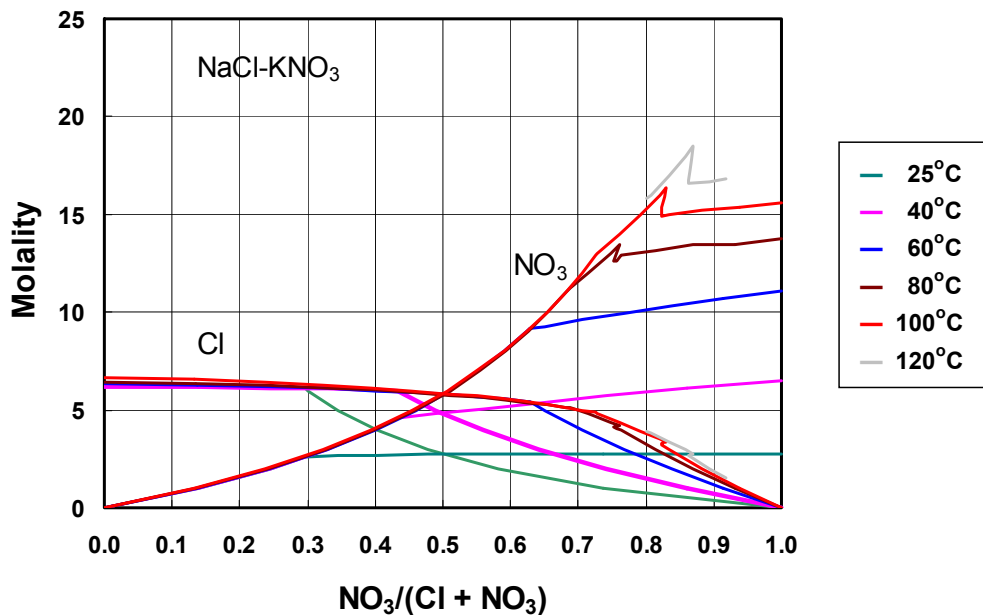
The NaCl-KNO₃-H₂O system illustrates the complication. Besides halite (NaCl) appearing to the left of the deliquescence RH (mutual saturation) point and niter (KNO₃) to the right, a third phase, sylvite (KCl) also appears under certain conditions. Figure 6.7-22 shows a set of traditional RH versus aqueous nitrate mole fraction curves for various temperatures in the range 25°C to 120°C. In general appearance, this figure resembles Figure 6.7-18, which contains a corresponding set of curves (though not for 120°C) for the NaCl-NaNO₃-H₂O system. However, the curves for 60°C and higher have a kink near the deliquescence RH (mutual saturation) point (the kink is not actually discernible on the 60°C curve in the figure). Close inspection shows that the kink causes the RH for certain values of the aqueous nitrate mole fraction variable to have as many as three values. Note that the 120°C curve only exists for relative humidity values that imply a partial pressure of water up to 0.90 bar, the total pressure limit adopted in this report. Figure 6.7-23 shows a set of traditional nitrate and chloride molalities versus aqueous nitrate mole fraction curves for the same set of temperatures. In general appearance, this figure resembles Figure 6.7-19, which contains the corresponding set of curves (though not for 140°C) for the NaCl-NaNO₃-H₂O system. For temperature of 60°C and higher, the kink is again expressed (though it is not really discernible on the 60°C curve in the figure).

Figure 6.7-24 (RH) and Figure 6.7-25 (molalities of nitrate and chloride) show the advantage of using the composite normalized reaction progress variable on the abscissa. The kinks are no longer present. In Figure 6.7-25, the curves for chloride molality for temperatures of 60°C and higher have a shallow depression near the right side of the figure corresponding to the precipitation of sylvite (KCl). In the case of the 60°C curve, this depression is not actually discernible in the figure. Sylvite only appears at temperatures of 60°C and above, and it is barely present at 60°C. For all temperatures at which sylvite is present, this mineral is present at the deliquescence RH (mutual saturation) point. Thus, that deliquescence RH is then associated with the presence of not two but three salt minerals. As the temperature increases from 60°C, the effect of sylvite precipitation becomes more pronounced and the interval of composite normalized progress variable space in which it is present increases in magnitude.



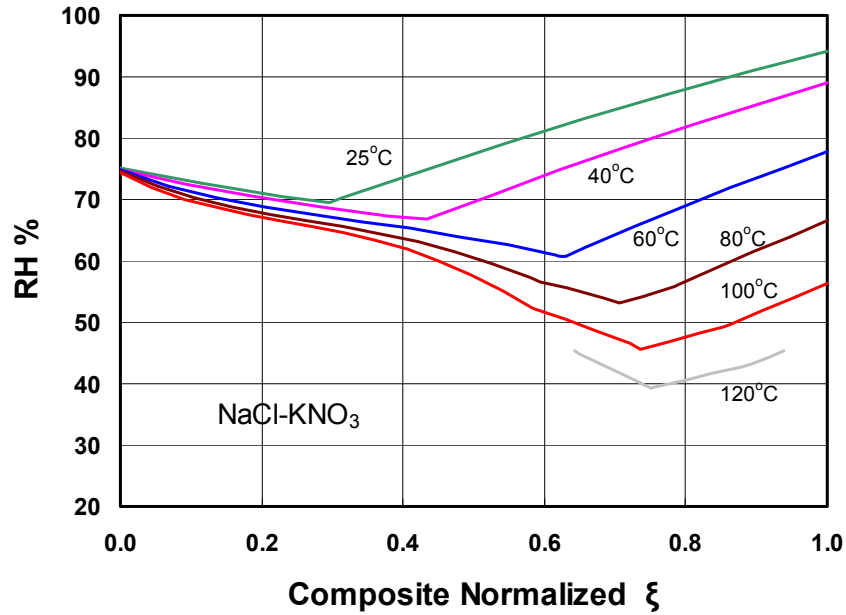
Source: Output DTN: LL040903723121.042, *RHTX_Minerals1_PlotsB_v2p1.xls*.

Figure 6.7-22. RH versus Nitrate Mole Fraction [$\text{NO}_3/(\text{Cl} + \text{NO}_3)$] in Aqueous Solution in the Halite-Niter (NaCl-KNO_3) System at Temperatures of 25°C, 40°C, 60°C, 80°C, 100°C, and 120°C



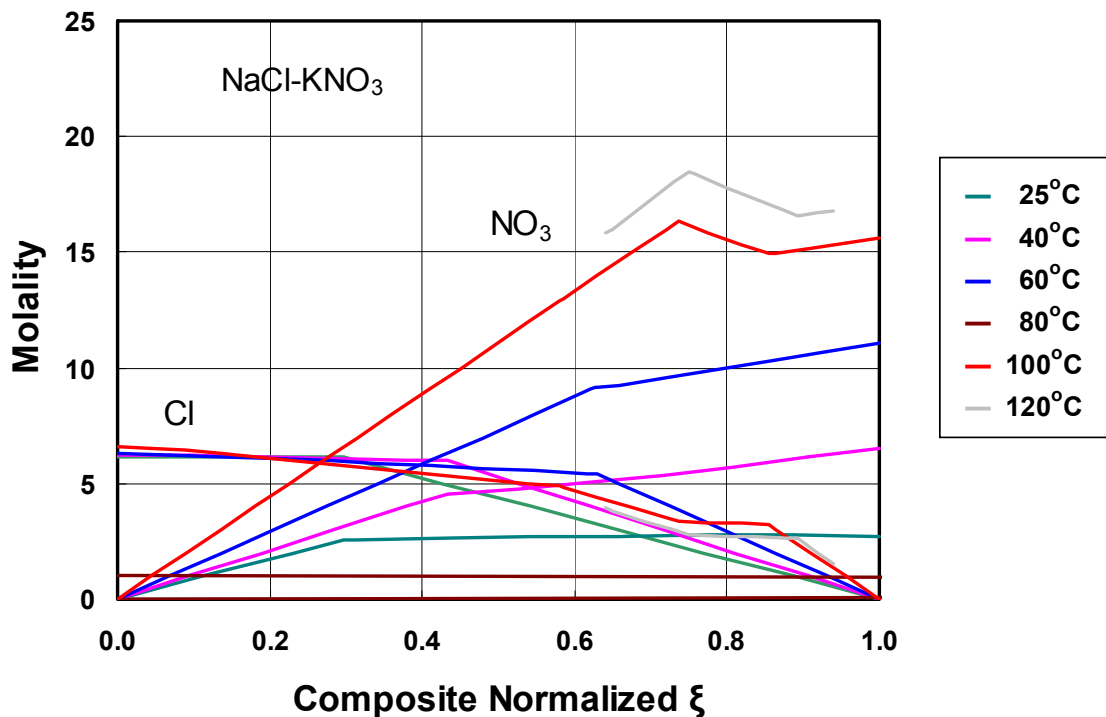
Source: Output DTN: LL040903723121.042, *RHTX_Minerals1_PlotsB_v2p1.xls*.

Figure 6.7-23. Nitrate and Chloride Molalities versus Nitrate Mole Fraction [$\text{NO}_3/(\text{Cl} + \text{NO}_3)$] in Aqueous Solution in the Halite-Niter (NaCl-KNO_3) System at Temperatures of 25°C, 40°C, 60°C, 80°C, 100°C, and 120°C



Source: Output DTN: LL040903723121.042, *RHTX_Minerals1_PlotsB_v2p1.xls*.

Figure 6.7-24. RH versus Composite Normalized Reaction Progress (ξ) in Aqueous Solution in the Halite-Niter (NaCl-KNO₃) System at Temperatures of 25°C, 40°C, 60°C, 80°C, 100°C, and 120°C

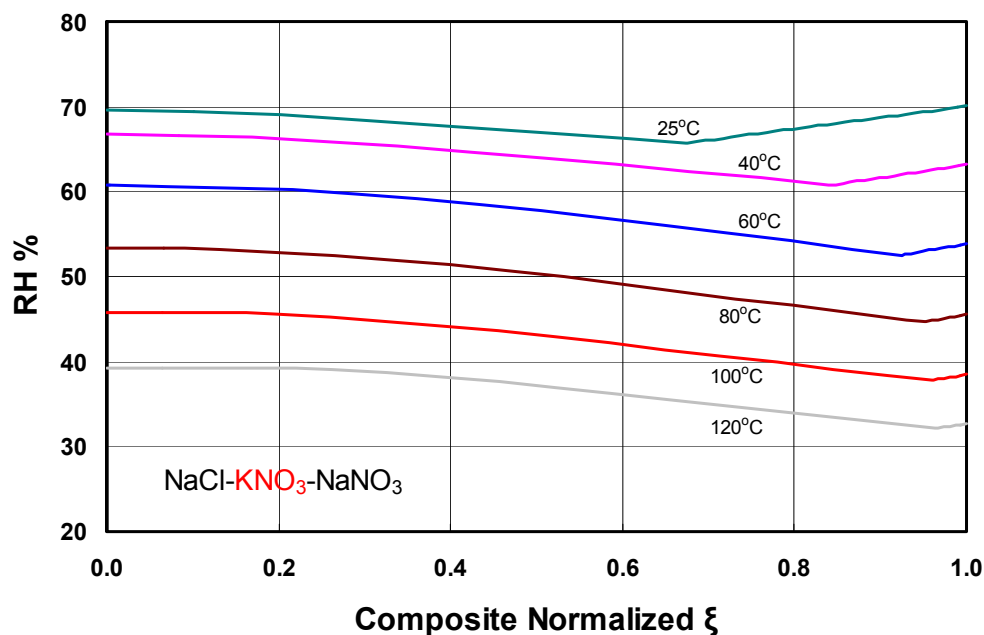


Source: Output DTN: LL040903723121.042, *RHTX_Minerals1_PlotsB_v2p1.xls*.

Figure 6.7-25. Nitrate and Chloride Molalities versus Composite Normalized Reaction Progress (ξ) in Aqueous Solution in the Halite-Niter (NaCl-KNO₃) System at Temperatures of 25°C, 40°C, 60°C, 80°C, 100°C, and 120°C

In interpreting plots where the composite normalized progress variable is used on the abscissa, it is important to keep in mind that the progress variable does not directly reflect the aqueous solution composition, as does, for example, the aqueous mole fraction of nitrate (or any other ion). Thus, if one is interested in the RH at which the NO_3/Cl ratio has a certain value (at a certain temperature), one must first consult a plot like Figure 6.7-25 to determine the value of the progress variable at which this occurs, then consult the corresponding plot for the RH (which in this case would be Figure 6.7-24).

Similar types of diagrams can be constructed for more complex mineral assemblages. A number of calculations are made for the assemblage halite niter-soda niter ($\text{NaCl-KNO}_3\text{-NaNO}_3$). An example is given in Figure 6.7-26. Thus is much like Figure 6.7-20, which shows the RH as a function of the normalized progress variable for the halite-soda niter (NaCl-NaNO_3) assemblage. The difference is the presence of the third mineral (niter, KNO_3) at saturation throughout. Thus the left side (“NaCl”) actually corresponds to a saturated solution of halite and niter, and the right side to one of soda niter and niter.



Source: Output DTN: LL040903723121.042, *RHTX_Minerals1_PlotsB_v2p1.xls*.

NOTE: KNO_3 is present throughout. Compare with Figure 6.7-20, in which KNO_3 is not present as an “extra” solid.

Figure 6.7-26. RH Versus Composite Normalized Reaction Progress (ξ) in Aqueous Solution on the $\text{NaCl+KNO}_3\text{-NaNO}_3\text{+KNO}_3$ join in the Halite–Niter–Soda Niter ($\text{NaCl-KNO}_3\text{-NaNO}_3$) System at Temperatures of 25°C, 40°C, 60°C, 80°C, 100°C, and 120°C

Additional plots of this type (including ones showing aqueous solution compositional relations) are included in *RHTX_Minerals1_PlotsB_v2p1.xls* in output DTN: LL040903723121.042.

This subsection has presented various EQ3/6 calculations of salt mineral deliquescence to provide a background on this important topic. The actual significance of these calculations is apparent in the following subsections. Additional EQ3/6 results are presented in the following subsections.

6.7.2.10 Analysis of Dust Compositions Taken from the Repository Drifts

The actual application of the IDPS model to deliquescence to describe the anticipated chemical environment on the drip shield and waste package outer barrier surfaces depends on what salt mineral assemblages are likely to be present. This section addresses that topic in regard to salts present in dust. The source of the dust is likely to be varied, with some component being generated in situ from tunneling, boring, and other operations. This component will consist mainly of rock dust, but other constituents may also be present, generated by processes including combustion and welding. Dust is also expected to be brought into the tunnels from the outside air in the course of repository ventilation. As is noted in Section 6.7.2.8, such dust may include material from local, regional, and global sources.

The approach in this report is to use dust sampled from the Yucca Mountain tunnels as the primary indicator of the composition (specifically the soluble salt portion) of the dust that will likely accumulate on the metal barrier surfaces in the repository. The information on deliquescent salts gathered from study of this dust is compared with information on deliquescent salts from other potential sources, such as playa deposits and chemical reactions in the atmosphere, to assess the reasonableness of the results based on the tunnel dust.

The data for Yucca Mountain tunnel dusts are taken from the data sets noted in Section 4.1.14 from DTN: MO0207EBSDUSTS.020 [DIRS 162556] and DTN: MO0209EBSDUST2.030 [DIRS 162557]. These contain data for Phase I and Phase II studies, respectively. Only the data for leachable components are used in the present analysis. The Phase I results are given in Table 4.1.19, those for Phase II in Table 4.1.20. The questions to be answered are, what are the soluble minerals (presumably represented by the calculated evaporation of the leachate solutions), and what is the salt content of the dust? There is no direct information on the identity of the actual salt minerals.

EQ3/6 calculations using the IDPS model are made to “reverse” the leaching process. These runs simulate evaporation at 25°C. Because the inputs on leachate compositions do not include measurements of aqueous carbonate and pH, the CO₂ fugacity is fixed at the atmospheric value (10^{-3.5} bar) and pH is required to satisfy charge balance. Three dust samples (“s79a,” “s79b,” and “s79c”) of the original 57 are excluded from the EQ3/6 calculations because these samples were collected outside the tunnels (behind a sign-in shack) in a zone of possible contamination (e.g., involving possible materials such as construction materials, tobacco ash, urine). The EQ3/6 calculations are made for the remaining 54 samples. The results are contained in output DTN: LL040603612251.104.

Determining pH by charge balance in such calculations is generally not desirable as the result may be impacted by cumulative errors in the overall chemical analysis (due to analytical uncertainties or failure to include some chemical components in the analytical panel, or both). The use of an assigned constant pCO₂ often tends to alleviate these problems to at least some

extent by the buffering effect it has on the pH. One test of the appropriateness of determining pH by charge balance is to compare the resulting calculated values with an expected reasonable range. Salts were by definition neither acids nor bases, and highly soluble salts generally do not produce or consume hydrogen ions in any significant quantity when they were dissolved in water. Acidic species were generally gases or aqueous solutions. Some less-soluble salts can be somewhat basic, and many basic compounds (generally oxides and hydroxides) exist as solids. As a result, one would expect the calculated pH values to be in the near-neutral range to slightly basic (e.g., in the pH range 6 to 8). That is generally the result in the present calculations (those data are not presented in this report, but can be found in the EQ3NR output (.3o) files, EQ3_Initializing_Runs folder, in output DTN: LL040603612251.104. The pH addressed here is for the original leachate solutions, not the evaporated leachates. The remaining uncertainty in leachate pH could have had some minor effect on the final mineral assemblages, but this is not explicitly addressed in the present report. Two (“s81a” and “s87a”) of the three leachate calculations that failed to converge to the eutectic in the EQ6 evaporation calculations (these are addressed below) had calculated pH values below 3. This problem is thought to trace to an insufficient analytical panel (i.e., the samples apparently contain unexpected chemical components for which quantitative analyses were not conducted). It is not likely that these leachates were actually acidic (for the reasons discussed above).

Similar calculations of leachate evaporation are conducted in Section 6.10 of the *Engineered Barrier System: Physical and Chemical Environment* (BSC 2004 [DIRS 169860]). Those calculations are made using the same version 8.0 of the EQ3/6 software and the IDPS high-temperature Pitzer model as the calculations made in the present report. The results of the runs, from *Engineered Barrier System: Physical and Chemical Environment* (BSC 2004 [DIRS 169860]), are contained in DTN: SN0310T0510102.010 [DIRS 168705]. In those calculations, a stoichiometric error is present in the input data for the silica concentrations in the dust leachates (ppm Si are not corrected to ppm SiO₂ as required for the EQ3/6 calculations). This error and a resulting sensitivity analysis are described in Section 6.10.8 of *Engineered Barrier System: Physical and Chemical Environment* (BSC 2004 [DIRS 169860]). The error reduces the silica concentrations by a factor of approximately 2.14 and results in minor but obvious changes in the eutectic phase assemblages (the minerals produced by dryout). The present report begins its analysis from these mineral assemblages; hence, the corrected calculations, as presented in output DTN: LL040603612251.104.

The desired results of the evaporation calculations pertain to the final stage of evaporation, when a terminal eutectic mineral composition and solution composition are achieved. The output data of interest focus on the eutectic mineral assemblages and, for corroborative purposes, the associated water activities. The eutectic mineral assemblage for a run is determined by the minerals listed in the “Summary of Solid Phases (ES)” table at the final “print point” of the corresponding output file. The eutectic water activity is extracted from the same “print point.” That can be found by searching for the string “Activity of water=” backward from the end of the file. The runs for three samples (“s81a”, “s81c,” and “s87a”) do not converge to the eutectic state and these samples are excluded from further analysis. Chemical analysis of these three samples include high phosphate concentrations (indicative of probable contamination), which is ignored in the EQ3/6 calculations. When the run for s81c ends, the solution is nearly saturated with Ca(NO₃)₂:4H₂O and undersaturated with KBr, which in all the successful runs was the last phase to form. It is likely that the eutectic assemblage for s81c would have included these

phases. It would then have matched the p07 assemblage, but with sellaite (MgF_2) substituting for fluorite (CaF_2). The run for s81c is included in the corresponding evaporation simulation results reported in *Engineered Barrier System: Physical and Chemical Environment* (BSC 2004 [DIRS 169860]). Thus, the calculations in that report are based on 52 dust samples, and the calculations in the present report on 51.

The extracted mineral assemblages for the 51 successful runs are summarized in Table 6.7-7. Sixteen unique assemblages are identified, in which a total of 20 minerals are involved. The number of minerals in each eutectic assemblage is the same, 10. This number is required by the mineralogic phase rule for the number of chemical components considered (Wolery 1979 [DIRS 156741], pp. 22 and 23). The set of components is the same in all the runs. The dust leachate samples sharing a common unique assemblage are noted in the table. Each unique assemblage is named after the tag (e.g., "p07") for the first leachate sample run to show this assemblage. The number of occurrences for each unique assemblage is tabulated with results separated out for the Phase I ("p") and Phase II ("s") samples. The EQ6 output file contains data on the relative proportions of the minerals in the eutectic assemblage for a given run. However, these data are neither extracted nor used in this report. The data in Table 6.7-7 are used to develop an understanding of what is significant in the dust sample salt mineral assemblages (key mineral assemblages consisting of the most deliquescent salts). These key assemblages are used to generate tables of the corresponding deliquescence RHs as functions of temperature, as well as to generate constraints on the chemical compositions of aqueous solutions created by deliquescence of these assemblages.

The extracted eutectic water activities and RHs are summarized in Table 6.7-8. These are used to verify the correctness of the analysis of a small number of deliquescence RH-controlling mineral subassemblages from the sixteen unique mineral assemblages.

Table 6.7-7. EQ3/6 Calculations of Reconstituted Salt Minerals in Dust Samples – Eutectic Mineral Assemblages at 25°C

Mineral	Formula	p07	p10	p12	p14	p18	p22	p24	p27	p30	s80a	s82c	s90b	s91a	s91b	s92a	S92b
Anhydrite	CaSO ₄	X	—	—	X	—	X	—	—	—	—	—	X	—	X	—	—
Calcite	CaCO ₃	X	X	X	X	X	X	X	X	X	X	X	X	X	X	X	X
Nitrocalcite	Ca(NO ₃) ₂ ·4H ₂ O	X	—	—	—	—	—	—	—	—	—	—	—	—	—	—	—
Fluorite	CaF ₂	X	X	X	X	X	—	—	X	—	X	—	X	X	—	X	—
Halite	NaCl	X	X	X	X	X	X	X	X	X	X	X	X	X	X	X	X
KBr	KBr	X	X	X	X	X	X	X	X	X	X	X	X	X	X	X	X
Niter	KNO ₃	X	X	X	X	X	X	X	X	X	X	X	X	X	X	X	X
Sepiolite	Mg ₄ Si ₆ O ₁₅ (OH) ₂ ·6H ₂ O	X	X	X	X	X	X	X	X	X	X	X	X	X	X	X	X
SiO _{2(am)}	SiO _{2(am)}	X	X	X	X	X	—	—	—	—	X	—	—	X	—	X	—
Soda Niter	NaNO ₃	X	—	—	X	—	X	—	—	—	—	X	—	—	—	—	—
Glauberite	Na ₂ Ca(SO ₄) ₂	—	X	X	X	—	X	—	X	X	—	X	X	X	X	—	—
Syngenite	K ₂ Ca(SO ₄) ₂ ·H ₂ O	—	X	—	—	—	—	—	—	—	X	—	—	X	—	—	—
Thenardite	Na ₂ SO ₄	—	X	X	—	X	—	X	X	X	X	—	—	—	—	—	X
Darapskite	Na ₃ NO ₃ SO ₄ ·H ₂ O	—	—	X	—	—	—	X	X	X	—	X	—	—	—	—	—
Arcanite	K ₂ SO ₄	—	—	—	—	X	—	—	—	—	X	—	—	—	—	X	X
Pirssonite	Na ₂ Ca(CO ₃) ₂ ·2H ₂ O	—	—	—	—	X	—	X	—	—	—	—	—	—	—	X	X
Huntite	CaMg ₃ (CO ₃) ₄	—	—	—	—	—	X	X	—	X	—	X	—	—	X	—	X
Sellaite	MgF ₂	—	—	—	—	—	X	X	X	X	—	X	X	—	X	—	X
Sylvite	KCl	—	—	—	—	—	—	—	—	—	—	—	—	—	—	X	—
Pentasalt	K ₂ Ca ₅ (SO ₄) ₆ ·H ₂ O	—	—	—	—	—	—	—	—	—	—	—	X	X	X	—	—

Table 6.7-7. EQ3/6 Calculations of Reconstituted Salt Minerals in Dust Samples – Eutectic Mineral Assemblages at 25°C (Continued)

Mineral	Formula																
p-series (Phase I) Samples		p07	p10 p11 p32 p33	p12 p15 p19 p26 p31	p14 p16 p17 p28	p18 p20	p22 p23 p25	p24 p29	p27	p30							
s-series (Phase II) Samples		s80c	s81b s85a s85b s86b s90a s90c s91c	s85c	s86c s87b s87c	s82a s83a s84a s86a	s80b s83c			s82b s83b	s80a s92c	s82c	s90b	s91a	s91b	s92a	S92b

Source: Output DTN: LL040603612251.104.

NOTE: Samples s79a, s79b, and s79c are excluded from the EQ3/6 evaporation runs because the dust samples were collected outside the tunnel in a zone of likely contamination. Three other samples (s81a, s87a, and s81c) are excluded from further analysis because the runs did not converge to the eutectic (dryout) state. See text for further discussion.

Table 6.7-8. EQ3/6 Calculations of Reconstituted Salt Minerals in Dust Samples – Eutectic Water Activities and Relative Humidities

Sample	Activity of Water	RH%
p07	0.3895	38.95
p10	0.6019	60.19
p11	0.6019	60.19
p12	0.5983	59.83
p14	0.5480	54.80
p15	0.5983	59.83
p16	0.5480	54.80
p17	0.5480	54.80
p18	0.6107	61.07
p19	0.5983	59.83
p20	0.6107	61.07
p22	0.5480	54.80
p23	0.5480	54.80
p24	0.5953	59.53
p25	0.5480	54.80
p26	0.5983	59.83
p27	0.5983	59.83
p28	0.5480	54.80
p29	0.5953	59.53
p30	0.5983	59.83
p31	0.5983	59.83
p32	0.6019	60.19
p33	0.6019	60.19
s80a	0.6141	61.41
s80b	0.5480	54.80
s80c	0.3891	38.91
s81b	0.6019	60.19
s82a	0.6107	61.07
s82b	0.5983	59.83
s82c	0.5472	54.72
s83a	0.6107	61.07
s83b	0.5983	59.83
s83c	0.5480	54.80
s84a	0.6107	61.07
s85a	0.6019	60.19
s85b	0.6019	60.19
s85c	0.5983	59.83
s86a	0.6107	61.07
s86b	0.6019	60.19
s86c	0.5480	54.80
s87b	0.5480	54.80
s87c	0.5480	54.80
s90a	0.6019	60.19

Table 6.7-8. EQ3/6 Calculations of Reconstituted Salt Minerals in Dust Samples – Eutectic Water Activities and Relative Humidities (Continued)

Sample	Activity of Water	RH%
s90b	0.6063	60.63
s90c	0.6019	60.19
s91a	0.6071	60.71
s91b	0.6062	60.62
s91c	0.6019	60.19
s92a	0.6184	61.84
s92b	0.6109	61.09
s92c	0.6141	61.41

Source: Output DTN: LL040603612251.104.

The occurrence of each unique assemblage is identified in Table 6.7-7 by grouping together those samples sharing a common mineral assemblage. This is repeated in Table 6.7-9, but with occurrences weighted by assigning each Phase I or “p” sample a weighting factor of three, while assigning each Phase II or “s” sample weighting factor of unity. The Phase I samples are treated in chemical analysis as unit samples. However, the original Phase II samples are split into three size fractions that are then analyzed and reported separately; since each “sample” is actually a size fraction split of an original sample, the weighting is adjusted accordingly. The total weighting for the three size fractions of a Phase II sample is three, matching the weighting for a Phase I sample.

Table 6.7-10 summarizes the occurrences of the minerals in the assemblages. Calcite (CaCO_3), halite (NaCl), niter (KNO_3), KBr , and sepiolite ($\text{Mg}_4\text{Si}_6\text{O}_{15}(\text{OH})_2 \cdot 6\text{H}_2\text{O}$) are present in all 16 assemblages. Fluorite (CaF_2) and glauberite [$\text{Na}_2\text{Ca}(\text{SO}_4)_2$] are each present in 10, $\text{SiO}_{2(\text{am})}$ in eight, and thenardite (Na_2SO_4) and sellaite (MgF_2) each in eight. Others are present in fewer assemblages (Table 6.7-10). Soda niter (NaNO_3 ; also known as nitratine) appears in only four assemblages, and sylvite (KCl), a fairly well-known salt mineral, appears in only one.

Table 6.7-9. (Table 6.7-7 with Additional Weighted Occurrences) EQ3/6 Calculations of Reconstituted Salt Minerals in Dust Samples at 25°C

Mineral	Formula	p07	p10	p12	p14	p18	p22	p24	p27	p30	s80a	s82c	s90b	s91a	s91b	s92a	s92b
Anhydrite	CaSO ₄	X	—	—	X	—	X	—	—	—	—	—	X	—	X	—	—
Calcite	CaCO ₃	X	X	X	X	X	X	X	X	X	X	X	X	X	X	X	X
Nitrocalcite	Ca(NO ₃) ₂ ·4H ₂ O	X	—	—	—	—	—	—	—	—	—	—	—	—	—	—	—
Fluorite	CaF ₂	X	X	X	X	X	—	—	X	—	X	—	X	X	—	X	—
Halite	NaCl	X	X	X	X	X	X	X	X	X	X	X	X	X	X	X	X
KBr	KBr	X	X	X	X	X	X	X	X	X	X	X	X	X	X	X	X
Niter	KNO ₃	X	X	X	X	X	X	X	X	X	X	X	X	X	X	X	X
Sepiolite	Mg ₄ Si ₆ O ₁₅ (OH) ₂ ·6H ₂ O	X	X	X	X	X	X	X	X	X	X	X	X	X	X	X	X
SiO _{2(am)}	SiO _{2(am)}	X	X	X	X	X	—	—	—	—	X	—	—	X	—	X	—
Soda Niter	NaNO ₃	X	—	—	X	—	X	—	—	—	—	X	—	—	—	—	—
Glauberite	Na ₂ Ca(SO ₄) ₂	—	X	X	X	—	X	—	X	X	—	X	X	X	X	—	—
Syngenite	K ₂ Ca(SO ₄) ₂ ·H ₂ O	—	X	—	—	—	—	—	—	—	X	—	—	X	—	—	—
Thenardite	Na ₂ SO ₄	—	X	X	—	X	—	X	X	X	X	—	—	—	—	—	X
Darapskite	Na ₃ NO ₃ SO ₄ ·H ₂ O	—	—	X	—	—	—	X	X	X	—	X	—	—	—	—	—
Arcanite	K ₂ SO ₄	—	—	—	—	X	—	—	—	—	X	—	—	—	—	X	X
Pirssonite	Na ₂ Ca(CO ₃) ₂ ·2H ₂ O	—	—	—	—	X	—	X	—	—	—	—	—	—	—	X	X
Huntite	CaMg ₃ (CO ₃) ₄	—	—	—	—	—	X	X	—	X	—	X	—	—	X	—	X
Sellaite	MgF ₂	—	—	—	—	—	X	X	X	X	—	X	X	—	X	—	X
Sylvite	KCl	—	—	—	—	—	—	—	—	—	—	—	—	—	—	X	—
Pentasalt	K ₂ Ca ₅ (SO ₄) ₆ ·H ₂ O	—	—	—	—	—	—	—	—	—	—	—	X	X	X	—	—

Table 6.7-9. (Table 6.7-7 with Additional Weighted Occurrences) EQ3/6 Calculations of Reconstituted Salt Minerals in Dust Samples at 25°C (Continued)

Mineral	Formula																
		p07	p10 p11 p32 p33	p12 p15 p19 p26 p32	p14 p16 p17 p28	p18 p20	p22 p23 p25	p24 p29	p27	p30	—	—	—	—	—	—	—
p-series (Phase I) Samples																	
s-series (Phase II) Samples		s80c	s81b s85a s85b s86b s90a s90c s91c	s85c	s86c s87b s87c	s82a s83a s84a s86a	s80b s83c	—	—	s82b s83b	s80a s92c	s82c	s90b	s91a	s91b	s92a	s92b
p-series Occurrences		1	4	5	4	2	3	2	1	1	—	—	—	—	—	—	—
s-series Occurrences		1	7	1	3	4	2	0	0	2	2	1	1	1	1	1	1
Weighted Occurrences		4	19	16	15	10	11	6	3	5	2	1	1	1	1	1	1
Percentage Weighted Occurrences		4.1	19.6	16.5	15.5	10.3	11.3	6.2	3.1	5.2	2.1	1.0	1.0	1.0	1.0	1.0	1.0

Source: Output DTN: LL040603612251.104.

NOTES: Samples s79a, s79b, and s79c are excluded from the EQ3/6 evaporation runs because the dust samples were collected outside the tunnel in a zone of likely contamination. Three other samples (s81a, s81c, and s87a) are excluded from further analysis because the runs did not converge to the eutectic (dryout) state. The number of successful runs is 51.

In subsequent analysis, each sample from the Phase I (P) series is given a weighting factor of three. Each sample from the Phase II (S) series is assigned a weighting factor of 1. Each of the three Phase II dust samples is split into three size fractions, designated a, b, and c, for which leaching and other data are obtained. The total weighting factor for all three splits of a Phase II sample is, therefore, three. The "weighted occurrences" for all samples totaled 97.

Table 6.7-10. Summary of Mineral Occurrences in the 16 Assemblages in Table 6.7-9

Mineral	Formula	Occurrences
Anhydrite	CaSO ₄	5
Calcite	CaCO ₃	16
Nitrocalcite	Ca(NO ₃) ₂ ·4H ₂ O	1
Fluorite	CaF ₂	10
Halite	NaCl	16
KBr	KBr	16
Niter	KNO ₃	16
Sepiolite	Mg ₄ Si ₆ O ₁₅ (OH) ₂ ·6H ₂ O	16
SiO _{2(am)}	SiO _{2(am)}	8
Soda Niter	NaNO ₃	4
Glauberite	Na ₂ Ca(SO ₄) ₂	10
Syngenite	K ₂ Ca(SO ₄) ₂ ·H ₂ O	3
Thenardite	Na ₂ SO ₄	8
Darapskite	Na ₃ NO ₃ SO ₄ ·H ₂ O	5
Arcanite	K ₂ SO ₄	4
Pirssonite	Na ₂ Ca(CO ₃) ₂ ·2H ₂ O	4
Huntite	CaMg ₃ (CO ₃) ₄	6
Sellaite	MgF ₂	8
Sylvite	KCl	1
Pentasalt	K ₂ Ca ₅ (SO ₄) ₆ ·H ₂ O	3

Source: Output DTN: LL040603612251.104.

A clearer picture is obtained by noting only those minerals that are the most deliquescent. Anhydrite, calcite, fluorite, sepiolite, SiO_{2(am)}, huntite [CaMg₃(CO₃)₄], and sellaite (MgF₂) (seven of the 20 minerals) are not ordinarily considered deliquescent. Arcanite (K₂SO₄), thenardite (Na₂SO₄), and all of the double salts except darapskite (Na₃SO₄NO₃·H₂O) are only moderately deliquescent. That focuses attention on nitrocalcite [Ca(NO₃)₂·4H₂O], niter (KNO₃), soda niter (NaNO₃), halite (NaCl), sylvite (KCl), KBr, and darapskite.

Consideration of the most deliquescent minerals combined with occurrence in the 16 unique mineral assemblages suggests the key subassemblages (hereafter, "key assemblages") shown in Table 6.7-11. The two principal key assemblage cases are "A," NaCl- KNO₃-KBr, and "B," NaCl-KNO₃-NaNO₃-KBr. Key Assemblage Case A is itself a subassemblage of Key Assemblage Case B (lacking the soda niter, NaNO₃). These two key assemblages account for 95.9 percent of the total occurrence in the 51 dust samples. Key assemblage "C" is characterized by the presence of nitrocalcite [Ca(NO₃)₂·4H₂O], one of the more deliquescent salts. Key Assemblage Case C is composed of nitrocalcite plus the salts of Key Assemblage Case B. Nitrocalcite only appears in the calculated mineral assemblages for 2 of the 51 dust samples (one of which has a unit weighting factor, the other, a weighting factor of three; hence, the weighted occurrence of 4.1 percent).

Table 6.7-11. Key Sub-Assemblages of Reconstituted Salt Minerals in Dust Samples

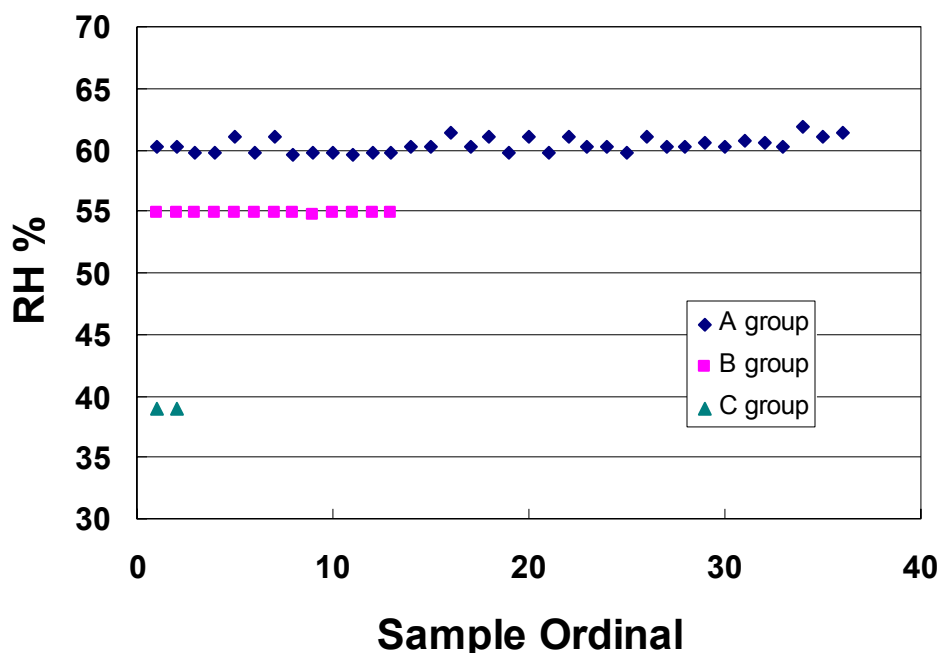
Key Assemblages Case	Key Salts	Unique Mineral Assemblages Represented	Total Occurrence Percentage
A	NaCl-KNO ₃ -KBr	P10, P12, P18, P24, P27, P30, S80a, S90b, S91a, S91b, S92a, S92b	68.1
B	NaCl-KNO ₃ -NaNO ₃ -KBr	P14, P22, S82c	27.8
C	NaCl-KNO ₃ -NaNO ₃ -Ca(NO ₃) ₂ -KBr	P07	4.1

Source: Table 6.7-9.

NOTE: The percentage occurrence values for unique phase assemblages as given in Table 6.7-9 sum to 99.9 percent. Here the value for key assemblage B is calculated so that the sum for the three key assemblages sums to 100 percent.

If the notion of three key salt mineral assemblages is correct, then the computed activity of water (or RH) for the eutectic solution composition in the EQ3/6 calculations of evaporation of the dust leachate solutions should closely congregate around only three values. The distribution of computed RH values is shown in the RH versus sample ordinal plot in Figure 6.7-27. The samples assigned above to the three key assemblage groups are plotted separately. The plot overall is somewhat like a bar graph on its side. The validity of the “three value” hypothesis is clearly visible. The question at this point is whether a set of adequate key assemblages has been identified. Confirmation of the hypothesis is best obtained by comparing the deliquescence RH of the pure key assemblages with the results obtained in the EQ3/6 evaporation calculations. This comparison is shown in Table 6.7-12 and is good.

The least favorable comparison in Table 6.7-12 is for Key Assemblage Case A, for which the pure assemblage has a deliquescence RH nearly two percentage points higher than that obtained from the evaporation calculations for the dust samples. This is considered acceptable, especially in that such differences would be expected to diminish at elevated temperature. Key Assemblage Case A is fairly deliquescent at 25°C, but becomes much more so as temperature increases (Figure 6.7-28). For such an assemblage, the effect of omitting one or more less deliquescent minerals results in less error as the assemblage per se becomes more deliquescent. This is illustrated, for example, in Figure 6.7-10, where the difference in the deliquescence RH curves for soda niter (NaNO₃) and halite-soda niter (NaCl-NaNO₃) decreases substantially with increasing temperature (thus showing that the consequences of ignoring the halite diminish with temperature). Another example is shown in Figure 6.7-14, where the difference in the deliquescence RH curves for niter-soda niter (KNO₃-NaNO₃) and halite-niter-soda niter (NaCl-KNO₃-NaNO₃) also decreases significantly with increasing temperature.



Source: Output DTN: LL040903723121.042, *DustLeachateActWaterRev02.xls*.

NOTE: The "Sample Ordinal" is defined such that the samples in a group follow their order as listed first in Table 4.1-19, then Table 4.1-20. There are essentially only three values of water activity represented in the 51 samples shown.

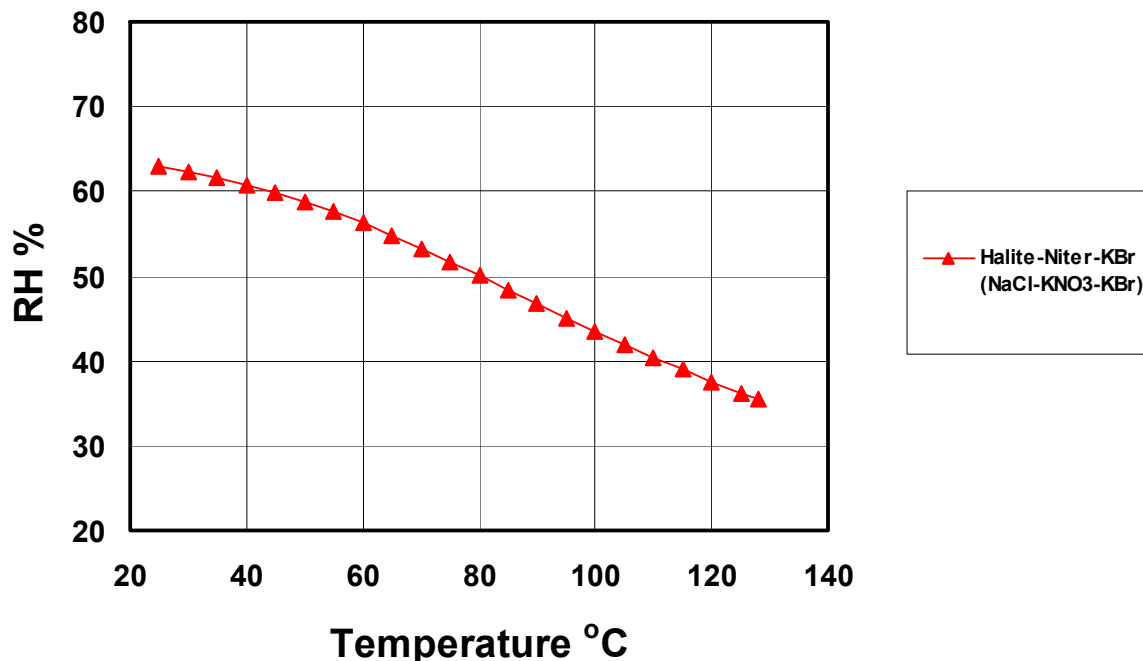
Figure 6.7-27. Eutectic RH percent Values from EQ3/6 Calculations of Reconstituted Salt Minerals in Yucca Mountain Tunnel Dust

Table 6.7-12. Calculated Deliquescence RH Values for Key Assemblages at 25°C

Key Assemblages Case	Key Salts	DRH% for Pure Key System	DRH% for Actual Associated Sample Cases
A	NaCl-KNO ₃ -KBr	62.97	60.38±0.60
B	NaCl-KNO ₃ -NaNO ₃ -KBr	54.91	54.79±0.02
C	NaCl-KNO ₃ -NaNO ₃ - Ca(NO ₃) ₂ -KBr	38.98	38.93±0.02

Source: Output DTN: LL040903723121.042.

NOTE: For "pure key system" data, see EQ3/6 output (.6o) files, folder ABCD, in *Pack048.zip*. For the "actual associated sample cases" data, see *DustLeachateActWaterRev02.xls*.



Source: Output DTN: LL040903723121.042, *RHTE_Minerals1_PlotsA_v2p1.xls*.

Figure 6.7-28. Deliquescence RH as a Function of Temperature for the Three-Mineral Assemblage Halite–Niter–KBr (NaCl–KNO₃–KBr)

KBr is a highly deliquescent salt (Figure 6.7-4). It appears in all the dust leachate evaporation calculations and thence in the three key salt mineral assemblages. Its presence in the evaporation calculations traces back to the bromide concentrations in the dust leachate solutions as shown in Table 4.1-19 and Table 4.1-20. These levels of bromide seem high in comparison to chloride (e.g., for the Phase I samples, from Table 4.1-19 mean Br is 28.7 ppm, mean Cl is 181 ppm).

Lithium bromide (LiBr) was used as a component of water used for construction and fire suppression in the development of the repository tunnels, as stated in *Chemical Tracer Injection System Analysis for Construction Process and Firewater Usage* (CRWMS M&O 1993 [DIRS 153976], p. 8):

The chemical tracer used for process and firewater is Lithium Bromide, LiBr.
The target concentration for the water is 20 ppm ± 10 ppm...

Data in DTN: LAJF831222AQ98.003 [DIRS 146310]) confirm this usage. Mitchell (1998 [DIRS 146795]) addresses the likely degree of loss of construction water during tunnel construction. Mitchell (1998 [DIRS 146802], the attachment by A. Flint and others) provides a more detailed study on this topic.

LiBr, NaBr, KBr, and CaBr₂ are also used in hydrologic tracer tests in the tunnels (Mitchell 1997 [DIRS 107654], p. 1; Mitchell 1998 [DIRS 107958], pp. 1 and 2; Mitchell 1998 [DIRS 107949], pp. 1 and 2; Mitchell 1998 [DIRS 107939], p. 1; Mitchell 1998 [DIRS 107946], pp. 1 and 2; Mitchell 1998 [DIRS 107972], pp. 1 and 2; Mitchell 1999 [DIRS 107977], pp. 1 to 3; Mitchell 1999 [DIRS 148008], p. 1; Mitchell 1999 [DIRS 148010], p. 1; Mitchell 1999

[DIRS 107978], pp. 1 and 2; Mitchell 2000 [DIRS 148049], p. 1). The specified amounts of individual bromide salts in these tests ranged from a few tens of grams to somewhat more than 150 kg. Some or all of these tracers were recovered by methods including mineback of the rock masses involved in the tests. Mitchell (2000 [DIRS 152962]) also mentions the use of humidifiers in niches used for hydrologic testing. It is stated that these might be “plumbed into the existing mine water supply.” It is not clear that water supply actually employed contained LiBr, but if so the humidifiers might have served as a source of bromide aerosol.

It is, therefore, likely that the level of bromide observed in the dust samples taken from the tunnels is an artifact due to the use of bromide in tunnel construction and hydrologic testing. This is not to say that there would otherwise be absolutely no soluble bromide in the dusts that would settle on the metal barrier surfaces, only that lower levels would be expected. Accordingly, it is appropriate to remove the bromide component from the key mineral assemblages, and, in this report, the bromide is removed. Operationally, this is done by removing KBr from the key assemblages. The results of doing this are first discussed, then various issues surrounding this action are discussed.

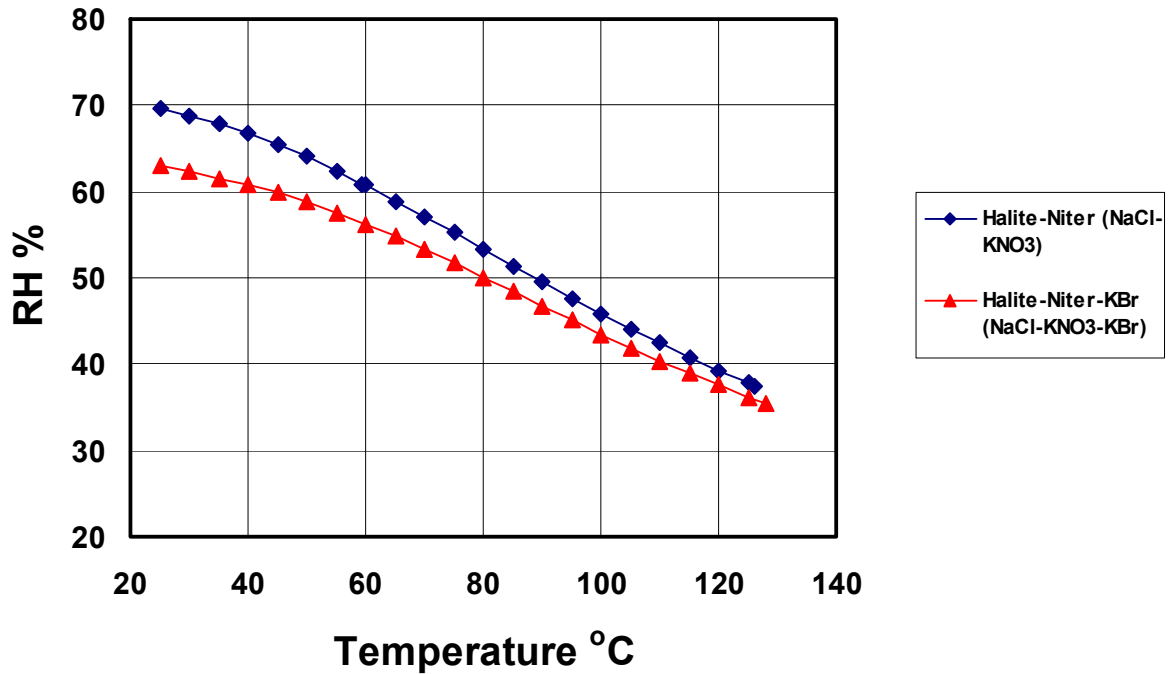
The principal effect of removing KBr from the key salt mineral assemblages is twofold. One, it removes relatively high levels of a potentially corrosive chemical species (bromide). Second, it results in mineral assemblages that are less deliquescent. This is illustrated in Table 6.7-13, which compares the results of EQ3/6 calculations at 25°C and atmospheric CO₂ pressure for the cases of KBr present and not present. The changes are fairly substantial for all three cases. The effect for Key Assemblage Case A as a function of temperature is shown in Figure 6.7-29, and that for Key Assemblage Case B in Figure 6.7-30. These plots show that the effect on the deliquescence RH of eliminating the KBr is diminished at higher temperature. This is the result of KNO₃ (and NaNO₃ in the case of Key Assemblage Case B) becoming much more deliquescent at higher temperature, while KBr becomes only somewhat more deliquescent (Figure 6.7-4). This effect would also hold for the relatively minor Key Assemblage Case C.

Table 6.7-13. Calculated Deliquescence RH values for Key Assemblages at 25°C, with and without KBr

Key Assemblage Case	Key Salts	DRH% Including KBr	DRH% Excluding KBr
A	NaCl-KNO ₃ -KBr	62.97	69.53
B	NaCl-KNO ₃ -NaNO ₃ -KBr	54.91	65.70
C	NaCl-KNO ₃ -NaNO ₃ - Ca(NO ₃) ₂ -KBr	38.98	49.47

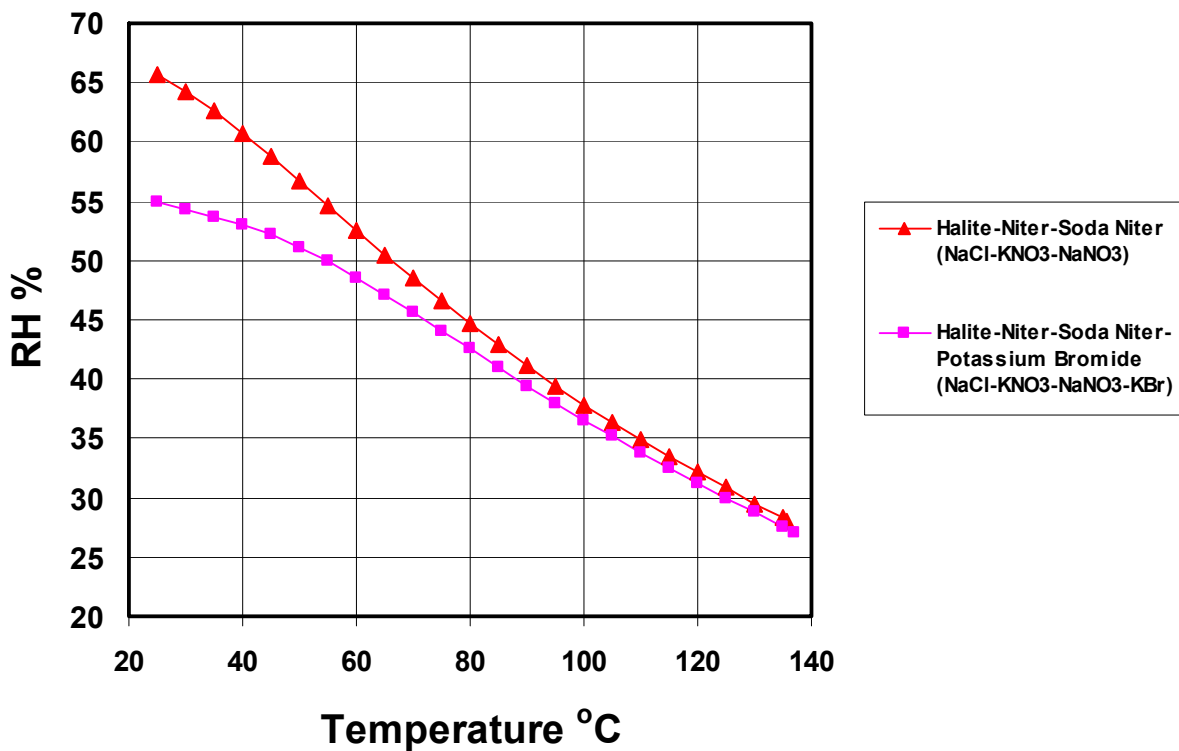
Source: Output DTN: LL040903723121.042.

NOTE: For “DRH Including KBr” data, see EQ3/6 output (.6o) files, ABCD folder, in *Pack048.zip*. For “DRH Excluding KBr” data, see EQ3/6 output (.6o) files, ABCD_NoBr folder, in *Pack048.zip*.



Source: Output DTN: LL040903723121.042, *RHTE_Mineral1_PlotsA_v2p1.xls*.

Figure 6.7-29. Deliquescence RH as a Function of Temperature for the Assemblages Halite-Niter (NaCl-KNO₃) and Halite-Niter-KBr (NaCl-KNO₃-KBr)



Source: Output DTN: LL040903723121.042, *RHTE_Mineral1_PlotsA_v2p1.xls*.

Figure 6.7-30. Deliquescence RH as a Function of Temperature for the Assemblages Halite-Niter-Soda Niter (NaCl-KNO₃-NaNO₃) and Halite-Niter-Soda Niter-KBr (NaCl-KNO₃-NaNO₃-KBr)

A potential issue in removing the bromide by taking out the KBr is that if Br should not be present, why not remove Na, Ca, or Mg instead of K to balance charge? The bromide, though present at a significant level, is generally less abundant in the dust leachate waters than any of these alkali or alkaline earth elements, and is generally less abundant than sulfate, nitrate, and chloride (Tables 4.1-19 and 4.1-20). It is probably less abundant than bicarbonate, which is not included in the original leachate analytical data (in the evaporation calculations bicarbonate and pH are determined by setting atmospheric CO₂ pressure and requiring charge balance). The various solutes are distributed in the evaporation calculations over ten minerals, so there is room for some reshuffling to accommodate changes in the amounts of the alkali and alkaline earth metals without actually changing the minerals appearing in the eutectic assemblages.

Taking out Na, Ca, or Mg instead of K would have little overall effect. In systems with all nitrate present in KNO₃, the extra potassium would likely simply go into one of the other K-bearing minerals (arcanite or one of the K-bearing double salts), with the reduced amount of one of the other alkali or alkaline earth metals spread over the existing phases. In the case of those systems in which other nitrate salts are present, the additional K would probably first go into KNO₃ and might eliminate one or more of these other nitrate salts from a eutectic assemblage. If that is the case, one new mineral would have to appear for each one lost to maintain to the required number of 10. This would be a sulfate, carbonate, or double salt of one of the unchanged alkali or alkaline earth metals.

As the issue of possible contamination of the dust samples is raised, it is appropriate to address whether the minor Key Assemblage Case C is the result of such contamination. Its low occurrence suggests that this might be the case.

Key Assemblage Case C is the same as Key Assemblage Case B, except for the addition of nitrocalcite, Ca(NO₃)₂·4H₂O. This assemblage is only associated with two samples, p07 and s80c (Table 6.7-9). Examination of the original dust leachate compositions (p07: Field Number SPC00573607 in Table 4.1-19; s80c: Sample No. 00574980C in Table 4.1-20) suggests nothing unusual relative to the majority of leachate samples. Furthermore, there is nothing particularly unusual about nitrocalcite in regard to mineral occurrences, given the presence of other nitrates (see the discussion of occurrences and potential sources in Section 6.7.2.8). Although the origin of nitrocalcite in Yucca Mountain tunnel dust is uncertain at this time, there are sufficient possible explanations to conclude that Key Assemblage Case C is simply a logical extension of Key Assemblage Case B.

An important issue is the relevance of the tunnel dusts for this analysis, including determining its difference from outside (atmospheric) dust, and whether the analysis using the tunnel dust results still applies. The two dust data packages (DTN: MO0207EBSDUSTS.020 [DIRS 162556]; DTN: MO0209EBSDUST2.030 [DIRS 162557]) indicate total salt content of the tunnel dusts is typically less than 0.5 percent by weight. Most of the dust material appears to consist of silicates (see other data presented by these data packages). A low percentage of soluble salts seems more consistent with an origin mostly from rock dust. That is, the tunnel dusts are mostly “rock flour.” This is supported by the overall analytical data and by the widespread presence of bromide, which was used as a tracer in construction water.

Information on the percentage of soluble salts in local and regional atmospheric dusts appears to be sparse. However, Blank et al. (1999 [DIRS 163486], Table 2, p. 370) report that playa dusts in Nevada may contain about 44 percent soluble salts. Some data from other parts of the world (e.g., Orlovsky and Orlovsky 2001 [DIRS 163413]) suggest that such a high (or indeed higher) percentage is not unreasonable. Reheis reported total soluble salt contents of 8 to 30 percent in dusts originating from the Owens (dry) Lake in California; however, regional values are reported in the range of 9 to 16 percent. (Reheis 1997 [DIRS 168715], Figure 3B). These regional values appear to represent the most likely common soluble salt content in atmospheric dust in the vicinity of Yucca Mountain. Information on the percentage of soluble salts in local and regional atmospheric dusts is fairly sparse, but the information cited above indicates that values in the range 9 to 16 percent are common, and much higher values are known. Apart from the excess bromide, the gross salt content of the tunnel dusts could be explained by the mixing of approximately 1 part of outside (atmospheric) dust with approximately 99 parts of rock flour. The general ubiquity of halite and nitrate minerals in desert terrains (not to mention the usual nondriver salt minerals including gypsum, anhydrite, calcite, glauberite, pirssonite, and thenardite) suggests that the deliquescence picture drawn from the tunnel dusts is likely consistent with one that might be drawn from a similar study of local, regional, or global atmospheric dusts.

Data supporting the representativeness of the tunnel dust soluble fractions (excluding excess Br) are presented in Table 6.7-14. The soluble fraction ionic ratios of three representative tunnel dusts (from DTN: MO0207EBSDUSTS.020 [DIRS 162556]) are compared with 2002 mean annual solute data for precipitation (rainfall) at three meteorological stations roughly bracketing Yucca Mountain (NV00, Red Rock Canyon, Clark County, Nevada: NADP/NTN 2003 [DIRS 171291]; NV05, Great Basin National Park-Lehman Caves, White Pine County, Nevada: NADP/NTN 2003 [DIRS 171292]; and CA95, Death Valley National Park-Cow Creek, Inyo County, California: NADP/NTN 2003 [DIRS 171293]) and with three composite compositions of Asian dust samples (Topping et al. 2004 [DIRS 171290]). The regional precipitation results would be expected to correlate with the soluble fractions of local atmospheric dusts. The Asian dust results are composite data for dusts originating in northern China and Mongolia (and sampled in Korea). Asian dusts are indirectly relevant because they represent certain effects and processes that determine the compositions of atmospheric dust generated in a desert or playa environment. They are also directly relevant because of the global transport of atmospheric dust; Asian dust reaches Nevada. The point of Table 6.7-14 is that these results are broadly similar. Thus, it appears that the soluble fraction of the tunnel dusts (less the excess Br) is compositionally representative of outside (atmospheric) dust.

Table 6.7-14. Ionic Ratios (mol/mol) for the Soluble Fraction of Three Representative Tunnel Dusts, Three Regional Precipitation (Rainfall) Stations Surrounding Yucca Mountain, and Three Composite Results for Asian Dust

Ionic Ratios (mol/mol)	Tunnel Dust Samples -Three Representative Cases from DTN: MO0207EBSDUSTS.020 [DIRS 162556]			Mean Annual 2002 Precipitation (Rainfall) Solute Data from Three National Atmospheric Deposition Program Stations Roughly Bracketing Yucca Mountain			Asian Dust, ACE Campaign Results (Topping et al. 2004 [DIRS 171290])		
	P07	P14	P10	CA95 ^a	NV00 ^b	NV05 ^c	Whole Campaign Total	Chinese Course Total	Korean Course Total
Na/Cl	2.699	4.069	2.894	2.070	1.127	1.828	2.169	1.309	2.222
K/Cl	1.221	1.528	1.237	0.158	0.139	0.207	0.513	0.387	0.515
NH ₄ /Cl	N/A	N/A	N/A	2.605	5.514	4.633	4.670	2.245	4.041
Mg/Cl	0.072	0.305	0.175	0.336	0.555	0.417	0.220	0.210	0.219
Ca/Cl	8.472	6.389	2.348	3.101	2.973	2.907	0.664	0.874	0.649
NO ₃ /Cl	4.002	1.671	0.776	2.969	5.146	3.839	1.754	1.440	1.719
SO ₄ /Cl	3.123	3.293	1.458	1.009	1.384	1.555	2.473	1.679	2.006
CO ₃ /Cl	4.839	4.737	2.057	2.860	2.461	2.683	0.711	0.155	0.892

Source: Output DTN: LL040603712251.105, *IonicRatiosInDustAndRainfallRev00.xls*.

NOTES: The tunnel dust leachates are not analyzed for NH₄.
CO₃ is estimated from charge balance.

^aDeath Valley National Park-Cow Creek, Inyo County, California: NADP/NTN 2003 [DIRS 171293].

^bRed Rock Canyon, Clark County, Nevada: NADP/NTN 2003 [DIRS 171291].

^cGreat Basin National Park-Lehman Caves, White Pine County, Nevada: NADP/NTN 2003 [DIRS 171292].

A comparison of the data in Table 6.7-14 shows that the ionic ratios (molar ratio of a given ion to the chloride ion) are broadly similar among the leachable component of tunnel dusts, the solute content of regional precipitation (rainfall), and the leachable component of Asian dusts. This supports the notion that the analysis based on the tunnel dusts is giving basically the correct picture. A potential point of concern is that NH₄⁺ (ammonium ion) was not measured in the analytical panel for the tunnel dust leachates and, therefore, is not included in the present analysis. Ammonium often acts in geochemical systems as a kind of potassium analogue, suggesting a potential role for NH₄NO₃ in the key assemblages for deliquescence. The Nevada rainfall and Asian dust data indicate that NH₄⁺ is generally more abundant (relative to Cl) than either K or Na, offering further support to this notion. Although the potential significance of NH₄⁺ is noted, the present analysis will otherwise remain focused on the reported tunnel dust compositions.

For corrosion, it is important to note that the first-formed solutions resulting from deliquescence contain more nitrate than chloride, owing to the generally higher solubilities in the deliquescing solutions of the expected nitrate minerals (K, Na, and Ca nitrates) versus those of the expected chlorides (NaCl and KCl). As the solutions continue to deliquesce and the original salt mineral assemblage is changed by complete dissolution of one salt mineral after another, the solutions become even more nitrate rich if nitrate abundance in the dust exceeds the chloride abundance, else they become more chloride rich. Regardless, any solution obtained after complete

dissolution of nitrate and chloride must have (at least in the absence of acid–gas volatility) a nitrate to chloride ratio that matches that in the soluble component of the original dust.

The soluble ratios in the dust, therefore, provide a compositional limit. Table 6.7-15 gives the NO_3/Cl ratios in the soluble component of the Phase I dust samples. These data put the ratio at 1.2919 ± 0.7920 (one standard deviation), with minimum and maximum values of 0.2963 and 4.0024, respectively. The minimum ratio guarantees that the NO_3/Cl ratio in any solution deliquescing in association with these dust samples will have at least this value. The precision of the results stated here and in Table 6.7-15 is somewhat overstated; the actual number of significant figures is, at best, three.

Table 6.7-16 gives the NO_3/Cl ratios in the soluble component of the Phase II dust samples. These data put the ratio at 1.3713 ± 0.7146 (one standard deviation), with minimum and maximum values of 0.4084 and 3.3634, respectively. These values are roughly comparable to those obtained for the Phase I samples as discussed above. The minimum ratio again guarantees that the NO_3/Cl ratio in any solution deliquescing in association with these dust samples will have at least this value. The precision of the numbers is again somewhat overstated as the number of significant figures is, at most, three.

It can be shown that although the apparent dust salt mineral assemblages are generally highly deliquescent, at least at elevated temperature, these tend to have high NO_3/Cl ratios at the relatively low RH values at which deliquescence first occurs. Lower NO_3/Cl ratios (of say 0.2 to 1.0) are only achievable at significantly higher RH values (much closer to the deliquescence RH for pure halite).

This fact is illustrated in Figure 6.7-31 for the NaCl-KNO_3 system. In addition to the usual deliquescence RH curve, this figure depicts as a function of temperature the minimum RH required to obtain NO_3/Cl ratios of 1.0 and 0.2. The minimum RH curves are obtained by referring to the data plotted in Figures 6.7-22 and 6.7-23 (they can also be obtained by referring to the data plotted in Figures 6.7-24 and 6.7-25). Note that the minimum RH curves correspond to essentially constant values above 60°C . Below this temperature, the “1.0” curve rises and crosses the “0.2” curve (which remains nearly flat) near 40°C . This crossover is due to a reversal in the relative solubilities of the two salts. At 25°C , NaCl is more soluble than KNO_3 . The solubility of KNO_3 increases rapidly with temperature, while that of NaCl increases more slowly. At 100°C , for example, KNO_3 is substantially more soluble than NaCl (Table 4.1-9).

Similar relations are illustrated in Figure 6.7-32 for the $\text{NaCl-KNO}_3\text{-NaNO}_3$ system. Here, the “1.0” curve is more nearly constant and does not cross the “0.2” curve. Note that the minimum RH curves in the present case are otherwise nearly identical to those for the NaCl-KNO_3 case.

Table 6.7-15. NO₃/Cl Ratios for Phase I Dust Samples

Field Number	Meters	NO ₃ /Cl (mol/mol)
SPC00573629	202	0.7458
SPC00573622	558	2.5133
SPC00573630	669	0.8168
SPC00573623	901	1.8424
SPC00573624	901	0.6671
SPC00573631	1,100	0.6757
SPC00573625	1,272	1.2960
SPC00573632	1,510	0.2963
SPC00573633	1,720	0.3110
SPC00573626	1,808	1.1435
SPC00573627	2,273	0.9236
SPC00573628	2,708	1.3580
SPC00573620	3,109	0.8372
SPC00573619	3,514	1.2007
SPC00573618	3,900	1.5047
SPC00573617	4,300	1.7970
SPC00573616	4,721	1.7593
SPC00573615	5,040	1.3412
SPC00573614	5,300	1.6713
SPC00573612	6,297	1.2624
SPC00573611	6,700	0.9720
SPC00573610	6,895	0.7765
SPC00573607	7,798	4.0024
Mean	—	1.2919
StdDev	—	0.7920
Min	—	0.2963
Max	—	4.0024

Source: Output DTN: LL040903723121.042, *DustNO3toClRatios.xls*.

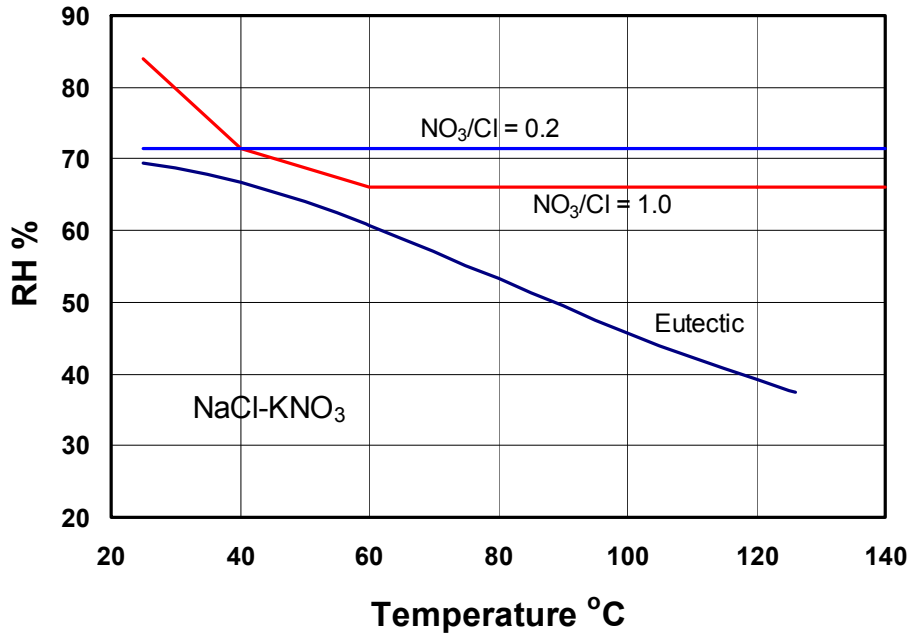
NOTE: The actual number of significant figures for the NO₃/Cl ratio is, at best, three. The precision shown matches that of the source spreadsheet.

Table 6.7-16. NO₃/Cl Ratios for Phase II Dust Samples

Sample Number	Lab Number	NO ₃ /Cl (mol/mol)
00574979A	C-203112	—
00574979B	C-203113	—
00574979C	C-203114	—
00574980A	C-203115	1.6551
00574980B	C-203116	2.3338
00574980C	C-203117	2.3762
00574981A	C-203118	0.8963
00574981B	C-203119	0.7351
00574981C	C-203120	3.1447
00574982A	C-203121	1.5956
00574982B	C-203122	2.5197
00574982C	C-203123	3.3634
00574983A	C-203124	0.9931
00574983B	C-203125	1.1875
00574983C	C-203126	1.5565
00574984A	C-203127	0.9827
00574984B	C-203128	—
00574984C	C-203129	1.2995
00574985A	C-203130	1.1435
00574985B	C-203131	1.6336
00574985C	C-203132	1.7222
00574986A	C-203133	0.8696
00574986B	C-203134	1.0090
00574986C	C-203135	1.1435
00574987A	C-203136	1.8248
00574987B	C-203137	0.8577
00574987C	C-203138	0.9291
00574990A	C-203139	1.1046
00574990B	C-203140	1.2332
00574990C	C-203141	1.2613
00574991A	C-203142	0.7927
00574991B	C-203143	1.1736
00574991C	C-203144	1.1435
00574992A	C-203145	0.4084
00574992B	C-203146	0.4742
00574992C	C-203147	0.5167
Mean	—	1.3713
StdDev	—	0.7146
Min	—	0.4084
Max	—	3.3634

Source: Output DTN: LL040903723121.042, *DustNO3toClRatios.xls*.

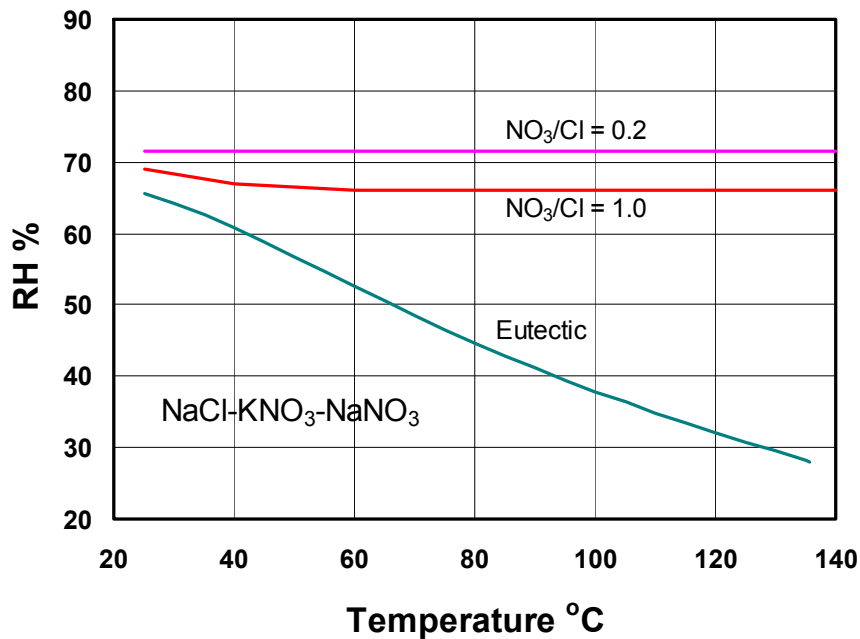
NOTE: The actual number of significant figures for the NO₃/Cl ratio is, at best, three. The precision shown matches that of the source spreadsheet.



Source: Output DTN: LL040903723121.042, *RHTX_Minerals1_PlotsB_v2p1.xls*.

NOTE: The crossover of the two minimum RH curves is caused by an inversion in the relative solubilities of NaCl and KNO₃.

Figure 6.7-31. Deliquescence RH and Minimum RH Values to Achieve NO_3/Cl Ratios of 1.0 and 0.2 as a Function of Temperature for the Assemblage Halite-Niter (NaCl-KNO₃)



Source: Output DTN: LL040903723121.042, *RHTX_Minerals1_PlotsB_v2p1.xls*.

Figure 6.7-32. Deliquescence RH and Minimum RH Values to Achieve NO_3/Cl Ratios of 1.0 and 0.2 as a Function of Temperature for the Assemblage Halite-Niter-Soda Niter (NaCl- KNO₃- NaNO₃)

6.7.2.11 Deliquescence of Salt Minerals Created by Evaporation of Seepage Waters

The purpose of the preceding section is to develop an analysis of deliquescence in the “no-dripping” case, which largely equates to deliquescence of dust deposited on the metal barrier surfaces. There is also a potential “dripping” case in which salt minerals formed by evaporation of seepage water later deliquesce. Due to the expected dryness during the ventilation period, little seepage is expected then. Because of the consequent dryout of the rock around the drift during that period, seepage during the heating up phase of the thermal pulse event is expected to be negligible as such water as is present in and around the tunnels is driven out. Although some salt might be formed in the ventilation and heating-up periods, it is likely to be quite minimal in comparison to salt deposited as part of dust. During the cooldown period, seepage eventually breaks through into the drifts. The possibility exists that salts can form on the metal barriers by evaporation of seepage water. These salts might deliquesce as temperature decreases and relative humidity rises. Such salts would form at the loci of seepage. However, the dripping of seepage water might also result in the formation of salts as aerosols that are deposited over a larger area.

The salts and concentrated solutions that form due to evaporation of seepage water depend on various factors, including the parent groundwater composition, the thermal history, reaction with rock and minerals, and reaction with the gas phase in the thermally perturbed unsaturated zone. Of all these factors, the most important is the composition of the parent groundwater or groundwaters. For many years, the relevant groundwater composition was considered to be represented by that of J-13 well water (Harrar et al. 1990 [DIRS 100814]), whose nominal composition (DTN: MO0006J13WTRCM.000 [DIRS 151029]) is shown in Table 4.1-21. This is a calcium-sodium-bicarbonate water from the saturated zone considered to share some affinity with perched water in the unsaturated zone. The shared affinity is probably based on a higher extent of long-term interaction with the rock, resulting in the observed high bicarbonate levels. More recently, recognition has shifted to porewaters, the compositions for two of which (EBS-HD-PERM-2 and EBS-HD-PERM-3; DTN: MO0005PORWATER.000 [DIRS 150930]) are given in Table 4.1-22. These contain higher levels of calcium, magnesium, chloride, and sulfate than the J-13 well water. Although porewater compositions vary, a characteristic is that the exact compositions are difficult to explain in terms of genesis. They seem more related to a variable pickup of highly soluble salts in the atmosphere (as rain), in the soil zone (as recently fallen rain), and in the deeper unsaturated zone (as groundwater) than to more classical and long-term rock–water interaction involving silicates and carbonates.

This report does not address the known variability of porewater in all the samples collected from Yucca Mountain, but simply notes that such variability exists. Small differences in the concentrations of the dissolved constituents in water can result in the following of different paths during the evaporative process, as various chemical divides come into play. Thus, a small increase in say dissolved calcium may result in more calcium than sulfate, thus leaving an excess of calcium instead of an excess of sulfate, after precipitation of a calcium sulfate minerals (e.g., gypsum or anhydrite).

Although experiments and modeling calculations can be done to study the evaporation of heated parent groundwaters, the applicability of such results is limited because the actual seepage waters derived from such groundwaters will differ owing to chemical interactions with the rock and the

gas phase at elevated temperatures. Because the chemistry of potential parent waters may cover a wide range, one looks to processes that might help to define a smaller range of ultimate outcomes.

One process theme is the precipitation of magnesium in clays or related silicates, such as sepiolite. The parent groundwaters contain elevated silica compared to many other, non-Yucca Mountain groundwaters. However, silica is also readily available at elevated temperatures from the dissolution of volcanic glass or cristobalite, or both, and other silicate minerals in the rock at Yucca Mountain. This will also be true of rock dust or dust blown into the repository. Sufficiency of available silica is not the only factor. The precipitation of magnesium from solution effectively adds hydrogen ions to solution that must then be largely neutralized (else a low-pH solution develops). Neutralization is possible by several mechanisms, including acid-gas evolution (e.g., of $\text{CO}_{2(g)}$), ion exchange reactions with minerals (e.g., H^+ for Na^+), and generally slower “weathering” reactions. This process of magnesium removal ensures that that a brine of the magnesium sulfate or magnesium chloride type will not form in the repository. The potential direct role of acid-gas evolution on sequestering magnesium in precipitated minerals is discussed in Section 6.7.2.14.

The theme of sequestration of aqueous magnesium in silicate minerals is observed in a variety of environments. Wolery (1978 [DIRS 151346]) pointed this out in the context of the removal of magnesium from seawater in hydrothermal reactions with the basalt of the oceanic crust (basalt is fairly Mg-rich to begin with, pointing to the strength of the theme). It is also seen in hydrothermal reaction of seawater with peridotite (Janecky 1982 [DIRS 157907]), an even more Mg-rich silicate rock. The theme has also been observed in a variety of calculations and experiments in other systems where silicate rock interacts with water at elevated temperature. Of immediate relevance to the repository, the theme of Mg sequestration in secondary silicates is observed in both groundwater evaporation experiments at near-boiling temperatures (Rosenberg et al. 1999 [DIRS 125338]; Rosenberg et al. 1999 [DIRS 125339]; and Rosenberg et al. 2001 [DIRS 154862]) and experimental studies of groundwater-tuff hydrothermal interaction, mostly between 90°C and 150°C (e.g., Knauss and Beiriger 1984 [DIRS 106441]; Knauss et al. 1985 [DIRS 143694]; Knauss et al. 1985 [DIRS 141586]; Knauss and Peifer 1986 [DIRS 100151]; and Knauss et al. 1987 [DIRS 100152]). Most of these studies of evaporation and tuff-groundwater interaction also include examples of modeling that is consistent with the theme of Mg sequestration in secondary silicates. Delany (1985 [DIRS 100134]) provides a pure modeling study of tuff-groundwater hydrothermal interaction. This theme is also reflected in more recent THC analyses of modification of groundwater chemistry due to rock-water interaction driven by thermal pulse (e.g., BSC 2004 [DIRS 169860]; DTN: MO0303MWDSCMAB.000 [DIRS 162551]).

Engineered Barrier System: Physical and Chemical Environment (BSC 2004 [DIRS 169860]) deals with seepage waters in greater detail. The present report will assume that calcium chloride minerals provide a sufficient bound for deliquescence of salt minerals generated from seepage waters. This would correspond to a pure calcium chloride seepage water. A close approximation to this analysis is shown in Figure 6.7-8, which points out the role of antarcticite ($\text{CaCl}_2 \cdot 6\text{H}_2\text{O}$), $\text{CaCl}_2 \cdot 4\text{H}_2\text{O}$, and $\text{CaCl}_2 \cdot 2\text{H}_2\text{O}$ at successively higher temperatures. The actual results, as presented in Section 6.7.2.13, is a blend of EQ3/6 calculations with experimental data (Section 6.7.2.12).

The (pure) calcium chloride case is chosen because it is considered the most plausible worst-case scenario. The development of a solution high in magnesium (e.g., magnesium chloride), whether from seepage or from dust, appears most unlikely given the data supporting the theme of magnesium sequestration into secondary silicates discussed above. Other plausible brine types developing from seepage water would include the bicarbonate type with elevated fluoride and pH characteristic; for example, of J-13 well water evaporation (e.g., Rosenberg et al. 1999 [DIRS 125338]; Rosenberg et al. 2001 [DIRS 154862]), which in the limit of the eutectic state may evolve into more of a nitrate brine and sulfate or sulfate–nitrate brines, or both, (BSC 2004 [DIRS 169863]), and *Engineered Barrier System: Physical and Chemical Environment* (BSC 2004 [DIRS 169860]).

As this report demonstrates, adding additional salt minerals to a salt mineral or salt mineral assemblage can only lower the deliquescence RH. Hence, one may ask if a pure calcium chloride case is sufficient. As the deliquescence RH data in Figure 6.7-8 indicate, the calcium chloride minerals are very strong drivers. They provide very low deliquescence RH by themselves, such that it is difficult to obtain further significant depression. There is no compelling reason to consider the addition of relatively weak driver salts such as anhydrite (CaSO_4), calcite (CaCO_3), or glauberite [$\text{Na}_2\text{Ca}(\text{SO}_4)_2$], as the effect of doing so is not significant. Even halite (NaCl) is a weak driver by comparison. Furthermore, considering the case CaCl_2 - NaCl , the extremely high chloride due to the calcium chloride would strongly depress the solubility of NaCl due to the common ion effect, hence strongly reduce any extra depression of the deliquescence RH due to the presence of NaCl . The same effect would also be true if one considers KCl instead of NaCl . The alkali metal sulfates such as thenardite (Na_2SO_4) are not strong drivers, so there is not much to consider there. Furthermore, the effect of adding a soluble sulfate to calcium chloride would be to precipitate calcium sulfate, leading to an aqueous solution that looks more like a mixture of aqueous CaCl_2 and NaCl . Adding some form of MgSO_4 would again result in CaSO_4 precipitation and possibly an aqueous solution dominated by MgCl_2 . However, with excess silica and other components present, the Mg would be expected to be removed by precipitation of Mg -bearing secondary silicates, to ultimately result in something far less deliquescent than pure CaCl_2 . Adding MgCl_2 or $\text{Mg}(\text{NO}_3)_2$ would lead to a similar result. The alkali metal nitrates (KNO_3 and NaNO_3) might have some effect at temperatures above 100°C . Even though no common ion effect would be involved, hardcore repulsive forces associated with extremely high solute concentrations would reduce the solubilities of these phases and correspondingly their ability to depress the deliquescence RH from that of the pure calcium chloride case. Adding $\text{Ca}(\text{NO}_3)_2$ would not be very effective because the calcium nitrate minerals are less effective drivers and there is a common ion effect through the calcium. Adding K_2CO_3 would not change the deliquescence RH much because calcium carbonate would precipitate, leaving a solution composed largely of CaCl_2 and KCl . The common ion effect would then reduce the solubility of the KCl and, hence, largely mask depression of the deliquescence RH relative to that for pure CaCl_2 .

One may also ask if the calcium chloride case is realistic. The likelihood is that only a minor fraction of seepage waters, possibly a very small fraction, would have compositions that would lead to the formation of calcium chloride brines. Furthermore, should the seepage waters have compositions that would allow this to occur, the effect of acid–gas volatility may limit the existence of such CaCl_2 brines, at least at sufficiently elevated temperature. This effect is discussed in Section 6.7.2.14.

6.7.2.12 Additional Deliquescence RH Data for Saturated Calcium Nitrate and Saturated Calcium Chloride Solutions

The purpose of Section 6.7.2.10 is to describe the implementation of the IDPS model for deliquescence in the “no-dripping” case, which for the most part equates to deliquescence of dust deposited on the metal barrier surfaces. Convergence difficulties are encountered in some of the calculations for systems saturated with calcium nitrate minerals and, to a much lesser extent, calcium chloride minerals. Calculations with such minerals involve extremely concentrated solutions that are at the limit of what current models can handle with reasonable accuracy. Consequently, some experimental data were developed to compensate for these problems.

Vapor pressure data for saturated calcium nitrate solutions are taken from Kracek (1928 [DIRS 122125], p. 368). These are reproduced in Tables 4.1-5 and 6.7-17. These data are used in conjunction with the vapor pressure data for pure water taken from Weast and Astle (1981 [DIRS 100833], pp. D-168 to D-169; reproduced in Table 4.1-4) to calculate deliquescence RH of the saturated calcium nitrate solutions as a function of temperature. The vapor pressures over the saturated solutions are also converted from mm Hg to bar units. In addition, the dryout temperature corresponding to the maximum expected repository total pressure of 0.90 bar is calculated by linear interpolation. All these calculated data are included in Table 6.7-17.

Table 6.7-17. Water Vapor Pressure and RH of Saturated Calcium Nitrate Solutions as a Function of Temperature

Temp (°C)	Pressure(m m Hg)	Pressure (bar)	RH (decimal)	RH (%)
α-Ca(NO₃)₂·4H₂O				
0	2.7	0.0036	0.5896	58.96
5	3.9	0.0052	0.5961	59.61
10	5.2	0.0069	0.5647	56.47
15	6.9	0.0092	0.5396	53.96
20	9.4	0.0125	0.5361	53.61
25	12.0	0.0160	0.5051	50.51
30	14.9	0.0199	0.4682	46.82
35	17.7	0.0236	0.4197	41.97
37	18.9	0.0252	0.4014	40.14
39	19.5	0.0260	0.3718	37.18
40	19.7	0.0263	0.3561	35.61
41	19.7	0.0263	0.3377	33.77
42	19.3	0.0257	0.3139	31.39
42.5	19.0	0.0253	0.3010	30.10
42.7	18.6	0.0248	0.2916	29.16
α-Ca(NO₃)₂·4H₂O + Ca(NO₃)₂·3H₂O				
42.7	18.0	0.0240	0.2822	28.22
Ca(NO₃)₂·3H₂O				
44	18.8	0.0251	0.2755	27.55
46	19.8	0.0264	0.2618	26.18
48	20.5	0.0273	0.2449	24.49
49	20.6	0.0275	0.2341	23.41

Table 6.7-17. Water Vapor Pressure and RH of Saturated Calcium Nitrate Solutions as a Function of Temperature (Continued)

Temp (°C)	Pressure(m m Hg)	Pressure (bar)	RH (decimal)	RH (%)
Ca(NO₃)₂:3H₂O (continued)				
50	20.5	0.0273	0.2216	22.16
50.5	20.2	0.0269	0.2130	21.30
51.1	19.0	0.0253	0.1945	19.45
51	16.8	0.0224	0.1728	17.28
Ca(NO₃)₂:3H₂O + Ca(NO₃)₂:2H₂O				
50.6	15.4	0.0205	0.1616	16.16
Ca(NO₃)₂:3H₂O + Ca(NO₃)₂				
49.8	14.3	0.0191	0.1561	15.61
Ca(NO₃)₂:2H₂O + Ca(NO₃)₂				
51.9	16.0	0.0213	0.1575	15.75
Ca(NO₃)₂				
55	19	0.0253	0.1610	16.10
60	24.9	0.0332	0.1667	16.67
140.5	675.1	0.9000	0.2025	20.25
151	760.0	1.01325	0.2072	20.72

Source: Output DTN: LL040903723121.042, *CalciumSaltsExptlDRHCalcsRev01.xls*.

NOTE: The vapor pressure of pure water used to calculate RH values is taken from Table 4.1-4, which gives results for 5°C-increments in the temperature. For temperatures not multiples of 5°C, values for the vapor pressure of pure water are obtained by linear interpolation (*CalciumSaltsExptlDRHCalcsRev01.xls*). The temperature of 140.5°C for a total pressure of 0.90 bar is determined by linear interpolation.

Vapor pressure data for saturated calcium chloride solutions are also taken from Kracek (1928 [DIRS 122125], p. 368). These are reproduced in Tables 4.1-6 and 6.7-18. These data are used in conjunction with the above-cited vapor pressure data for pure water to calculate deliquescence RH of the saturated calcium chloride solutions as a function of temperature. The vapor pressures over the saturated solutions are also converted from mm Hg to bar units. In addition, the dryout temperature corresponding to the maximum expected repository total pressure of 0.90 bar is calculated by linear interpolation. All these calculated data are included in Table 6.7-18.

Table 6.7-18. Water Vapor Pressure and RH of Saturated Calcium Chloride Solutions as a Function of Temperature

Temperature (°C)	Pressure (mm Hg)	Pressure (bar)	RH (decimal)	RH (%)
CaCl₂:6H₂O				
0	2.08	0.0028	0.4542	45.42
5	2.74	0.0037	0.4188	41.88
10	3.71	0.0049	0.4029	40.29
15	4.76	0.0063	0.3722	37.22
20	6.06	0.0081	0.3456	34.56
25	6.97	0.0093	0.2934	29.34
27	7.28	0.0097	0.2724	27.24

Table 6.7-18. Water Vapor Pressure and RH of Saturated Calcium Chloride Solutions as a Function of Temperature (Continued)

Temperature (°C)	Pressure (mm Hg)	Pressure (bar)	RH (decimal)	RH (%)
CaCl₂·6H₂O (continued)				
28.5	7.36	0.0098	0.2522	25.22
29	7.33	0.0098	0.2440	24.40
29.5	7.22	0.0096	0.2335	23.35
CaCl₂·6H₂O				
29.95	6.70	0.0089	0.2111	21.11
CaCl₂·6H₂O + α-CaCl₂·4H₂O				
29.93	6.85	0.0091	0.2161	21.61
α-CaCl₂·4H₂O				
35	8.63	0.0115	0.2046	20.46
40	10.53	0.0140	0.1903	19.03
α-CaCl₂·4H₂O + CaCl₂·2H₂O				
45.3	12.06	0.0161	0.1653	16.53
CaCl₂·2H₂O				
50	15.5	0.0207	0.1675	16.75
60	25.7	0.0343	0.1720	17.20
70	41.2	0.0549	0.1763	17.63
80	63.9	0.0852	0.1799	17.99
90	95.2	0.1269	0.1811	18.11
100	138	0.1840	0.1816	18.16
120	268	0.3573	0.1800	18.00
140	467.5	0.6233	0.1725	17.25
CaCl₂·2H₂O				
156.5	675.1	0.9000	0.1581	15.81
160	719	0.9586	0.1551	15.51
170	815	1.0866	0.1372	13.72
172	825	1.0999	0.1323	13.23
CaCl₂·2H₂O				
175.7	771	1.0279	0.1133	11.33
CaCl₂·2H₂O + CaCl₂·H₂O				
175.5	796	1.0612	0.1175	11.75

Source: Output DTN: LL040903723121.042, *CalciumSaltsExptIDRHCalsRev01.xls*.

NOTE: The vapor pressure of pure water used to calculate RH values is taken from Table 4.1-4, which gives results for 5°C-increments in the temperature. For temperatures not some multiple of 5°C, values for the vapor pressure of pure water are obtained by linear interpolation (*CalciumSaltsExptIDRHCalsRev01.xls*). The temperature of 156.5°C for a total pressure of 0.90 bar is determined by linear interpolation.

6.7.2.13 Analysis of Deliquescence of Salt Minerals on the Metal Barriers

A summary of salt mineral deliquescence on the drip shield and waste package outer barrier is created based on the analysis in previous subsections. The summary considers a “no-dripping” case (dust deliquescence) and a “dripping” case (deliquescence of minerals formed by evaporation of seepage waters). The no-dripping case applies until dripping of seepage occurs; then the dripping case applies.

The no-dripping case is based on the three key salt assemblages identified in Section 6.7.2.10, with the KBr component removed for the reasons discussed in that section. Each salt assemblage is applied to a specified percentage of the waste packages as shown in Table 6.7-19. These percentages are based on the occurrence of key salt assemblages in the tunnel dust samples as determined in Table 6.7-11. The spatial scale on which the dust samples are taken extends over 7.5 km of tunnel for the Phase I samples, justifying this approach. This scale is indicated in Table 4.1-19 (in the column headed by “meters,” denoting distance inside the tunnel from the North Portal). The same data show that the typical distance between sampling locations is on the order of 300 meters. The distance over which the samples extend in the tunnel and the typical distance between sampling locations greatly exceed the spatial scale (e.g., length) of a single waste package. It is presumed that spatial scales applicable to the Phase II samples are similar to those for the Phase I samples, though this information is not included in the data package for the Phase II samples (DTN: MO0209EBSDUST2.030 [DIRS 162557]).

Table 6.7-19. Cases, Associated Key Salts, and Percentage of Affected Waste Packages for the No-Dripping Condition (Dust Deliquescence)

Key Dust Assembly Case	Key Salts	% of Waste Packages
A	NaCl-KNO ₃	68.1
B	NaCl-KNO ₃ -NaNO ₃	27.8
C	NaCl-KNO ₃ -NaNO ₃ -Ca(NO ₃) ₂	4.1

Source: Output DTN: LL040603912251.107, *RHvsTempLookUpTablesRev01.xls*.

As is noted in Section 6.7.2.12, the dripping case is based on calcium chloride minerals, starting with antarcticite (CaCl₂:6H₂O) at low temperature, CaCl₂:4H₂O at intermediate temperatures, and CaCl₂:2H₂O at higher temperatures extending to the dryout point (at which there is near-equilibrium also with anhydrous CaCl₂). The mineral assemblage for this case is represented in Table 6.7-20, where “CaCl₂” refers to whichever calcium chloride mineral is the most stable at any given temperature.

Table 6.7-20. Case, Associated Key Salt, and Percentage of Affected Waste Packages for the Dripping Condition (Deliquescence of Salts Formed from Seepage Waters)

Case	Key Salt	% of Waste Packages
A	CaCl ₂	100

Source: Output DTN: LL040603912251.107, *RHvsTempLookUpTablesRev01.xls*.

The tables for the four cases included in Tables 6.7-19 and 6.7-20 are presented in Tables 6.7-21, 6.7-22, 6.7-23, and 6.7-24. Each table comprises pairs of temperature and RH (actually deliquescence RH) values. If the RH in the IDPS model, in which this analysis is utilized is

greater than or equal the corresponding RH in the appropriate table, the system is considered wet (aqueous solution present). Otherwise, the system is dry. If the temperature exceeds the highest value in the table, the system should be taken as dry. Note that the highest temperature in each table is specific to that table. In each table the highest temperature corresponds to dryout imposed by the total pressure limit of 0.90 bar.

The table for the no-dripping Key Dust Assembly Case A (NaCl-KNO₃) is given in Table 6.7-21. This is based entirely on the EQ3/6 calculations for this mineral assemblage presented in Section 6.7.2.9.

Table 6.7-21. Deliquescence RH as a Function of Temperature: No-Dripping Key Dust Assembly Case A (“NaCl-KNO₃”)

Temperature (°C)	RH (decimal)	RH (%)
25	0.6953	69.53
30	0.6871	68.71
35	0.6778	67.78
40	0.6671	66.71
45	0.6545	65.45
50	0.6401	64.01
55	0.6242	62.42
59.45	0.6090	60.90
60	0.6071	60.71
65	0.5892	58.92
70	0.5707	57.07
75	0.5519	55.19
80	0.5329	53.29
85	0.5139	51.39
90	0.4949	49.49
95	0.4760	47.60
100	0.4573	45.73
105	0.4404	44.04
110	0.4239	42.39
115	0.4079	40.79
120	0.3925	39.25
125	0.3777	37.77
126.08	0.3746	37.46

Source: Output DTN: LL040603912251.107,
RHvsTempLookUpTablesRev01.xls.

NOTE: These data trace further back to file *halntr.csv*, folder RHTx2, in *Pack048.zip* in output DTN: LL040903723121.042.

The table for the no-dripping Key Dust Assembly Case B (NaCl-KNO₃-NaNO₃) is given in Table 6.7-22. This is based entirely on the EQ3/6 calculations for this mineral assemblage presented in Section 6.7.2.9.

Table 6.7-22. Deliquescence RH as a Function of Temperature: No-Dripping Key Dust Assembly Case B ("NaCl-KNO₃-NaNO₃")

Temperature (°C)	RH (decimal)	RH (%)
25	0.6570	65.70
30	0.6426	64.26
35	0.6259	62.59
40	0.6073	60.73
45	0.5875	58.75
50	0.5669	56.69
55	0.5461	54.61
60	0.5253	52.53
65	0.5049	50.49
70	0.4850	48.50
75	0.4656	46.56
80	0.4469	44.69
85	0.4289	42.89
90	0.4114	41.14
95	0.3945	39.45
100	0.3782	37.82
105	0.3636	36.36
110	0.3493	34.93
115	0.3353	33.53
120	0.3216	32.16
125	0.3082	30.82
130	0.2953	29.53
135	0.2828	28.28
135.79	0.2809	28.09

Source: Output DTN: LL040603912251.107;
RHvsTempLookUpTablesRev01.xls.

NOTE: These data trace further back to file *hanrsn.csv*, folder RHTx3, in *Pack048.zip* in output DTN: LL040903723121.042.

The table for the no-dripping Key Dust Assembly Case C [NaCl-KNO₃-NaNO₃-Ca(NO₃)₂] is given in Table 6.7-23. This is partly based on the EQ3/6 calculations for this mineral assemblage (reference files *HNS_CN4.csv*, *HNS_CN3.csv*, *HNS_CN2.csv*, and *HNS_CN0.csv* in output DTN: LL040903723121.042). The calculations with calcium nitrate represented as nitrocalcite [Ca(NO₃)₂·4H₂O] are run to 60.40°C, at which point the nitrocalcite “melts.” Subsequent attempts to run the IDPS model on the system at higher temperature with Ca(NO₃)₂·3H₂O and Ca(NO₃)₂·2H₂O failed to generate any useful results due to predicted “melting” at the starting temperature. This behavior in essence parallels that for the pure Ca(NO₃)₂ case presented in more detail in Section 6.7.2.9 (Figure 6.7-9). There, it is pointed that all results above some temperature between 25°C and 30°C fall outside the IDPS experimental validation criterion on the RH. It can be said that the relative humidity data for this assemblage must be lower than the corresponding data for the pure Ca(NO₃)₂ system (one of the key rules of deliquescence discussed earlier).

Table 6.7-23. Deliquescence RH as a Function of Temperature: No-Dripping Key Dust Assembly Case C ("NaCl-KNO₃-NaNO₃-Ca(NO₃)₂")

Temperature (°C)	RH (decimal)	RH (%)
25	0.4947	49.47
30	0.4845	48.45
35	0.4720	47.20
40	0.4564	45.64
45	0.4370	43.70
50	0.4127	41.27
55	0.3803	38.03
60	0.3210	32.10
60.40	0.3051	30.51
155	0.1656	16.56

Source: Output DTN: LL040603912251.107;
RHvsTempLookUpTablesRev01.xls.

NOTES: These data (except for 155°C) trace further back to file *hns_cn4.csv*, folder RHTx4, in *Pack048.zip* in output DTN: LL040903723121.042; see the text above for an explanation of the data for 155°C.

The data in this table carry exceptional uncertainty and are only intended to illustrate the best-estimate picture of the behavior for this case (see text).

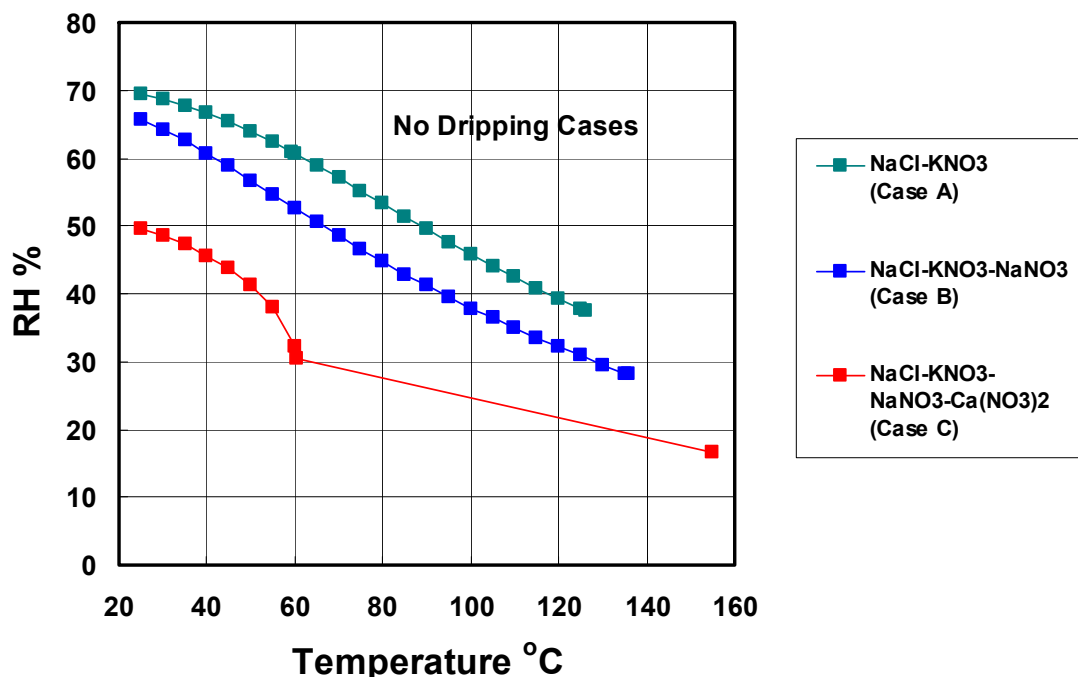
However, the IDPS model results for the Key Dust Assembly Case C assemblage are lower than those for the pure Ca(NO₃)₂ system (by about 12 RH percent at 25°C). The validation range criterion for RH is clearly exceeded above 40°C, as the difference between the IDPS model results and the experimental data for the pure Ca(NO₃)₂ system (Table 6.7-17) is greater than the 10 RH percent validation limit. The common ion effect must reduce the solubility of Ca(NO₃)₂·4H₂O in the instance of the Key Dust Assembly Case C eutectic because KNO₃ and NaNO₃ are also present. It cannot be said with certainty that the IDPS model RH results in the 25°C to 60.40°C range are outside the validation range of the model, but that may be the case, as suggested by the situation for the pure Ca(NO₃)₂-H₂O system (Section 6.7.2.9). The way in which the IDPS model validation range is defined precludes resolution of this issue in the absence of experimental data for this particular four-salt system.

Experimental data for saturated pure calcium nitrate solutions (Table 6.7-17) indicate a boiling temperature of 151°C for a total pressure of 1 atm (1.01325 bar) and about 140.5°C for the expected repository maximum pressure of 0.90 bar. To construct the table, results from the EQ3/6 run are used from 25°C to 60.40°C (despite the reservations noted above). To complete the table, a boiling temperature of 155°C for 0.90 bar total pressure is assumed for saturated Ca(NO₃)₂-NaCl-KNO₃-NaNO₃, about fifteen degrees higher than the estimated 140.5°C for pure Ca(NO₃)₂ at the same total pressure. As indicated in Table 6.7-17, a vapor pressure of 0.90 bar is 675.1 mm Hg. The vapor pressure of pure water at this temperature is 4,075.88 mm Hg (Table 4.1-4). This implies an RH at dryout of 16.56 percent (a fairly low value). As the table implies, the deliquescence RH for the no-dripping Key Dust Assembly Case C is assumed to vary linearly between 60.40°C and 155°C. Table 6.7-23 carries additional uncertainty in the range 25°C to 60.40°C owing to the problems in the IDPS model, particularly the limited

adequacy of the $\text{Ca}(\text{NO}_3)_2$ parameterization (Section 6.7.2.9) and the fact that at higher temperature only a rough estimate can be made of the deliquescence RH for this system. The data in this table are presented to give a best-estimate picture of the behavior of this system. These data are not used in the total system performance assessment for the license application (TSPA-LA).

The deliquescence RH versus temperature curves for the three no-dripping cases are shown in Figure 6.7-33. Note that the minor Key Dust Assembly Case C is more deliquescent than the two major Key Dust Assembly Cases (A and B). All three cases are highly deliquescent at elevated temperature.

The table for the single dripping case (CaCl_2) is given in Table 6.7-24. This is based partly on the EQ3/6 calculations for CaCl_2 minerals presented in Section 6.7.2.9 (Figure 6.7-8). Those calculations indicate a dryout temperature just above the IDPS model validation limit of 140°C for the limit of 0.90 bar total pressure. The reported measured data for pure saturated CaCl_2 solutions in Table 6.7-18 suggest a higher boiling (dryout) temperature, perhaps as high as 176°C for 1 atm (1.01325 bar) total pressure, and an estimated value of 156.5°C for the expected maximum repository pressure of 0.90 bar. The table is, therefore, constructed by using the IDPS model calculation data up to 46.02°C , where $\text{CaCl}_2 \cdot 2\text{H}_2\text{O}$ becomes controlling. Thereafter, the more conservative elements of the measured data are employed (there is some inconsistency in these data, as is noted in Section 6.7.2.12).



Source: Output DTN: LL040603912251.107, *RHvsTempLookupTablesRev01.xls*.

NOTE: The curve for Key Dust Assembly Case C carries exceptional uncertainty and is only provided to give a best-estimate picture of the behavior for this case (see text).

Figure 6.7-33. Deliquescence RH as a Function of Temperature for the Three No-Dripping Cases

Table 6.7-24. Deliquescence RH as a Function of Temperature: Dripping Case ("CaCl₂")

Temperature (°C)	RH (decimal)	RH (%)
25	0.2819	28.19
30	0.2223	22.23
30.02	0.2214	22.14
35	0.2103	21.03
40	0.1961	19.61
45	0.1756	17.56
46.02	0.1744	17.44
50	0.1675	16.75
60	0.1720	17.20
70	0.1763	17.63
80	0.1799	17.99
90	0.1811	18.11
100	0.1816	18.16
120	0.1800	18.00
140	0.1725	17.25
156.5	0.1581	15.81

Source: Output DTN: LL040603912251.107,
RHvsTempLookUpTablesRev01.xls.

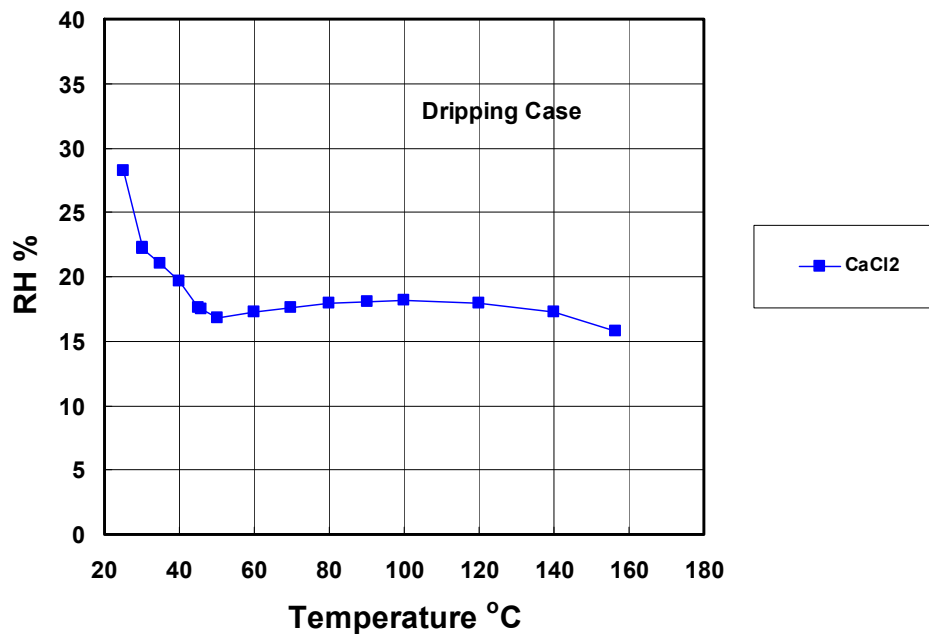
NOTE: See text above for further information regarding the origin of these data. The dryout temperature of 156.5°C corresponds to the expected repository maximum pressure of 0.90 bar.

Figure 6.7-34 shows the deliquescence RH as a function of temperature for the single dripping case. Comparison with Figure 6.7-8 indicates that near 100°C, there is a divergence between the IDPS model calculations and the experimental measurements. In the IDPS model calculations (Figure 6.7-8) the deliquescence RH continues to increase slowly with temperature. In the experimental results (Table 6.7-18, for temperatures above 46.02°C), the deliquescence RH decreases, then flattens out (actually rising very slightly), and finally decreases again near the boiling temperature.

6.7.2.14 Role of Acid-Gas Volatility in Determining the Chemical Environment on the Metal Barriers

6.7.2.14.1 Background

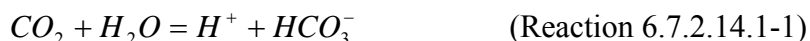
The chemical system of the repository in the thick vadose zone at Yucca Mountain consists of solid phases, aqueous solutions, and a gas phase. The influence of the gas phase as a source and sink of chemical species poses a major difference between a hydrologically unsaturated system and a saturated system. This is well recognized in terms of the effects of O₂ (which imposes oxidizing conditions) and CO₂. CO₂ is an acid-gas volatile in that it is the anhydride of carbonic acid.



Source: Output DTN: LL040603912251.107, *RHvsTempLookUpTablesRev01.xls*.

Figure 6.7-34. Deliquescence RH as a Function of Temperature for the Single Dripping Case

Transfer of CO₂ from the gas phase to aqueous solution results in the formation of hydrogen ions according to a reaction such as:



This tends to reduce the pH. Conversely, transfer of CO₂ from the aqueous solution to the gas phase consumes hydrogen ions and tends to increase the pH.

O₂ and CO₂ are important constituents of air. The components of atmospheric air exclusive of water vapor are given in Table 6.7-25 (reproducing Table 4.1-13).

Table 6.7-25. Components of Atmospheric Air Exclusive of Water Vapor

Constituent	Content (%) by Volume	Content (ppm) by Volume
N ₂	78.084 ± 0.004	—
O ₂	20.946 ± 0.002	—
CO ₂	0.033 ± 0.001	—
Ar	0.934 ± 0.001	—
Ne	—	18.18 ± 0.04
He	—	5.24 ± 0.004
Kr	—	1.14 ± 0.01
Xe	—	0.087 ± 0.001
H ₂	—	0.5
CH ₄	—	2
N ₂ O	—	0.5 ± 0.1

Source: Weast and Astle 1981 [DIRS 100833], p. F-172.

The composition of the air in the mountain (excluding water vapor) is assumed to be that of normal atmospheric air. This report does not require specific data for O₂, N₂, or Ar or use such in the development of technical product output. Rather, it only requires a general assumption of mildly oxidizing conditions.

The data in Table 4.1-14 show a broad range of CO₂ abundance as a function of borehole depth. A partial pressure of 10^{-3.0} bar is equivalent to 1,000 ppm (by volume). For purposes of this analysis a value of 10^{-3.0} bar was used for the partial pressure of CO₂.

Transfer of CO₂ from aqueous solution to the gas phase occurs due to evaporation or boiling associated with the thermal pulse. Condensation of CO₂-laden steam at some distance from the drifts produces a CO₂-rich vapor and a dilute carbonic acid solution. The effect of mass transfer of CO₂ in the repository is a phenomenon that is incorporated into current THC modeling, as exemplified by the data included in Tables 6.7-26, 6.7-27, 6.7-28, 6.7-29, and 6.7-30 (reproducing Tables 4.1-15, 4.1-16, 4.1-17, 4.1-18, and 4.1-23, respectively) for calculated CO₂ pressures associated with seepage waters. Uptake of CO₂ into aqueous solution produces only a mild acid. However, such uptake can be helpful in neutralizing even strong bases (any weak acid can neutralize any strong base, and vice versa). The CO₂ data shown in Tables 6.7-26, 6.7-27, 6.7-28, and 6.7-29 are direct results of THC calculations (DTN: LB0108DSTTHC01.001 [DIRS 156285]). The gas fugacity data (for CO₂, HF, HCl, HNO₃, and N₂O₅) in Table 6.7-30 are derived from (non-Pitzer) EQ3/6 calculations (BSC 2004 [DIRS 169860]; DTN: MO0303MWDSCMAB.000 [DIRS 162551]) for water compositions near the drift wall determined by preceding THC calculations described in *Drift-Scale THC Seepage Model* (BSC 2004 [DIRS 169856]).

Tables 6.7-26, 6.7-27, 6.7-28, and 6.7-29 do not list any acid-gas species other than CO₂. Nevertheless, acid-gas species such as HCl and HNO₃ do exist in the atmosphere at trace levels. These levels are generally thought to be quite variable, reflecting transient processes. In that, these gases differ from better-known components like O₂, N₂, and even CO₂ in more than relative abundance. Fugacity data for four additional acid-gas species (HF, HCl, HNO₃, and N₂O₅) in calculated seepage waters are included in Table 6.7-30. These data can be considered as providing time-dependent boundary conditions on the chemical potentials of these acid-gas species in the relatively open parts of the drifts. These relatively open parts include the exposed surfaces of the drip shield and waste package outer barrier. Before directly addressing the consequences of this, however, some additional background information on acid-gases are reviewed.

Table 6.7-26. Calculation Results for High Temperature and Low Carbon Dioxide Partial Pressure in the Tptpll Lithology for Seepage at the Crown of the Drift

Parameter	Preclosure	Boiling	Cool Down	Extended Cool Down	Transition to Ambient	Ambient
	(0 to 50 yr)	(51 to 1,500 yr)	(1,501 to 4,000 yr)	(4,001 to 25,000 yr)	(25,001 to 100,000 yr)	(100,001 to 1,000,000 yr)
Actual THC Model Simulation Time (yr)	49.97	300.00	1,800.01	10,000.00	50,001.50	Averaged
Temperature (°C)	79.30	122.87	95.80	54.02	27.37	23.60
PCO ₂ (v.frac)	9.20E-04	8.91E-06	1.66E-05	1.62E-03	5.71E-04	4.39E-04

Source: DTN: LB0108DSTTHC01.001 [DIRS 156285].

yr = year.

Table 6.7-27. Calculation Results for High Temperature and High Carbon Dioxide Partial Pressure in the Tptpll Lithology for Seepage at the Crown of the Drift

Parameter	Preclosure	Boiling	Cool Down	Extended Cool Down	Transition to Ambient	Ambient
	(0 to 50 yr)	(51 to 1,500 yr)	(1,501 to 4,000 yr)	(4,001 to 25,000 yr)	(25,001 to 100,000 yr)	(100,001 to 1,000,000 yr)
Actual THC Model Simulation Time (yr)	49.97	300.00	1,800.01	10,000.00	50,001.50	Averaged
Temperature (°C)	79.30	122.86	95.80	54.02	27.37	23.20
PCO ₂ (v.frac)	9.20E-04	8.92E-06	2.26E-05	3.45E-03	1.06E-03	7.67E-04

Source: DTN: LB0108DSTTHC01.001 [DIRS 156285].

yr = year.

Table 6.7-28. Calculation Results for Low Temperature and Low Carbon Dioxide Partial Pressure in the Tptpll Lithology for Seepage at the Crown of the Drift

Parameter	Preclosure	Postclosure Hot	Cool Down	Transition to Ambient	Ambient
	(0 to 300 yr)	(301 to 10,000 yr)	(10,001 to 30,000 yr)	(30,001 to 100,000 yr)	(100,001 to 1,000,000 yr)
Actual THC Model Simulation Time (yr)	53.00	700.00	20,000.00	51,411.30	Averaged
Temperature (°C)	52.92	73.40	35.59	25.89	23.60
PCO ₂ (v.frac)	1.19E-03	1.48E-03	8.75E-04	5.11E-04	4.39E-04

Source: DTN: LB0108DSTTHC01.001 [DIRS 156285].

yr = year.

Table 6.7-29. Calculation Results for Low Temperature and High Carbon Dioxide Partial Pressure in the Tptpll Lithology for Seepage at the Crown of the Drift

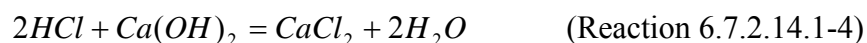
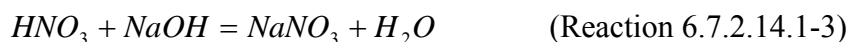
Parameter	Preclosure	Postclosure Hot	Cool Down	Transition to Ambient	Ambient
	(0 to 300 yr)	(301 to 10,000 yr)	(10,001 to 30,000 yr)	(30,001 to 100,000 yr)	(100,001 to 1,000,000 yr)
Actual THC Model Simulation Time (yr)	53.00	700.00	20,000.00	51,411.30	Averaged
Temperature (°C)	52.92	73.40	35.59	25.89	23.20
PCO ₂ (v.frac)	1.19E-03	1.48E-03	1.71E-03	9.38E-04	7.67E-04

Source: DTN: LB0108DSTTHC01.001 [DIRS 156285].

yr = year

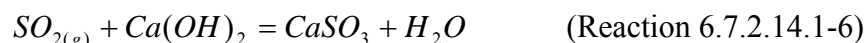
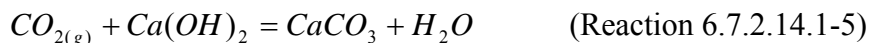
Acid-gas species are of considerable interest in atmospheric science (e.g., Ansari and Pandis 1999 [DIRS 162167]; von Glasow and Sander 2001 [DIRS 162162]; and Arimoto 2001 [DIRS 163485]) and in gas purification and environmental technology (e.g., Elm et al. 2001 [DIRS 163186]). Von Glasow and Sander (2001 [DIRS 162162]) proposed that the pH of aqueous sea salt aerosols is controlled by equilibrium with HCl gas in the atmosphere (the theory accounts for the observation that pH decreases with increasing aerosol size, which is contrary to what one would expect if the acid content of an aerosol particle is fixed when the particle first forms). Acid-gas species are also of interest, of course, in corrosion studies (e.g., Opila et al. 1989 [DIRS 140330]; Falk et al. 1998 [DIRS 163489]).

A salt is defined as the product of the neutralization of an acid by a base. The following reactions exemplify this process:



The question is whether and if so under what conditions this process can be reversed (acidic and basic species regenerated). It is obvious that it can be reversed, especially by the application of heat and in a system in which the acidic and basic components can be separated by volatilization of one or the other (more commonly it is the acidic component).

The following reactions are also neutralizing reactions:



Here, the two gas species are the respective anhydrides of carbonic and sulfurous acids.

Opila et al. (1989 [DIRS 140330]) noted the apparent long-term (nine-year) generation of HCl gas from a saturated NaCl solution, which resulted in the corrosion of a copper coupon placed above the solution. They presented thermodynamic calculations supporting the generation of small (but ultimately significant) amounts of HCl gas from the concentrated salt solution.

Creahan (1991 [DIRS 163395]) proposed the use of concentrated calcium nitrate solutions to control RH in museum cases. This prompted some concern about the long-term generation of acidic volatiles that might damage the case contents (Creahan 1991 [DIRS 163396]). As a test, a sodium bicarbonate solution was placed in a case along with a calcium nitrate solution and its pH was monitored for one month. No change was observed, and it was concluded that the calcium nitrate solution was safe to use in the absence of a sodium bicarbonate solution.

Pulvirenti et al. (2003 [DIRS 163184]) reported generating acid–gas volatiles including HCl, HF, and HNO₃ by boiling down various salt mixtures. These include the “UZ porewater” of Rosenberg et al. (2001 [DIRS 154862]) and salts and salt mixtures including CaCl₂ + KNO₃, MgSO₄ + KNO₃, Ca(NO₃)₂, Mg(NO₃)₂, CaCl₂, and MgCl₂. Condensate was trapped in a condenser and the pH was measured. In some cases, pH values less than 1 are reported. The salt MgSO₄ was found not to generate acid–gas, since no evidence of sulfate was reported from the condensate. Mg(NO₃)₂ appeared to be more efficient in generating acid–gases than Ca(NO₃)₂, CaCl₂, and MgCl₂, at least at the temperatures considered (in the range 90°C to 130°C).

Table 6.7-30. Log Fugacities of Five Acid-Gas Species in the Drift Wall as Functions of Time in Repository History

W0 THC Abstraction													
TF4							BF4						
Time (yrs)	Temp (°C)	CO ₂	HF	HCl	HNO ₃	N ₂ O ₅	Time (yrs)	Temp (°C)	CO ₂	HF	HCl	HNO ₃	N ₂ O ₅
10	52.50	-2.978	-11.703	-15.703	-17.407	-39.928	10	51.30	-2.897	-11.724	-15.713	-17.412	-39.935
51	91.80	-3.215	-10.336	-14.222	-15.991	-37.148	51	86.10	-2.776	-10.334	-14.266	-16.026	-37.212
100	96.10	-3.485	-10.249	-14.609	-16.388	-37.944	100	111.00	-3.607	-9.973	-12.438	-14.233	-33.641
150	95.90	-3.453	-10.120	-14.309	-16.085	-37.339	150	110.00	-3.322	-9.864	-12.937	-13.934	-33.042
250	95.50	-3.400	-10.030	-13.790	-15.534	-36.237	250	109.00	-3.361	-9.913	-13.171	-14.432	-34.037
350	95.70	-3.461	-9.978	-13.352	-15.115	-35.398	350	108.00	-3.611	-10.067	-13.324	-14.774	-34.721
500	95.90	-3.164	-9.850	-12.793	-14.546	-34.259	500	106.00	-3.431	-10.035	-13.456	-14.976	-35.125
750	95.70	-2.707	-9.900	-13.864	-15.637	-36.443	750	103.00	-2.805	-9.814	-13.523	-15.094	-35.360
1,000	94.60	-2.405	-9.812	-13.918	-15.694	-36.554	1,000	100.00	-2.457	-9.658	-13.456	-15.087	-35.345
2,401	88.30	-2.126	-9.899	-14.024	-15.787	-36.738	2,401	88.30	-1.995	-9.765	-13.744	-15.507	-36.176
5,003	73.20	-2.218	-10.407	-14.613	-16.354	-37.857	5,003	73.30	-2.083	-10.281	-14.467	-16.205	-37.558
10,006	56.20	-2.202	-11.165	-15.334	-17.047	-39.216	1,0006	56.30	-2.179	-11.142	-15.305	-17.015	-39.153
20,013	40.20	-2.393	-11.962	-16.129	-17.815	-40.716	2,0013	40.30	-2.418	-11.986	-16.151	-17.837	-40.760
50,034	27.00	-2.712	-12.703	-16.880	-18.548	-42.142	5,0034	27.00	-2.922	-12.900	-17.079	-18.748	-42.542
W4 THC Abstraction													
TF4							BF4						
Time (yrs)	Temp (°C)	CO ₂	HF	HCl	HNO ₃	N ₂ O ₅	Time (yrs)	Temp (°C)	CO ₂	HF	HCl	HNO ₃	N ₂ O ₅
10	52.50	-2.401	-11.496	-16.382	-17.620	-40.354	10	51.30	-2.351	-11.500	-16.381	-17.618	-40.348
51	91.90	-2.534	-10.287	-15.200	-16.505	-38.175	51	86.201	-2.061	-9.999	-14.962	-16.257	-37.674
100	96.10	-2.718	-9.977	-15.172	-16.484	-38.136	100	111.00	-2.825	-9.602	-12.926	-14.262	-33.699
150	96.00	-2.516	-9.833	-14.898	-16.209	-37.586	150	110.00	-2.493	-9.468	-13.469	-13.935	-33.043
250	95.50	-2.405	-9.703	-14.566	-15.855	-36.878	250	109.00	-2.393	-9.445	-13.453	-14.440	-34.053
350	95.70	-2.580	-9.651	-14.141	-15.434	-36.035	350	108.00	-2.583	-9.567	-13.589	-14.747	-34.668
500	95.90	-3.051	-9.715	-13.725	-15.024	-35.217	500	106.00	-3.102	-9.887	-14.033	-15.206	-35.585
750	95.70	-2.861	-9.982	-14.696	-16.006	-37.179	750	103.00	-3.056	-9.953	-14.354	-15.546	-36.263

Table 6.7-30. Log Fugacities of Five Acid-Gas Species in the Drift Wall as Functions of Time in Repository History (Continued)

W4 THC Abstraction													
TF4							BF4						
Time (yrs)	Temp (°C)	CO ₂	HF	HCl	HNO ₃	N ₂ O ₅	Time (yrs)	Temp (°C)	CO ₂	HF	HCl	HNO ₃	N ₂ O ₅
1,000	94.60	-2.481	-9.890	-14.753	-16.062	-37.291	1,000	100.00	-2.542	-9.765	-14.304	-15.524	-36.219
2,401	88.30	-2.107	-9.888	-14.786	-16.084	-37.330	2,401	88.30	-1.985	-9.762	-14.486	-15.780	-36.723
5,003	73.20	-2.117	-10.344	-15.339	-16.610	-38.369	5,003	73.30	-1.992	-10.239	-15.188	-16.460	-38.069
10,006	56.20	-2.002	-11.105	-16.003	-17.247	-39.616	10,006	56.30	-1.983	-11.092	-15.971	-17.215	-39.552
20,013	40.20	-2.080	-11.876	-16.735	-17.954	-40.993	20,013	40.30	-2.085	-11.891	-16.736	-17.956	-40.997
50,034	27.00	-2.391	-12.679	-17.519	-18.720	-42.485	50,034	27.00	-2.521	-12.802	-17.645	-18.846	-42.738
W5 THC Abstraction													
TF4							BF4						
Time (yrs)	Temp (°C)	CO ₂	HF	HCl	HNO ₃	N ₂ O ₅	Time (yrs)	Temp (°C)	CO ₂	HF	HCl	HNO ₃	N ₂ O ₅
10	52.50	-2.565	-11.526	-16.460	-17.814	-40.743	10	51.30	-2.522	-11.546	-16.470	-17.822	-40.756
51	91.80	-2.811	-10.367	-15.299	-16.719	-38.603	51	86.10	-2.288	-10.098	-15.073	-16.483	-38.126
100	96.10	-3.024	-10.068	-15.321	-16.748	-38.664	100	111.00	-3.133	-9.750	-13.166	-14.619	-34.411
150	96.00	-2.833	-9.949	-15.090	-16.517	-38.202	150	110.00	-2.818	-9.626	-13.803	-14.352	-33.878
250	95.50	-2.761	-9.819	-14.787	-16.184	-37.537	250	109.00	-2.772	-9.625	-13.928	-14.833	-34.839
350	95.70	-3.021	-9.811	-14.364	-15.770	-36.707	350	108.00	-3.046	-9.789	-13.951	-15.158	-35.490
500	95.90	-3.264	-9.813	-14.010	-15.421	-36.010	500	106.00	-3.526	-10.092	-14.365	-15.609	-36.390
750	95.70	-2.760	-9.965	-14.845	-16.268	-37.704	750	103.00	-2.915	-9.874	-14.487	-15.757	-36.685
1,000	94.60	-2.428	-9.864	-14.858	-16.281	-37.729	1,000	100.00	-2.495	-9.678	-14.425	-15.736	-36.643
2,401	88.30	-2.112	-9.891	-14.877	-16.290	-37.744	2,401	88.30	-2.006	-9.772	-14.426	-15.828	-36.818
5,003	73.20	-2.171	-10.373	-15.471	-16.859	-38.867	5,003	73.30	-2.016	-10.248	-15.286	-16.674	-38.495
10,006	56.20	-2.125	-11.115	-16.155	-17.515	-40.151	10,006	56.30	-2.098	-11.097	-16.112	-17.471	-40.065
20,013	40.20	-2.249	-11.881	-16.898	-18.234	-41.553	20,013	40.30	-2.251	-11.896	-16.897	-18.232	-41.550
50,034	27.00	-2.596	-12.690	-17.698	-19.016	-43.076	50,034	27.00	-2.725	-12.813	-17.824	-19.142	-43.329

Table 6.7-30. Log Fugacities of Five Acid-Gas Species in the Drift Wall as Functions of Time in Repository History (Continued)

W6 THC Abstraction													
TF4							BF4						
Time (yrs)	Temp (°C)	CO ₂	HF	HCl	HNO ₃	N ₂ O ₅	Time (yrs)	Temp (°C)	CO ₂	HF	HCl	HNO ₃	N ₂ O ₅
10	52.50	-2.424	-11.384	-16.257	-16.835	-38.785	10	51.30	-2.389	-11.404	-16.277	-16.853	-38.818
51	91.80	-2.591	-10.293	-15.080	-15.725	-36.615	51	86.00	-1.942	-9.898	-14.745	-15.379	-35.919
100	96.10	-2.850	-9.982	-15.210	-15.862	-36.892	100	111.00	-2.962	-9.650	-13.051	-13.727	-32.628
150	95.80	-2.707	-9.864	-14.948	-15.599	-36.367	150	110.00	-2.733	-9.564	-13.750	-14.064	-33.302
250	95.30	-2.783	-9.929	-14.871	-15.516	-36.200	250	109.00	-2.768	-9.608	-14.279	-14.696	-34.565
350	95.60	-3.063	-9.933	-14.465	-15.111	-35.389	350	108.00	-3.098	-9.798	-14.425	-14.200	-33.574
500	95.90	-3.390	-9.993	-14.193	-14.840	-34.849	500	106.00	-3.650	-10.136	-14.606	-14.987	-35.148
750	95.60	-2.724	-9.936	-14.788	-15.436	-36.040	750	103.00	-2.948	-9.869	-14.467	-14.979	-35.129
1,000	94.50	-2.453	-9.872	-14.837	-15.484	-36.136	1,000	100.00	-2.525	-9.690	-14.430	-14.985	-35.140
2,401	88.30	-2.131	-9.903	-14.844	-15.482	-36.127	2,401	88.30	-2.041	-9.790	-14.211	-14.846	-34.856
5,003	73.20	-2.235	-10.411	-15.481	-16.093	-37.334	5,003	73.30	-2.051	-10.266	-15.272	-15.883	-36.914
10,006	56.20	-2.222	-11.075	-16.136	-16.720	-38.561	10,006	56.30	-2.191	-11.058	-16.090	-16.674	-38.470
20,013	40.20	-2.413	-11.867	-16.916	-17.477	-40.039	20,013	40.30	-2.414	-11.892	-16.842	-17.395	-39.876
50,034	27.00	-2.672	-12.615	-17.656	-18.197	-41.440	50,034	27.00	-2.790	-12.729	-17.771	-18.313	-41.671
W7 THC Abstraction													
TF4							BF4						
Time (yrs)	Temp (°C)	CO ₂	HF	HCl	HNO ₃	N ₂ O ₅	Time (yrs)	Temp (°C)	CO ₂	HF	HCl	HNO ₃	N ₂ O ₅
10	52.50	-2.428	-11.438	-15.885	-17.279	-39.673	10	51.30	-2.415	-11.487	-15.924	-17.314	-39.740
51	92.00	-2.670	-10.187	-14.649	-16.107	-37.380	51	86.20	-2.309	-10.104	-14.616	-16.064	-37.290
100	96.10	-2.921	-10.009	-14.830	-16.298	-37.764	100	111.00	-3.030	-9.692	-12.586	-14.075	-33.325
150	96.00	-2.740	-9.863	-14.547	-16.012	-37.193	150	110.00	-2.715	-9.564	-13.049	-13.738	-32.649
250	95.50	-2.668	-9.709	-14.097	-15.542	-36.252	250	109.00	-2.673	-9.572	-13.164	-14.235	-33.644
350	95.70	-2.912	-9.755	-13.622	-15.068	-35.303	350	108.00	-2.942	-9.736	-13.320	-14.590	-34.354
500	95.90	-3.326	-9.915	-13.271	-14.720	-34.607	500	106.00	-3.474	-10.056	-13.779	-15.082	-35.337
750	95.70	-2.790	-9.946	-14.290	-15.755	-36.677	750	103.00	-2.935	-9.878	-13.920	-15.245	-35.661
1,000	94.60	-2.443	-9.870	-14.359	-15.825	-36.817	1,000	100.00	-2.499	-9.699	-13.847	-15.212	-35.595
2,401	88.30	-2.121	-9.896	-14.437	-15.889	-36.942	2,401	88.30	-2.014	-9.777	-14.237	-15.692	-36.547

Table 6.7-30. Log Fugacities of Five Acid-Gas Species in the Drift Wall as Functions of Time in Repository History (Continued)

W7 THC Abstraction													
TF4							BF4						
Time (yrs)	Temp (°C)	CO ₂	HF	HCl	HNO ₃	N ₂ O ₅	Time (yrs)	Temp (°C)	CO ₂	HF	HCl	HNO ₃	N ₂ O ₅
5,003	73.20	-2.171	-10.379	-15.005	-16.433	-38.013	5,003	73.30	-2.047	-10.260	-14.865	-16.291	-37.730
10,006	56.20	-2.115	-11.127	-15.691	-17.089	-39.300	10,006	56.30	-2.090	-11.103	-15.656	-17.056	-39.235
20,013	40.20	-2.227	-11.891	-16.438	-17.812	-40.710	20,013	40.30	-2.238	-11.906	-16.445	-17.822	-40.729
50,034	27.00	-2.524	-12.672	-17.209	-18.564	-42.173	50,034	27.00	-2.689	-12.826	-17.366	-18.722	-42.490

Source: DTN: MO0303MWDSCMAB.000 [DIRS 162551].

Aqueous salt solutions with the necessary components (e.g., H^+ and Cl^- , to generate HCl) react to come to equilibrium with a coexisting vapor phase. Acid–gas volatiles may be produced or consumed in this process. The equilibrium for the reaction (here written as the dissolution reaction, for consistency with EQ3/6 convention):



is described by the mass action equation:

$$\log K_{HCl} = \log a_{H^+} + \log a_{Cl^-} - \log f_{HCl} \quad (\text{Eq. 6.7.2.14.1-8})$$

Another way of writing this is that:

$$\log f_{HCl} = -\log K_{HCl} - pH + \log a_{Cl^-} \quad (\text{Eq. 6.7.2.14.1-9})$$

Since a chloride-bearing solution has some pH, an equilibrium fugacity is defined for the given fluid composition. Fugacities of common gases, including acid–gas volatiles, are in fact routinely computed in EQ3/6 calculations.

Normally an equilibrium involving a gas species at two distinct locations would be established by comparing the fugacities or partial pressures (in the following discussion, the differences between fugacities and partial pressures are ignored). If the pressure of the gas at both locations is the same, then an equilibrium exists and there is no thermodynamic driving force to move the gas from one location to the other. However, that is true only in the isothermal case. If a temperature difference exists, then one must compare chemical potentials. The chemical potential of the i -th gas species at absolute temperature T is given by (Equation 4.1.25-3):

$$\mu_i(T) = \mu_i^o(T) + RT \ln p_i \quad (\text{Eq. 6.7.2.14.1-10})$$

where $\mu_i^o(T)$ is the standard state chemical potential at temperature T , R is the gas constant (8.3143 J/K-mol; Table 3, from Weast and Astle 1981 [DIRS 100833], p. F-96), and p_i is the partial pressure of the gas. For an equilibrium between two locations (1 and 2) with respective temperatures (T_1 and T_2), the chemical potentials must be the same. Hence:

$$\mu_i^o(T_2) + RT_2 \ln p_{i,2} = \mu_i^o(T_1) + RT_1 \ln p_{i,1} \quad (\text{Eq. 6.7.2.14.1-11})$$

where $p_{i,1}$ is the pressure of the i -th gas at the location 1 and $p_{i,2}$ is the corresponding pressure at location 2. Rearranging yields:

$$T_2 \ln p_{i,2} - T_1 \ln p_{i,1} = \frac{(\mu_i^o(T_1) - \mu_i^o(T_2))}{R} \quad (\text{Eq. 6.7.2.14.1-12})$$

Less symmetrically, this can be written as:

$$\ln p_{i,2} = \frac{T_1}{T_2} \ln p_{i,1} + \frac{(\mu_i^o(T_1) - \mu_i^o(T_2))}{RT_2} \quad (\text{Eq. 6.7.2.14.1-13})$$

In the present example, location 1 might be at the drift wall and location 2 might be either the surface of the drip shield or that of the waste package outer barrier. If the pressure of a gas species can be constrained at one location, the equilibrium value of the pressure at another location can then be calculated. The applicability of this equilibrium requires that transport of the gas between the two locations be rapid. Given the distances between the drift wall, the drip shield, and the waste package outer barrier, and the facts that backfill is not present and that convection and diffusion in the gas phase are relatively fast processes, the applicability is justified.

Making such calculations requires that the standard state chemical potential of a gas be known as a function of temperature. There is potentially more than one way to define this; however, only the difference expressed in Equations 6.7.2.14.1-11, 6.7.2.14.1-12, and 6.7.2.14.1-13 matters. A reasonable choice is to use the apparent Gibbs energy of formation (apparent $\Delta G_{f,i}^o$), which is equivalent to the actual Gibbs energy of formation at 298.15K at 1 bar pressure (actually any pressure for a gas species). At higher temperature, the apparent Gibbs energy of formation is equal to the value at 298.15K plus the difference in the Gibbs energy of the chemical species in question at the actual temperature and that at 298.15K. Helgeson et al. (1978 [DIRS 101596], pp. 28 and 29) provide a more detailed discussion of this concept.

Values of the apparent standard molar Gibbs energies for HF, HCl, HBr, HNO₃, and N₂O₅ gases are calculated from the data summarized in Tables 4.1-11 and 4.1-12 using Equation 4.1.24-5, which allows calculation of the apparent Gibbs energy as a function of temperature. The results are summarized in Table 6.7-31 (here presented in five-degree temperature increments; results in one-degree increments are also included in *Gases_j_AppDelGof_1_TJW.xls* in output DTN: LL030500812251.061). It can be seen from the table that the apparent Gibbs energy of each of the five gas species decreases with increasing temperature.

Consider the case of HCl, in which the temperature at the drift wall (T_1) is 90°C (363.15K) and that on a metal barrier surface (T_2) is 100°C (373.15K). The respective values of the standard chemical potential from the above table are -107,634.1 J/mol and -109,564.4 J/mol, respectively. The difference is 1,930.3 J/mol. The second term on the right hand side of Equation 6.2.7.14.1-13 then evaluates to $1,930.3/(8.3143 \times 373.15) = 0.622$. Assuming that the partial pressure at the drift wall is 10^{-14} bar (roughly consistent with many of the data in Table 6.7-30) then $\ln p_1 = -32.236$. Then $\ln p_2 = (363.15/373.15)(-32.236) + 0.622 = -31.372 + 0.622 = -30.750$. Hence $p_2 = 4.420 \times 10^{-14}$ bar. This value is 4.420 times that for p_1 , but is within an order of magnitude. This calculation illustrates that because of the temperature difference, a somewhat higher partial pressure of an acid-gas volatile at a metal barrier surface would be in effective equilibrium with a somewhat smaller partial pressure at the drift wall. A still higher pressure at the metal barrier surface would drive transport to the drift wall. Therefore, one may conclude that effective partial pressures of acid-gas volatiles on the metal barrier surfaces cannot be significantly greater than those on the drift wall, assuming that there is

good physical communication between the two locations. Therefore, the data in Table 6.7-30 (or data of this type for similar THC calculations) provide an important constraint on the chemical environment of the drip shield and waste package outer barrier.

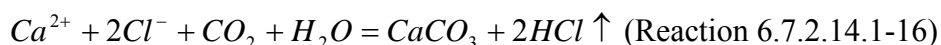
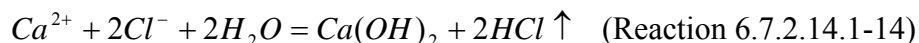
Table 6.7-31. The Apparent Standard Gibbs Energy of Formation (J/mol) of the gases HF, HCl, HBr, HNO₃, and N₂O₅ as a Function of Temperature

Temp. (°C)	Apparent ΔG_f° (J/mol)				
	HF	HCl	HBr	HNO ₃	N ₂ O ₅
0	-270,332.0	-90,652.0	-48,513.1	-67,358.7	126,575.6
5	-271,189.4	-91,575.1	-49,495.1	-68,670.6	124,879.8
10	-272,049.5	-92,500.7	-50,479.8	-69,987.2	123,175.6
15	-272,912.2	-93,429.0	-51,467.0	-71,308.2	121,463.2
20	-273,777.3	-94,359.7	-52,456.8	-72,633.9	119,742.7
25	-274,645.0	-95,293.0	-53,449.0	-73,964.0	118,014.0
30	-275,515.1	-96,228.7	-54,443.7	-75,298.6	116,277.2
35	-276,387.6	-97,166.8	-55,440.8	-76,637.7	114,532.5
40	-277,262.5	-98,107.3	-56,440.2	-77,981.1	112,779.8
45	-278,139.7	-99,050.0	-57,442.0	-79,329.0	111,019.1
50	-279,019.2	-99,995.1	-58,446.1	-80,681.3	109,250.7
55	-279,900.9	-100,942.4	-59,452.4	-82,037.8	107,474.4
60	-280,784.9	-101,892.0	-60,461.0	-83,398.7	105,690.4
65	-281,671.1	-102,843.7	-61,471.7	-84,763.9	103,898.7
70	-282,559.4	-103,797.6	-62,484.5	-86,133.3	102,099.5
75	-283,449.8	-104,753.6	-63,499.5	-87,506.9	100,292.6
80	-284,342.3	-105,711.7	-64,516.6	-88,884.7	98,478.3
85	-285,236.9	-106,671.9	-65,535.8	-90,266.7	96,656.5
90	-286,133.6	-107,634.1	-66,556.9	-91,652.9	94,827.3
95	-287,032.2	-108,598.3	-67,580.1	-93,043.2	92,990.8
100	-287,932.8	-109,564.4	-68,605.3	-94,437.5	91,147.0
105	-288,835.4	-110,532.6	-69,632.4	-95,836.0	89,296.0
110	-289,739.9	-111,502.6	-70,661.4	-97,238.4	87,437.9
115	-290,646.2	-112,474.6	-71,692.4	-98,644.9	85,572.6
120	-291,554.5	-113,448.4	-72,725.2	-100,055.4	83,700.2
125	-292,464.6	-114,424.1	-73,759.9	-101,469.8	81,820.9
130	-293,376.6	-115,401.6	-74,796.4	-102,888.2	79,934.6
135	-294,290.4	-116,381.0	-75,834.7	-104,310.5	78,041.4
140	-295,205.9	-117,362.1	-76,874.8	-105,736.7	76,141.3
145	-296,123.2	-118,345.0	-77,916.6	-107,166.8	74,234.4
150	-297,042.3	-119,329.6	-78,960.2	-108,600.8	72,320.8
155	-297,963.1	-120,315.9	-80,005.6	-110,038.5	70,400.5
160	-298,885.5	-121,304.0	-81,052.6	-111,480.1	68,473.5
165	-299,809.7	-122,293.7	-82,101.4	-112,925.5	66,539.9
170	-300,735.5	-123,285.1	-83,151.8	-114,374.6	64,599.7
175	-301,663.0	-124,278.2	-84,203.8	-115,827.5	62,653.0
180	-302,592.1	-125,272.9	-85,257.5	-117,284.1	60,699.8
185	-303,522.8	-126,269.2	-86,312.8	-118,744.4	58,740.2
190	-304,455.1	-127,267.1	-87,369.7	-120,208.4	56,774.3
195	-305,389.0	-128,266.6	-88,428.2	-121,676.1	54,801.9
200	-306,324.4	-129,267.6	-89,488.3	-123,147.4	52,823.3

Source: Ouput DTN: LL030500812251.061, Gases_j_AppDelGof_1_TJW.xls.

NOTE: The spreadsheet also contains these data in one-degree increments.

If acid–gas volatiles evolved from hot salt solutions condense in a tight locus on or over a metal barrier surface, the resulting acidic solution could pose a problem to the performance of that metal barrier. It is assumed in this report that they will instead be dispersed to the drift wall, and either diffuse or advect into it or be neutralized by reaction with the rock. If there is not such a condensation problem, the evolution of acid–gas volatiles may have significantly beneficial effects on the chemical environment on the metal barrier surfaces. Potential highly concentrated calcium chloride solutions (as might be formed by any means, but evaporation of seepage water seems to offer the greatest potential for this possibility) may be effectively unstable owing to reactions such as:



Little is known about the solid CaOHCl, though it apparently exists (e.g., Lutz et al. 1993 [DIRS 163487]; Allal 1997 [DIRS 162579]). The magnesium analogue, in contrast, is quite well known (its thermodynamic properties are listed in Barin and Platzki (1995 [DIRS 157865], p. 1,017). Note that similar reactions could also occur involving HF, HBr, HNO₃, and N₂O₅ in place of HCl, as expected.

Recent experimental evidence indicates that such reactions impose a real limit on potential calcium chloride brine formation on the metal barrier surfaces. This is discussed in the following subsection.

6.7.2.14.2 Thermogravimetric Thin Aqueous Film Studies of Calcium Chloride Solutions at Elevated Temperature

The experiment described here was originally designed to examine the extent of reaction of Alloy 22 with a thin film of concentrated aqueous calcium chloride (CaCl₂). Thin aqueous film corrosion processes can produce changes in the aqueous film chemistry that significantly affect the extent of corrosion reactions. At cathodic sites, oxygen reduction to hydroxyl ions can elevate the local pH, and at anodic sites dissolved metal hydrolysis can lower the pH. Electrolyte migration occurs to maintain electrical neutrality. These changes in solution chemistry can result in precipitation reactions and acid–gas generation. Precipitation of insoluble species is reported for example in the atmospheric corrosion of zinc (Falk et al. 1998 [DIRS 163489]; Lindstrom et al. 2002 [DIRS 163488]). These electrochemical processes were observed in the cited zinc corrosion studies to ultimately limit the extent of corrosion for a given amount of aqueous salt film.

Alloy 22 specimens with nominal dimensions 51 mm × 13 mm × 1.5 mm were polished to a mirror finish, with a final polish using 1µm Al₂O₃. A dilute calcium chloride solution was prepared by dissolving 5g CaCl₂-dihydrate (reagent grade, Mallinckrodt) in 500mL deionized water. The calcium chloride solution was sprayed into a coating chamber as an aerosol for uniform specimen coating. Specimens were coated with a thin CaCl₂ film as follows. Specimens were first warmed for 10 seconds with a heat gun; specimen preheating and

subsequent heating or drying between coating steps was necessary in order to achieve a uniform coating. Heated specimens were introduced into the coating chamber for approximately 2 seconds, then removed and dried with the heat gun; this process was repeated until the desired coating was achieved. Specimens were weighed before salt deposition, and periodically during the coating process to determine how much salt had been deposited. A final mass of $3.0 \text{ mg} \pm 0.2 \text{ mg}$ of CaCl_2 was ultimately deposited on the surface of each specimen.

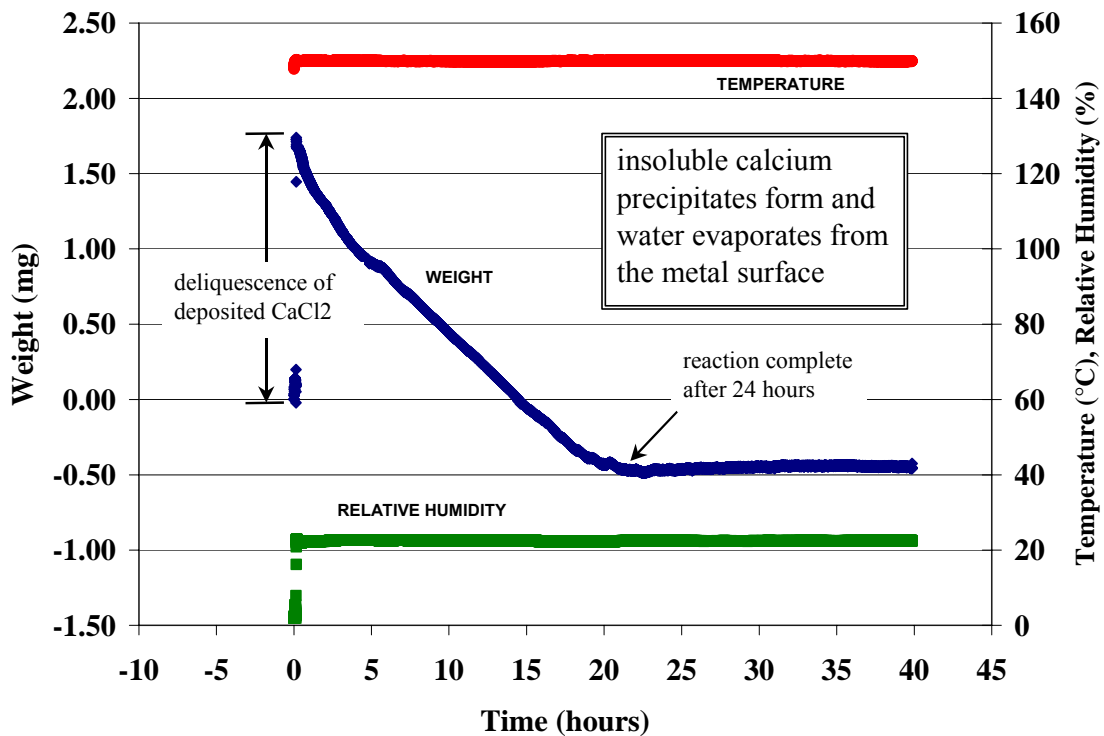
A Cahn TG-100 thermogravimetric analyzer (TGA) was modified such that the sample chamber would be capable of achieving stable temperature and relative humidity conditions. The sample chamber is unpressurized and separated from the external environment in part by the use of a transparent plastic curtain. Uncertainty in temperature is $\pm 0.2^\circ\text{C}$; uncertainty in RH is ± 3 percent. Environmental conditions for the tests discussed were 22.5 percent RH and 150°C , 125°C , and 100°C . The reactant gas was a continuous flow of purified humidified laboratory air; the microbalance housing was purged with ultra high purity helium (He) gas. The flow rate is specified by the source of these data. Humidity was achieved and controlled by varying the ratios of dry air and air that was bubbled through a heated water column. Temperature and RH were measured continuously using sensors that were situated within the sample chamber. Specimen mass was recorded as a function of time via the TGA microbalance, which is sensitive to changes of $\pm 1\mu\text{g}$, with an average noise resolution of $\pm 5\mu\text{g}$.

Immediately following the coating process, specimens were introduced into the TGA sample chamber and allowed to equilibrate at the desired temperature and a very low relative humidity (nominally 2 percent RH). After an equilibration period of 10 to 15 minutes, the balance was tared and the relative humidity in the sample chamber was increased to the desired set point. As a function of time, the specimen weight was recorded and physical changes on the surface monitored visually.

Various methods of analysis were performed on posttest specimens in an attempt to characterize the reaction products. Raman spectroscopy was performed on precipitate species using an HR800 spectrograph with a 633 nm HeNe laser. Scanning electron microscopy and X-ray elemental mapping were performed using a JEOL-JXA8600 electron probe micro analyzer.

The reaction of CaCl_2 on the surface of Alloy 22 at 150°C and 22.5 percent RH is displayed gravimetrically as a function of time in Figure 6.7-35. An increase in specimen weight was observed as the RH was increased to above the deliquescence point of CaCl_2 . After approximately 30 minutes in a constant temperature and RH environment, the initial solid salt coating formed a visible thin aqueous film on the surface of the specimen. Subsequent reaction progress was monitored as a function of specimen weight change. Insoluble crystalline precipitates were observed to form on the specimen surface, which in turn became gradually drier as the nondeliquescent crystals allowed water to evaporate from the surface. This process was observed gravimetrically as a steady weight loss. After sufficient time (approximately 24 hours), the specimen surface appeared completely dry and covered uniformly with crystalline precipitates, and no further weight change was observed. Figure 6.7-36 shows before and after pictures of a typical metal coupon. These are from a repetition of the original experiment and are associated with a slightly different reported RH (19 percent versus 22.5 percent).

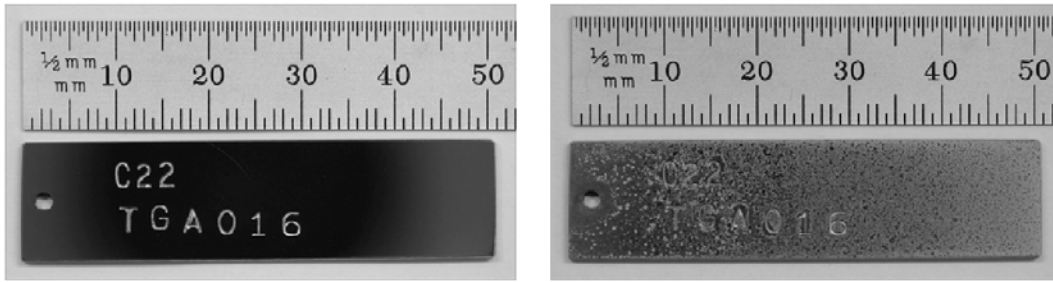
Temperature effects on the reaction rate of CaCl_2 on the surface of Alloy 22 at a constant relative humidity of 22.5 percent are illustrated in Figure 6.7-37. At 100°C there was no observable change in weight following the initial increase due to deliquescence, and the specimen surface remained wet and visually unchanged throughout the test. At 125°C a very subtle yet steady weight loss was observed for more than 600 hours (not shown to test completion in the figure). During this time, the specimen surface was observed to slowly lose water, although precipitate formation was not as pronounced as at higher temperatures. At 150°C a sharp decline in weight was observed following initial deliquescence, and reaction completion was reached in approximately 24 hours (as noted previously).



Source: DTN: LL030308812251.017 [DIRS 163775].

NOTE: The weight is a signal that tracks weight change. The numbers on the scale on the left side of this figure have no absolute meaning.

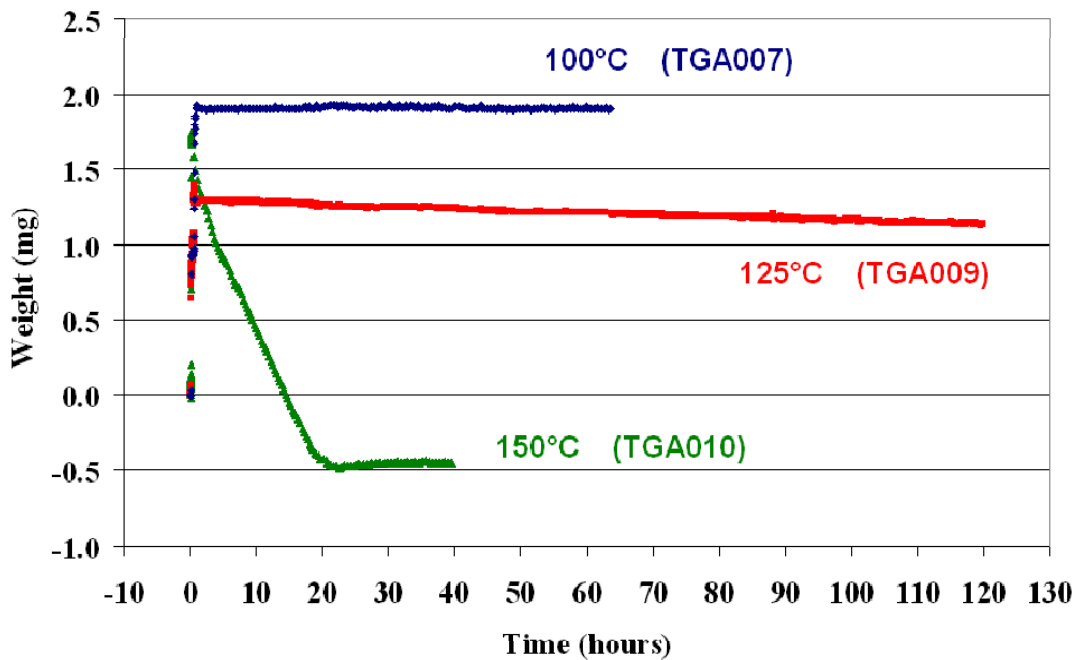
Figure 6.7-35. Weight Change Curve for a Typical Test at 150°C and 22.5 Percent RH for Alloy 22



Source: DTN: LL030309012251.018 [DIRS 163774].

NOTE: Reaction was complete at approximately 24 hours.

Figure 6.7-36. Images of Alloy 22 Specimen (ID#TGA016) Before (left) and After (right) Reaction With a Thin Aqueous Layer of Calcium Chloride at 150°C and 19 Percent RH for Approximately 40 Hours



Source: DTN: LL030308812251.017 [DIRS 163775].

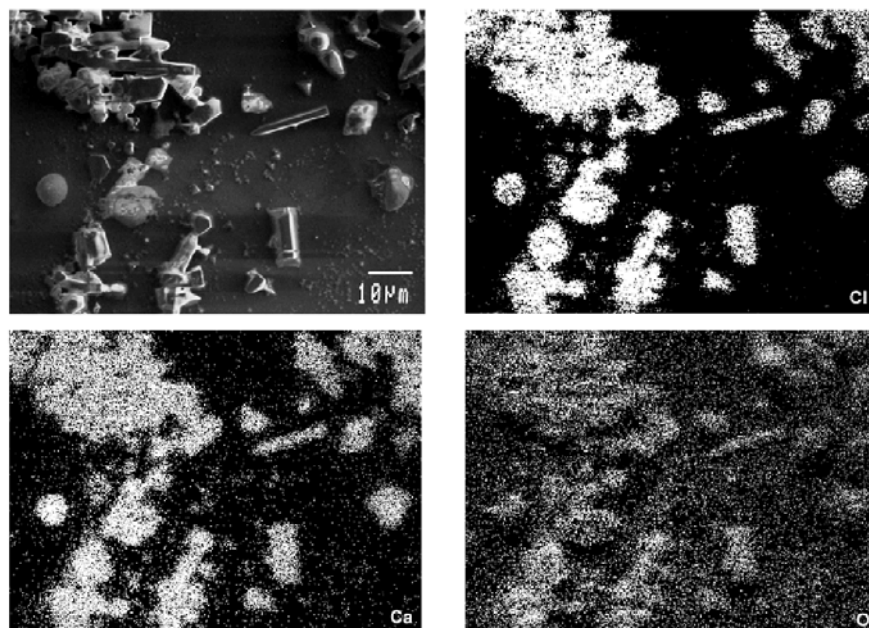
NOTES: The weight is a signal that tracks weight change. The numbers on the scale on the left side of this figure have no absolute meaning.

Variations in water mass absorbed through deliquescence are most likely due to slightly differing amounts of salt deposited during the coating process.

Figure 6.7-37. Comparison of Weight Changes of Alloy 22 Specimens Coated With a Thin Film of Calcium Chloride and Subjected to a 22.5 Percent RH Environment at the Various Temperatures Shown

Post test electron probe microanalysis and x-ray elemental mapping were performed on the Alloy 22 sample that had been in the 150°C, 22.5 percent RH environment. Figure 6.7-38 shows the elemental distribution of chloride, calcium, and oxygen relative to a secondary electron image. The chloride, calcium, and oxygen distributions indicate a uniform precipitate composition with respect to these three elements. No other elements were detected within the precipitates.

Lack of metal ion incorporation in the precipitates suggests that the primary reaction responsible for the gravimetric changes is not an electrochemical one, and may thus be independent of the substrate. Various substrates were, therefore, tested in conditions identical to the Alloy 22 experiment at 150°C and 22.5 percent RH in order to probe the nature of the CaCl_2 -substrate interaction. In addition to Alloy 22, substrate specimens of platinum and glass were tested. The tests with these other substrates were performed for reference only. The gravimetric reaction progress for calcium chloride films on the surface of these three different substrates was essentially the same in all cases, allowing for variances in weight loss slopes and final overall mass losses are likely due to minor differences in coating uniformity.



Source: DTN: LL030309012251.018 [DIRS 163774].

NOTE: Formed on the surface of an Alloy 22 specimen (ID#TGA010) after reaction with an aqueous calcium chloride film at 150°C and 22.5 percent RH for approximately 40 hours (reaction was complete at approximately 24 hours).

Figure 6.7-38. Scanning Electron Microscopy (top left) and Energy Dispersive X-ray Spectroscopy Elemental Mapping (Cl, top right; Ca, bottom left; and O, bottom right) of Precipitate Constituents

Raman spectroscopy confirmed the presence of identical crystalline precipitates on the Alloy 22, glass, and platinum substrates. The Raman spectra for these precipitates are not consistent with either $\text{Ca}(\text{OH})_2$ or CaCO_3 (CaCl_2 is not Raman active). As noted above, these precipitates contain calcium, oxygen, and chloride. The existence of CaOHCl is noted in the literature (Lutz et al. 1993 [DIRS 163487]; Allal et al. 1997 [DIRS 162579]), though information on this or related species is scarce.

At high temperatures (150°C), thin aqueous calcium chloride films undergo precipitation reactions that ultimately serve to limit the extent of reaction with the substrates with which they are in contact. These reactions appear to be coupled with the loss of chloride as HCl gas to the gas stream used in the experiments, which flows through in a single pass mode. In a constant temperature and relative humidity environment, the soluble calcium chloride is converted to insoluble calcium-, chloride-, and oxygen-containing precipitates, and water is free to evaporate from the aqueous layer in a self-limiting process. This reaction is shown to be temperature dependent, and accounts for the majority of gravimetric change seen on Alloy 22, glass, and platinum substrates at high temperatures. No evidence of corrosion was observed in the experiments using Alloy 22.

There is thus experimental evidence that acid-gas volatility limits the possible formation of calcium chloride brines. This was readily demonstrated at 150°C and 125°C , but not at 100°C . The mechanism may be active at or below 100°C , but if so these experiments did not demonstrate it.

6.7.2.14.3 EQ3/6 Calculations of the Evaporation to Near Dryness of a Dilute Calcium Chloride Solution, Subject to Fixed Fugacities of CO_2 and HCl

A number of EQ3/6 calculations are made to determine what thermodynamic data indicate in regard to the experimental observations. The method employed is to evaporate a very dilute calcium chloride solution to near-dryness at specified CO_2 and HCl fugacities. To obtain a useful reference, some runs are first made with the HCl fugacity not fixed. This treats an open system. Water and CO_2 are treated as volatile (can move between the aqueous solution and a gas phase), but HCl is treated as nonvolatile. Consequently, the equilibrium HCl fugacity of the fluid can rise as a result of increasing chloride in solution. The fixed CO_2 pressure may act to bring CO_2 into solution and (after reaction with water) provide a source of hydrogen ions, which would also act to increase the equilibrium HCl fugacity. Some results for these reference runs are shown in Table 6.7-32. Basically, all of these runs produce concentrated CaCl_2 as expected (the small amount of calcite precipitated does not significantly change the stoichiometric balance between Ca and Cl). There is a strong temperature effect on the calculated HCl fugacities. These values are also notably higher than those for THC-calculated seepage waters as tabulated in Table 6.7-30. This suggests that imposing reasonable values on the HCl fugacity could lead to significant effects.

Table 6.7-32. Calculated Log Fugacities for HCl, RH Percent Values, and Ca and Cl Molalities Obtained in EQ3/6 Calculations of the Evaporation to Near-Dryness of Dilute CaCl₂ Solution

Temperature (°C)	Log Fugacity CO ₂	Log Fugacity HCl	RH%	Ca Molality	Cl Molality	Minerals Formed	EQ3/6 Output File
0	-3.5	-11.265	34.32	6.216	12.422	antarctite, calcite	<i>ecc000p_.6o</i>
25	-3.5	-9.712	28.16	7.612	15.217	antarctite, calcite	<i>ecc025p_.6o</i>
25	-3.0	-9.461	28.15	7.619	15.225	antarctite, calcite	<i>ecc0253_.6o</i>
90	-4.0	-7.205	18.92	13.384	26.757	CaCl ₂ ·2H ₂ O, calcite	<i>ecc0904_.6o</i>

Source: Output DTN: LL030500812251.061, files *ecc*__.6o* (as indicated above).

NOTE: HCl fugacities not fixed.

Table 6.7-33 shows the effect of imposing fixed fugacities of CO₂ and HCl on the evaporation of dilute calcium chloride solution at 90°C and 150°C. Now HCl is treated as volatile along with water and CO₂. Note that the range of values for the log CO₂ fugacity is reasonable for these temperatures (though some rather low values of -10 and -12 are included). The range of imposed HCl fugacities is generally on the high side of expected values for seepage waters (e.g., the values given in Table 6.7-30), even allowing for temperature differences between the metal barrier surfaces and the drift wall. These results indicate that limits on the HCl partial pressure (imposed by conditions at or near the drift wall, or in the rock beyond) can markedly reduce the concentrations of the final solutions near complete dryout.

 Table 6.7-33. Calculated RH Percent Values and Ca and Cl Molalities Obtained in EQ3/6 Calculations of the Evaporation to Near-Dryness of Dilute CaCl₂ Solution at Fixed Log Fugacities of CO₂ and HCl

Temperature (°C)	Log Fugacity CO ₂	Log Fugacity HCl	RH%	Ca Molality	Cl Molality	Minerals Formed	EQ3/6 Output File
90	-3.0	-10.0	92.93	1.274	2.547	calcite	<i>ecc0903a.6o</i>
90	-4.0	-8.0	39.67	7.170	14.335	calcite	<i>ecc09038.6o</i>
90	-4.0	-10.0	86.56	2.070	4.140	calcite	<i>ecc0904a.6o</i>
90	-4.0	-12.0	99.45	0.122	0.243	calcite	<i>ecc0904c.6o</i>
90	-4.0	-14.0	99.98	0.00332	0.00652	calcite	<i>ecc0904e.6o</i>
90	-5.0	-10.0	77.53	3.025	6.047	calcite	<i>ecc0905a.6o</i>
90	-6.0	-10.0	66.17	4.151	8.290	calcite	<i>ecc0906a.6o</i>
150	-6.0	-8.0	56.59	6.304	12.174	calcite	<i>ecc15068.6o</i>
150	-6.0	-10.0	96.45	0.777	1.518	calcite	<i>ecc1506a.6o</i>
150	-6.0	-12.0	99.89	0.0247	0.0443	calcite	<i>ecc1506c.6o</i>
150	-6.0	-14.0	99.99	0.00234	0.00112	calcite	<i>ecc1506e.6o</i>
150	-10.0	-10.0	90.92	1.901	3.541	portlandite	<i>ecc150aa.6o</i>
150	-12.0	-12.0	99.70	0.0725	0.1201	portlandite	<i>ecc150cc.6o</i>

Source: Output DTN: LL030500812251.061, files *ECC090*.6o* and *ECC150*.6o* (as indicated above).

The point of dryout itself would be shifted in the case of the 150°C runs from what is shown in Table 6.7-33. These calculations do not account for the limit of aqueous solution existence imposed by the total pressure limit of 0.90 bar adopted in this report. At 150°C, the systems must be dry unless the relative humidity is less than about 18 percent (Figure 6.7-3). That is not the case for any of the 150°C cases included in Table 6.7-33. If the IDPS model calculations for this temperature had been modified to take the pressure limit effect into account, the final solution compositions would have been more concentrated, but less concentrated than if HCl had been treated as nonvolatile.

Transport by convection (driven by temperature differences between the metal barrier surfaces and the drift wall) and diffusion within the drift between the metal barrier surfaces and the drift wall is assumed (Section 5.7) to be sufficient to connect the hypothesized source and sink loci. No assumptions are made about transport along the drift axis, only between the metal barrier surfaces and the drift wall (in directions essentially normal to the drift axis). With sufficiently low imposed HCl fugacities, a less concentrated solution as the final result is always obtained. With somewhat higher HCl fugacities, higher CO₂ fugacities are needed to help drive HCl from the evaporating fluid. This effect is illustrated by the reaction:



Note that except for the most dilute solutions, the original stoichiometric relationship between Ca and Cl (1:2) is preserved. The thermodynamic calculations do not consider the possible formation of CaOHCl or other possible similar phases owing to a lack of representation on the supporting thermodynamic data file (*data0.ypf.R1*; DTN: SN0302T0510102.002 [DIRS 162572]).

6.7.2.15 Comments on In-Drift Precipitates/Salts Model Accuracy for the Present Analysis

Niter (KNO₃) is a key component in the analysis of deliquescence on the metal barrier surfaces. As is pointed out earlier in this report, the Pitzer interaction coefficients for KNO₃ in the present supporting thermodynamic database (*data0.ypf.R1*; (DTN: SN0302T0510102.002 [DIRS 162572])) are just the reported 25°C values. They appear to predict RH adequately up to about 50°C, at which point there are fewer data with which to compare. Another approach to evaluating the adequacy of the IDPS model is to compare calculated niter solubilities with measured values, which are more extant. Such a comparison is shown in Figure 6.7-39, which covers the range 25°C to 200°C (no pressure cutoff is imposed, and the IDPS model validation limit of 140°C is ignored here for illustrative purposes). The IDPS model calculations appear to agree reasonably well up to about 75°C. At higher temperature, the measured values (based on Linke 1965 [DIRS 166191], p. 250; Table 4.1-24) continue to increase rapidly, while the IDPS model values taper off. At 200°C, the measured value is about four times the calculated value. This is suggestive that the deliquescence RH of niter may decrease more rapidly than indicated by the IDPS model. However, the IDPS model prediction for the deliquescence RH (as shown in Figures 6.7-4 and 6.7-14) already shows a strong decrease with temperature to rather low values at higher temperature. This suggests that the deliquescence RH curve for niter might not show a major further decrease at higher temperature were the Pitzer parameterization for KNO₃ to be improved. A decrease of five or more points in the RH (expressed as a percentage) in the

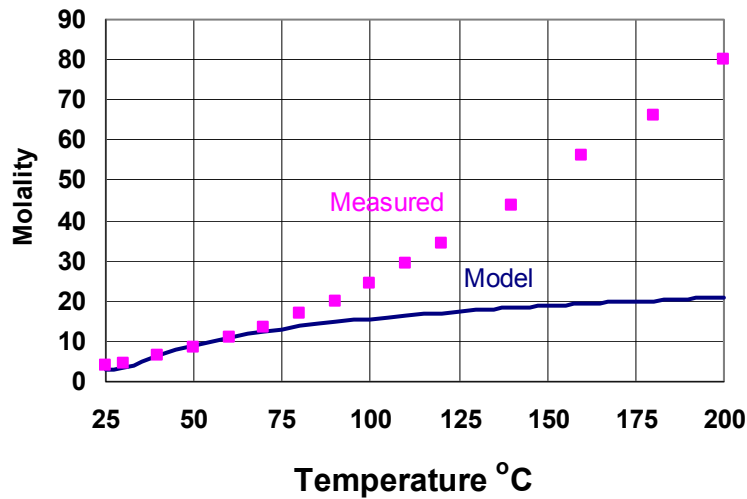
vicinity of 140°C is quite possible. However, the available data do not permit the actual uncertainty to be accurately quantified at such temperatures.

Figure 6.7-40 shows the same comparison, but for a more limited temperature range. It can be more clearly seen that the IDPS model, though based on a 25°C Pitzer parameterization, does only a fair job of predicting the solubility of niter at 25°C. The IDPS model actually does better at higher temperatures, up to about 70°C.

The effect of the IDPS model uncertainty for KNO_3 extends to those mineral assemblages in which niter is a relative strong driver (which it is only at elevated temperatures). This would be the case for NaCl-KNO_3 and to a lesser extent, $\text{NaCl-KNO}_3\text{-NaNO}_3$ (because soda niter is also a relatively strong driver at elevated temperature). There would be much less effect for the assemblage $\text{NaCl-KNO}_3\text{-NaNO}_3\text{-Ca(NO}_3)_2$ owing to the fact that the governing $\text{Ca(NO}_3)_2$ solids at elevated temperatures are extremely strong drivers.

As the results shown in Figures 6.7-39 and 6.7-40 depend on the binary system Pitzer coefficients for $\text{KNO}_3\text{-H}_2\text{O}$, one might reasonably ask if the discrepancy could not be resolved by adjusting these coefficients to make the IDPS model calculations better fit the actual solubility data. Binary system Pitzer coefficients are closely tied to activity coefficient or alternatively vapor pressure data over the whole concentration range (up to and occasionally somewhat beyond solubility limits). Solubility data in a binary system only reflect one end of this range. Attempts to fit (or adjust) binary Pitzer parameters to these data (and only these data) suffer from a significant uniqueness problem. Furthermore, any values obtained would depend strongly on the assumed Gibbs energy of the solid (or, equivalently, the equilibrium constant for the corresponding dissolution reaction). The adequacy of such fitted or adjusted data (or the lack thereof) would become apparent in modeling higher-order mixtures containing the binary system in question.

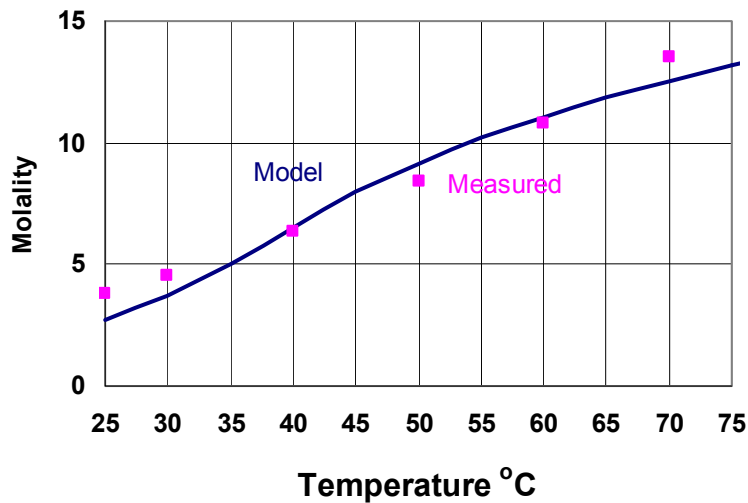
The model for calcium nitrate in the thermodynamic data file *data0.yypf.R1* (DTN: SN0302T0510102.002 [DIRS 162572]) also has some problems, as indicated by the inability to compute systems saturated with $\text{Ca(NO}_3)_2\cdot 3\text{H}_2\text{O}$ and $\text{Ca(NO}_3)_2\cdot 2\text{H}_2\text{O}$ in the appropriate temperature ranges in the calculations presented in Section 6.7.2.9.



Source: Output DTN: LL040903723121.042, *NiterSolubility.xls*.

NOTES: IDPS model results are from file *Niter.csv* in the above DTN; reported measurements are from Linke 1965 [DIRS 166191], p. 250; reported values, given in g/100g solution, are converted to molality. IDPS model results above 140°C are beyond the validation range of the model.

Figure 6.7-39. In-Drift Precipitates/Salts Model Calculations versus Reported Measurements of the Solubility (Molality) of Niter (KNO_3) from 25°C to 200°C



Source: Output DTN: LL040903723121.042, *NiterSolubility.xls*.

NOTE: IDPS model results are from file *Niter.csv* in the above DTN; reported measurements are from Linke 1965 [DIRS 166191], p. 250; reported values, given in g/100g solution, are converted to molality.

Figure 6.7-40. In-Drift Precipitates/Salts Model Calculations Versus Reported Measurements of the Solubility (Molality) of Niter (KNO_3) from 25°C to 75°C (Showing More Detail in this Region than Figure 6.7-39)

6.7.2.16 Uncertainties

The calculations made in the present report consist of two principal types, relatively simple spreadsheet calculations and thermodynamic calculations made using the EQ3/6 software with the high-temperature Pitzer supporting data file *data0.ypf.R1* (DTN: SN0302T0510102.002 [DIRS 162572]). In the case of the spreadsheet calculations, as exemplified by the calculation of the atmospheric pressure at the repository elevation (Section 6.7.2.1), the output uncertainties are negligible for the purposes of this report. Several of the spreadsheet calculations involve little more than unit conversions of handbook data that are highly accurate to begin with. In the case of the EQ3/6 calculations, the output uncertainties are more difficult to deal with. In general, these can be described as thermodynamic calculations, here employed to simulate processes including the deliquescence of salt minerals and the formation of acid-gas volatiles. The sources of output uncertainty include uncertainties in the thermodynamic data that comprise part of the thermodynamic model and uncertainties in the problem-specific inputs (including conceptual definitions such as “equilibrium applies”) to the thermodynamic calculations.

The thermodynamic calculation algorithms employed in this report do not extend to automatic estimation of output uncertainties from input uncertainties, as might be obtained by embedding simple “linear” propagation-of-errors formulas. The thermodynamic models are in effect calibrated by the choice of thermodynamic data, including standard state data and data for parameters representing deviation from thermodynamic ideality (including Pitzer interaction coefficients). Uncertainty in these fundamental underlying data tends to be highly correlated, often in a complex manner.

The need for a consistent approach is illustrated by the fact that results of consequence often depend more on the difference between the Gibbs energies of formation of two compositionally equivalent mineral assemblages (as this is what determines which assemblage is more stable) than the Gibbs energies themselves, which would be calculated from tabulated values of the Gibbs energies of the individual minerals. It is thus important for those tabulated values to be mutually consistent as well as accurate in an individual sense. Indeed, an analysis of the propagation of the individual uncertainties associated with such tabulated values (ignoring the correlation associated with consistency constraints) could easily lead to the incorrect conclusion that the uncertainty in the Gibbs energies of two mineral assemblages is too large to determine which assemblage is actually the more stable. Nordstrom and Munoz (1986 [DIRS 153965], p. 332 to 334) illustrate this principle in the case of some simple mineral assemblage transformations (they focus on enthalpy instead of Gibbs energy, but the principle is the same). This theme is repeated in still other areas. Pitzer interaction coefficients describing nonideality in aqueous electrolyte solutions also have correlated uncertainty.

Quantitative estimation of uncertainties in thermodynamics is generally limited to the treatment of experimental data in relatively simple systems. Thus, for example, uncertainties in the standard enthalpies and Gibbs energies of minerals determined by a technique such as drop calorimetry are routinely reported along with the data for these parameters. Because of the consistency issue (correlated uncertainties), standard tabulations of thermodynamic data such as those presented by Barin and Platzki (1995 [DIRS 157865]) generally give the recommended data without such associated uncertainty values. In effect, there would be no useful way to use them in calculations of error propagation for complex systems. In theory, one could develop a

description of uncertainties that includes the correlative effects. This would include far more than just a one-to-one association of an uncertainty value with each datum; it would require a complex matrix of cross-uncertainties, potentially to high order. Such an approach has yet to be developed, or at least applied other than in narrow confines. Consequently, current thermodynamic modeling codes such as EQ3/6 do not consider propagation of uncertainties, and they use supporting data files containing no uncertainty information. A different approach is, therefore, required, and one such is used by the IDPS model; this is described later in this section.

In general, the uncertainty associated with the results of thermodynamic modeling is established by validation experience (testing how well calculated results compare with reality) in laboratory, industrial, and natural (geologic, surface hydrologic, and atmospheric) systems. In this respect, there is a lot of experience documented in a body of literature spanning, but not limited to, the fields of geochemistry, chemical engineering, and atmospheric sciences. Typical pitfalls are associated with an incomplete set of supporting thermodynamic data, extrapolation of such data out of range (e.g., to temperatures unconstrained by measurements), failure to consider all types of chemical reactions that may be occurring, and kinetic and transport factors that limit the degree of approach to thermodynamic equilibrium. In general, successful application requires a sense of how these factors might come into play when attacking a given problem. Sufficient validation is the key to estimating the final uncertainty. This may come from both tests and observations of natural systems.

For the types of problems addressed by this report, validation experience to assess uncertainties in results of thermodynamic modeling comes from a combination of evaporation tests, deliquescence tests, solubility tests, comparison with natural systems, and experimental results reported in the scientific literature. Here the usual focus is on the development of quantitative metrics incorporating such data (which is exemplified by the approach taken in the IDPS model as is discussed below). However, another approach (which can be complementary) is to constrain the operative processes and boundary conditions that limit the range of possibilities. One such process discussed in this report concerns the formation and transport of trace acid-gas volatiles, as this alone may suffice to limit if not entirely prevent the formation of potentially corrosive brines (Section 6.7.2.14.3). This process could also be a significant natural long-term control on the range of ambient porewater compositions in a thick desert vadose zone such as is present at Yucca Mountain. The general theme of the near-quantitative removal of magnesium from hydrothermal solutions into silicate minerals (Section 6.7.2.11) is another example.

In-Drift Precipitates/Salts Model (BSC 2004 [DIRS 169863]) addresses uncertainties in terms of the validation criteria summarized in Table 7-1 of that report. The key criteria used in the IDPS model and of note for the present report are (1) uncertainty in relative humidity within 10 RH percent (0.1 units in the activity of water), (2) concentrations of “readily equilibrated components” within a factor of ten, and (3) concentrations of “less rapidly equilibrated” components within a factor of 100. Other criteria apply to pH (within 1 pH unit) and ionic strength (within a factor of ten). These criteria are thus broad and in many instances would overstate the actual uncertainties in IDPS model calculations.

In particular, *In-Drift Precipitates/Salts Model* (BSC 2004 [DIRS 169863], Section 7, p. 7-4) notes that:

...the validation criteria used here do not necessarily imply large uncertainties in the model outputs. Uncertainties must be individually assessed for the specific applications of the model.

The uncertainties in the deliquescence tables in output DTN: LL040603912251.107 require special comment. The key salt mineral assemblages that these tables are based on have some associated uncertainty. These assemblages are highly deliquescent at elevated temperatures, and other possible assemblages (e.g., those involving NH_4 salts) are similarly deliquescent under these conditions. The higher solubility of nitrate minerals relative to corresponding chloride minerals indicates that NO_3/Cl ratios would remain high even if the exact identities of the minerals involved are changed (e.g., involving NH_4). The most uncertain aspects of these deliquescence tables are probably the dryout temperatures imposed by the total pressure limit of 0.90 bar. If the deliquescence RH is as much as 10 RH percent (0.1 units in the activity of water) lower than predicted, the dryout temperature associated with the pressure limit can rise, on the order of 10°C to 25°C for RH values less than 50 percent (Figures 6.7-2 and 6.7-3).

Given the salt mineral assemblages developed in this report, one can address the uncertainties in the thermodynamic calculations. If the assemblages involved the salt minerals and aqueous components for which the available thermodynamic data are the most accurate, the uncertainty in the deliquescence RH at temperatures in the range considered would be about 1-3 percentage points. See for example plots for such systems given in *In-Drift Precipitates/Salts Model* (BSC 2004 [DIRS 169863], Figure 7-18: $\text{NaCl-H}_2\text{O}$; Figure 7-19: $\text{KCl-H}_2\text{O}$, and Figure 7-40: $\text{NaCl-KCl-H}_2\text{O}$). For the three no-dripping case assemblages, that level of uncertainty may be approached at low temperature.

At elevated temperatures (above 50°C to 70°C), the uncertainty is greater owing to specific problems with the Pitzer parameterization, especially for the KNO_3 Pitzer parameters (and in Case C, also for the $\text{Ca}(\text{NO}_3)_2$ parameters). There are also some issues with the NaNO_3 parameters as extrapolated above the dryout point for the pure $\text{NaNO}_3\text{-H}_2\text{O}$ system (120.59°C from Table 4.1-5), as well as some further issues regarding mixture parameters involving nitrate at elevated temperature.

The uncertainty in the RH percent for the pure $\text{KNO}_3\text{-H}_2\text{O}$ system is likely in the range 5 to 10 percent up to the IDPS model validation limit of 140°C . This is supported by the comparison of IDPS model and experimental RH data shown in Figure 7-37 of *In-Drift Precipitates/Salts Model* (BSC 2004 [DIRS 169863]). The RH data from the IDPS model at higher temperature are about 10 percent lower than the experimental data. Thus, the IDPS model indicates that KNO_3 is more deliquescent than it actually is. Figure 7-37 of *In-Drift Precipitates/Salts Model* (BSC 2004 [DIRS 169863]) also compares solubility data (the same data shown in Figure 6.7-39 of the present report). This comparison indicates that the actual concentration of dissolved KNO_3 in the $\text{KNO}_3\text{-H}_2\text{O}$ system at saturation close to 140°C is about twice that predicted by the IDPS model. The IDPS model error in the RH seems unusual compared with that in the solubility. Normally, higher concentrations are associated with lower water activities (and lower relative humidities). Hence, underestimation of solubility would be thought of as associated with

overestimation of RH. Here that is clearly not the case. The solutions here are in the “super-concentrated” realm (e.g., 40 molal or greater), and some of the rules of thumb that apply in the lower concentration ranges do not apply here.

In-Drift Precipitates/Salts Model (BSC 2004 [DIRS 169863] Figure 7-36) shows similar model versus experiment comparisons for the relative humidity and the solubility for the pure $\text{NaNO}_3\text{-H}_2\text{O}$ system. The RH data from the IDPS model at higher temperatures are about 2 to 6 RH percent higher than the experimental data in the range of about 80°C to 121°C . Thus, the IDPS model indicates that NaNO_3 is less deliquescent than it actually is. The solubility comparison is excellent (within the 1-3 percent range) up to about 121°C . For the pure $\text{NaNO}_3\text{-H}_2\text{O}$ system, convergence problems are encountered at higher temperature. Model RH results for higher temperature shown in Figure 7-36 of *In-Drift Precipitates/Salts Model* (BSC 2004 [DIRS 169863]) are for unsaturated solutions (the most concentrated for which convergence could be obtained).

In-Drift Precipitates/Salts Model (BSC 2004 [DIRS 169863], Figure 7-38) shows similar comparisons for the pure $\text{Ca}(\text{NO}_3)_2\text{-H}_2\text{O}$ system. The IDPS model will only converge for the saturated system up to about 62°C . The RH model data are higher than the experimental data by about 10 to 23 RH percent over the range 25°C to 62°C (as is discussed previously). The IDPS model solubility is low by nearly 25 percent at 25°C and by about 50 percent near 62°C .

Figure 7-20 of *In-Drift Precipitates/Salts Model* (BSC 2004 [DIRS 169863]) shows similar comparisons for the pure $\text{CaCl}_2\text{-H}_2\text{O}$ system. The RH deviations are relatively small (a few RH percent) over most of the temperature range, but close to 10 RH percent at 140°C . The solubility deviations are within a few percent.

The no-dripping Key Dust Assemblage Case A (NaCl-KNO_3) contains one component (NaCl) that is represented accurately in the corresponding IDPS model single-salt case and another (KNO_3) that is much less accurately represented in its corresponding single-salt case. For the mixture, there are additional considerations. The lower order Pitzer mixture parameters (for Na-K and Cl- NO_3 interactions) are usually the more important. However, of the higher order mixture parameters (for Na-K-Cl, Na-K- NO_3 , Na-Cl- NO_3 , and K-Cl- NO_3 interactions), only that for Na-K-Cl is well constrained (from data for the $\text{NaCl-KCl-H}_2\text{O}$ system). Those parameters for combinations involving NO_3 are of special concern in systems such as this because at high temperature the concentration of nitrate can become extremely high, amplifying these interactions. The uncertainty in the relative humidity for this case is likely the full validation limit of 10 RH percent. Because the KNO_3 results from the IDPS model underpredicts the concentration of nitrate, there is little chance that the corresponding model NO_3/Cl ratios could be any lower. It is more likely that they would be higher by about a factor of two near the 140°C validation limit. Also for this assemblage, KCl (sylvite) joins in at elevated temperatures (such that the assemblage present is actually $\text{NaCl-KNO}_3\text{-KCl}$). This mineral is a sink for chloride.

The no-dripping Key Dust Assemblage Case B ($\text{NaCl-KNO}_3\text{-NaNO}_3$) contains the additional NaNO_3 component, which is inaccurately represented in the corresponding single salt case above about 121°C . The uncertainty in the relative humidity for these cases is again likely the full validation limit of 10 RH percent. It is probably no worse because it involves no additional higher order Pitzer interactions and the nitrate concentration should be slightly depressed by the

common ion effect (two nitrate salts present). Because the KNO_3 model results underpredict concentration of nitrate, there is again little chance that the IDPS model NO_3/Cl ratios would be any lower. It is more likely that they are higher, especially at higher temperature. Again KCl joins in at elevated temperature. This is a more deliquescent assemblage than Key Dust Assemblage Case A. Therefore, the uncertainty in the maximum dryout temperature associated with the 0.90 bar pressure limit is greater (note for example the trend in Figure 6.7-3).

For the no-dripping Key Dust Assemblage Case C, the uncertainty in the IDPS model RH up to about 60°C exceeds the validation limit of 10 RH percent over at least the upper part of this range. It could be 15 to 20 RH percent near 60°C . Above 60°C , IDPS model calculations did not converge. The behavior at higher temperature is extrapolated from experimental data for the pure $\text{Ca}(\text{NO}_3)_2$ system (Section 6.7.2.10), so the resulting uncertainty there is tied to the mixture effect. This would still probably exceed 10 RH percent. The presence of the Ca introduces two additional lower-order mixture combinations (Ca-Na, Ca-K), but these are fairly well constrained. However, it also introduces some additional higher-order mixture combinations (Ca-Na-Cl, Ca-Na- NO_3 , Ca-K-Cl, Ca-K- NO_3 , and Ca-Cl- NO_3). The effects of the interactions for these combinations involving nitrate are not well constrained, and those effects are amplified by very high nitrate concentrations, particularly at elevated temperature. As the single-salt IDPS models for KNO_3 and $\text{Ca}(\text{NO}_3)_2$ significantly underpredict solubility, there is again little chance that predicted NO_3/Cl ratios for this assemblage are overestimated. Again KCl joins in at elevated temperature. The results presented for this case comprise only a best-estimate of likely actual behavior.

The uncertainty in the RH for the first two no-dripping cases (Key Dust Assemblage Cases A and B) suggests a potential uncertainty in the associated boiling temperatures (or temperature for the limit of deliquescence associated with the expected maximum pressure of 0.90 bar) of about 10°C to 25°C (as noted above). For the no-dripping Key Dust Assemblage Case C the potential uncertainty in the boiling temperature is higher, perhaps 20°C to 40°C .

For the dripping case (based on the pure $\text{CaCl}_2\text{-H}_2\text{O}$ system) the uncertainties over the range are rather small as discussed above. Experimental data are employed at temperatures above about 46°C . Thus, the uncertainty in the RH is in the range of 1 to 3 RH percent at low and high temperatures. The uncertainty in the boiling temperature appears to be about 10°C to 15°C as indicated by the scatter of data in Table 6.7-18 near the boiling point for standard atmospheric pressure (extrapolating the same degree of scatter to a pressure of 0.90 bar). That is an experimental uncertainty, not a model uncertainty.

Table 7-8 of *In-Drift Precipitates/Salts Model* (BSC 2004 [DIRS 169863]), which is also summarized in DTN: MO0312SPAESMUN.002 [DIRS 166329], provides specific guidance for assignment of uncertainties to calculations made using the IDPS model (including those to be used in TSPA-LA). This table along with its footnotes is reproduced here as Table 6.7-34. “ RH_d ” denotes the deliquescence RH. The general scheme is to assign uncertainties to IDPS model outputs based on the range of calculated (output) RH. As noted in the table, the results are only applicable to the lower temperature ranges for no-dripping Key Dust Assemblage Case C (below about 62°C) and for the single-dripping case with pure CaCl_2 seepage waters (below about 46°C), as IDPS model calculations are generated only in those ranges.

Table 6.7-34. Estimated In-Drift Precipitates/Salts Model Uncertainties for Temperatures Between 25°C and 140°C

Parameter	Units	RH Range 100% to 85%	RH Range 85% to 65%	RH Range 65% to 60%	RH Range 60% to 40%	RH Range 40% to 0%
pH	pH units	± 1	± 1	± 1	± 2	± 2
Ionic Strength	log molal	± 0.1	na ^a	Na	na	na
Cl	log molal	± 0.0	± 0.2	± 0.5	± 0.7	± 0.7
NO ₃	log molal	± 0.0	± 0.2	± 0.2	± 0.7	± 0.9
Cl:NO ₃	log mole ratio	± 0.0	± 0.2	± 0.5	± 0.7	± 1
RH _d	%RH units	± 5%	± 10%	± 10%	± 10% ^b	± 15% ^b

Source: BSC 2004 [DIRS 169863], Table 7-8.

^aNot applicable to TSPA-LA. Prediction of ionic strength is for colloids model. At RH below 85 percent, ionic strength is greater than 1 molal, which is far above the critical ionic strength where colloids are unstable.

^bThe exception for this estimated uncertainty is for a brine with a large Ca(NO₃)₂ component. IDPS model predictions in binary Ca(NO₃)₂ systems operationally provide RH_d values that are 20 to 25 percent higher than reported measurements. Because the validation criterion for the IDPS model is to predict RH_d within ±10 percent RH (Table 7-1), the IDPS model is not valid for predicting RH_d below 40 percent or when Ca(NO₃)₂ is a large component of the brine at RH below 60 percent.

For the no-dripping Key Dust Assemblage Case A (NaCl-KNO₃) and Key Dust Assemblage Case B (NaCl-KNO₃-NaNO₃), the uncertainty in RH would be 10 RH-percent over nearly the entire ranges of the curves depicted in Figure 6.7-33. However, a small part of the curve for Key Dust Assemblage Case A and a larger part of that for Key Dust Assemblage Case B extend into the region below 40 percent RH, where an uncertainty of 15 RH percent would be assigned. For Key Dust Assemblage Case A, this occurs at about 118°C; for Key Dust Assemblage Case B, at about 93°C. For the no-dripping Key Dust Assemblage Case C, between 25°C and 30°C, the IDPS model calculations do not meet the validation criteria and the above table does not specify an uncertainty. As previously noted, the uncertainty is likely about 16 RH percent near 60°C, the highest temperature at which the IDPS model would converge for the saturated case. Also as previously noted, the uncertainty in the analysis for Key Dust Assemblage Case C is exceptional and the analysis is only intended to give a best-estimate picture of actual behavior. Table 6.7-34 also specifies uncertainties for the Cl/NO₃ ratio (the inverse of the NO₃/Cl ratio used in this report). For the three no-dripping dust deliquescence key assemblage cases, the actual uncertainties are much more one-sided than implied by this table in that calculated NO₃/Cl ratios would be significantly lower than in reality.

For the single no-dripping case based on the pure CaCl₂-H₂O system, the RH (from the IDPS model or from experimental data) is already well below 40 percent at 25°C, and at higher temperatures it is lower still (Figure 6.7-34). The analysis for this case is based on IDPS model calculations only up to near 46°C. Table 6.7-34 would imply an uncertainty of 15 RH percent. However, the IDPS model is considerably more accurate for this particular system as is noted above. There is, of course, no nitrate in a pure CaCl₂-H₂O system, so consideration of uncertainty in the NO₃/Cl ratio is moot.

Although the above uncertainties are difficult to quantify in some important instances, they are small in relation to the span of RH values in the deliquescence RH tables in output DTN: LL040603912251.107. The RH values at the highest temperatures for the cases

represented in these tables are fairly low, about 30 percent or less (Figures 6.7-33 and 6.7-34). In simple terms, the salt mineral assemblages associated with the tables output from this analysis are highly deliquescent at the maximum (boiling) temperatures as currently represented. The uncertainty is that they could be somewhat more or less deliquescent than represented, but they would still be highly deliquescent.

7. CONCLUSIONS

7.1 SUMMARY OF SCIENTIFIC ANALYSES

This scientific analysis specifies anticipated environments on the surfaces of the drip shield and the waste package outer barrier in the repository at Yucca Mountain, Nevada. It estimates the conditions of temperature (T) and relative humidity (RH) under which liquid water can be present on the metal barrier surfaces, and, if liquid water is present, it then estimates its chemical composition. The presence of liquid water is a key factor in metal barrier corrosion, and the water composition is also a key factor in controlling the mechanisms and rates of corrosion (BSC 2004 [DIRS 169845], Sections 1.2 and 6.3.3; BSC 2004 [DIRS 169984], Sections 1.2 and 6.3). The present analysis emphasizes the effects of deliquescence of dusts that are expected to be deposited on the metal barrier surfaces during the ventilation period. It also includes an analysis of the effect of brine formation by seepage of a calcium chloride groundwater onto the metal barrier surfaces.

This report is one of three addressing chemical environments in the repository drifts. The others are *In-Drift Precipitates/Salts Model* (BSC 2004 [DIRS 169863]) and *Engineered Barrier System: Physical and Chemical Environment* (BSC 2004 [DIRS 169860]). The former is the source of the IDPS high-temperature Pitzer thermodynamic model used extensively in the latter report and in the present report. The latter report is the main source of the chemical environment inputs to the Total Systems Performance Assessment (TSPA-LA). The present analysis is intended to be complementary and supportive of *Engineered Barrier System: Physical and Chemical Environment* (BSC 2004 [DIRS 169860]) and more directly support other objectives such as Key Technical Issues and features, events, and processes screening.

The present report presents background material on the deliquescence and evaporation processes, the thermodynamic controls on these processes, and a summary of what is known about the compositions of Yucca Mountain tunnel dusts and atmospheric dusts. It discusses processes that appear to determine the compositions of both dust types, such as the formation of nitrate in the atmosphere associated with electrical discharges. It defines the concept of key mineral assemblages that control the onset of deliquescence in conjunction with changes in temperature and RH. It determines the apparent key assemblages in Yucca Mountain tunnel dusts (Key Dust Assemblage Cases A: NaCl-KNO₃; B: NaCl-KNO₃-NaNO₃; and C: NaCl-KNO₃-NaNO₃-Ca(NO₃)₂), and addresses the likelihood of these or similar assemblages pertaining also to atmospheric dusts. Here for the tunnel dusts the presence of bromide as KBr from the use of LiBr as a tracer in construction water is factored out because this tracer will not be used in future operations. The present report also determines a value (0.90 bar) for the maximum (sustained) total pressure in the repository drifts, which is another factor in conjunction with temperature that controls the existence of liquid water independent of the RH. This provides a cut-off for deliquescence RH (deliquescence relative humidity)-temperature curves for any saturated salt mineral assemblages. This report further addresses the generation of acid-gas volatiles including HCl_(g) and HNO_{3(g)} from deliquescing salt minerals or evaporating brines, the likely controls on the fate of such volatiles, the role of generation of such volatiles as a control on mineral and brine transformations, and hence on chemical compositions of material and the sustainable existence of liquid water on the metal barrier surfaces. Experimental data and thermodynamic calculations pertinent to these effects are presented.

This analysis determines bounds associated with the repository location and design, based on two important cases. These are:

1. The no-dripping case, corresponding to deliquescence of the salt component of dust
2. The dripping case, corresponding to either the evaporation of seepage water or the deliquescence of salts that may have previously formed from seepage water.

This analysis indicates, as a function of local temperature and RH, whether or not liquid water is present due to the deliquescence of salt minerals on the metal surfaces. For the no-dripping case, this report considers potential dust salts and their sources, and evaluates the key features of dust deliquescence using chemical data obtained from dusts taken from the repository drifts. For the dripping case, it provides an analysis based on the formation of a calcium chloride brine. Tables are provided summarizing the no-dripping and dripping cases. Uncertainties in these analyses are discussed in Section 6.7.2.16.

This report establishes an expected maximum (sustainable) pressure in the drifts of 0.90 bar. It uses two methods to establish values for the ambient pressure at the repository elevation. The first method is to apply a relation for the mean atmospheric pressure as a function of elevation (Fleagle and Businger 1980 [DIRS 108591]). The second method is to examine actual recorded pressure measurements behind a bulkhead in the current tunnel system (DTN: GS030108312242.001 [DIRS 163118]). This part of the analysis shows that ambient pressure values above 0.90 bar may occur only infrequently, in association with weather phenomena. It is assumed (Assumption 5.3) that pressure within the drift will not significantly exceed the ambient pressure. The expected maximum pressure imposes a limit on the existence of liquid water at a given temperature, as shown in Figures 6.7-2 and 6.7-3. This limit is independent of the deliquescence properties of any salt mineral or salt mineral assemblage.

This analysis provides background on the deliquescence process and related processes (Sections 6.7.2.7 and 6.7.2.8). Extensive scientific literature is cited (Section 6.7.2.8) that confirms that deliquescence is tightly controlled by equilibrium thermodynamics. Each salt mineral has a deliquescence RH that is a function of temperature (though that of NaCl is fairly constant over a wide range). In most instances, the deliquescence RH decreases with temperature, though in a smaller number of instances it increases. Every assemblage of two or more salt minerals has its own characteristic deliquescence RH, also a function of temperature. This deliquescence RH must be lower (though not sensibly so) than any contained mineral or mineral subassemblage. The deliquescence RH for most salt mineral assemblages decreases with increasing temperature. Deliquescence may be further affected by mineral decomposition or transformation and by reaction with volatiles other than H₂O, notably CO₂, HCl, and HNO₃. Certain minerals are only stable in certain temperature ranges (e.g., antarcticite, CaCl₂·6H₂O, to about 29°C).

The characteristics of the environment of the drip shield and waste package outer barrier are discussed in terms of the compositions of Yucca Mountain waters, the temperature of the EBS components, the effective RH at the EBS components, the gas-phase composition, and dust and aerosol deposition of hygroscopic (deliquescent) salts. Water vapor is implicitly included in the gas-phase composition through RH. For this analysis, it is expected that most interactions

between aqueous solutions, minerals on the metal surfaces, and the components of the adjoining gas phase are effectively governed by thermodynamic equilibrium (local equilibrium). Thus, mineral and gas solubilities are key elements to understanding whether aqueous solution is present under given conditions (e.g., T, RH, and $p\text{CO}_2$) and, if that is the case, the composition of that solution. The expectation of local thermodynamic control is supported by several factors. These include the long time periods available for equilibrium to be reached (e.g., T and RH are relatively constant for long periods), the low thickness of any aqueous film or layer, and the ready availability of nucleation sites (“rough” surfaces and small particles).

This scientific analysis then uses the IDPS model (BSC 2004 [DIRS 169863]), a high-temperature Pitzer thermodynamic model, to study the deliquescence relative humidity of various salt minerals and salt mineral assemblages and the compositions of the corresponding aqueous solutions. Salt deliquescence calculations are made for selected one-salt to four-salt salt mineral assemblages. In one type of calculation, the deliquescence RH for a given salt mineral or assemblage is determined over a temperature range starting at 25°C and extending to 140°C. Another type of calculation is made to determine the aqueous solution composition and RH moving off the eutectic point of selected salt mineral assemblages.

The IDPS model is also applied to “reconstitute” from chemical analysis of leachates the salt minerals originally present in Yucca Mountain tunnel dusts. The concept of deliquescence control by key mineral assemblages that are present within larger mineral assemblages is developed and applied to the tunnel dusts. The concept is demonstrated to be appropriate by comparing predicted RH values for the full assemblages with those for the key assemblages without other minerals present. The results are applied to develop the no-dripping (deliquescence) case based on the three key salt assemblages from the tunnel dust analysis (factoring out bromide as KBr from the past use of LiBr in construction water). These are Key Dust Assemblage Case A: NaCl-KNO₃; Key Dust Assemblage Case B: NaCl-KNO₃-NaNO₃; and Key Dust Assemblage Case C: NaCl-KNO₃-NaNO₃-Ca(NO₃)₂. The salt mineral sylvite (KCl) also appears in these systems starting at moderately elevated temperatures (approximately 40°C) and is implicitly present though not always explicitly noted. Otherwise, these assemblages are stable to the IDPS model validation limit of 140°C (and beyond). The percentages of these three assemblages (as determined by occurrence in dust samples and recommended for application to corresponding percentages of waste packages) from Table 6.7-19 are Key Dust Assemblage Case A: 68.1 percent; Key Dust Assemblage Case B: 27.8 percent; and Key Dust Assemblage Case C: 4.1 percent. The deliquescence RH vs. temperature results for these cases are given as tables (Key Dust Assemblage Case A: Table 6.7-21; Key Dust Assemblage Case B: Table 6.7-22; and Key Dust Assemblage Case C: Table 6.7-23). One of the important results of this scientific analysis is that at elevated temperature, the initial brines formed by deliquescence of these assemblages contain very high concentrations of nitrate relative to chloride. This is significant because nitrate acts as an inhibitor of localized corrosion of Alloy 22 the WPOB alloy, while chloride is a promoter. In essence, the nitrate minerals dissolve more fully earlier in the process. As temperature in the repository drifts falls and the RH rises, complete dissolution of the nitrate followed by dissolution of the remaining chloride salt will cause the nitrate to chloride ratio to decline. However, the susceptibility of Alloy 22 to corrosion decreases with temperature (BSC 2004 [DIRS 169984]).

The dripping case is an upper bound based on calcium chloride mineral. The deliquescence RH is a function of temperature, noting that, at about 100°C, there is a divergence between the IDPS model calculations and the experimental measurements. In the IDPS model calculations, the deliquescence RH continues to increase slowly with temperature, while, in the experimental results for temperatures above 46.02°C, the deliquescence RH begins decreasing, and begins decreasing rapidly near the boiling temperature. The table (Table 6.7-24) is based on the IDPS model calculations up to about 46°C, and directly on reported experimental data at higher temperatures.

The above no-dripping and dripping cases ignore the potential effects of acid-gas volatilization, which may further reduce the range of existence of aqueous solutions and limit the types of potential brine compositions. The influence of the gas phase as a source and sink of chemical species is a major difference between a hydrologically unsaturated system and a saturated system. For Yucca Mountain, acid-gas volatility in determining the chemical environment on the metal barriers is studied in terms of developing values of the apparent standard molar Gibbs energies for HF, HCl, HBr, HNO₃, and N₂O₅, as a function of temperature. The results provided in this report include tables of Gibbs energy of formation that can be used to assess potential differences between drift wall and metal barrier surfaces. Experimental data show the effects of acid-gas volatilization from aqueous brine films are also presented. In particular, it is noted that such data show that volatilization of HCl gas is a strong limiting factor on the existence of CaCl₂ brines at elevated temperature. In the particular case discussed, the Alloy 22 is shown to behave as an inert substrate.

Niter (KNO₃) is a key component in the analysis of deliquescence on the metal barrier surfaces. The Pitzer interaction coefficients for KNO₃ are the reported 25°C values. They appear to predict RH adequately up to about 50°C, at which point there are fewer data. An alternative approach to evaluating the adequacy of the results using Pitzer's method is to compare calculated niter solubilities with measured values. The results appear to agree reasonably well up to about 75°C. At higher temperature, the measured values continue to increase rapidly, while the Pitzer's values taper off. At 140°C, the measured value is more than twice the calculated (IDPS model) value. The accuracy limits for modeling of systems containing this salt are recognized and incorporated into the output uncertainty description for the IDPS model. There are additional limitations for Ca(NO₃)₂ in that the IDPS model does not represent experimental data with sufficient accuracy at very high ionic strength (near saturation with calcium nitrate minerals). This is also recognized and incorporated in the application of the IDPS model in TSPA-LA.

A final important point is that the analysis of the tunnel dusts (e.g., identification of key salt assemblages) likely also pertains to outside (atmospheric) dusts. The ionic ratios (molar ratio for an ion other than chloride to chloride) for the tunnel dusts are compared with ratios for precipitation (rainfall) at three meteorological stations roughly bracketing Yucca Mountain and with ratios for three statistical composites representing Asian dust. These results are all broadly similar. The total salt content in Yucca Mountain tunnel dusts is quite small, only a few tenths of a percent, while outside dusts will likely show many values in the 9 to 16 percent range. Thus, apart from bromide contamination introduced from the use of LiBr as a tracer in construction water, the tunnel dusts could be a mixture of 98 to 99 percent rock flour and 1 to 2 percent outside dust. Ammonium ion (NH₄) was not analyzed for in the tunnel dust leachates, but is a

significant component of the salt content of regional precipitation (rainfall) and Asian dusts. Ammonium ion often behaves much like potassium ion in geochemical systems.

7.2 DEVELOPED OUTPUT

The eight output DTNs for the report are summarized in Table 7.2-1. The principal output (DTN: LL040603912251.107) consists of deliquescence tables. This output is described in detail in Section 6.7.2.13 and in the Excel workbook in the DTN package. This description (in Section 6.7.2.13 and in the workbook) specifies how this output can be used. It will, therefore, not be repeated here. Five of the seven remaining output DTNs (LL040903723121.042, LL030500612251.059, LL030500712251.060, LL040603712251.105, and L040601512251.103) contain calculations used quantitatively or qualitatively in the construction of output DTN: LL040603912251.107. The output DTN: LL040603712251.105 contains calculations that indirectly support that analysis by showing that the salts in tunnel dusts are largely similar to salts in atmospheric dusts and in regional rainfall. The output DTN: LL030500812251.061 contains material pertinent to acid–gas volatility; this is presented as supplementary material.

Table 7.2-1. Output DTN Packages

DTN Number	Purpose
LL030500612251.059	Atmospheric pressure at the repository elevation; in support of DTN: LL040603912251.107
LL030500712251.060	Calculations pertaining to the vapor pressure of pure water and accessible RH; in support of DTN: LL040603912251.107
LL030500812251.061	Calculations pertaining to acid–gas volatility
LL040601512251.103	Extension of calculations in LL030500712251.060; contains additional plots
LL040603612251.104	Calculation of evaporation of dust leachate solutions at 25°C, to determine the eutetic (dryout) mineral assemblages
LL040603712251.105	Calculation of ionic ratios in Yucca mountain tunnel dust leachates, Asian dust leachates, and the solute content of Nevada regional precipitation (rainfall)
LL040903723121.042	Thermodynamic calculations and plots analyzing salt mineral deliquescence on the drip shield and waste package outer barrier; contains most of the plots in this report
LL040603912251.107	Deliquescence tables for the no-dripping and dripping cases

The principal output DTN (LL040603912251.107) can be used to determine when liquid water is present. The tables require the RH and temperature to make this determination. There are three tables for the no-dripping (dust deliquescence) case, corresponding to three key salt mineral assemblages (A, B, and C). Each of these tables applies to a percentage of the waste packages, or to a percentage of probabilistic realizations, based on reported tunnel dust compositions as discussed in Section 6.7.2.13. If the temperature is greater than the highest temperature in the relevant table, the system is dry. If that is not the case, the RH obtained from thermal history data is compared with the deliquescence RH at the matching temperature in the table (interpolating as necessary). If the system RH equals or exceeds the deliquescence RH, the system is wet; otherwise, it is dry. There is one table for the dripping case (deliquescence of salt minerals created by evaporation of seepage water); this describes a very conservative case of a CaCl₂ brine. This table can be used in the same fashion as the three tables for the no-dripping case. The tables in this DTN are not used to determine brine compositions when the system RH

is greater than the deliquescence RH. That information is derived from output of *Engineered Barrier System: Physical and Chemical Environment* (BSC 2004 [DIRS 169860]).

The output developed in this report contains no uncertainty. The major sources of uncertainty are discussed in Section 6.7.2 and are mainly related to limitations on available data. For example, there is limited data on the composition of salts that might enter the repository from the outside air during the ventilation period. There are sources of uncertainty related to the currently available thermodynamic data, noted particularly in Section 6.7.2.15.

7.3 ACCEPTANCE CRITERIA SUMMARY

This section summarizes how and where in this report each of the applicable criteria/subcriteria established in *Yucca Mountain Review Plan, Final Report* (NRC 2003 [DIRS 163274]) is addressed. The determination of applicability is summarized in Section 4.2.

Acceptance Criterion 1 – System Description and Model Integration are Adequate

- (1) Total system performance assessment adequately incorporates important design features, physical phenomena, and couplings, and uses consistent and appropriate assumptions throughout the quantity and chemistry of water contacting engineered barriers and waste forms abstraction process.

Response: This report does not provide direct feeds to Total System Performance Assessment for the License Application (TSPA-LA). This report is mainly used for FEPs screening, technical basis documents, and key technical issues. However, the analyses in this report also support results from other reports that provide direct inputs to TSPA-LA, chiefly *Engineered Barrier System: Physical and Chemical Environment* (BSC 2004 [DIRS 169860]). This report provides an analysis of the factors expected to control the chemical environment on the drip shield and waste package outer barrier. This report adequately incorporates important design features, physical phenomena, and couplings as described in Sections 6.2, 6.3, 6.5 and 6.7 (primarily in 6.7.2). Analysis assumptions in this report are consistent and appropriate for the quantity and chemistry of water contacting engineered barriers (Section 5).

- (2) The abstraction of the quantity and chemistry of water contacting engineered barriers and waste forms uses assumptions, technical bases, data, and models, that are appropriate and consistent with other related U.S. Department of Energy abstractions...[examples omitted here]. The descriptions and technical bases provide transparent and traceable support for the abstraction of quantity and chemistry of water contacting engineered barriers and waste forms.

Response: The analysis developed in this report uses the same technical bases and other information as are used in other TSPA-LA-supporting documents concerned with the chemistry of water contacting engineered barriers. The assumptions that form the basis for this analysis (Section 5) are consistent with other system conceptual models and assumptions, and are appropriate for the quantity and chemistry of water contacting engineered barriers. This report provides an analysis of the factors expected to control the chemical environment on the drip shield and waste package outer barrier. As such, it is tied to other cited reports and other sources regarding the expected temperature and relative humidity in the drift and, to a limited extent, to

the predicted composition of groundwaters seeping into the drifts during the cool down period. It supports use of the IDPS model for brine–salt mineral interactions (BSC 2004 [DIRS 169860]). The descriptions and technical bases presented in Sections 6.2, 6.3, 6.5 and 6.7 (primarily in 6.7.2) of this report provide transparent and traceable support for the use of quantity and chemistry of water contacting engineered barriers.

- (4) Spatial and temporal abstractions appropriately address physical couplings (thermal-hydrologic-mechanical-chemical).

Response: This report deals with potential couplings with the surrounding TH and THC system. Assumption 5.3 and Section 6.7.2.1 develop the maximum expected pressure of 0.90 bar. Assumption 5.5 states that the temperature, RH, and CO₂ pressure at the surface of a metal barrier are not perturbed either by seepage-water evaporation or by the deliquescence of dust. The amounts of liquid water vaporized or condensed are small in comparison with the amount of water vapor in and around the drifts. Assumption 5.6 states that the composition of the water that contacts the drip shield and waste package outer barrier (via seepage or deliquescence) will not change significantly because of chemical interaction with the metal barriers themselves. Assumption 5.7 provides rationale that acid–gas species (such as HCl_(g) and HNO_{3(g)}) volatilized by heating of concentrated salt solutions present on the drip shield and waste package outer barrier surfaces are dispersed by convection and diffusion to the drift wall, where they advect or diffuse farther into the rock and/or are neutralized by chemical reaction. Spatial and temporal parameters used in this analysis appropriately address physical couplings.

- (10) Likely modes for container corrosion (Section 2.2.1.3.1 of the Yucca Mountain Review Plan) are identified and considered in determining the quantity and chemistry of water entering the engineered barriers and contacting waste forms.

Response: The analyses of the chemical environment on the drip shield and waste package outer barrier in this report focus attention on two key issues related to corrosion (1) the existence of liquid water and (2) the nitrate to chloride ratio, which are considered important factors in localized corrosion of Alloy 22. This information is given in Sections 6.7.2.9, 6.7.2.10, 6.7.2.11, 6.7.2.12, 6.7.2.13, and 6.7.2.14.

Acceptance Criterion 2 – Data are Sufficient for Model Justification

- (1) Geological, hydrological, and geochemical values used in the license application are adequately justified. Adequate description of how the data were used, interpreted, and appropriately synthesized into the parameters is provided.

Response: This report uses as direct inputs data on the compositions of leachates of tunnel dust, which reflect the salt content of the original samples. These data are compared with other data for regional precipitation (rainfall) and for Asian dusts as addressed in Section 6.7.2.10. Other geochemical data are drawn upon in Section 6.7.2.

- (2) Sufficient data were collected on the characteristics of the natural system and engineered materials to establish initial and boundary conditions for conceptual models of thermal-hydrologic-mechanical-chemical coupled processes, that affect seepage and flow and the engineered barrier chemical environment.

Response: This report uses as direct inputs data on the compositions of leachates of tunnel dust, which reflect the salt content of the original samples. These data are sufficient to establish initial and boundary conditions and are compared with other data for regional precipitation (rainfall) and for Asian dusts. This is addressed in Section 6.7.2.10. Also, temperature ranges, pressures, and other boundary conditions are representative of repository conditions

- (4) Sufficient information to formulate the conceptual approach(es) for analyzing water contact with the drip shield, engineered barriers, and waste forms is provided.

Response: This report analyzes the existence of liquid water as formed by deliquescence of salts in dust. Sufficient information to formulate the approach for analyzing water in contact with the drip shield and WPOB is provided in Sections 6.7.2.9, 6.7.2.10, 6.7.2.11, 6.7.2.12, 6.7.2.13, and 6.7.2.14.

Acceptance Criterion 3 – Data Uncertainty Is Characterized and Propagated Through the Model Abstraction

- (1) Models use parameter values, assumed ranges, probability distributions, and bounding assumptions that are technically defensible, reasonably account for uncertainties and variabilities, and do not result in an under-representation of the risk estimate.

Response: This report provides an analysis of the factors expected to control the chemical environment on the drip shield and waste package outer barrier, principally by combining available geochemical data pertinent to the site (mainly on dust compositions) and applying the IDPS model (a high-temperature Pitzer thermodynamic model for aqueous systems) to analyze dust deliquescence. The parameter ranges and bounding assumptions of this analysis are defined in Sections 4.1 and 5 and are considered representative of the system. It also uses other chemical and geochemical data directly, as in the formulation for the conservative dripping (seepage) case based on a CaCl_2 composition (Section 6.7.2.13). This subcriterion is broadly addressed in Section 6.7.2. Input parameters (Table 4.1-1) are developed in this report to be consistent with the expected ranges of values for upstream and downstream modeled systems. Values and ranges of these parameters used in this analysis are reasonable and do not result in underrepresentation of the risk estimate.

- (4) Adequate representation of uncertainties in the characteristics of the natural system and engineered materials is provided in parameter development for conceptual models, process-level models, and alternative conceptual models. The U.S. Department of Energy may constrain these uncertainties using sensitivity analyses or conservative limits.

Response: Uncertainty in the natural system is adequately characterized in parameter development this analysis. This report addresses uncertainties at the conceptual and process level by referencing a broad range of pertinent data, and using wide uncertainty ranges and conservative limits where necessary. This is addressed throughout Section 6.7.2.

Acceptance Criterion 4 – Model Uncertainty Is Characterized and Propagated Through the Model Abstraction

- (3) Consideration of conceptual model uncertainty is consistent with available site characterization data, laboratory experiments, field measurements, natural analog information and process-level modeling studies; and the treatment of conceptual model uncertainty does not result in an under-representation of the risk estimate.

Response: This report provides an analysis of the expected chemical environment on the drip shield and waste package outer barrier surfaces. It primarily uses the IDPS model, which does not allow direct propagation of uncertainties in inputs (Section 6.7.2.16). Instead, uncertainties in the IDPS model outputs are based on the magnitude of error in IDPS model predictions for independent data (BSC 2004 [DIRS 169863] Section 7.3). Uncertainties in the IDPS conceptual model are based on natural analogues, model comparisons, and laboratory experiments (BSC 2004 [DIRS 169863], Sections 6.3, 6.6.2.6, and 7). IDPS model validation is consistent with these uncertainties.

Treatment of IDPS conceptual model uncertainty does not result in a biased underrepresentation of the risk estimate (BSC 2004 [DIRS 169863], Section 7.5). Uncertainties in the site-specific inputs to the analyses in the present report are estimated from a broad base of information. For example, the issue of uncertainty in the applicability of the tunnel dusts is addressed in Section 6.7.2.10 by comparing the ionic ratios in the tunnel dust leachates with corresponding ratios in Nevada regional precipitation (rainfall) and Asian dust leachates. This subcriterion is broadly addressed in Section 6.7.2.

INTENTIONALLY LEFT BLANK

8. INPUTS AND REFERENCES

The following is a list of references cited in this document. Column 2 represents the unique six-digit numerical identifier (the DIRS number), which is placed in the text following the reference callout (e.g., BSC 2004 [DIRS 167969]). The purpose of these numbers is to assist in locating a specific reference. Within the reference list, multiple sources by the same author (e.g., BSC 2002) are sorted alphabetically by title.

8.1 DOCUMENTS CITED

- Allal, K.M.; Dolignier, J.-C.; and Martin, G. 1997. "Determination of Thermodynamical Data of Calcium Hydroxide." *Revue de l'Institut Francais du Petrole*, 52, (3), 361-368. Paris, France: Éditions Technip. TIC: 254737. 162579
- Ansari, A.S. and Pandis, S.N. 1999. "Prediction of Multicomponent Inorganic Atmospheric Aerosol Behavior." *Atmospheric Environment*, 33, (5), 745-757. New York, New York: Pergamon. TIC: 254406. 162167
- Arimoto, R. 2001. "Eolian Dust and Climate: Relationships to Sources, Tropospheric Chemistry, Transport and Deposition." *Earth-Science Reviews*, 54, (1-3), 29-42. New York, New York: Elsevier. TIC: 254407. 163485
- Barin, I. and Platzki, G. 1995. *Thermochemical Data of Pure Substances*. 3rd Edition. Two volumes. New York, New York: VCH Publishers. TIC: 251934. 157865
- Blank, R.R.; Young, J.A.; and Allen, F.L. 1999. "Aeolian Dust in a Saline Playa Environment, Nevada, U.S.A." *Journal of Arid Environments*, 41, (4), 365-381. New York, New York: Academic Press. TIC: 254405. 163486
- Böhlke, J.K.; Ericksen, G.E.; and Revesz, K. 1997. "Stable Isotope Evidence for an Atmospheric Origin of Desert Nitrate Deposits in Northern Chile and Southern California, U.S.A." *Chemical Geology*, 136, (1-2), 135-152. New York, New York: Elsevier. TIC: 254348. 163354
- Bromley, L.A. 1973. "Thermodynamic Properties of Strong Electrolytes in Aqueous Solutions." *AIChE Journal*, 19, (2), 313-320. New York, New York: American Institute of Chemical Engineers. TIC: 253813. 163123
- BSC 2001. *Temperature - Relative Humidity Time Plot for Operating Mode 50-Yr Forced Ventilation and Indefinite Natural Ventilation*. Input Transmittal 00439.T. Las Vegas, Nevada: Bechtel SAIC Company. ACC: MOL.20010409.0185. 154276
- BSC 2002. *Scientific Processes Guidelines Manual*. MIS-WIS-MD-000001 REV 01. Las Vegas, Nevada: Bechtel SAIC Company. ACC: MOL.20020923.0176. 160313

BSC 2003. <i>Repository Design, Repository/PA IED Subsurface Facilities.</i> 800-IED-EBS0-00402-000-00B. Las Vegas, Nevada: Bechtel SAIC Company. ACC: MOL.20030109.0146.	161727
BSC 2004. <i>Abstraction of Drift Seepage.</i> MDL-NBS-HS-000019, Rev. 01. Las Vegas, Nevada: Bechtel SAIC Company. ACC: DOC.20041103.0003.	169131
BSC 2004. <i>D&E / PA/C IED Emplacement Drift Configuration and Environment.</i> 800-IED-MGR0-00201-000-00B. Las Vegas, Nevada: Bechtel SAIC Company. ACC: ENG.20040326.0001.	168489
BSC 2004. <i>D&E / PA/C IED Interlocking Drip Shield and Emplacement Pallet.</i> 800-IED-WIS0-00401-000-00D. Las Vegas, Nevada: Bechtel SAIC Company. ACC: ENG.20040503.0018.	169220
BSC 2004. <i>D&E / PA/C IED Subsurface Facilities.</i> 800-IED-WIS0-00101-000- 00A. Las Vegas, Nevada: Bechtel SAIC Company. ACC: ENG.20040309.0026.	164519
BSC 2004. <i>D&E / PA/C IED Typical Waste Package Components Assembly.</i> 800-IED-WIS0-00201-000-00E. Las Vegas, Nevada: Bechtel SAIC Company. ACC: ENG.20040517.0007.	169480
BSC 2004. <i>Drift-Scale THC Seepage Model.</i> MDL-NBS-HS-000001, Rev. 03. Las Vegas, Nevada: Bechtel SAIC Company. ACC: DOC.20041111.0001.	169856
BSC 2004. <i>Engineered Barrier System Features, Events, and Processes.</i> ANL-WIS-PA-000002, Rev. 03. Las Vegas, Nevada: Bechtel SAIC Company.	169898
BSC 2004. <i>Engineered Barrier System: Physical and Chemical Environment.</i> ANL-EBS-MD-000033, Rev. 03. Las Vegas, Nevada: Bechtel SAIC Company.	169860
BSC 2004. <i>General Corrosion and Localized Corrosion of the Drip Shield.</i> ANL EBS-MD-000004 REV 02. Las Vegas, Nevada: Bechtel SAIC Company. ACC: DOC.20040921.0002.	169845
BSC 2004. <i>General Corrosion and Localized Corrosion of Waste Package Outer Barrier.</i> ANL-EBS-MD-000003 REV 02. Las Vegas, Nevada: Bechtel SAIC Company. ACC: DOC.20041004.0001.	169984
BSC 2004. <i>In-Drift Natural Convection and Condensation.</i> MDL-EBS-MD-000001 REV 00. Las Vegas, Nevada: Bechtel SAIC Company. ACC: DOC.20041025.0006.	164327
BSC 2004. <i>In-Drift Precipitates/Salts Model.</i> ANL-EBS-MD-000045, Rev. 02. Las Vegas, Nevada: Bechtel SAIC Company. ACC: DOC.20041111.0002.	169863

BSC 2004. *Multiscale Thermohydrologic Model*. ANL-EBS-MD-000049 REV 02. 169565
 Las Vegas, Nevada: Bechtel SAIC Company. ACC: DOC.20041014.0008.

BSC 2004. *Q-List*. 000-30R-MGR0-00500-000-000 REV 00. Las Vegas, Nevada: 168361
 Bechtel SAIC Company. ACC: ENG.20040721.0007.

BSC 2004. *Technical Work Plan for: Near-Field Environment and Transport* 171156
In-Drift Geochemistry Model Report Integration. TWP-MGR-PA-000016 REV 02.
 Las Vegas, Nevada: Bechtel SAIC Company. ACC: DOC.20040806.0008.

Canori, G.F. and Leitner, M.M. 2003. *Project Requirements Document*. 166275
 TER-MGR-MD-000001 REV 02. Las Vegas, Nevada: Bechtel SAIC Company.
 ACC: DOC.20031222.0006.

Creahan, J. 1991. "Controlling Relative Humidity with Saturated Calcium Nitrate 163395
 Solutions." *WAAC Newsletter*, 13, (1), Pages 17-18. Los Angeles, California:
 Western Association for Art Conservation. TIC: 254503.

Creahan, J. 1991. "Update and Feedback: Controlling Relative Humidity with 163396
 Saturated Calcium Nitrate Solutions. Follow-Up Report: Calcium Nitrate Solutions
 for RH Control." *WAAC Newsletter*, 13, (2), Page 11. Los Angeles, California:
 Western Association for Art Conservation. ACC: 254502.

CRWMS (Civilian Radioactive Waste Management System) M&O (Management 153976
 and Operating Contractor) 1993. *Chemical Tracer Injection System Analysis for
 Construction Process and Firewater Usage*. BABFAE000-01717-0200-00030
 REV 01. Las Vegas, Nevada: CRWMS M&O. ACC: MOL.19951019.0473.

Delany, J.M. 1985. *Reaction of Topopah Spring Tuff with J-13 Water: A* 100134
Geochemical Modeling Approach Using the EQ3/6 Reaction Path Code.
 UCRL-53631. Livermore, California: Lawrence Livermore National Laboratory.
 ACC: HQS.19880517.2419.

Drever, J.I. 1997. "Evaporation and Saline Waters." Chapter 15 of *The* 147480
Geochemistry of Natural Waters: Surface and Groundwater Environments. 3rd
 Edition. Upper Saddle River, New Jersey: Prentice Hall. TIC: 246732.

Duncan, M.S. 1997. "Examining Early Nineteenth Century Saltpeter Caves: An 163338
 Archaeological Perspective." *Journal of Cave and Karst Studies*, 59, (2), 91-94.
 Huntsville, Alabama: National Speleological Society. TIC: 254349.

Dunning, G.E. and Cooper, J.F., Jr. 1969. "A Second Occurrence of Antarcticite, 162578
 from Bristol Dry Lake, California." *American Mineralogist*, 54, (7-8), 1018-1025.
 Washington, D.C.: Mineralogical Society of America. TIC: 254451.

- Elm, N.; Zipprian, J.; and Schaber, K. 2001. "Vapour-Liquid Equilibria of Binary and Ternary Aqueous Systems with HCl, HBr and CaCl₂ at Highly Diluted Vapour Phases." *Fluid Phase Equilibria*, 189, (1-2), 163-178. New York, New York: Elsevier. TIC: 254413. 163186
- Eugster, H.P. and Hardie, L.A. 1978. "Saline Lakes." *Lakes, Chemistry, Geology, Physics*. Lerman, A., ed. Pages 237-293. New York, New York: Springer-Verlag. TIC: 240782. 100743
- Falk, T.; Svensson, J.-E.; and Johansson, L.-G. 1998. "The Role of Carbon Dioxide in the Atmospheric Corrosion of Zinc." *Journal of the Electrochemical Society*, 145, (1), 39-44. Pennington, New Jersey: Electrochemical Society. TIC: 254417. 163489
- Farmer, J.; McCright, D.; Gdowski, G.; Wang, F.; Summers, T.; Bedrossian, P.; Horn, J.; Lian, T.; Estill, J.; Lingenfelter, A.; and Halsey, W. 2000. "General and Localized Corrosion of Outer Barrier of High-Level Waste Container in Yucca Mountain." *Transportation, Storage, and Disposal of Radioactive Materials, 2000, Presented at the 2000 ASME Pressure Vessels and Piping Conference, Seattle, Washington, July 23-27, 2000*. Hafner, R.S., ed. PVP-Vol. 408. Pages 53-69. New York, New York: American Society of Mechanical Engineers. TIC: 251259. 156521
- Fleagle, R.G. and Businger, J.A. 1980. *An Introduction to Atmospheric Physics*. 2nd Edition. Pages 10, 34, 40. Orlando, Florida: Academic Press. TIC: 245634. 108591
- Garrels, R.M. and Christ, C.L. 1990. *Solutions, Minerals, and Equilibria*. Boston, Massachusetts: Jones and Bartlett Publishers. TIC: 223483. 144877
- Ge, Z.; Wexler, A.S.; and Johnston, M.V. 1998. "Deliquescence Behavior of Multicomponent Aerosols." *Journal of Physical Chemistry A*, 102, (1), 173-180. Washington, D.C.: American Chemical Society. TIC: 254410. 162165
- Greenberg, J.P. and Moller, N. 1989. "The Prediction of Mineral Solubilities in Natural Waters: A Chemical Equilibrium Model for the Na-K-Ca-Cl-SO₄-H₂O System to High Concentration from 0 to 250°C." *Geochimica et Cosmochimica Acta*, 53, 2503-2518. New York, New York: Pergamon Press. TIC: 249020. 152684
- Greenspan, L. 1977. "Humidity Fixed Points of Binary Saturated Aqueous Solutions." *Journal of Research of the National Bureau of Standards*, 81A, (1), 89-96. Washington, D.C.: U.S. Department of Commerce. TIC: 241138. 104945
- Hardie, L.A. 1991. "On the Significance of Evaporites." *Annual Review of Earth and Planetary Sciences*, 19, 131-168. Palo Alto, California: Annual Reviews. TIC: 254409. 162777
- Hardie, L.A. and Eugster, H.P. 1970. *The Evolution of Closed-Basin Brines*. Mineralogical Society of America Special Paper 3. Pages 273-290. Washington, D.C.: Mineralogical Society of America. TIC: 254408. 162776

- Harrar, J.E.; Carley, J.F.; Isherwood, W.F.; and Raber, E. 1990. *Report of the Committee to Review the Use of J-13 Well Water in Nevada Nuclear Waste Storage Investigations*. UCID-21867. Livermore, California: Lawrence Livermore National Laboratory. ACC: NNA.19910131.0274. 100814
- Harvie, C.E.; Moller, N.; and Weare, J.H. 1984. "The Prediction of Mineral Solubilities in Natural Waters: The Na-K-Mg-Ca-H-Cl-SO₄-OH-HCO₃-CO₃-CO₂-H₂O System to High Ionic Strengths at 25°C." *Geochimica et Cosmochimica Acta*, 48, (4), 723-751. New York, New York: Pergamon Press. TIC: 239849. 118163
- Helgeson, H.C.; Delany, J.M.; Nesbitt, H.W.; and Bird, D.K. 1978. "Summary and Critique of the Thermodynamic Properties of Rock Forming Minerals." *American Journal of Science*, 278-A. New Haven, Connecticut: Yale University, Kline Geology Laboratory. TIC: 220013. 101596
- Hill, C. and Forti, P. 1997. *Cave Minerals of the World*. 2nd Edition. Huntsville, Alabama: National Speleological Society. TIC: 254549. 164320
- Hill, C.A. 1999. "Mineralogy of Kartchner Caverns, Arizona." *Journal of Cave and Karst Studies*, 61, (2), 73-78. Huntsville, Alabama: National Speleological Society. TIC: 254351. 163340
- Janecky, D.R. 1982. *Serpentinization of Peridotite within the Oceanic Crust: Experimental and Theoretical Investigations of Seawater-Peridotite Interaction at 200°C and 300°C, 500 Bars*. Ph.D. dissertation. Minneapolis, Minnesota: University of Minnesota. TIC: 246544. 157907
- Johnson, J.W.; Oelkers, E.H.; and Helgeson, H.C. 1992. "SUPCRT92: A Software Package for Calculating the Standard Molal Thermodynamic Properties of Minerals, Gases, Aqueous Species, and Reactions from 1 to 5000 Bar and 0 to 1000°C." *Computers & Geosciences*, 18, (7), 899-947. New York, New York: Pergamon Press. TIC: 234273. 101632
- Knauss, K.G. and Beiriger, W.B. 1984. *Report on Static Hydrothermal Alteration Studies of Topopah Spring Tuff Wafers in J-13 Water at 150°C*. UCRL-53576. Livermore, California: Lawrence Livermore National Laboratory. ACC: HQS.19880517.2007. 106441
- Knauss, K.G. and Peifer, D.W. 1986. *Reaction of Vitric Topopah Spring Tuff and J-13 Ground Water Under Hydrothermal Conditions Using Dickson-Type, Gold-Bag Rocking Autoclaves*. UCRL-53795. Livermore, California: Lawrence Livermore National Laboratory. ACC: NNA.19891102.0117. 100151
- Knauss, K.G.; Beiriger, W.J.; and Peifer, D.W. 1985. *Hydrothermal Interaction of Crushed Topopah Spring Tuff and J-13 Water at 90, 150, and 250°C Using Dickson-Type, Gold-Bag Rocking Autoclaves*. UCRL-53630. Livermore, California: Lawrence Livermore National Laboratory. ACC: NNA.19931005.0010. 143694

- Knauss, K.G.; Beiriger, W.J.; and Peifer, D.W. 1987. *Hydrothermal Interaction of Solid Wafers of Topopah Spring Tuff with J-13 Water at 90 and 150°C Using Dickson-Type, Gold-Bag Rocking Autoclaves: Long-Term Experiments*. UCRL-53722. Livermore, California: Lawrence Livermore National Laboratory. ACC: NNA.19870713.0081. 100152
- Knauss, K.G.; Delany, J.M.; Beiriger, W.J.; and Peifer, D.W. 1985. "Hydrothermal Interaction of Topopah Spring Tuff with J-13 Water as a Function of Temperature." *Scientific Basis for Nuclear Waste Management VIII, Symposium held November 26-29, 1984, Boston, Massachusetts*. Jantzen, C.M.; Stone, J.A.; and Ewing, R.C., eds. 44, 539-546. Pittsburgh, Pennsylvania: Materials Research Society. TIC: 203665. 141586
- Kracek, F.C. 1928. "P-T-X Relations for Systems of Two or More Components and Containing Two or More Phases (L-V, L_I-L_{II}-V and S-L-V Systems)." *International Critical Tables of Numerical Data, Physics, Chemistry and Technology*. Washburn, E.W., ed. Volume III. 1st Edition. New York, New York: McGraw-Hill. TIC: 243268. 122125
- Levy, D.B.; Schramke, J.A.; Esposito, K.J.; Erickson, T.A.; and Moore, J.C. 1999. "The Shallow Ground Water Chemistry of Arsenic, Fluorine, and Major Elements: Eastern Owens Lake, California." *Applied Geochemistry*, 14, (1), 53-65. New York, New York: Pergamon. TIC: 254418. 163397
- Lewis, G.N. and Randall, M. 1961. *Thermodynamics*. 2nd Edition. New York, New York: McGraw-Hill. TIC: 240735. 119458
- Li, J.; Lowenstein, T.K.; and Blackburn, I.R. 1997. "Responses of Evaporite Mineralogy to Inflow Water Sources and Climate During the Past 100 k.y. in Death Valley, California." *Geological Society of America Bulletin*, 109, (10), 1361-1371. Boulder, Colorado: Geological Society of America. TIC: 247723. 148201
- Lindström, R.; Svensson, J-E.; and Johansson, L.G. 2002. "The Influence of Salt Deposits on the Atmospheric Corrosion of Zinc." *Journal of the Electrochemical Society*, 149, (2), B57-B64. Pennington, New Jersey: Electrochemical Society. TIC: 254416. 163488
- Linke, W.F. 1965. *Solubilities, Inorganic and Metal-Organic Compounds*. 4th Edition. Volume II, K-Z. Washington, D.C.: American Chemical Society. TIC: 222176. 166191
- Lutz, H.D.; Schmidt, M.; and Weckler, B. 1993. "Infrared and Raman Studies on Calcium, Zinc and Cadmium Hydroxide Halides Ca{O(H,D)}Cl, Cd{O(H,D)}Cl, Zn{O(H,D)}F and β-Zn{O(H,D)}Cl." *Journal of Raman Spectroscopy*, 24, 797-804. New York, New York: John Wiley & Sons. TIC: 254787. 163487

- Maier, C.G. and Kelley, K.K. 1932. "An Equation For The Representation Of High Temperature Heat Content Data." *Journal of the American Chemical Society*, 54, 3243-3246. Washington, D.C.: American Chemical Society. TIC: 239023. 101691
- Mitchell, A. 1997. "Notice of Planned Tracers, Fluids, and Materials to be Utilized for Exploratory Studies Facility Site Characterization Testing in Support of Field Work Package FWP-ESF-96-004 Moisture Studies in the ESF." Memorandum from A. Mitchell (LANL) to P. Hastings (CRWMS M&O), March 5, 1997, LA-EES-13-LV-03-97-006, with attachments. ACC: MOL.19971103.0143; MOL.19971103.0144. 107654
- Mitchell, A. 1998. "Intent to Use Aqueous Tracers in Various Concentrations for Tests to be Conducted in Upper Tiva Canyon Alcove – Alcove 1 in Association with Infiltration and Percolation Studies in the Exploratory Studies Facility, in Support of Field Work Package FWP-ESF-96-004." Memorandum from A. Mitchell (LANL) to Distribution, June 17, 1998, LA-EES-7-06-98-017, with attachments. ACC: MOL.19981124.0073. 107958
- Mitchell, A. 1998. "Tracers, Fluids and Materials Evaluation for Gases and Aqueous Tracers in Various Concentrations for Tests to be Conducted in Alcove 6 in Association with the Moisture Seepage and Percolation Studies in the ESF in Support of Field Work Package FWP-ESF-96-004." Memorandum from A. Mitchell (LANL) to D. Gwyn (CRWMS M&O), May 28, 1998, LA-EES-7-05-98-022, with attachments. ACC: MOL.19980923.0208. 107949
- Mitchell, A. 1998. "Tracers, Fluids and Materials Evaluation for Gases and Aqueous Tracers in Various Concentrations for Tests to be Conducted in Niches #3 and #4 in Association with the Drift Scale Niche Studies in Support of Field Work Package FWP-ESF-96-004 Moisture Studies in the ESF." Memorandum from A. Mitchell (LANL) to D. Gwyn (CRWMS M&O), May 29, 1998, LA-EES-7-05-98-021, with attachments. ACC: MOL.19980923.0209. 107939
- Mitchell, A. 1998. "Tracers, Fluids, and Materials Evaluation for Gases and Aqueous Tracers in Various Concentrations for Tests to be Conducted in Alcove 4 in Association with the Moisture Seepage and Percolation Studies in the Exploratory Studies Facility in Support of Field Work Package FWP-ESF-96-004." Memorandum from A. Mitchell (LANL) to D. Gwyn (CRWMS M&O), June 1, 1998, LA-EES-7-06-98-002. ACC: MOL.19980923.0210. 107946
- Mitchell, A. 1998. "Transmittal of Preliminary Water Use in the East-West Cross-Drift Information." Memorandum from A. Mitchell (LANL) to R. Wemheuer (CRWMS M&O), June 22, 1998, LA-EES-7-06-98-019. ACC: MOL.19990218.0202. 146802
- Mitchell, A. 1998. "Water Data." E-mail from A. Mitchell to R. Wemheuer (CRWMS M&O), February 23, 1998. ACC: MOL.19990305.0201. 146795

Mitchell, A. 2000. "Humidifiers in the Niches." E-mail from A. Mitchell to K. Fitzgerald (CRWMS M&O), J. Wang (CRWMS M&O), and R. Kovach (CRWMS M&O), October 30, 2000. ACC: MOL.20001031.0167. 152962

Mitchell, A.J. 1998. "Notice of Intent to Use Conservative Tracers in Various Concentrations for Tests to be Conducted in Niche #2 in Association with the Drift Scale Niche Studies in Support of Field Work Package FWP-ESF-96-004, Moisture Studies in the Exploratory Studies Facility." Interoffice correspondence from A.J. Mitchell (CRWMS M&O) to G.A. Fasano and T.H. Pysto, August 4, 1998, LV.NEPO.TEST.AJM.08/98-333, with enclosures. ACC: MOL.19981124.0075. 107972

Mitchell, A.J. 1999. "Request for Additional Water for Phase II of Infiltration and Percolation Study Being Conducted in Upper Tiva Canyon Alcove – Alcove 1 in Support of Field Work Package FWP-ESF-96-004." Interoffice correspondence from A.J. Mitchell (CRWMS M&O) to D. Gwyn, October 25, 1999, LV.NEPO.TEST.AJM.10/99-374, with enclosure. ACC: MOL.20000204.0133. 148010

Mitchell, A.J. 1999. "Tracers, Fluids, and Materials Evaluation for Gases and Aqueous Tracers for Testing to be Conducted in Niche 1620 (Niche #5) in Accordance with FWP-ESF-96-004, Moisture Studies in the ESF." Interoffice correspondence from A.J. Mitchell (CRWMS M&O) to D. Gwyn, March 15, 1999, LV.NEPO.TEST.AJM.03/99-262. ACC: MOL.19990329.0086. 107977

Mitchell, A.J. 1999. "Tracers, Fluids, and Materials Evaluation for Gases and Aqueous Tracers for the Systematic Hydrological Investigation of the Fracture Flow and Transport in the East-West Cross Drift." Interoffice correspondence from A.J. Mitchell (CRWMS M&O) to D. Gwyn, December 14, 1999, LV.NEPO.TEST.AJM.12/99-410, with enclosures. ACC: MOL.20000204.0132. 148008

Mitchell, A.J. 1999. "Tracers, Fluids, and Materials Evaluation for Tracers to be Conducted in Alcove 8 in Association with Infiltration Testing in Support of Field Work Package FWP-ESF-96-004." Interoffice correspondence from A.J. Mitchell (CRWMS M&O) to D. Gwyn, March 10, 1999, LV.NEPO.TEST.AJM.03/99-259. ACC: MOL.19990329.0083. 107978

Mitchell, A.J. 2000. "Request for Additional Water for the Infiltration and Percolation Study Being Conducted in Upper Tiva Canyon Alcove – Alcove 1, in Support of Field Work Package FWP-ESF-96-004, Moisture Studies in the ESF." Interoffice correspondence from A.J. Mitchell (CRWMS M&O) to D. Gwyn, January 7, 2000, LV.NEPO.TEST.AJM.01/00-105, with enclosure. ACC: MOL.20000204.0134. 148049

NADP/NTN (National Atmospheric Deposition Program/National Trends Network) 2003. *2002 Annual & Seasonal Data Summary for Site CA95. Part 1: Summary of Sample Validity and Completeness Criteria*. Champaign, Illinois: National Atmospheric Deposition Program Office, Illinois State Water Survey. TIC: 256216. 171293

- NADP/NTN 2003. *2002 Annual & Seasonal Data Summary for Site NV00. Part 1: Summary of Sample Validity and Completeness Criteria*. Champaign, Illinois: National Atmospheric Deposition Program Office, Illinois State Water Survey. TIC: 256214. 171291
- NADP/NTN 2003. *2002 Annual & Seasonal Data Summary for Site NV05. Part 1: Summary of Sample Validity and Completeness Criteria*. Champaign, Illinois: National Atmospheric Deposition Program Office, Illinois State Water Survey. TIC: 256215. 171292
- Nordstrom, D.K. and Munoz, J.L. 1986. *Geochemical Thermodynamics*. Palo Alto, California: Blackwell Scientific Publications. TIC: 208228. 153965
- NRC (U.S. Nuclear Regulatory Commission) 2003. *Yucca Mountain Review Plan, Final Report*. NUREG-1804, Rev. 2. Washington, D.C.: U.S. Nuclear Regulatory Commission, Office of Nuclear Material Safety and Safeguards. TIC: 254568. 163274
- Opila, R.L., Jr.; Weschler, C.J.; and Schubert, R. 1989. "Acidic Vapors Above Saturated Salt Solutions Commonly Used For Control of Humidity." *IEEE Transactions on Components, Hybrids, and Manufacturing Technology*, 12, (1), 114-120. New York, New York: The Institute of Electrical and Electronic Engineers. TIC: 246611. 140330
- Orlovsky, N. and Orlovsky, L. 2001. "White Sandstorms in Central Asia." Chapter 8 of *Global Alarm: Dust and Sandstorms from the World's Drylands*. Youlin, Y.; Squires, V.; and Qi, L., eds. Beijing, China: United Nations Convention to Combat Desertification. TIC: 254449. 163413
- Pabalan, R.T. and Pitzer, K.S. 1987. "Thermodynamics of Concentrated Electrolyte Mixtures and the Prediction of Mineral Solubilities to High Temperatures for Mixtures in the System Na-K-Mg-Cl-SO₄-OH-H₂O." *Geochimica et Cosmochimica Acta*, 51, (9), 2429-2443. New York, New York: Pergamon Journals. TIC: 253508. 162096
- Pabalan, R.T.; Yang, L.; and Browning, L. 2002. *Effects of Salt Formation on the Chemical Environment of Drip Shields and Waste Packages at the Proposed Nuclear Waste Repository at Yucca Mountain, Nevada*. CNWRA 2002-03. San Antonio, Texas: Center for Nuclear Waste Regulatory Analyses. TIC: 254207. 163067
- Pilinis, C. 1999. "Modeling Atmospheric Aerosols Using Thermodynamic Arguments - A Review." *Global Nest: the International Journal*, 1, (1), 5-13. Athens, Greece: Global Nest. TIC: 254346. 163126
- Pitzer, K.S. 1991. "Ion Interaction Approach: Theory and Data Correlation." Chapter 3 of *Activity Coefficients in Electrolyte Solutions*. 2nd Edition. Pitzer, K.S., ed. Boca Raton, Florida: CRC Press. TIC: 251799. 152709

- Pulvirenti, A.; Adel-Hadadi, M.A.; Barkatt, A.; Marks, C.; Gorman, J.A.; and Staehle, R.W. 2003. *Continuing Investigations of Local Environments on Waste Container Surfaces*. Presented at Nuclear Waste Technical Review Board Meeting, Las Vegas, Nevada, January 28, 2003. Carson City, Nevada: State of Nevada, Agency for Nuclear Projects. TIC: 254428. 163184
- Reheis, M.C. 1997. "Dust Deposition Downwind of Owens (Dry) Lake, 1991-1994: Preliminary Findings." *Journal of Geophysical Research*, 102, (D22), 25,999-26,008. Washington, D.C.: American Geophysical Union. TIC: 255971. 168715
- Reheis, M.C. and Kihl, R. 1995. "Dust Deposition in Southern Nevada and California, 1984-1989: Relations to Climate, Source Area, and Source Lithology." *Journal of Geophysical Research*, 100, (D5), 8893-8918. Washington, D.C.: American Geophysical Union. TIC: 234886. 106653
- Reheis, M.C.; Budahn, J.R.; and Lamothe, P.J. 2002. "Geochemical Evidence for Diversity of Dust Sources in the Southwestern United States." *Geochimica et Cosmochimica Acta*, 66, (9), 1569-1587. New York, New York]: Pergamon. TIC: 254213. 163132
- Rosenberg, N.D.; Gdowski, G.E.; and Knauss, K.G. 2001. "Evaporative Chemical Evolution of Natural Waters at Yucca Mountain, Nevada." *Applied Geochemistry*, 16, (9-10)], 1231-1240. New York, New York]: Pergamon. TIC: 249879. 154862
- Rosenberg, N.D.; Knauss, K.G.; and Dibley, M.J. 1999. *Evaporation of J13 Water: Laboratory Experiments and Geochemical Modeling*. UCRL-ID-134852. Livermore, California: Lawrence Livermore National Laboratory. TIC: 246322. 125338
- Rosenberg, N.D.; Knauss, K.G.; and Dibley, M.J. 1999. *Evaporation of Topopah Spring Tuff Pore Water*. UCRL-ID-135765. Livermore, California: Lawrence Livermore National Laboratory. TIC: 246231. 125339
- SNL (Sandia National Laboratories) 2003. *Software User's Manual, EQ3/6, Version 8.0*. SDN: 10813-UM-8.0-00. Albuquerque, New Mexico: Sandia National Laboratories. ACC: MOL.20030312.0084. 162494
- Stumm, W. and Morgan, J.J. 1996. *Aquatic Chemistry, Chemical Equilibria and Rates in Natural Waters*. 3rd Edition. New York, New York: John Wiley & Sons. TIC: 246296. 125332
- Tang, I.N. and Munkelwitz, H.R. 1993. "Composition and Temperature Dependence of the Deliquescence Properties of Hygroscopic Aerosols." *Atmospheric Environment*, 27A, (4), 467-473. New York, New York: Pergamon. TIC: 254415. 163124

- Tang, I.N. and Munkelwitz, H.R. 1994. "Aerosol Phase Transformation and Growth in the Atmosphere." *Journal of Applied Meteorology*, 33, (7), 791-796. Boston, Massachusetts: American Meteorological Society. TIC: 254414. 163125
- Thorstenson, D.C.; Weeks, E.P.; Haas, H.; and Woodward, J.C. 1990. "Physical and Chemical Characteristics of Topographically Affected Airflow in an Open Borehole at Yucca Mountain, Nevada." *Proceedings of the Topical Meeting on Nuclear Waste Isolation in the Unsaturated Zone, Focus '89, September 17-21, 1989, Las Vegas, Nevada*. Pages 256-270. La Grange Park, Illinois: American Nuclear Society. TIC: 212738. 100831
- Topping, D.; Coe, H.; McFiggans, G.; Burgess, R.; Allan, J.; Alfarra, M.R.; Bower, K.; Choularton, T.W.; Decesari, S.; and Facchini, M.C. 2004. "Aerosol Chemical Characteristics from Sampling Conducted on the Island of Jeju, Korea During ACE Asia." *Atmospheric Environment*, 38, 2111-2123. New York, New York]: Elsevier. TIC: 256037. 171290
- Torii, T. and Ossaka, J. 1965. "Antarcticite: A New Mineral, Calcium Chloride Hexahydrate, Discovered in Antarctica." *Science*, 149, (3687), 975-977. Washington, D.C.]: American Association for the Advancement of Science. TIC: 254426. 162577
- von Glasow, R. and Sander, R. 2001. "Variation of Sea Salt Aerosol pH with Relative Humidity." *Geophysical Research Letters*, 28, (2), 247-250. Washington, D.C.: American Geophysical Union. TIC: 254352. 162162
- Weast, R.C. and Astle, M.J., eds. 1981. *CRC Handbook of Chemistry and Physics*. 62nd Edition. Boca Raton, Florida: CRC Press. TIC: 240722. 100833
- Weber, C.F. 2001. *Thermodynamic Modeling of Savannah River Evaporators*. ORNL/TM-2001/102. Oak Ridge, Tennessee: Oak Ridge National Laboratory. TIC: 254353. 163110
- Wolery, T.J. 1978. *Some Chemical Aspects of Hydrothermal Processes at Mid-Oceanic Ridges - A Theoretical Study. I. Basalt-Sea Water Reaction and Chemical Cycling Between the Oceanic Crust and the Oceans. II. Calculation of Chemical Equilibrium Between Aqueous Solutions and Minerals*. Ph.D. dissertation. Evanston, Illinois: Northwestern University. TIC: 219640. 151346
- Wolery, T.J. 1979. *Calculation of Chemical Equilibrium Between Aqueous Solution and Minerals: The EQ3/6 Software Package*. UCRL-52658. Livermore, California: Lawrence Livermore Laboratory. ACC: HQS.19880517.2586. 156741

Yang, I.C.; Rattray, G.W.; and Yu, P. 1996. *Interpretation of Chemical and Isotopic Data from Boreholes in the Unsaturated Zone at Yucca Mountain, Nevada*. Water-Resources Investigations Report 96-4058. Denver, Colorado: U.S. Geological Survey. ACC: MOL.19980528.0216. 100194

8.2 CODES, STANDARDS, REGULATIONS, AND PROCEDURES

10 CFR 63. Energy: Disposal of High-Level Radioactive Wastes in a Geologic Repository at Yucca Mountain, Nevada. Readily available. 156605

ASTM C 1174-97. 1998. *Standard Practice for Prediction of the Long-Term Behavior of Materials, Including Waste Forms, Used in Engineered Barrier Systems (EBS) for Geological Disposal of High-Level Radioactive Waste*. West Conshohocken, Pennsylvania: American Society for Testing and Materials. TIC: 246015. 105725

ASTM E 104-85 (Reapproved 1996). 1985. *Standard Practice for Maintaining Constant Relative Humidity by Means of Aqueous Solutions*. West Conshohocken, Pennsylvania: American Society for Testing and Materials. TIC: 247404. 146039

AP-2.22Q, Rev. 1, ICN 1. *Classification Analyses and Maintenance of the Q-List*. Washington, D.C.: U.S. Department of Energy, Office of Civilian Radioactive Waste Management. ACC: DOC.20040714.0002.

AP-SIII.9Q, Rev. 1, ICN 7. *Scientific Analyses*. Washington, D.C.: U.S. Department of Energy, Office of Civilian Radioactive Waste Management. ACC: DOC.20040920.0001.

LP-SI.11Q-BSC, Rev. 0, ICN 1. *Software Management*. Washington, D.C.: U.S. Department of Energy, Office of Civilian Radioactive Waste Management. ACC: DOC.20041005.0008.

8.3 SOURCE DATA, LISTED BY DATA TRACKING NUMBER

GS030108312242.001. Temperature, Relative Humidity and Barometric Pressure Behind the Bulkhead in Alcove 8 from June 22, 2000 to August 26, 2002. Submittal date: 02/20/2003. 163118

GS970908312271.003. Unsaturated Zone Hydrochemistry Data, 2-1-97 to 8-31-97, Including Chemical Composition and Carbon, Oxygen, and Hydrogen Isotopic Composition: Porewater from USW NRG-7A, SD-7, SD-9, SD-12 and UZ-14; and Gas from USW UZ-14. Submittal date: 09/08/1997. 111467

LAJF831222AQ98.003. Chloride, Bromide, Sulfate, and Chlorine-36 Analysis of Construction Water. Submittal date: 09/09/1998. 146310

LB0108DSTTHC01.001. THC Simulations of the Drift Scale Test and THC Seepage Model: 1. Data Summary. Submittal date: 08/10/2001.	156285
LL001100931031.008. Aqueous Chemistry of Water Sampled from Boreholes of the Drift Scale Test (DST). Submittal date: 11/10/2000.	153288
LL030308812251.017. The Effect of Temperature on the Reaction Rate of Calcium Chloride on the Surface of Alloy-22 at 22.5% Relative Humidity and Atmospheric Pressure. Submittal date: 05/07/2003.	163775
LL030309012251.018. Images Illustrating the Formation of Precipitates Through the Reaction of Calcium Chloride on the Surface of Alloy-22 at 150 C and 19-22.5 Per Cent Relative Humidity and Atmospheric Pressure. Submittal date: 05/07/2003.	163774
LL991212305924.108. Environment on the Surfaces of the Drip Shield and Waste Package Outer Barrier. Submittal date: 12/20/1999.	144927
MO0005PORWATER.000. Perm-Sample Pore Water Data. Submittal date: 05/04/2000.	150930
MO0006J13WTRCM.000. Recommended Mean Values of Major Constituents in J-13 Well Water. Submittal date: 06/07/2000.	151029
MO0101SEPFDDST.000. Field Measured Data of Water Samples from the Drift Scale Test. Submittal date: 01/03/2001.	153711
MO0207EBSDUSTS.020. Geochemical Composition of Dust Samples. Submittal date: 07/11/2002.	162556
MO0209EBSDUST2.030. Geochemical Composition of Dust Samples (Phase II). Submittal date: 09/30/2002.	162557
MO0302SPATHDYN.000. Thermodynamic Data Input Files - Data0.YMP.R2. Submittal date: 02/05/2003.	161756
MO0302SPATHDYN.001. Thermodynamic Data Supporting Spreadsheet Files - Data0.YMP.R2. Submittal date: 02/05/2003.	161886
MO0303MWDSCMAB.000. THC Seepage Chemistry Model Abstraction Binning EQ3 Input, Pickup and Output Files. Submittal date: 03/06/2003.	162551
MO0303SPAMNSUP.000. Baseline YPF Pitzer Database MineralSuppressions for the In-Drift Precipitates/Salts Model. Submittal date: 03/04/2003.	171426
MO0312SPAESMUN.002. Estimated Model Uncertainties in IDPS Model Outputs. Submittal date: 12/03/2003.	166329
MO0407SEPFEPPLA.000. LA FEP List. Submittal date: 07/20/2004.	170760

SN0203F3903102.001. Drift Scale Test Water Sampling (with Results from 4/17/2001 through 1/14/2002). Submittal date: 03/29/2002. 159133

SN0302T0510102.002. Pitzer Thermodynamic Database (data0.ypf, Revision 1). Submittal date: 02/06/2003. 162572

SN0310T0510102.010. Analysis of In-Drift Dust Leachates at 25 Degrees C to Various Evaporation Relative Humidity (RH) Levels. Submittal date: 10/08/2003. 168705

8.4 OUPUT DATA, LISTED BY DATA TRACKING NUMBER

LL030500612251.059. Atmospheric Pressure at the Repository Elevation. Submittal Date: 05/24/2003.

LL030500712251.060. Vapor Pressure of Water as a Function of Temperature and Water Activity; Range of Accessible Relative Humidity (Rh) at Standard Atmospheric Pressure and at Repository Ambient Pressure. Submittal date: 05/24/2003.

LL030500812251.061. Calculations Pertaining To Acid Gas Volatility. Submittal Date: 07/02/2003.

LL040601512251.103. Vapor Pressure of Water as a Function of Temperature and Water Activity; Range of Accessible Relative Humidity (Rh) at Standard Atmospheric Pressure at Expected Mean Repository Pressure, and at Expected Maximum Repository Pressure. Submittal date: 07/15/2004.

LL040603612251.104. EQ3/6 Dust Leachate Evaporation Calculations. Submittal date: 08/02/2004.

LL040603712251.105. Ionic Ratios in Dust and Rainfall, Comparing the Leachable Solute Content of YMP Tunnel Dusts with that of Asian Dusts and with the Dissolved Solute Content of Nevada Rainfall. Submittal date: 08/17/2004.

LL040903723121.042. Thermodynamic Calculations and Plots Analyzing Salt Mineral Deliquescence on the DS (Drip Shield) and WPOB (Waste Package Outer Barrier). Submittal date: 09/21/2004.

LL040603912251.107. Deliquescence Lookup Tables: Relative Humidity (Decimal) Vs. Temperature (C). Submittal date: 08/17/2004.

8.5 SOFTWARE CODES

BSC (Bechtel SAIC Company) 2003. *Software Code: EQ3/6. V8.0. PC w/ Windows 95/98/2000/NT 4.0. 10813-8.0-00.* 162228

LBNL (Lawrence Berkeley National Laboratory) 1999. *Software Code: SUPCRT92. V1.0. PC w/Windows OS and MAC w/MAC OS. 10058-1.0-00.* 153218